FAST COMBUSTION REACTIONS OF SILICON AND LEAD OXIDES

BY

SABEH SWADY AL-KAZRAJI

THESIS SUBMITTED FOR THE DEGREE OF DOCTOR OF PHILOSOPHY
IN THE DEPARTMENT OF CHEMICAL ENGINEERING

The award is that of the Council for National Academic Awards.

DEPARTMENT OF CHEMICAL ENGINEERING
POLYTECHNIC OF WALES
TREFOREST PONTYPRIDD
MID GLAMORGAN

JULY 1979

ACKNOWLEDGEMENTS

The author expresses his deepest appreciation to Dr. G. J. Rees for his guidance and supervision throughout this work. His suggestions and continued encouragement provided a real stimulus. The author also thanks I.C.I. (Nobel Explosives) Co., who, with Science Research Council, sponsored this research, and with whom some of this work was performed, especially Dr. J. Morman, Dr. J. McAuslan, Mr. T. McLoughlin and Mr. T. Turner, for their continued help.

Thanks are also due to Dr. M. S. Doulah for frequent discussions and the interest he has shown, his help is gratefully acknowledged. Sincere thanks to all the technical staff of the Chemical Engineering Department for their assistance in the construction and maintenance of the experimental equipment.

I acknowledge the help of Mr. D. Lee of the Electrical Engineering Department for his assistance with the construction of the firing system, and Dr. S. Wilde and Dr. Roberts of the Science Department, for their advice in the use of the X-ray diffraction and thermal conductivity equipment.

CONTENTS

ABSTRACT OF THESIS

A survey of earlier work in the field of reactions of solids introduces the thesis. The conclusions derived from these researches are discussed.

Reactions of trilead tetraoxide (red lead) and lead dioxide as oxidants with powdered silicon were extensively studied. The experimental methods and apparatus used are described. The study can be divided into two parts:

(1) Study of the burning characteristics of the pelletted oxidant/fuel compositions.

(2) Study of small samples of powdered mixtures of the same compositions at controlled conditions by thermal analysis techniques.

In the first, the delay time and the rate of burning of the compositions are measured and the influence of diluents, ambient temperature and pressure, particle size and other variables are determined and mathematical relationships arrived at. Heats of reaction data are utilized to select the most probable reaction taking place, and a correlation between the heat evolved and the rate of burning is established.

A detailed study of the mechanism of the self-sustained reaction between red lead and silicon was performed by the method of temperature profile analysis and a mathematical model for the propagation

is put forward.

The temperatures of the burning compositions are measured and compared with theoretically calculated maximum temperatures, and a theory is put forward as to the temperature of reaction below which combustion reaction is no longer possible.

In the thermal analysis study, the stages of the reactions and the temperatures at which these reactions proceed are established. Also studies of the individual components such as oxidants, silicon and binder are carried out and the effect of varying conditions such as rate of heating, atmosphere under which reaction occurs, and the presence of binder, are investigated.

From DSC and TG, a mathematical model for the decomposition reaction of the oxide and the exothermic reactions of oxidant/fuel is put forward.

CHAPTER ONE

INTRODUCTION

In industry, rapid exothermic reaction processes which take place with the evolution of large amounts of heat are of considerable importance and interest. The basic feature of combustion phenomena is that the conditions necessary for the reaction to take place rapidly are created by the reaction itself. In solid reactions these conditions are constituted by a high temperature of the products.

When chemical reactions occur which involve two solids and liquefaction does not occur, the progress of chemical change depends on the area and defect structure of the contact areas between the reactant solids and the products. Reaction kinetics of a process may thus be influenced by the average particle size and particle size distribution. It is therefore important to know the form of sample, and any special treatments to which it has been subjected.

Combustion reactions in pyrotechnics are the main feature of this study, and hence understanding of the various applications determines their design and construction. Pyrotechnic compositions consist basically of mixtures of reducing and oxidising chemicals, which are capable of self-sustained combustion. These constituents are normally used in the form of consolidated crystalline or powdered solids.

The particular results from burning a pyrotechnic composition depend on various factors. The most important are the specific reducing agents and oxidants used, their physical form and particle size and also the method of containment and the environment in which burning takes place. The behaviour may be considerably modified by

additives included intentionally or by adventitious contamination.

The reducing agent is referred to as the fuel. Pyrotechnic compositions differ from fuel-air systems, such as household fires and furnaces, or from petrol and oil engines, in incorporating the oxidant for the combustion in the mixture. It is not essential that oxygen containing substances should be used. In certain cases, for example, sulphides are effective.

Relatively crude pyrotechnic compositions are employed in fireworks which have been used for centuries in entertainment and celebrations, and have long been used in wars, gun powder being the obvious example. In recent years more sophisticated formulation and design of pyrotechnics has resulted from the accuracy needed for space exploration as well as stringent requirements for military uses.

On ignition of a pyrotechnic composition, reaction propagates over all the available surface to yield the products of reaction and to release energy. According to the compositions used and the conditions of use, the energy may appear in the form of heat, light or sound, giving rise to ignition and incendiary sources, to visual or audible signals or to sources of irradiation. (1)

Burning suitable pyrotechnic compositions to transfer ignition between pyrotechnic or explosive components over a required interval of time, is referred to as "delay time", and the time delays can be very accurate and are used in virtually every type of device from the hand grenade to the sophisticated Apollo space vehicle.

At high altitudes, and in the confined spaces of systems where changes of pressure would affect the rate of burning of gas

producing compositions, rendering them unreliable, the use of "gasless" compositions becomes essential. These compositions give little, or no, gaseous products.

CHAPTER TWO

SUMMARY OF LITERATURE SURVEY

Work on the self-propagation of reactions in mixtures of oxidising and reducing agents was carried out by Hill, Sutton and Temple (2, 3, 4). The methods utilised included the recording of temperature changes as the reaction front passes a point, examination of combustion products and conductivity studies. The results they obtained were used to

(a) test the Mallard-Le Chatelier[5] theory of propagation by thermal conduction,

(b) investigate the stoichiometry of the reactions,

(c) obtain rate of burning and activation energies.

They concluded that the Mallard-Le Chatelier theory of propagation by thermal conduction is basically capable of explaining the behaviour of such reactions but that it is somewhat inadequate in its simplest form.

In more recent work Hill (6) has investigated the kinetics of chemical reactions of $Mo/KMnO_4$ and established that reaction takes place in two stages, the chemical kinetics of the first stage in the temperature range 25 - 110° have been derived by means of a thermal conduction theory of wave propagation. The observed activation energy decreased with temperature, from which it is deduced that there is a single reaction path having several successive energy barriers. The view is put forward that the first stage of reaction involves only the permanganate ions which are favourably placed at the boundaries of mosaic blocks and that these are decomposed by molybdenum atoms which have diffused through the dislocation network of the potassium permanganate.

Hill (7) also studied the influence of adding inert materials to compacts of iron/potassium permanganate by the temperature profile method and found that these inerts slow down the initial rate of the solid - gas - solid combustion reaction markedly. When comparing the initial reaction rate with independently measured rates of thermal decomposition of potassium permanganate it is concluded that in combustion, decomposition of permanganate is normally catalysed by contact with the iron and that this catalysis is explained in terms of a small amount of solid - solid reaction.

Previous work by Cackett (8) on the effects of certain variables showed that the rate of burning of compacted oxidizer/fuel mixtures is

(1) a function of composition
(2) dependent upon the pelletting pressure, the mass of material reacting per second being constant
(3) inversely proportional to the particle size, being roughly proportional to the area of contact
(4) increased by increase of thermal conductivity of the mass
(5) proportional to the initial temperature.

Spice and Stavely (9, 10) have reported work on the very slow reactions which proceed at temperatures just below the ignition temperature in barium perioxide/iron pellets, and also on the relationship between heat of evolution and rate of propagation. They concluded that

(1) the pre-ignition reactions involve the non-gaseous diffusion of the oxidizing agent as atoms or ions
(2) pre-ignition and burning reactions are probably different

(3) The maximum in rate of propagation usually occurs at a higher weight percentage of reducing agent than for the maximum heat of evolution per gramme, sometimes at the same one but never at a lower one. They attributed this to the inhibiting of the reaction by the film of product formed on the particles of the reducing agent

(4) in some systems the combustion reaction is essentially the same over the whole range of composition while in others there is a series of different reactions.

Rees (11) made a detailed study of the mechanism of the self-sustained reaction between powdered iron and potassium dichromate, as a simple system for the simulation of rocket propulsion reactions. Temperature changes as the reaction front passes a point were measured; propagation velocities derived from these records by means of the Mallard-Le Chatelier theory agreed fairly well with the directly-observed velocities. It was concluded that the thermal theory is a good representation of the behaviour of this particular composition. He also found that kinetics at low density differed greatly from those at high density and suggested that the difference may be explained on the hypothesis that reaction occurs at low density by means of the gas phase, and at high density, where contact is greater, by diffusion across solid - solid interfaces.

The reaction between selenium and barium peroxide was studied by Johnson (12) with the object of producing more closely timed delay fuses in order to be used more effectively and safely in mining, where successive detonation of charges is necessary. He found that the reaction between gray selenium and barium perioxide powders takes place

by three processes. The effect of the first, he claimed, can be measured after the powdered mixture is heated to temperatures as low as 50° C for as little as 32 hours, as a slight lowering of the heat output and activation energy and an increase in burning rate. He attributed this to be caused by an increased area of contact between the reactants brought about by the preheating. The second process appears to be a slow, exothermic product forming reaction between the materials, which is not self-sustaining. Its effects are a considerable decrease in the eventual heat output and burning rate, and an increase in the activation energy. The third is the ignition reaction which begins at 265°C, is extremely exothermic, and is self-propagating.

Thomson and Wild (13) described the burning rate dependence of a composition comprising titanium, strontium nitrate, boiled linseed oil and chlorinated rubber on the particle parameters of the titanium and strontium nitrate. They have concluded that the rate of burning of the composition

(1) decreases as the porosity of the titanium decreases and that of the strontium nitrate increases

(2) decreases as the particle size of the titanium increases.

They have also found that ball milling of titanium and hammer milling of strontium nitrate offer effective and easy means of altering widely the rate of burning of a given formulation containing Ti/Sr $(NO_3)_2$, and that porosity of the titanium and particle size of the strontium nitrate as measured by the Fisher sub-sieve sizer are major criteria.

McLain (14) studied heats of reactions and rate of burning of PbO_2/Si and B/$BaCrO_4$ systems. In accordance with the treatment by Spice and Stavely (10) he calculated the amount of heat given off by that weight of mixture that contains one mole of oxidizer (Q) and by plotting this against percent reductant, he found that Q increases as percent reductant increases up to a composition where the reducing agent uses up all the oxidising agent. This point corresponds to the stoichiometric composition. From these plots and calculation of Q for postulated reactions he determined the chemical nature of the products and what the reaction was on which stoichiometry should be based. He found that heat evolved per gramme reached a maximum at 10% silicon for PbO_2/Si reaction which corresponded to $PbO_2 + Si \rightarrow Pb + SiO_2$. He also found that Q does not conform to the Spice and Stavely Criterion or there may be more than one reaction operating over the burning range. However, he found that from 3 - 30% Si range, the Q plot showed that there is probably only one reaction but at a slightly higher value (approximately 15.0% Si).

In B/$BaCrO_4$ there is a good agreement between Q, ΔH and burning rate as they reached their maximum at approximately the same percent boron. The stoichiometric percentage composition for the system is about 15%, this value corresponds to a reaction

$$4B + BaCrO_4 \rightarrow 4BO + Ba + Cr$$

Another study of PbO_2/Si was made by Ripley (15) he found that the rate of burning of this composition varied from 2.97 gm/sec to 5.19 gm/sec by using PbO_2 from different suppliers due to variation of particle diameter, the apparent density, and the absolute density of the lead dioxide specimens, and the loaded density of the compositions.

Hardt and Holsinger (16,17) studied experimentally the reaction characteristics of several exothermic intermetallic reactions. The boron and carbon mixtures with titanium and zirconium, were found to be self propagating at room temperature but aluminide mixtures and other types of intermetallic reaction mixtures react only at elevated temperatures or must have additives which reduce their thermal conductivity before self-sustaining reactions can be initiated. The reaction mechanisms was studied using pyrometry and metallography. It was shown that the adiabatic reaction temperature must exceed the melting point of the alloy in order to ensure a self-propagating reaction, and that the ignition temperature may be below the melting point of either constituent. Linear reaction rates and thermal transport properties of the reaction mixtures are reported.

They suggested that these exothermic metallic reactions, which constitute a special type of gasless reaction may find application in pyrotechnic and ordnance devices owing to their comparative chemical inertness.

The use of compacted powders comprising an oxidiser, a fuel and some additives for pyrotechnic applications has been reported by many workers. Hale (18) found that Pb_3O_4/Si, together with graphite and nitrocellulose, can be used in the production of fuses for projectiles at high altitudes and so these compositions were developed to replace the older fuse compositions, based on gun-powder, which were erratic and unreliable under the conditions of low ambient pressure at high altitudes, since solid products rather than gases are produced upon combustion and so the term gas-less delay compositions was used to describe the new fuse materials.

(19)

Graff patented an invention which relates to a primer composition for use as a projectile or bomb fuse initiator particularly in connection with lead azide, but also utilized in initiating ignition of pyrotechnics. The composition comprising 45% lead dioxide, 20% calcium silicide and 25% zirconium and 15% sulphur.

Hans Goldschmidt (20) discovered that if calcium is admixed to silicon a smooth reaction takes place with ferric oxide. In igniting this mixture a molten iron and a slag of mainly calcium silicate are obtained, and this method was patented for producing the metal from the ore. The substances being thoroughly mixed with each other for best results.

Nash (21) invented a ventless cap with a fuse which, on burning, gave no substantial quantity of gas. For this delay fuse he suggested the use of red lead/sulphur/lead monoxide, in the weight ratio of 91/3/6. Selenium or tellurium may be substituted for sulphur. He explained that the red lead and sulphur composition will, on burning, produce a minimum of gas and at the same time will have the advantage of substantial resistance to moisture and a fixed burning rate.

Patterson (22) found that a mixture of zirconium and red lead in certain proportions when compressed in rigid tubes under a load of 10 tons per square inch, will give a delay fuse that burns at a rate of not more than 50×10^{-3} s/cm. The zirconium should be, for the fast burning delay tubes, of as fine particle size as practicable. These compositions, when ignited, propagate through themselves an exothermic reaction, with the formation of non-volatile products but not any considerable quantity of gaseous products, so as to be used in ventless assemblies whereby the access of moisture to them can most effectively be prevented.

Pearsall (23) investigated the use of a diluent to slow the burning velocity without the disadvantages obtained in the prior materials used, such as giving irregular and unpredictable burning velocity, which frequently rendered the explosive unsuitable for certain purposes including ordnance materials. He discovered that polyvinyl alcohol could be used in the proportion 5 - 55% with red lead/S/Fe Si 64/13/8 to give a slow burning composition.

McLain (24) invented a composition, to provide a first fire charge, which will be extremely easy to ignite from a primer or a power flash and yet not sensitive enough to frictional impact to cause undue hazard in mixing or pressing procedures. The delay charge mixture comprises essentially of dry litharge and powdered silicon in ratio 4 to 1 and inert materials, such as Fullers earth, to regulate the speed of burning. After burning, heavy slag is left which serves as a plug and to prevent backfiring.

A composition improvement to enable using it for a fuse in delay caps for firing commercial explosives was made by Piccard (25) The improvement was to prevent premature reaction of the ingredients in such compositions prior to burning, and she claimed that if either of the ingredients, or both, be coated with a protective coating, this will prevent reaction between the element and oxidising agent prior to burning. The coating material could be nitrostarch, shellac, a hard resin or nitro-cotton.

Thermal analysis techniques have been used to investigate the nature of the chemical changes that occur in powder mixtures of oxidants and fuels under controlled conditions. Howlett and May (26) investigated systems of boron-potassium dichromate and boron - silicon -

potassium dichromate by D.S.C.. They found that these systems are dependent on liquid phase transport for ignition, the reaction zone then propagates as a molten front and they suggested that this mechanism may account for the apparently anomalous effect of pressure on burning rate. Their D.S.C. studies showed that upon heating of 50/50 mixed oxidant/fuel composition, the D.S.C. curves show melting at the solidus of the oxidant accompanied by ignition and combustion of fuel. As the sample is further heated, excess potassium dichromate melts, providing a supply of molten oxidant for the burning fuel until the liquid phase is exhausted. In the boron - silicon - dichromate system, again ignition occurs immediately after fusion of oxidant, the boron burns in a matrix of molten oxidant, then at a later stage, the silicon reacts as a back-up reaction.

Sulacsik (27) studied the reactions of Fe Si 90-MnO_2 by M.O.M. derivatograph and found that

(1) there is a partial release of oxygen from MnO_2, this precedes the temperature where Fe - Si90 becomes reactive, thus a part of the oxygen leaves the system

(2) the decomposition reaction $MnO_2 \rightarrow Mn_2O_3$ is practically independent of component ratio

(3) Fe-Si90 becomes reactive at approximately 800^{o}C and the reaction is exothermic. The reaction is most violent in mixtures containing 72.8% MnO_2. The temperature and duration of the reaction are sufficient for the completion of all reactions, thus the release of oxygen and oxidation takes place simultaneously

$MnO_2 \rightarrow Mn_2O_3 \rightarrow Mn_3O_4$

$Fe \rightarrow Fe_2O_3$, $Si \rightarrow SiO_2$

Charsley et al (28) studied the reaction between boron and molybdenum trioxide using differential thermal analysis supplemented by X-ray diffraction and hot stage microscopy. The system was found to give a multistage exothermic reaction over the range 400°C to 900°C in which MoO_3 is initially reduced directly to MoO_2 while at higher temperatures reduction to MoO_2 takes place via the oxide Mo_4O_{11} according to the following

exotherm 1 & 2	$2\ B + 3MoO_3 \xrightarrow{partial} B_2O3 + 3\ MoO_2$
exotherm 3	$2\ B + 12\ MoO_3 \rightarrow B_2O_3 + 3\ MO_4O_{11}$
exotherm 4	$2\ B + Mo_4O_{11} \rightarrow B_2O_3 + 4\ MoO_2$
exotherm 5	$4\ B + 3MoO_2 \rightarrow 2B_2O_3 + 3Mo$

They however concluded that the ignition reactions differ from those under controlled conditions in that in the presence of excess boron, molybdenum oxides are formed, thus increasing the overall exothermicity of the reaction. Their D.T.A. studies of MoO_3-B mixtures have shown that a single stage exothermic reaction takes place over the range 900°C to 1100°C. It is possible that boride formation is being observed as the glowing reaction following ignition seen on the hot stage.

Miller (29) examined the effect of incorporating the boron particles into a crystalline matrix of the barium chromate during precipitation of the latter to see how it differs from the mechanical mixing of the two constituents. He found that the rate of burning of co-precipitated barium chromate/boron, was virtually unaffected by reduction of pressure to about 0.07 atmosphere, while that of mechanical mixing fell by some 15%, suggesting that air, played a part in the combustion of the latter but not the former. Ignition temperature

studies by DTA were found to differ little whether the samples were under argon or air, but those of the co-precipitated samples were some 70 to 80 degrees lower at the same rate of heating than those of the conventional samples. This he explained in terms of the surface to surface contact of the former. All the mechanical samples show indications of a pre-ignition reaction, which is virtually absent with the co-precipitated samples of lower boron content, but appears where the boron content is higher. Some of the boron is possibly external to the crystals of barium chromate or close to a disorganised surface structure.

Beardell and Kirshenbaum (30) investigated the kinetics of the solid state reaction between circonium powder and MoO_3 by isothermal and DTA methods. The reaction they found is a two stage process in which MoO_3 is first reduced to MoO_2 and then to Mo.

$$Zr + 2MoO_3 \rightarrow ZrO_2 + 2MoO_2$$

$$Zr + MoO_2 \rightarrow ZrO_2 + Mo$$

The isothermal kinetic study, performed between 440°C and 475°C revealed that the first stage reaction is diffusion controlled at the lower temperature but changes to a kinetically controlled mechanism at the higher temperature. The reaction rate was found to obey the Tamman equation from which the rate constants at the various temperatures were obtained which produced an activation energy of 40 k.cal/mol. A similar value was obtained by calculation of activation energy from binding energy considerations.

A kinetic analysis of the DTA curve, in which thermal activity is first observed above 475°C, revealed that the data follow the

Freeman-Carroll equation from which an activation energy of about 65 k Cal/mole was calculated for both the first and second stage processes, and that in the temperature range above 500°C, the reaction is kinetically controlled.

An argument, based on the thermal theory of ignition of condensed systems, is presented which tends to confirm the value of activation energy. Analysis of the DTA curve in terms of a diffusion controlled mechanism failed to produce a good correlation.

During their search for a gasless delay mixture for a composition burning at about 5 mm/sec, Boddington and Laye (31-33) found that tungsten/potassium dichromate was a particularly smooth burning composition when ingredients were mixed in equal proportions by weight. In their study they applied a multidisciplinary approach involving the application of calorimetry, thermal analysis and the measurement of temperature profiles in reacting system. They reported that an exothermic peak is noticed at 380°C which is below the fusion onset of the dichromate (398°C). This reaction corresponds to

$$W + 2K_2Cr_2O_7 \rightarrow 2\ K_2CrO_4 + WO_3 + Cr_2O_3$$

which is stoichiometric at 23.8% tungsten. The experimental value of the peak exothermicity is at a higher per cent tungsten due to incomplete reaction of the tungsten due to build up of reaction products on the surface. However, for very fine tungsten (0.5μ) the peak is at 28% which they concluded was in good agreement with the theoretical value. A second exotherm occurs at 703°C, a smaller exotherm at 830°C and a sharp endotherm at 920°C.

Exotherm 2 they found was due to

$$W + 2K_2CrO_4 + WO_3 \rightarrow 2K_2WO_4 + Cr_2O_3$$

The last peak was found by DTA and corresponds to the fusion of potassium tungstate at 925°C.

From the study of the temperature profile, Boddington et al (33) have shown that endotherms can be detected on the profile as regions of increased slope at 400°C and corresponds to the fusion of the dichromate. Another less defined endotherm at 924°C, due to fusion of potassium tungstate, and the third at above 1300°C due to volatalisation of tungsten trioxide.

Scanes and Martin (34,35) measured heats of reactions of a number of mixtures containing potassium chlorate and lactose by bomb calorimetry. From these values of heats of reactions they have established the chemical nature of the reactions taking place. They also carried DTA and TG studies of these mixtures which are used in vapourizing pyrotechnic compositions. They found that there are two principal exothermic reactions in the absence of air. The first, coinciding with the fusion of lactose at approximately 200°C, is the oxidation of lactose by the chlorate and may be represented by the stoichiometric reaction.

$$8\ K\ ClO_3 + C_{12}H_{22}O_{11} \quad H_2O \rightarrow \quad 8\ K\ Cl + 12\ CO_2 + 12\ H_2O$$

It is postulated that this reaction is initiated by the partial solution of the potassium chlorate in the lactose and terminates when there is no liquid lactose left in the mixture. This is followed immediately by the dehydration of lactose, represented by the equation

$$C_{12}H_{22}O_{11}. \quad H_2O \rightarrow \quad 12C + 12\ H_2O$$

This reaction terminates when approximately half the maximum possible

amount of water is evolved. The second exothermic reaction occurs at about 340°C and is probably initiated by the fustion of potassium chlorate. This reaction is the oxidation of carbonaceous organic residues by the remaining potassium chlorate.

The effects of diluents on the rate of burning of solid mixtures, have been investigated by several research workers. Yoshinaga et al (36) studied the effect of adding Sb_2S_3 to a mixture of Pb_3O_4 and ferrosilicon, the following conclusions were drawn from their work:

(1) The changes that take place to the Sb_2S_3 on heating, are the oxidation at 300°C to form Sb_2O_3 and So_2 gas.
The unoxidised Sb_2S_3 was melted at around 500°C

(2) The higher the purity of the Sb_2S_3 and the greater the amount added, the greater the inhibition of the combustion reaction. The cause of this inhibition of the combustion was attributed to the lowering of the temperature of the system due to absorption of heat or melting of Sb_2S_3, and to the fact that contact between Pb_3O_4/Si was obstructed by the melted Sb_2S_3.

(3) There is a reaction between SO_2 generated by oxidation of Sb_2S_3 and Pb_3O_4 , and therefore the Pb_3O_4/Si reaction was inhibited by the decrease in amount of Pb_3O_4 which reacted with silicon.

Dadley (37) investigated the effect of diluents on the titanium/lead chromate system, he used Cr_2O_3, TiO_2 and Pb as diluents and measured the effect of the inert materials on the burning rate by

(a) alteration of oxidant/inert ratio at constant fuel percentage

(b) alteration of percentage of inert at constant fuel/oxidant ratio.

He also measured calorimetrically the heat evolved from the reaction. He arrived at the following conclusions:

(i) from heat measurement, the reaction seems to indicate oxidation of titanium to the monoxide, TiO,

(ii) a theory advanced that for a self-propagation to be possible, the reaction must be sufficiently exothermic for the reaction zone to reach the temperature at which titanium oxide melts.

(iii) the burning rates of the titanium/lead chromate mixtures have been shown to be, to a limited extent, linearly dependent on the amount of inert material added. The proportionality constant is itself dependent on the fuel/oxidant ratio and increases as the ratio increases.

(iv) the replacement of any excess oxidant by inert material has virtually no effect on the rate of burning. This suggests that the rate determining step is not the thermal decomposition of the oxidant and must, therefore, be the oxidation of the metal. This is consistent with the fact that titanium oxide has to melt before propagation occurs.

Kirshenbaum, Campbell and Beardell (38) studied a delay train consisting of Zr/MoO_3 by DTA. They have given some account of

the effect of vinyl alcohol acetate resin binder (1%) and of the addition of Cr_2O_3 (16%). They found in a mixture with excess Zr 70/30. DTA showed two exotherms which appeared as a shoulder and a peak at 550 and 650°C, and by X-ray diffraction analysis of the products of the complete reaction and of those at each stage. They have concluded that the first exotherm is due to the following

$$Zr + 2MoO_3 \rightarrow Zr\ O_2 + 2MoO_2$$

and the second exotherm is due to

$$Zr + MoO_2 \rightarrow ZrO_2 + Mo$$

The effect of adding Cr_2O_3 is to influence the Zr - MoO_3 second stage reaction exotherm as some lowering of the energy output is noticed from the exotherm peak size. This is taken to indicate that the heat output of the second stage process controls the propagating reaction, since the overall effect of Cr_2O_3 is to lower the burning rate.

The authors noticed that the addition of resin promotes the ignition of the fuel/oxidant system, and suggested that from the pyrolysis of the resin the carbon formed gives an exothermic reaction at 490°C which is the same temperature as that at which Zr/MoO_3 reaction begins. They have suggested that the reaction is as follows

$$2\ MoO_3 + C \rightarrow 2MoO_2 + CO_2$$

The heat released from this reaction will be enough to produce ignition

CHAPTER THREE

SCOPE OF THE PRESENT INVESTIGATION

When pyrotechnic compositions are to be studied, it is essential to re-create the actual operating conditions under which these mixtures are normally prepared and used, if accurate findings are to be ensured. It also predisposes definite conclusions as to the means and conditions for making the delay compositions such as the ratio of oxidant/fuel, the compacting pressure, the particle size, the ambient temperature and pressure, the humidity of the ambient atmosphere, the length of the delay tube and the materials of construction.

The method of mixing the components is essential. Since the densities of the oxidant and the reductant are so different, segregation may occur, hence a binder is used which will hold the particles in good contact, and prevent segregation. The reproducibility of delay time is essential, therefore the methods of filling and compacting the compositions must be identical, necessitating an automatically operating press.

The reaction mechanism is studied by

(1) measurement of heats of reaction, and the values obtained for the differing ratios are utilized to select the probable reaction

(2) X-ray and infra red analysis to establish the reaction products

(3) Thermalanalysis studies to determine the temperature range of the different stages of the reaction, and the products at each stage.

As the reaction is determined, the adiabatic reaction temperature can be calculated from standard values, and these values are to be compared with directly measured values, by means of an U.V. recorder.

Formulation of a mathematical model for determining the rate of propagation of flame in the compacted mixture will be attempted as a supplementary proof of the solid reaction mechanism.

Relationships between rate of burning with (a) particle size, (b) ambient temperature, and (c) diluents will enhance the study of these reactions.

Solid reactions are difficult to investigate, and in the red lead/silicon and lead dioxide/silicon, the task is complicated further by the speed and exothermicity of the reactions which are in some composition ratios quite violent. The controlled conditions under which thermal analysis techniques are normally carried out, make these techniques extremely suitable for reaction analysis. In addition, only very small samples are needed to establish

(1) Individual constituents behaviour during heating

(2) stages of reaction at the temperature range studied

(3) temperature range for each reaction and the temperature at which rate of heat or weight change is maximum.

(4) the nature of the reaction

(5) the heat of reaction

(6) the weight loss or gain during a reaction and at what temperature it occurs.

(7) the influence of rate of heating on these reactions

(8) the reaction kinetics

CHAPTER FOUR

EXPERIMENTAL STUDY

4.1 SAFETY PRECAUTIONS

Appropriate precautions are necessary when dealing with pyrotechnic compositions since they are usually sensitive to impact, friction and static electricity, and also due to the toxic nature of the dusts. Sparkfree tools and equipment are used throughout, e.g. brass sieves and camel hair brushes for mixing ingredients. The sieves are earthed and placed behind armoured safety screens, with suction fans operating to extract any dust from sieving.

Safety clothing, including gloves, fireproof overall, electrically conducting shoes, protective glasses, respirator and gloves are used.

The pelletting and preparation for the firing is done in a portakabin located outside the main laboratory, with all electric points located externally. Specially designed doors for escape in case of fire, and a fire extinguisher was available.

4.2 DETERMINATION OF SURFACE AREA OF FINE POWDERS

The method is based on the low-temperature nitrogen adsorption according to Brunauer, Emmet and Teller (BET method). The equipment consists of

1. Heating block
2. Measuring apparatus

Heating Block:

In order to remove all foreign molecules which are already adsorbed on the sample at room temperature, the sample in the measuring flask is purged with dry measuring gas in the heating block at temperature between about 50 and 350°C.

It consists of a metal block with infra red heating and is insulated against the outside by a casing consisting of several shells. It is equipped to take eight adsorption vessels. When the samples are purged with the test gas (nitrogen) at 150°C for three hours, they are then cooled to room temperature without interrupting the purge gas flow; they are then closed with a stopper and stored as long as required.

The diagram (4.2.1) shows the heating block with the main compounds marked as follows:

a = measuring gas inlet with regulating valve

b = drying tube

c = flow meter

d = connector

e = arresting screw

g = connecting tube

h = purging capillaries

i = thermostate

FIG. 4.2.1

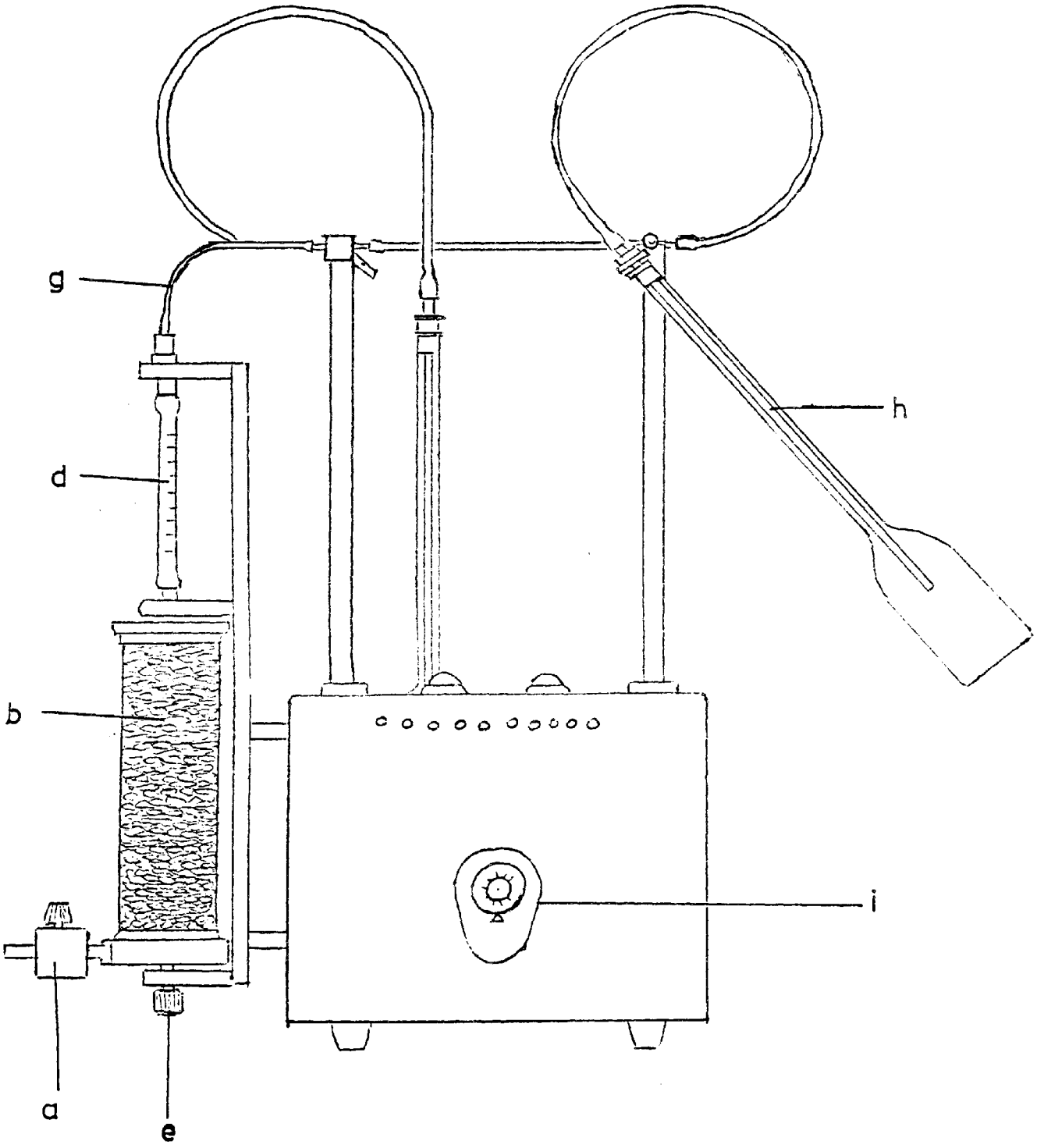

HEATING BLOCK

Measuring Apparatus:

The main parts are shown on diagram (4.2.2-3). A weighed sample is introduced into the adsorption vessel, the amount is chosen so that the differential pressure on the manometer was between 100 and 300 mm for accurate results. The vessel with sample are heated as described above with nitrogen flow adjusted to give a flow rate of 45 litres per hour.

After the samples have cooled to room temperature, the apparatus was purged thoroughly with nitrogen by opening the five valves and nitrogen was introduced at a flow rate 10 litres per hour, this is done in order to remove all the air from the various parts, especially the drying tube. During this purging operation the two adsorption vessels (the sample and the reference vessels) are placed in positions and into a bath of water at room temperature in order to balance the temperatures. Purging is continued for thirty minutes to ensure equilibrium and the valves are closed and the apparatus is now sealed against atmosphere. The two vessels are separated from each other and connected to one manometer limb each.

The water bath is removed and the vessels are then immersed in liquid nitrogen for five minutes and the difference in pressure due to nitrogen adsorbed on sample is noted by the manometer level difference when valve 5 was opened.

Numerical evaluation of specific surface area Sg

$$Sg = \frac{A\,\Delta h}{m} + \frac{B}{\rho p}$$

FIG. 4.2.2

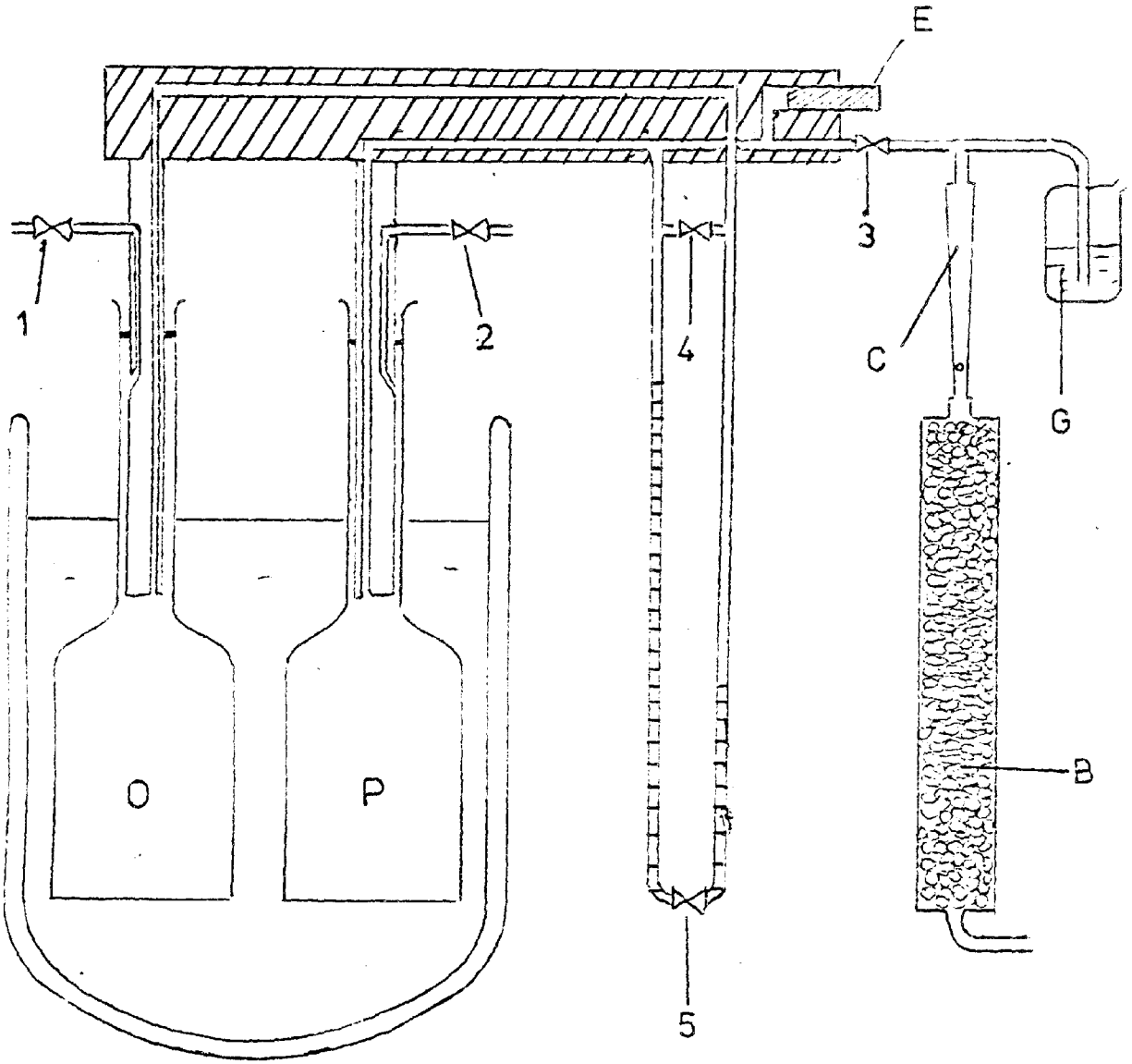

ADSORPTION APPARATUS

FIG. 4.2.3

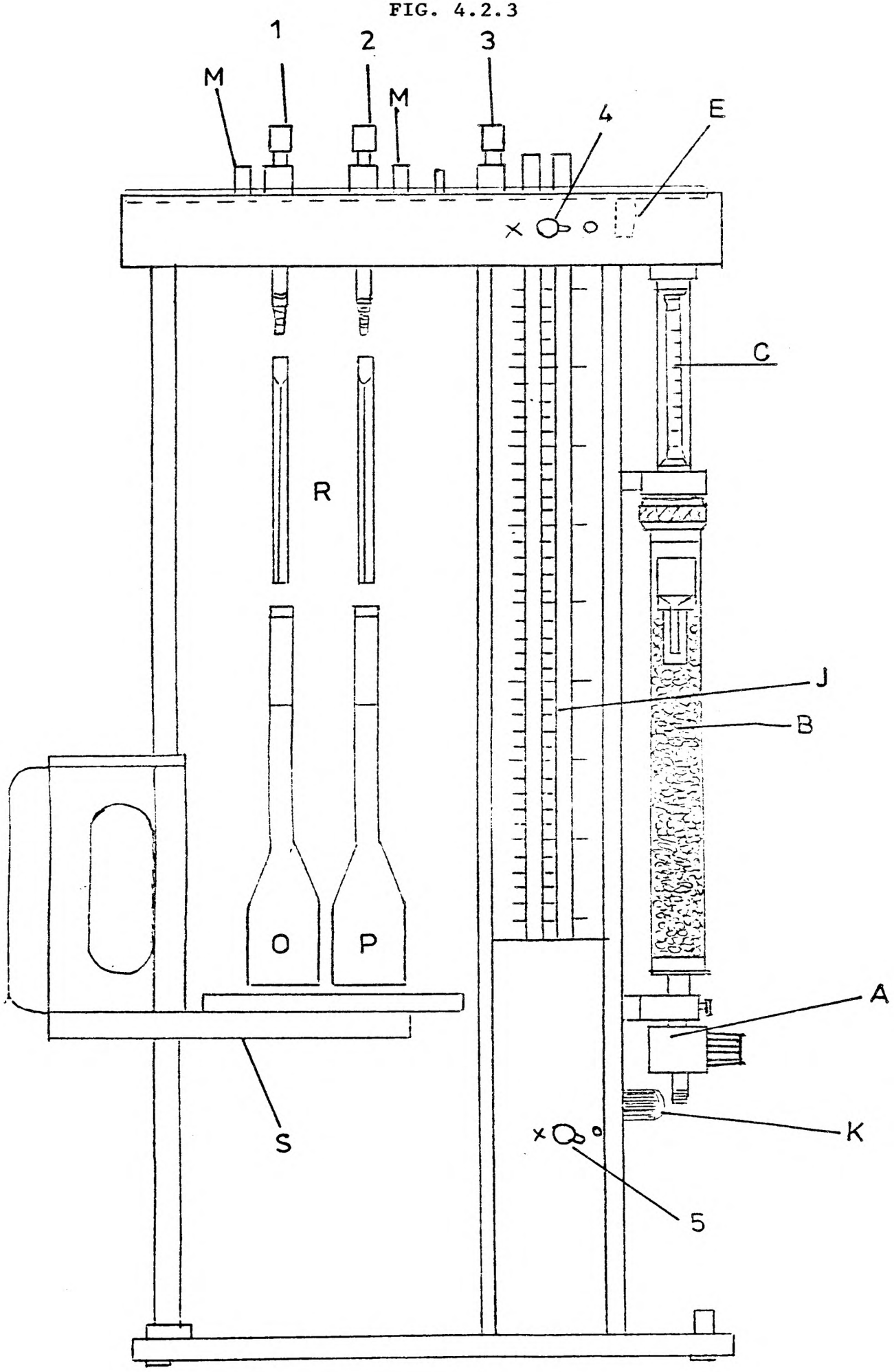

AREA METER

where A = apparatus coefficient

B = " "

m = sample weight (gm)

Sg = specific surface area m^2/gm.

Δh = pressure different on manometer (m.m)

ρ_p = specific weight of sample

Both A and B are obtained from nomogram

The main components of the measuring apparatus are marked as follows:

A = measuring gas inlet with regulating value

B = drying tube

C = flow meter

E = adjustment screw for volume balancing

G = overpressure vessel

J = adjustable scale

K = adjustment knob for scale

M = measuring gas outlet

O = empty adsorption vessel as reference

P = adsorption vessel with sample

R = displacement capillaries

S = adjustable table for baths

1 = outlet valve (reference vessel)

2 = outlet valve (adsorption vessel)

3 = inlet valve

4 = manometer valve

5 = stop valve

4.3 PARTICLE SIZE MEASUREMENT

Coulter counter model TA was used to measure particle size by suspending them in an electrolyte, then passed through an orifice with a specific path of current flow for a given sample volume.

As each particle passes through the aperture and displaces its own volume of electrolyte, the resistance in the path of current changes. The quantity of this change is directly proportional to the volumetric size of the particle.

The number of changes per unit time is directly proportional to the number of particles per unit volume of the sample suspension.

Each current pulse, which is representative of each particle count, is detected, amplified and fed to a threshold circuit by an amplifier and a pulse stretcher card, and two threshold circuit cards. These sized particle pulses are then sent to their respective integrators where they are converted to voltage representative of the volume of particles; these integrator voltages are then fed to the multiplexer card for differential date and cumulative date. The output of the multiplexer card is fed to the AGC card which adjusts these signals for X - Y recorder presentation relative to 100% for total sample.

4.4 MATERIALS

In making the delay compositions, silicon, minium, lead dioxide, binder and various chemicals as diluents were used.

1. Silicon Si:

The silicon is normally produced on an industrial scale by heating quartz silica with coke or carbide in an electric furnace.

$$SiO_2 + 2\,C = Si + 2\,CO$$

The silicon was then powdered by a grinding process and classified by a multiplex zigzag classifier to give the required size range.

The silicon used was not less than 98.0% pure with less than 1.0% metallic iron.

2. Minium Pb_3O_4

This was supplied in the form of dry soft powder, free from organic colouring matter. It was no less than 99.0% pure and according to fluorescent X-ray diffraction, the material did not contain any other metals. Loss in weight on heating the material at 100°C over four hours did not exceed 0.2%.

3. Lead dioxide:

The powder used was at least 98.0% pure. Its particle size distribution can be seen from the Coulter counter diagram.

Tables 4.1&4.2 show the values of average particle size, particle size distribution and specific surface area for Si, Pb_3O_4 PbO_2 and graphite, plus values of specific surface area for CaF_2 Fe and Pb. For the last three chemicals, it was not possible to obtain

values by the use of the Coulter counter, due to the large particle sizes of these materials.

4. Binder:

This is a sodium carboxymethyl cellulose, an anionic water-soluble polymer prepared from purified cellulose. The molecular structure of cellulose is represented by the general formula

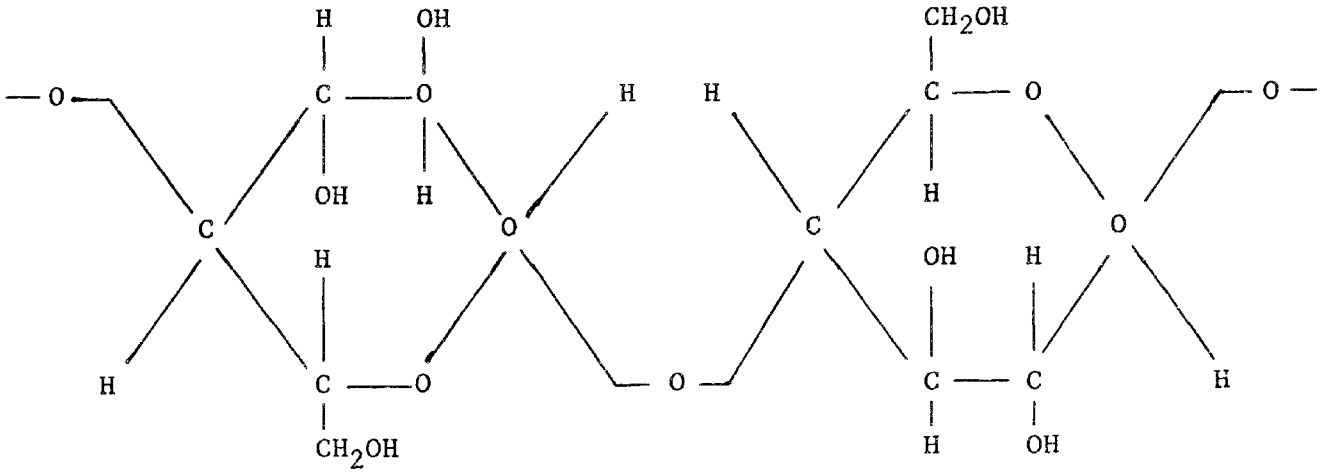

The material came in the form of granules, for ease of dissolving in cold water. It contains not less than 98% of active ingredient. The degree of substitution is between 0.7 and 0.8 (Carboxymethyl substituents per anhydroglucose unit).

TABLE 4.1 Average Particle size, particle size distribution and specific surface area for various chemicals.

Pb_3O_4 Av.particle size = 5.0 μm (m^2/g)		PbO_2 Av.particle size = 3.2 μm (m^2/g)		Graphite Av.particle size = 11.0 μm (m^2/g)		Material	Specific surface area.
particle size μm	%	particle size μm	%	particle size μm	%		m^2/g
1.2- 2	6.0	1.9- 1.5	15.0	0.9- 1.9	4.5	CaF_2	15.278
2.0-3.2	20.0	1.5- 2.5	22.5	1.9- 4.1	13.0		
3.2-4.0	14.5	2.5- 4.2	27.0	4.1- 7.0	15.0	Fe	0.241
4.0-5.0	15.5	4.2- 5.4	12.5	7.0 11.5	29.0	Pb	0.057
5.0-6.4	14.0	5.4- 7.0	4.5	11.5-15.0	13.5		
6.4-8.0	10.0	7.0-12.0	5.5	15.0-19.0	15.0		
8.0-10.0	6.0	12.0-20.0	7.0	19.0-24.0	9.0		
10.0-20.0	9.0	20.0-30.0	6.0	24.0-30.0	1.0		
20.0-30.0	5.0	-					

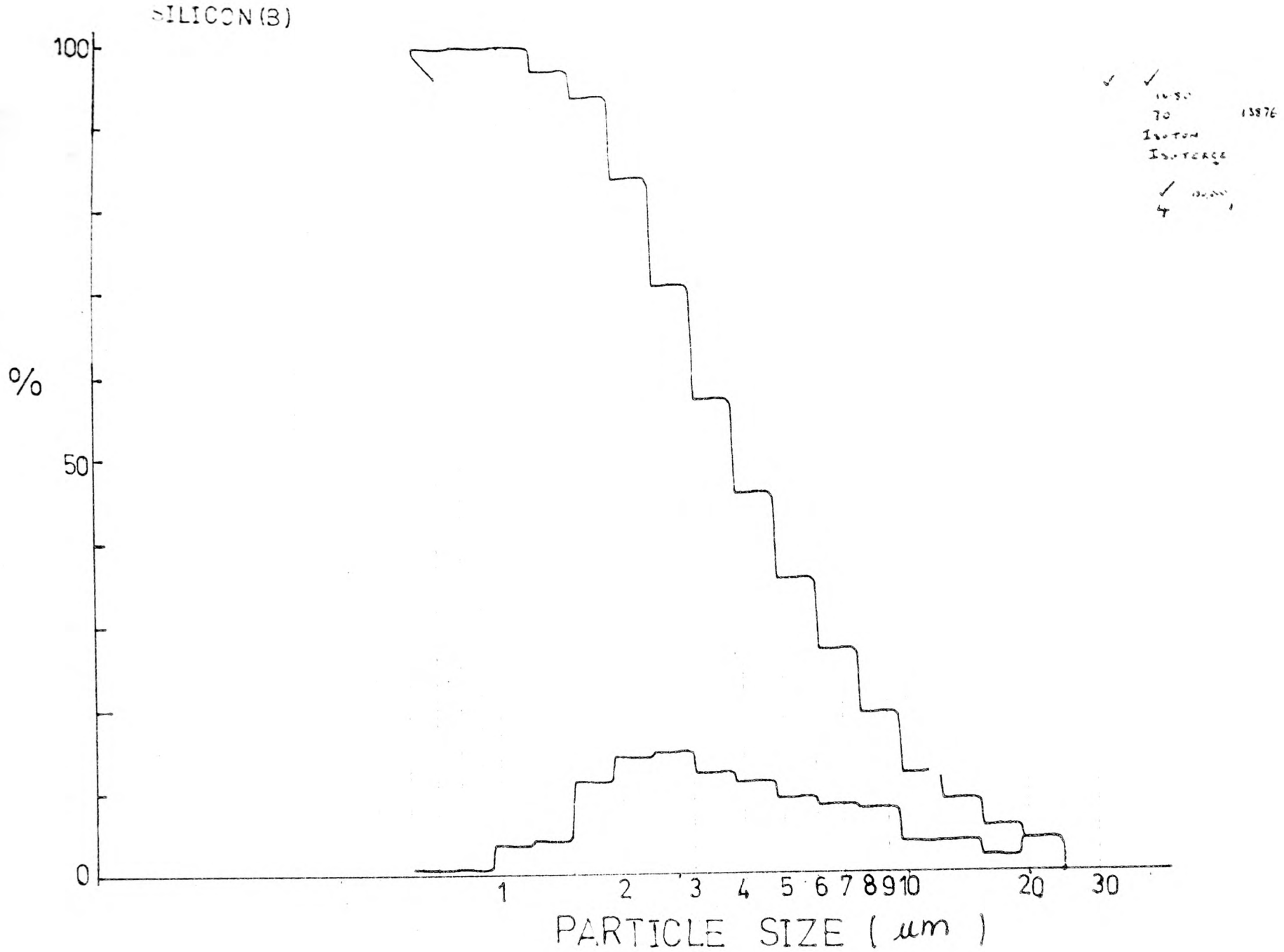

FIG. 4.4.1

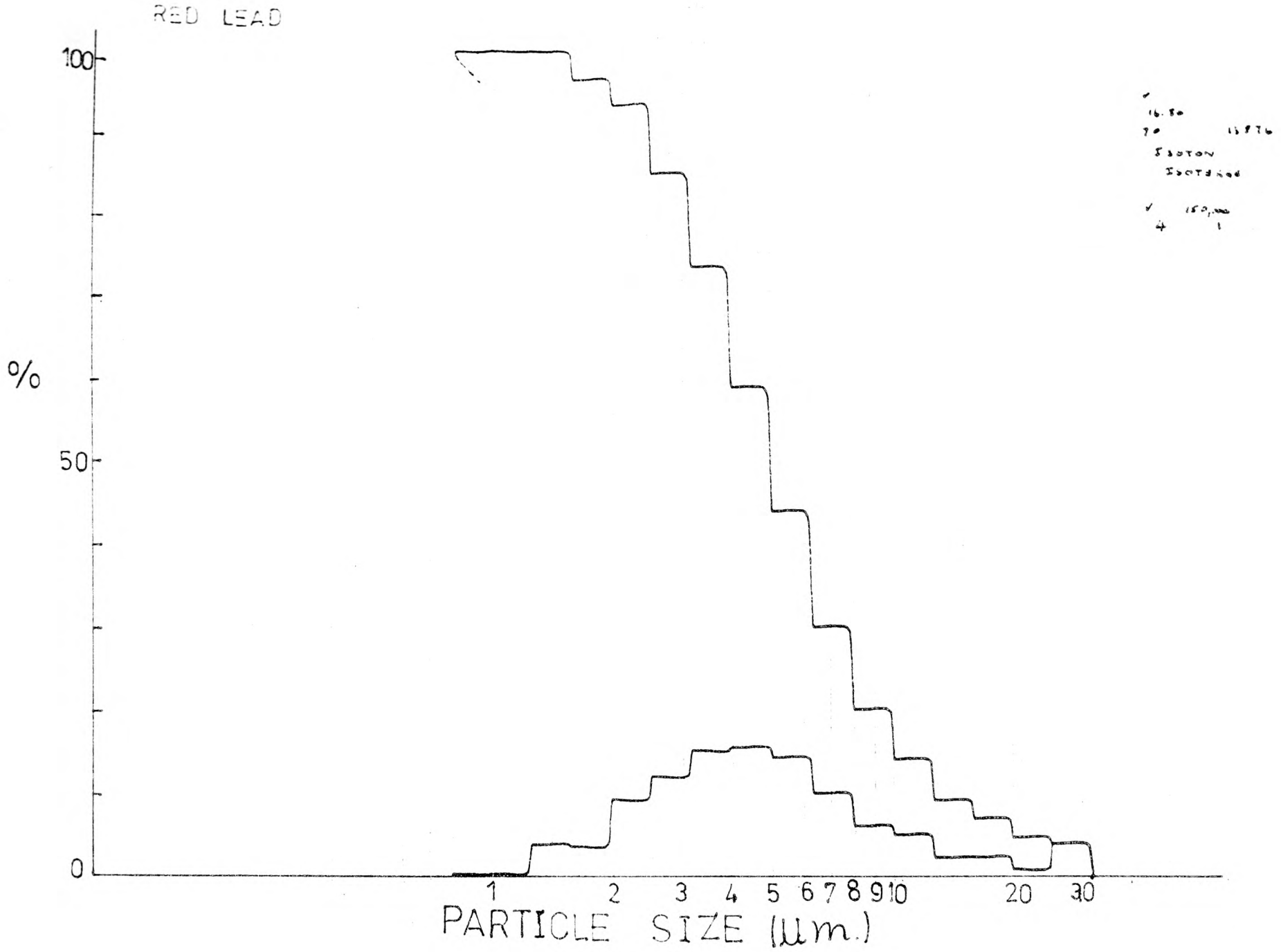

FIG. 4.4.2

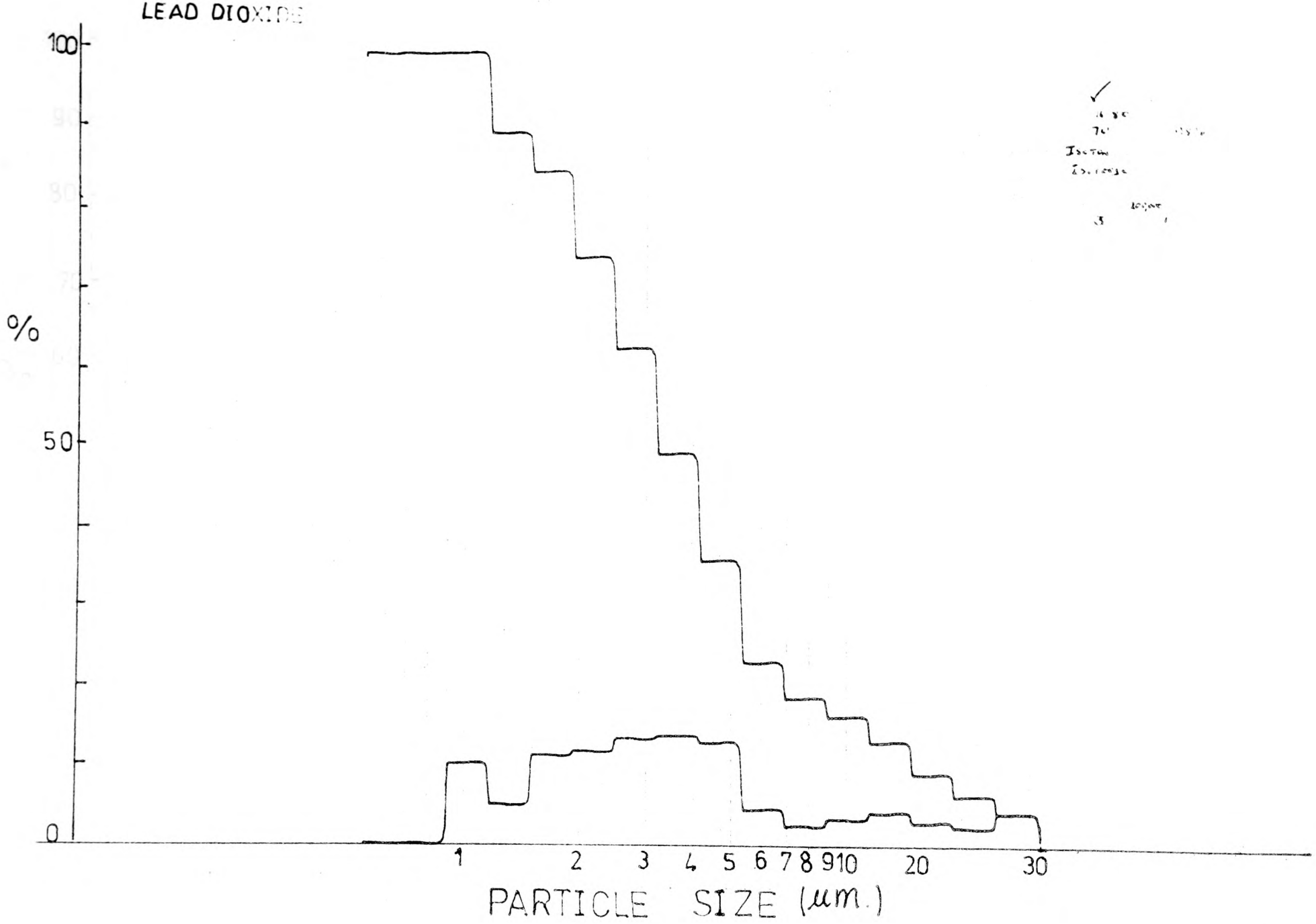

FIG. 4.4.3

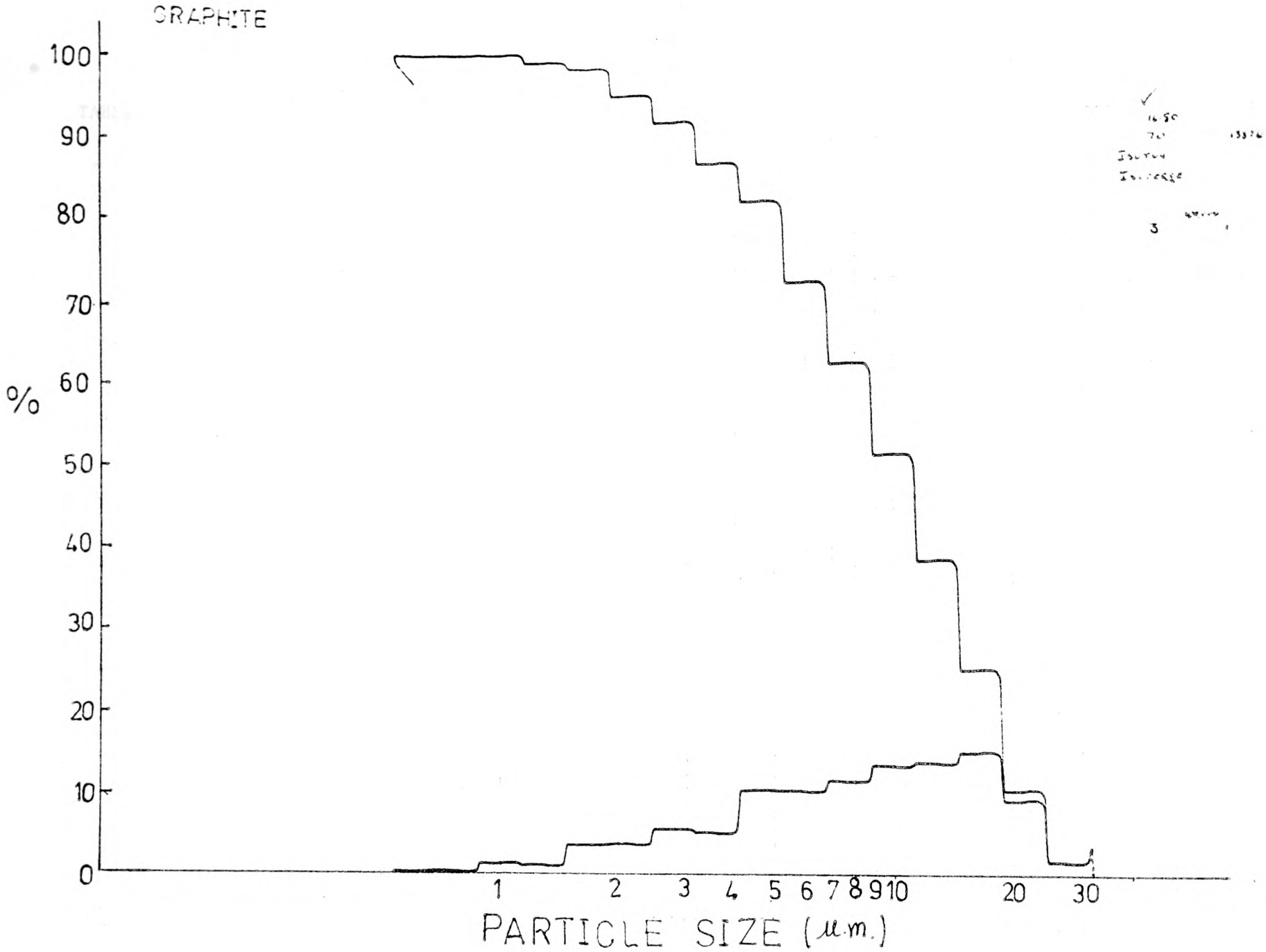
GRAPHITE
100
90
80
70
60
50
40
30
20
10
0
%
1
2
3
4
5
6
7
8
9
10
20
30
PARTICLE SIZE (μm.)

FIG. 4.4.4

TABLE 4.2 Average particle size, particle size distribution and specific surface area for various silicon powders

Silicon A Av. particle size = 1.9 μm specific surface area = 6.258 (m^2/g)		Silicon B Av. particle size = 3.9 μm specific surface area = 2.543 m^2/g)		Silicon C Av. particle size = 5.0 μm specific surface area = 1.448 (m^2/g)	
particle size μm	%	particle size μm	%	particle size μm	%
0 - 1.5	30.5	0 - 1.5	6.0	1.2 - 2.0	8.0
1.5 - 2.0	43.5	1.5 - 2.0	10.0	2.0 - 2.5	7.0
2.0 - 2.5	13.0	2.0 - 2.5	13.0	2.5 - 4.0	21.0
2.5 - 3.0	2.0	2.5 - 3.0	15.0	4.0 - 5.0	15.0
3.0 - 5.0	1.0	3.0 - 4.0	11.0	5.0 - 6.0	20.0
> 5	10.0	4.0 - 5.0	10.0	6.0 - 8.0	17.0
		5.0 - 6.0	8.0	8.0 -10.0	10.0
		6.0 - 8.0	8.0	>10	2.0
		8.0 -10.0	7.0		
		10.0 -12.0	3.0		
		12.0 -15.0	3.0		
		15.0 -20.0	2.0		
		>20	4.0		

4.5 PREPARATION OF THE DELAY COMPOSITIONS

The oxidant/fuel mixturesto be used in the delay elements were prepared by weighing accurately the required amounts of oxidant and the silicon. They were then transferred to a plastic beaker, and carefully mixed before binder solution was added. The contents were then stirred manually at first until slurried, then thoroughly mixed by a hydraulic stirrer to ensure thorough mixing of the constituents and also to break down any agglomeration of either component.

The uniform slurry obtained was poured into a shallow pyrex dish and left on a water heated plate, thermostatically controlled at 80°C, until the slurry was almost dry, forming a "cake." This cake was broken, then passed through a sieve BS 410, mesh No.18 of aperture 850 μm,and the granules were then left to dry for a further 24 hours at 80°C to complete the drying. These dried granules were then passed again through the same sieve into another sieve, BS 410, mesh No.52, of aperture 300 μm, so that any particles smaller than 300 μm were discarded, since it was possible that these finer granules contain a large percentage of "unbound" constituents.

The samples obtained of size 300 - 850 μm were kept at a steady ambient temperature of 20°C and relative humidity of 30% for 24 hours before being loaded into the delay tubes so that the delay compositions could be studied under the same conditions.

The binder, sodium carboxymethyl cellulose, was prepared by adding a weighed amount into cold water to give a 1.2% solution. The dissolving of the binder was accomplished by vigorous stirring by means of a hydraulic stirrer. The volume of the solution added was calculated so that the binder weight was 0.5% of the powders used.

4.6 LOADING AND PRESSING OF COMPOSITIONS

The granules comprising oxidant, fuel and binder were introduced into the diecast delay tubes one increment at a time. The height of each increment, after pressing, was approximately the same as the internal diameter of the tube. The loading and pressing was automatically performed to fill the whole tube. The column of mixture obtained thus was evenly compacted.

The equipment used was set up specially for this research, and all the operations of loading and compressing were hydraulically controlled. By use of a timer, the duration of the compression on the composition could be predetermined, and by regulating a valve the loading cylinder would regulate the movement of a slide which controlled the amount of chemicals that went into the tube.

Various valves were used to control the air into the pressing and loading cylinders, so that as the slide moved to feed a portion of the sample into the delay tube, it stayed in position for the plunger of the press to act on the powders via the punch at a controllable pressing load. As the plunger retracted, the slide would also retract to bring back more sample. The sequence of pressing and loading continued until the tube was filled.

The mains air pressure	=	700 k N/m^2
Pressing cylinder internal diameter	=	15 cm.
Loading cylinder internal diameter	=	2.5 cm.
Punch diameter	=	0.33 cm.
Dwell time of piston on sample	=	2 S

The air pressure into the pressing cylinder can be regulated from 70 - 350 k N/m^2

4.7 ASSEMBLING OF DELAY UNIT

The detonator tube was made of aluminum. This tube was punctured at the base and a perspex disc was inserted to plug it. The perspex disc replaced the base charge normally used in actual detonators. The delay element was then pushed in to be held firmly against the perspex disc. The fuse head was crimped at the top of the tube, leaving a free space approximately 3 cm between the top of the delay element and the neoprene plug, as illustrated in diagram 4.7.1

The assembly was now ready for firing, to measure the delay time to burn a certain length of compacted oxidant/fuel mixture. The perspex disc served the purpose of transmitting the light emitted from the end of the delay composition, and also prevented the ejection of any particles prior to burning.

4.8 DELAY TIME MEASUREMENT

A Racal Universal Counter timer, Model No. 9901 was used for measurement of the time. It was linked to a firing circuit, so that it could be started when the firing switch was depressed, and stopped by the signal picked from the photoelectric cell as it received the light which was emitted from the end of the delay composition through the perspex plug, as illusted in figure 4.8.1

Various lengths of a variety of compacted mixtures under different pressing loads were timed.

FIG. 4.7.1

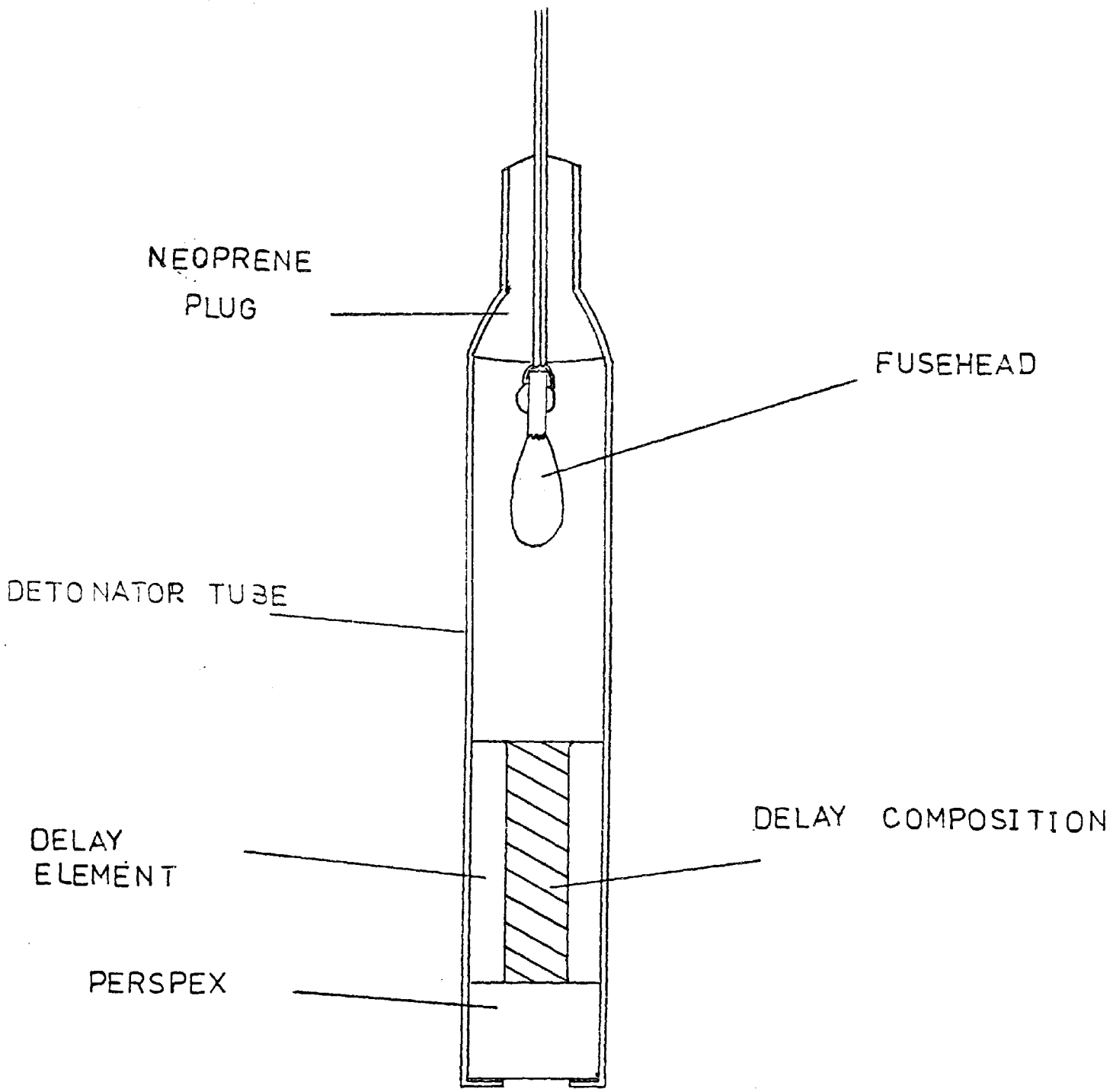

DELAY ASSEMBLY

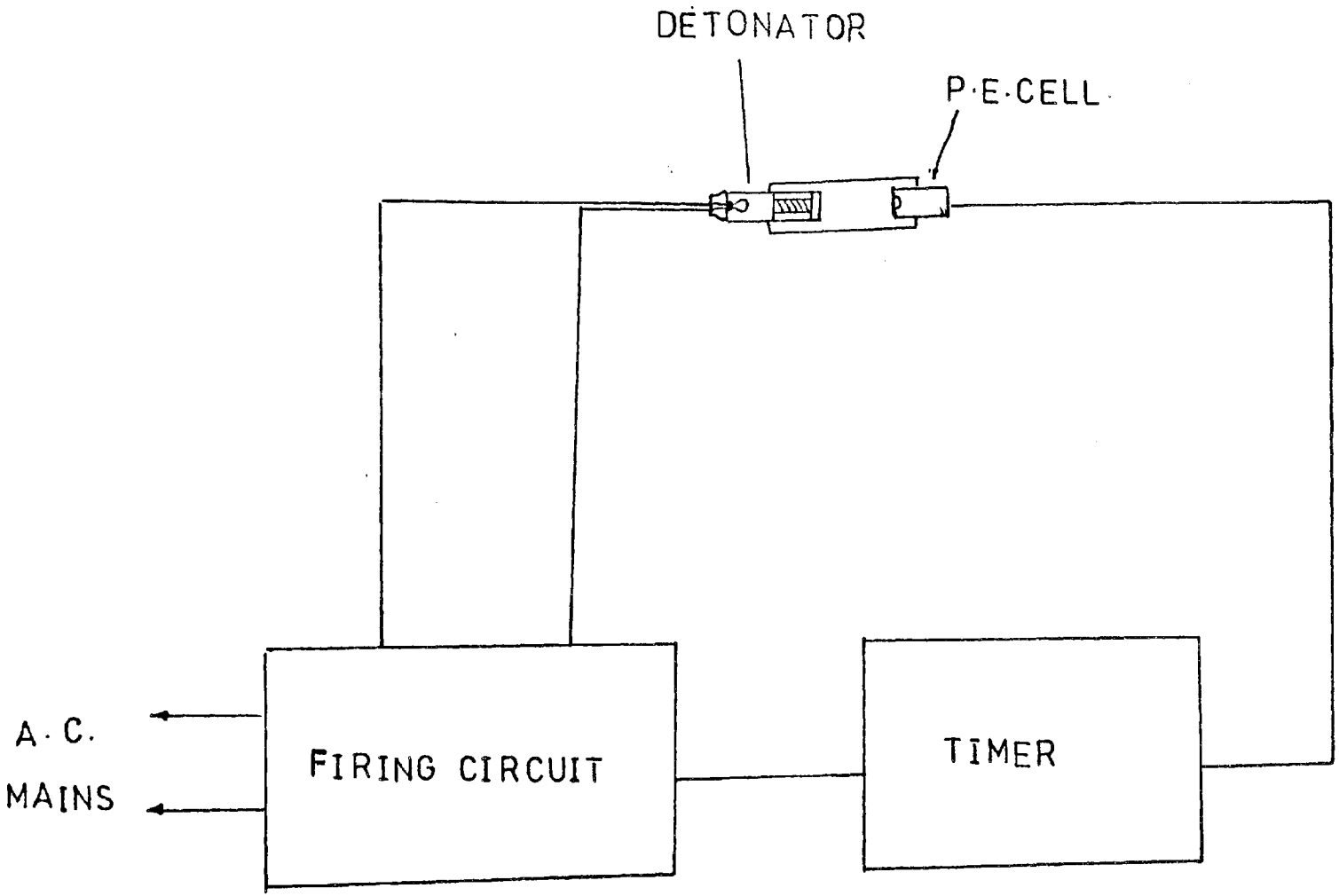

DELAY TIME MEASURING ASSEMBLY

FIG. 4 .8.1

4.9 HEAT OF REACTION MEASUREMENT

A Gallenkamp autobomb automatic adiabatic calorimeter, model CB-100 was used for the measurement of heat of reaction of red lead/silicon and lead dioxide/silicon compositions.

Ten aluminum tubes with the delay elements and fuseheads inside were placed inside the bomb then connected to the firing circuit. The air in the bomb was evacuated by a vacuum pump, then filled with nitrogen to atmospheric pressure, to eliminate reaction with oxygen of air.

Five Amperes current was then passed through the firing plug, this ignited the fuseheads which in turn, ignited the delay mixtures. The temperature rise of the water surrounding the bomb was recorded by a Beckmann thermometer which read with an accuracy of $0.001^{o}C$.

Heat losses to the surrounding were eliminated by having an outside jacket that was filled with water and kept at the same temperature as that of the calorimeter throughout the test, by a combination of very sensitive thermistors, (one immersed in the calorimeter and the other in the water of outside jacket), phase sensitive detector and instantaneous response of the electrode heaters that were fitted in the jacket.

The heat released from the fuseheads alone was determined by a separate experiment at identical conditions.

The water equivalent of the bomb itself was determined by burning a known weight of a combustible material (Benzoic acid) of a known calorific value and the temperature rise of the water was read

If ΔH is the total heat released

then ΔH = (weight of water in calorimeter + Bomb water equivalent) X (temperature rise)

4.10 MAXIMUM TEMPERATURE OF REACTION

An arrangement was used for measuring and recording reaction temperature, whereby a thermocouple was directly connected to a sensitive ultraviolet recording galvanometer. This system has the advantage of fast response and reliability. It is shown diagramatically in figure 4.10.1.

The overall static calibration of the system, i.e. galvanometer deflection per unit change in temperature is directly related to the voltage output per unit change in temperature of the thermocouple hot junction, and inversely related to the current requirement of the galvanometer per unit deflection.

The thermocouple used was Pt/Pt.10% Rh. of 0.05 mm diameter wires. This was embedded in the delay composition, which was pelleted in a tube. The temperature profile was recorded as the wave moved from point of ignition until it reached the thermojunction. This recording was achieved by using a recording oscillograph type 5 - 127, manufactured by Bell and Howell Ltd. This instrument is capable of making a record of any static or dynamic phenomenon which could be converted to an analogue voltage. The sensing of such a phenomenon was accomplished by using low voltage output transducers which converted the temperature change into an electrical signal. This signal was then fed to a high sensitive mirror galvanometer in the oscillograph, where it was used to vary the mirror position.

Light from a mercury arc ultra violet lamp was reflected by the galvanometer mirror through a simple optical system to focus a spot of light on a moving strip of light sensitive paper, the speed of which could be increased to 80 cm/s.

FIG. 4.10.1

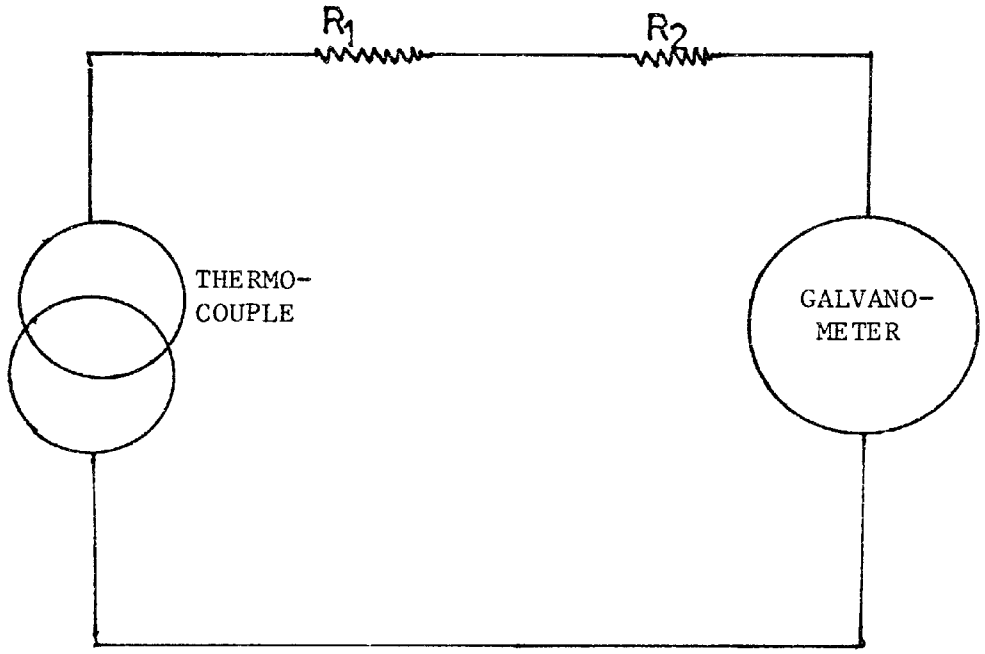

R_1 Ohmic resistance of the circuit external to the galvanometer

R_2 Ohmic resistance of the galvanometer

TEMPERATURE MEASURING SYSTEM

Calibration was then made of the output voltage trace by the use of a known temperature furnace to give a temperature-time curve.

4.11 THERMAL CONDUCTIVITY OF COMPACTED MIXTURES

The method (39) used is based on the temperature measurement at the interface between a material of a known melting point on which the specimen is placed and a pure material of a known thermal conductivity. Heating the assembly is controlled at a low rate to reach a quasi-steady state condition until melting of the material took place.

The specimen (Pb_3O_4/Si + 0.5% Carboxymethyl Cellulose binder) is obtained by compacting in a mould 40 mm diameter under a known pressure to give a disc approximately 6 mm thick.

A small amount of naphthalene (melting point 80.2^{o}C) was placed on top of the silica plate of the sample block assembly and the heating started until the naphthalene was completely molten and covered the top surface of the silica plate. The specimen supported by a fine film was placed on top of the molten naphthalene and the heating was stopped when naphthalene was still molten and formed a complete layer between the specimen and the silica plate. A weight (200 gm) was placed on top of the specimen to ensure a constant thickness of naphthalene layer and the whole assembly was left to cool to room temperature.

A microswitch operating a plunger was positioned horizontally to touch the specimen. Crushed ice was piled on a metal plate which was placed on top of the specimen. The heating was started at a low

voltage so that a quasi-steady state condition is reached at the approach to the melting point of the naphthalene.

When the specimen/silica interface has reached the melting point of the naphthalene, the specimen will be displaced because of the sideways force exerted by the actioned sprung microswitch which will cut off the heating automatically. The millivoltmeter was read immediately and the temperature was then determined. Figure 4.11.1 illustrates the equipment used.

4.12 THERMAL ANALYSIS EQUIPMENT

The equipment used was

1) A Stanton Redcraft mass flow thermal balance (model No. MFH-1), adapted for simultaneous differential thermal analysis (DTA) and thermal gravimetry (TG) was used. This has a temperature range of up to 1200°C. Thermocouples were of platinum/platinum - 13% Rhodium positioned in dimped platinum crucibles 6.5 mm diameter and 10 mm deep. The crucibles rest on the thermocouples within a high purity ceramic block.

2) Perkin Elmer differential scanning calorimeter DSC2. This has a temperature range of up to 725°C. Sample holder is made of platinum-iridium alloy for the body and structured members of the holder, a platinum wire for both the heater and sensor and α-alumina for electrical insulation. It reads with accuracy of ± 1.0°C.

Calorimetric sensitivity range from 0.1 to 20 mcal/second

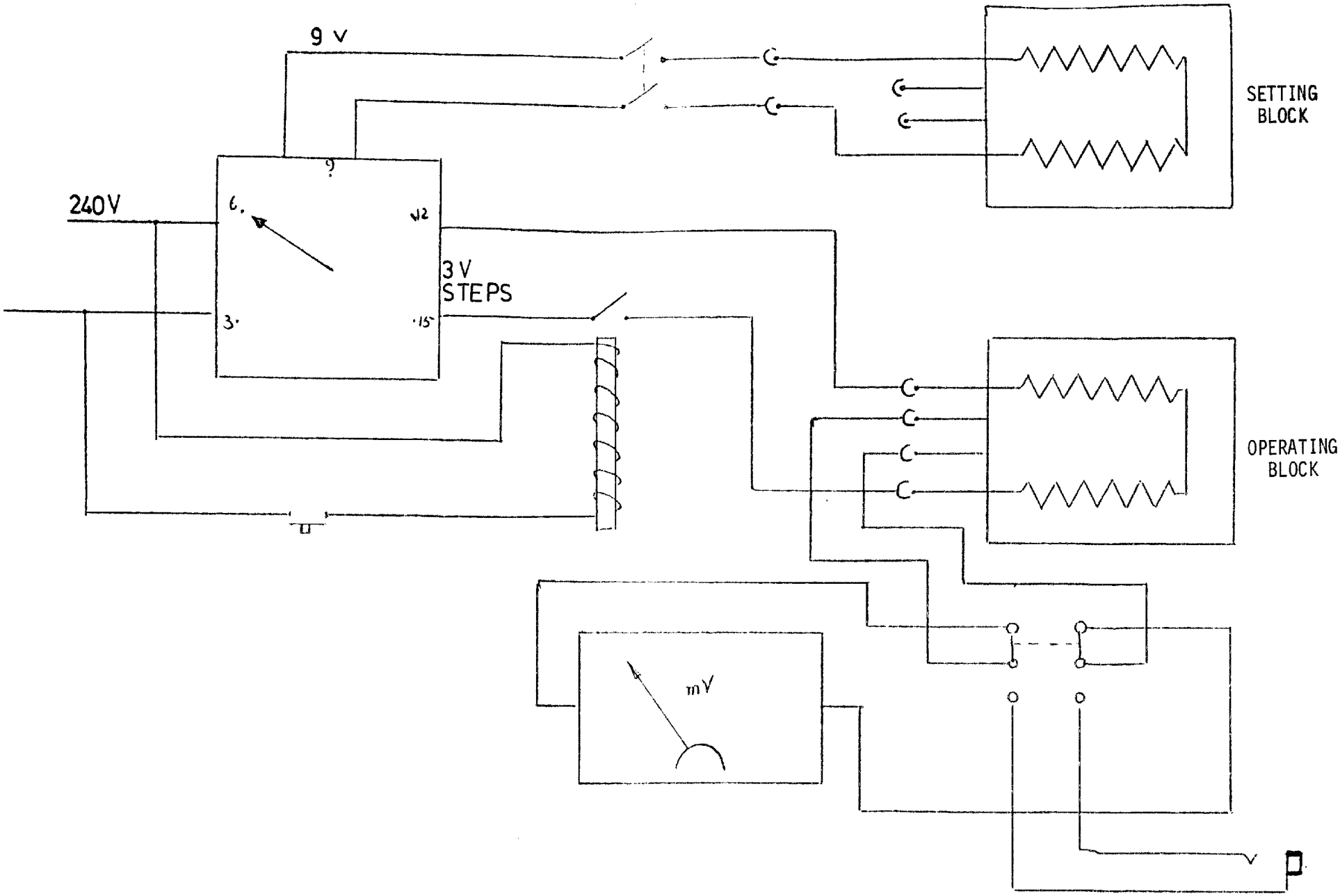

FIG. 4.11.1 CIRCUIT DIAGRAM FOR THERMAL CONDUCTIVITY APPARATUS

full scale deflection using 10 mv recorder. The furnace atmosphere may be varied according to requirements.

3) Perkin Elmer thermogravimetric system TGS-2

This is a system for measuring the weight loss or gain of a sample as it is subjected to a precisely controlled temperature environment.

Temperature range of instrument 20 - 1000°C.

Scanning rate 0.3 to 160°C per minute

The autobalance will support up to 1.0 gm of sample. Sample pans are made of platinum, 5.8 mm internal diameter x 1.8 mm deep. Recorder ranges - there are 16 fixed ranges from 0.01 mg. full scale deflection to 1000 mg full scale deflection.

It is possible in this equipment to suppress the weight electronically from 0 - 1000 mg to give an amplified percentage change.

A first derivative computer (FDC) was used to give an amplified derivative of the analyser signal, such as rate of change of sample weight and hence separates overlapping thermal weight loss phenomena.

The recorder used was a 2 pen strip chart recorder, the primary pen recorded weight changes while the event maker monitors the programme temperature. The second pen is used for simultaneous recording of thermocouple temperature, FDC output or weight changes on a different sensitivity range.

CHAPTER FIVE

RESULTS AND DISCUSSION

5.1 STUDIES ON COMPACTED COMPOSITIONS

The work was carried out with the objective of providing some knowledge as to how combustion reactions occur and to find the factors that influence them. Pb_3O_4/Si and PbO_2/Si delay compositions are used to study

1. delay time per specified length for different oxidant/fuel ratios
2. variation of delay time with length of pellet
3. effect of silicon particle size on rate of burning
4. effect of loading pressure on rate of burning
5. effect of ambient temperature on rate of burning
6. effect of ambient pressure on rate of burning
7. pressure inside the detonator tube
8. temperature of reaction
9. heat of reaction
10. effect of diluents on rate of burning.

5.1.1 DELAY TIME OF VARIOUS OXIDANT/FUEL RATIOS

Mixtures of Pb_3O_4/Si and PbO_2/Si (50/50, 55/45, 60/40, ... 95/5 W/W) with 0.5% of carboxymethyl cellulose binder are prepared as previously described and pressed into delay tubes at a pressure 15.7 kPa. In all cases 2 cm lengths were used and the time is measured as previously and as illustrated in figure 4.8.1.

From the plot of the delay time against percentage silicon,

for Pb_3O_4/Si, it can be seen that the delay time is reduced as the silicon percentage is reduced from 50 to 30% and then it increases as silicon is reduced further from 30 to 5% as can be seen in figure 5.1.1.

Compositions with silicon greater than 50% failed to burn, while compositions with less than 15% silicon gave erratic delay time and caused bursting of detonator tubes due to the high pressure created in the space above the delay element.

For PbO_2/Si prepared in the same way as above and tested under the same conditions as above, similar pattern is obtained but the delay time is maximum at 35% silicon. Silicon rich mixtures with 55 and 60% silicon, unlike Pb_3O_4/Si, still sustained burning reactions. The time taken to burn the 2 cm column of mixture is shorter for PbO_2/Si than that of Pb_3O_4/Si. However, bursting of the tubes occurred at a higher silicon percentage (up to 25%).

As the temperature in the layer of the column is increased by the heat from the fusehead, the heat will flow along the delay composition and when sufficient energy is conducted into the layer so that its ignition temperature is reached, the reactants will begin to combine chemically. This reaction causes additional heat to be conducted into unreacted material. At some point in time, sufficient energy will be conducted into the next layer to cause ignition here. The process of conducting energy and obtaining additional heat from the reaction will continue as the flame front proceeds through the column.

The heat of reaction at a layer is transferred to the next layer at a rate depending on the thermal conductivity of the mixture,

FIG. 5.1.1

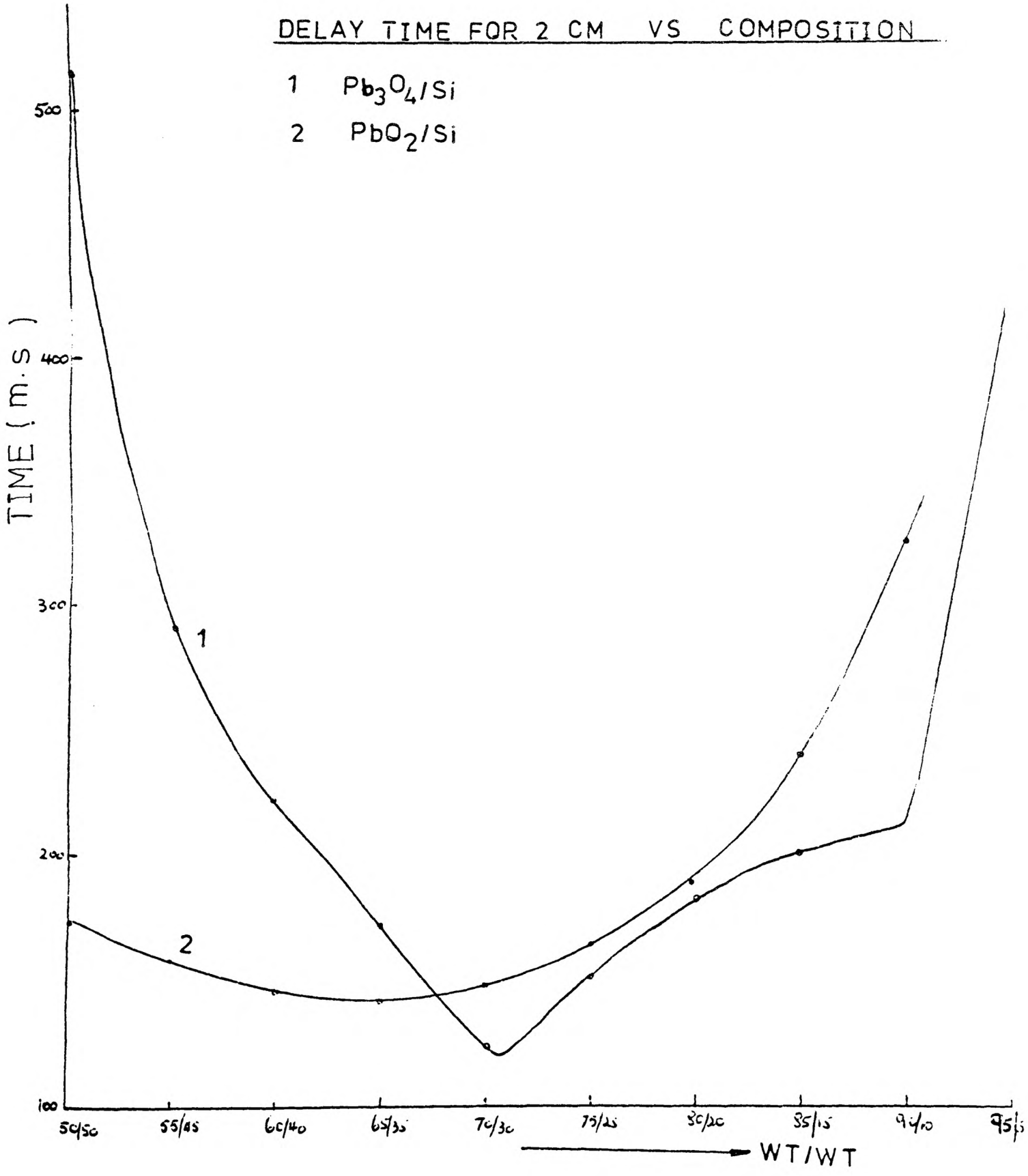
DELAY TIME FOR 2 CM VS COMPOSITION
1 Pb_3O_4/Si
2 PbO_2/Si
TIME (m.s)
500
400
300
200
100
1
2
50/50
55/45
60/40
65/35
70/30
75/25
80/20
85/15
90/10
95/5
WT/WT

the temperature gradient between the two layers and on the specific heat of the mixture.

Theoretically it would be expected that the maximum rate of burning coincides with the reaction stoichiometric proportions, i.e. 92.4/7.6 Pb_3O_4/Si and 89.5/10.5 PbO_2/Si as based on the formation of silicon dioxide and elemental lead which are confirmed by X-ray diffraction and infra red analysis. However, as seen from the figure 5.1.1, the burning rate is at a maximum at a higher silicon percent than required by the equations:

$$Pb_3O_4 + 2\ Si \rightarrow 3Pb + 2\ SiO_2$$

$$Pb\ O_2 + Si \rightarrow Pb + SiO_2$$

The reason for the discrepancy can be explained by the fact that as the reaction starts taking place on the surfaces of the silicon particles, a layer of SiO_2 will form on unreacted silicon cores, this layer becomes thicker as the Si% is reduced and the oxidant consequently increased, and so this SiO_2 acts as a barrier, making it more difficult for the oxygen to reach the unreacted silicon and so the maximum rate of burning occurs at a Si% higher than theoretically required. The difference between the theoretical and actual Si% at which maximum rate of burning occurs is narrowed as a finer silicon powder is used.

5.1.2 VARIATION OF DELAY TIME WITH LENGTH OF COLUMN

The time taken to burn a certain length of composition has been determined in all cases by averaging twenty readings. These results are tabulated in for Pb_3O_4/Si and for PbO_2/Si.

As can be seen in figure 5.1.2, the time delay is

FIG. 5.1.2

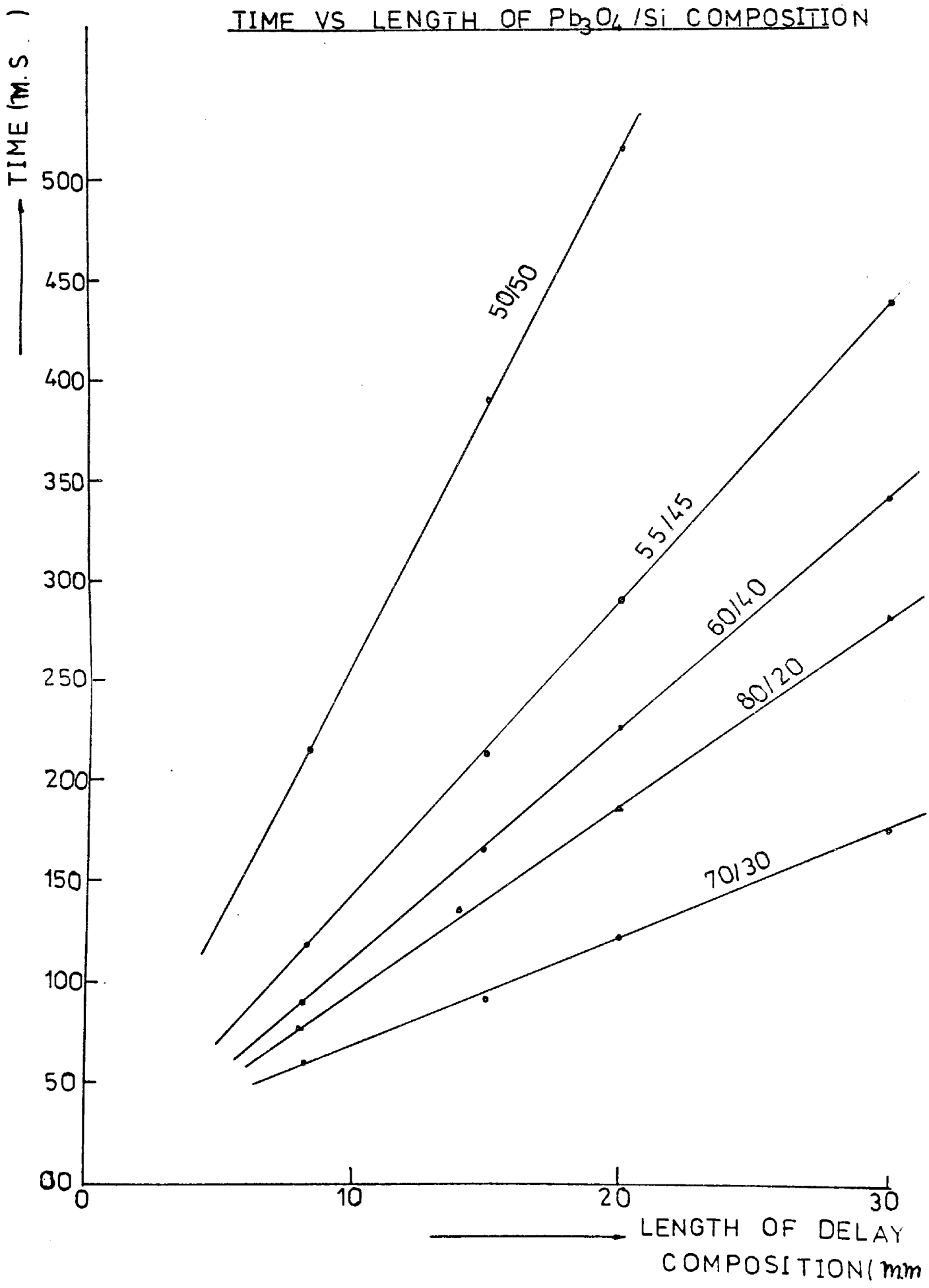
TIME VS LENGTH OF Pb_3O_4 /Si COMPOSITION
TIME (M.S.)
500
450
400
350
300
250
200
150
100
50
00
0
10
20
30
50/50
55/45
60/40
80/20
70/30
LENGTH OF DELAY COMPOSITION(mm

directly proportional to the length for all the oxidant/Si ratios, therefore the rate of burning is a linear relationship both in Cm/s and g/s with length of column.

5.1.3 EFFECT OF SILICON PARTICLE SIZE ON RATE OF BURNING

The silicon powder used was prepared by grinding, then classified into different sizes. The size recorded is an average of a wide range as seen from the Coulter Counter plot.

Three silicon sizes were studied extensively

silicon A of specific surface area 6.258 m^2/g and average size 1.9μm.

silicon B of specific surface area 2.543 m^2/g and average size 3.9μm.

silicon C of specific surface area 1.448 m^2/g and average size 5.0μm.

The silicon B is used in the mass production of delay mixtures, while A and C are silicon rejected as fine and coarse respectively, and are used for purpose of comparison.

The shapes of the particles are very irregular when viewed through electron microscope (see pictures). The average size is, therefore, taken for geometrically different particles and this is used as a rough guide for the purpose of comparison. It is obvious that different shapes which may give the same average size will offer different contact areas and the voidage produced will not by any means be uniform in different positions along and across the pellet.

The three silicon powders, A, B and C were used to examine the rate of burning of red lead/silicon and lead dioxide/silicon of

ratios ranging from 50/50 to 90/10 of oxidant/silicon. From figures 5.1.3 & 4 it is observed that the rate of burning increases with diminishing particle size of the silicon. This is as predicted, since finer powders give larger surfaces for the interaction or area of contact with the oxidant. As the burning of a pellet of the delay composition takes place by the passage of a reaction front along the column, it is therefore necessary to have a better surface contact between the reacting solids for a faster rate of burning.

Komatsu (40) puts forward the theory that the reaction product grows spherically from each contact point. After a time, these products will come into contact with one another to form a shell and reactants will advance from the outside towards the interior as the reaction proceeds.

From figure 5.1.3 for red lead/silicon, the (R.B.) of sample containing silicon A, was maximum at approximately 15.0% Si, while for silicon B and C it was maximum at approximately 30% Si.

For lead dioxide/silicon delay compositions, it is illustrated in figure 5.1.4 that the finer the silicon, as with red lead, the faster was the rate of burning and the lower the percentage of silicon at which the maximum (R.B.) occurred.

For silicon A, (R.B.) was at 20% Si
For silicon B, (R.B.) " " 35% Si
For silicon C, (R.B.) " " 40% Si
For silicon D, (R.B.) " " 50% Si

If the particle size distribution is narrowed down a more

FIG. 5.1.3 VARIATION OF BURNING RATE WITH Pb_3O_4/Si RATIO FOR VARIOUS Si PARTICLE SIZES

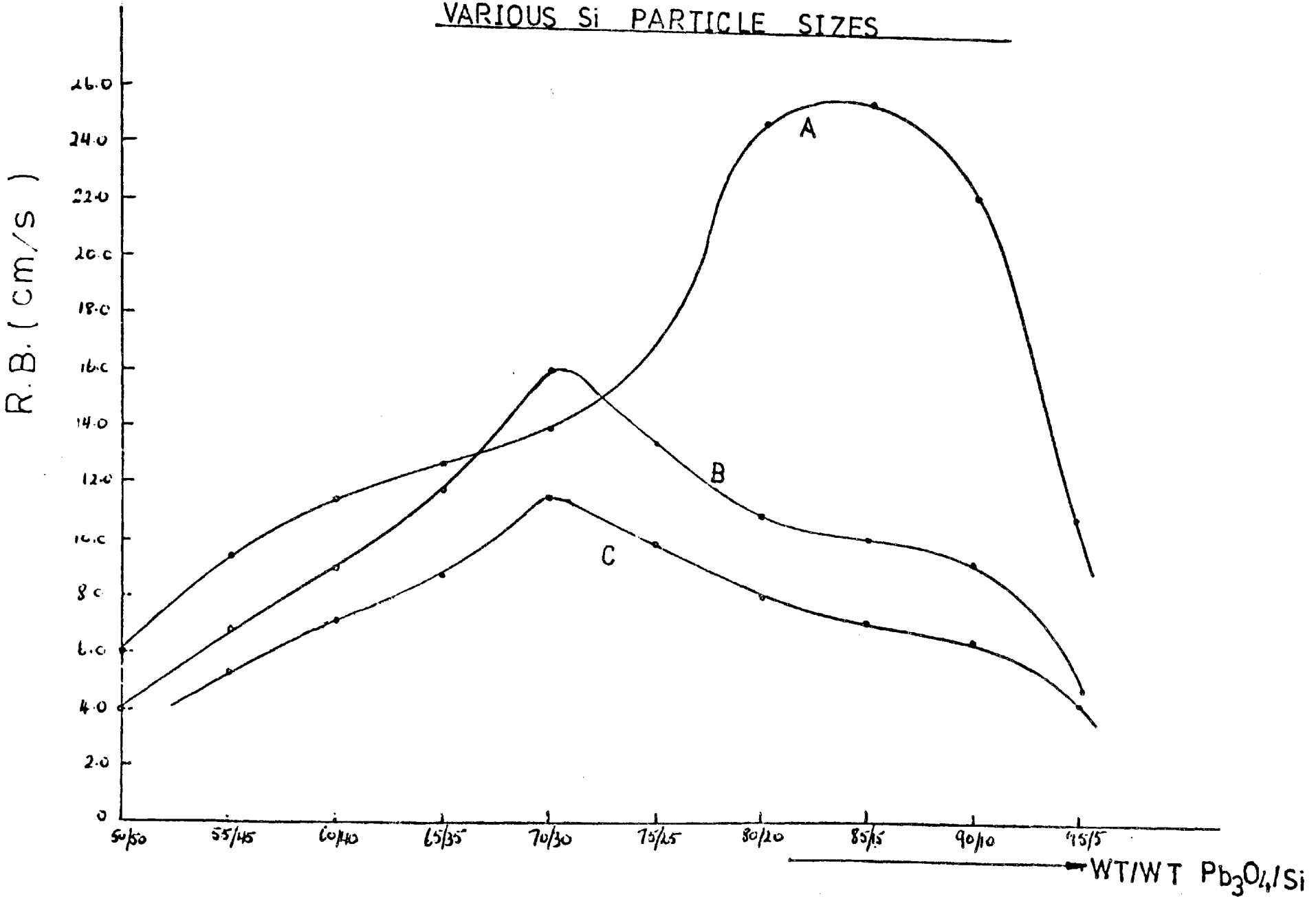

FIG. 5.1.4 VARIATION OF RATE OF BURNING WITH PbO_2/Si RATIO FOR VARIOUS SILICON PARTICLE SIZES

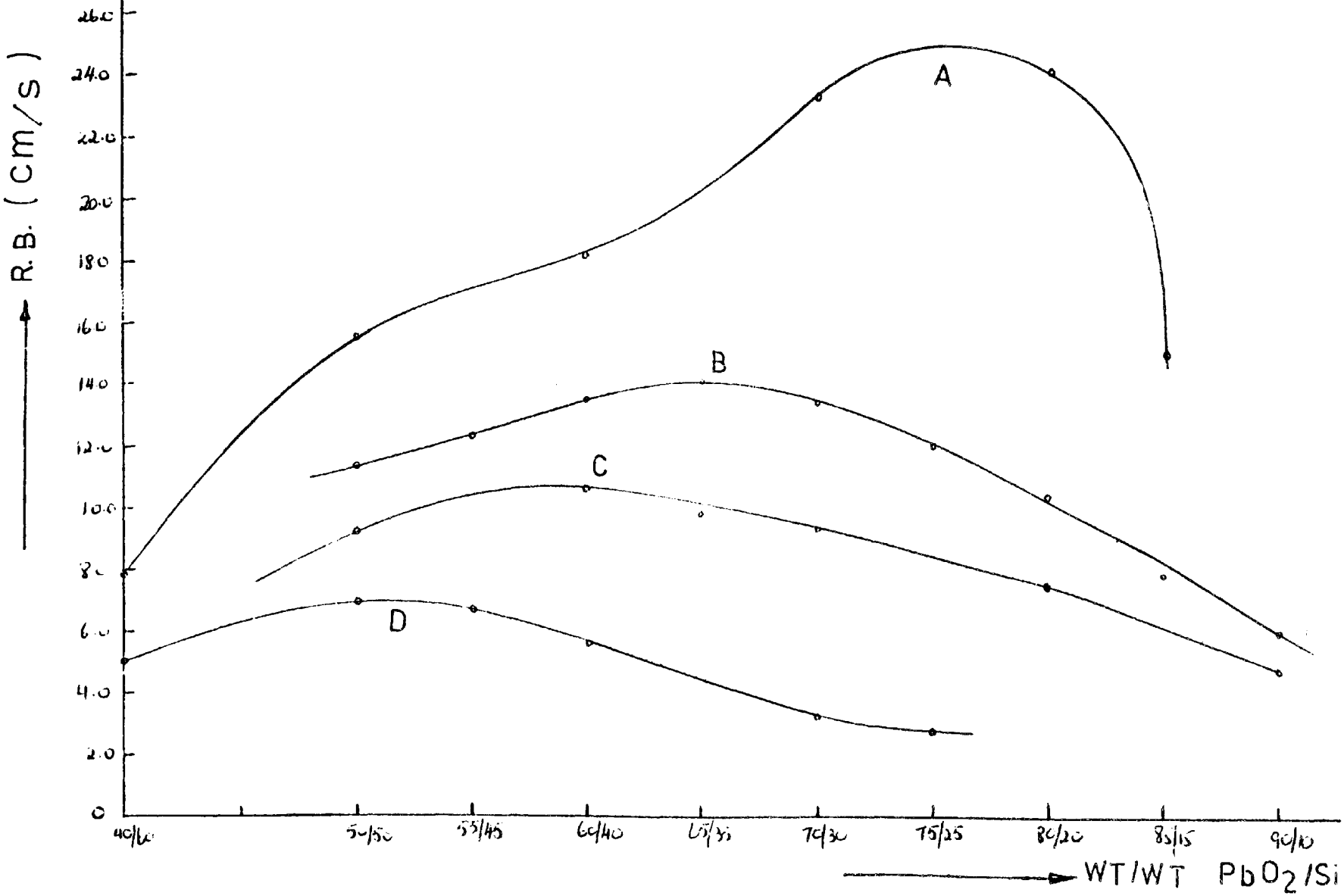

reliable average size can be obtained. By sieving the powder, sizes ≤ 2 μm to 48 μm were produced. When samples of delay compositions of each of these sizes with red lead were prepared in ratios 50/50, 60/40, 70/30, 80/20 and 90/10, the delay times were measured for a known length of column. The standard deviation of the delay time was observed to be very high for the coarser powders, making them unreliable for practical use.

The plot of $\frac{1}{v}$ against the silicon particle size for each ratio gave a straight line. The rate of burning is therefore related to particle size by the equation:

$$\frac{1}{v} = md + c$$

where m is the gradient of the straight line of the plot. (5.1.5) m was measured for each sample and was found to be

50/50 m = 0.0180

60/40 m = 0.0105

70/30 m = 0.0112

80/20 m = 0.0160

90/10 m = 0.0155

From the values of m, it can be concluded that samples 50/50, 80/20 and 90/10 are more influenced by the size d.

FIG. 5.1.5 $\frac{1}{V}$ VS PARTICLE SIZE OF Si IN Pb_3O_4/Si

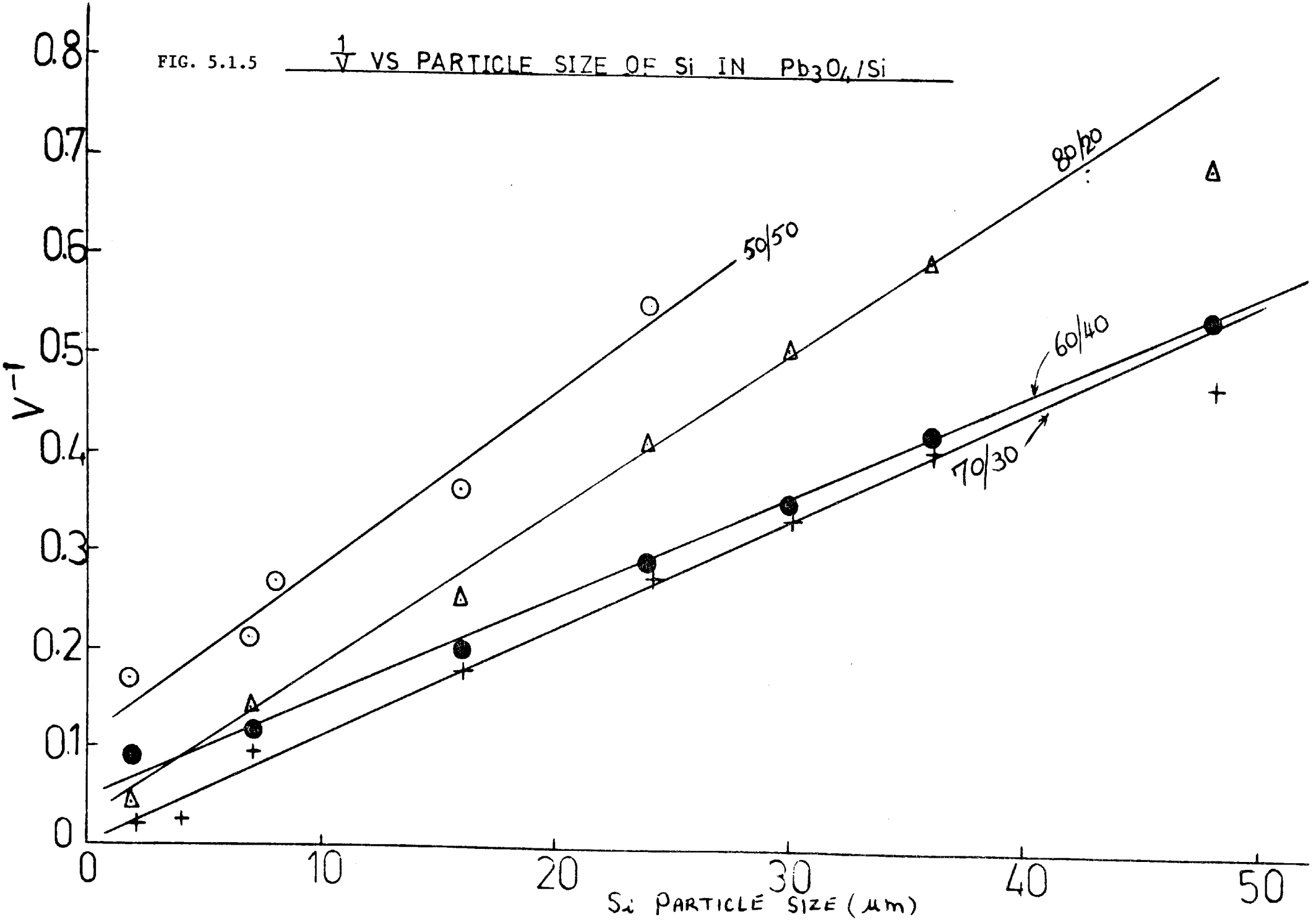

5.1.4 EFFECT OF LOADING PRESSURE ON RATE OF BURNING

Mixtures of Pb_3O_4/Si of different weight ratios were compacted in delay tubes under several pressures (17.6, 66.5, 143.0 and 181.0 Newton/Sq.m.metres) by the hydraulic press. All other aspects are kept the same and the time of burning was measured in the normal procedure. The results of rate of burning were plotted against the loading pressure as seen in Fig. 5.1.6. This graph shows that the rate of burning is increased for compositions rich with silicon viz (30 - 50%), but when silicon weight per cent was reduced below 30%, the rate of burning dropped and this drop continued down to 10% Si. It can also be seen that the peak of the rate of burning has shifted towards higher Si% with increase of loading pressure.

The direct effect of compaction is obviously increasing the density of composition inside the tube, and hence reducing the voidage existing between the particles and getting the oxidant and fuel particles closer, that is, better surface contact through which the reaction can proceed and so the increase in the rate of burning can be justified for 30 - 50% Si in a composition of Pb_3O_4/Si as in Fig. 5.1.7.

The thermal conductivity change with compaction as discussed in 5.1.11 and the results shown in Table 5.1.28 indicate that the change is rather small, and in all cases, the thermal conductivity was very small (much smaller than the thermal conductivity of either constituent).

In the region where Si is below 30% the rate of burning is reduced by increasing the pressure of compaction as in Fig. 5.1.8.

FIG. 5.1.6

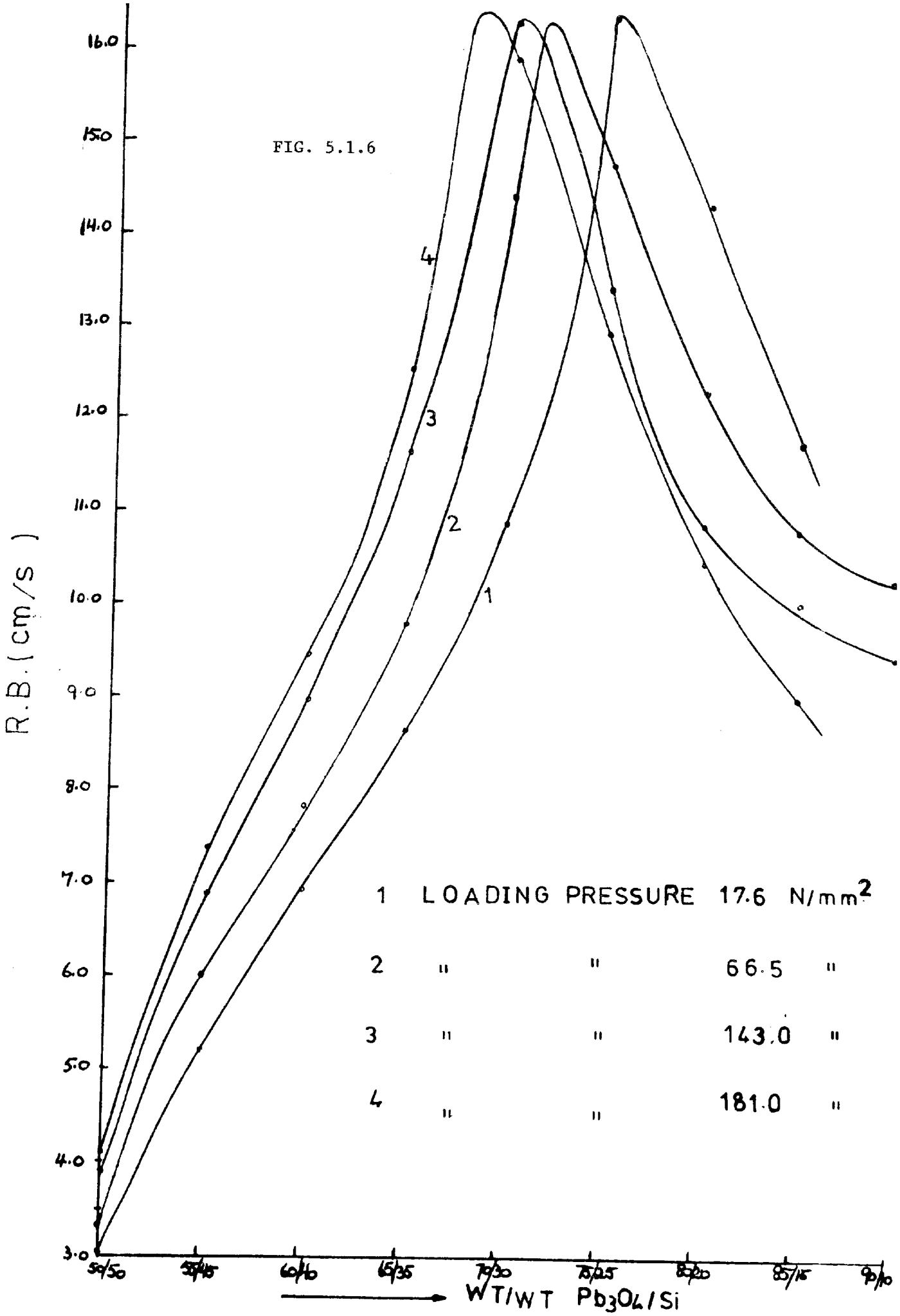
R.B. (cm/s)
16.0
15.0
14.0
13.0
12.0
11.0
10.0
9.0
8.0
7.0
6.0
5.0
4.0
3.0
1
2
3
4
1 LOADING PRESSURE 17.6 N/mm²
2 " " 66.5 "
3 " " 143.0 "
4 " " 181.0 "
50/50
55/45
60/40
65/35
70/30
75/25
80/20
85/15
90/10
WT/WT Pb3O4/Si

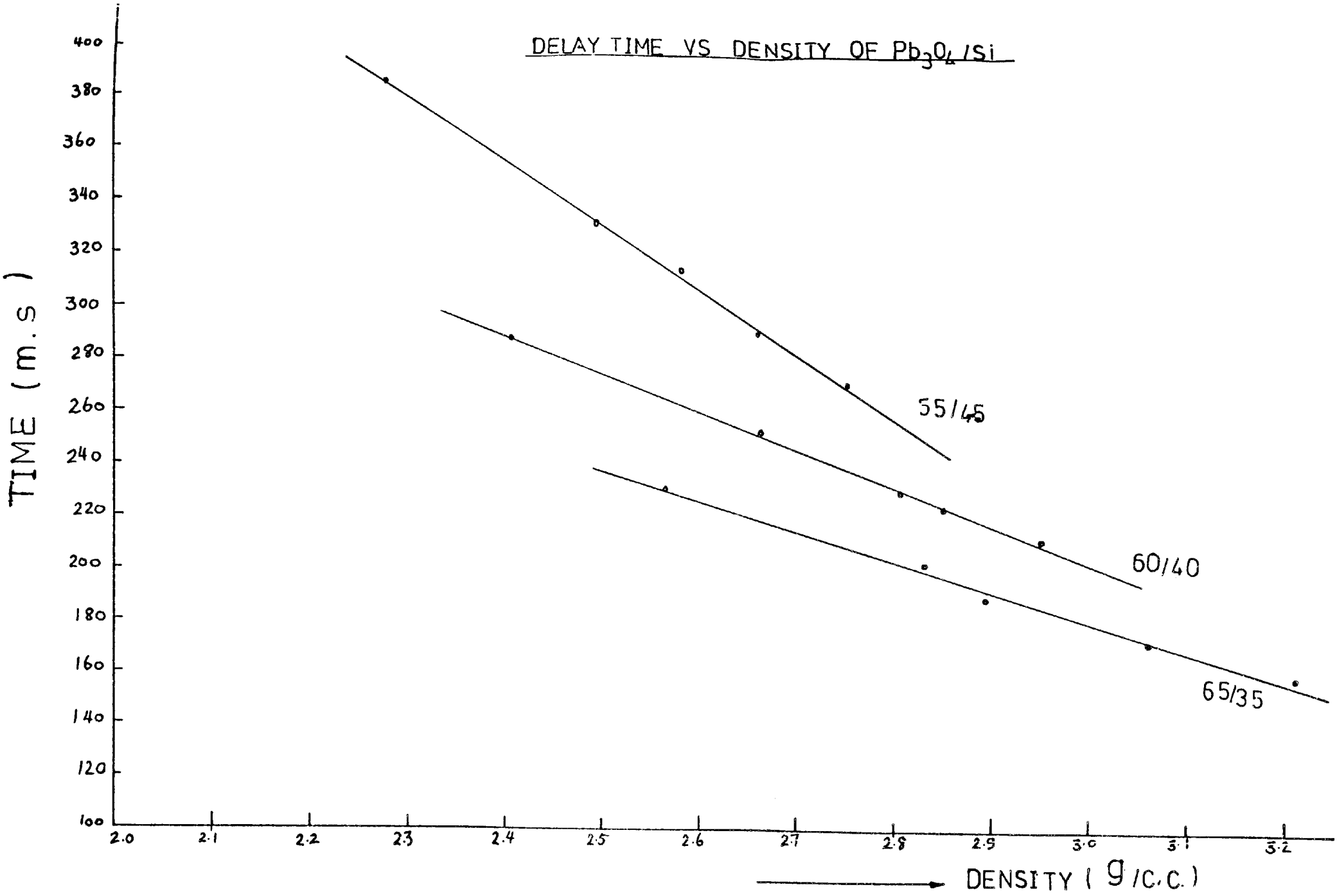
DELAY TIME VS DENSITY OF Pb_3O_4/Si
TIME (m.s)
400
380
360
340
320
300
280
260
240
220
200
180
160
140
120
100
2.0
2.1
2.2
2.3
2.4
2.5
2.6
2.7
2.8
2.9
3.0
3.1
3.2
DENSITY (g/c.c.)
55/45
60/40
65/35

FIG. 5.1.7

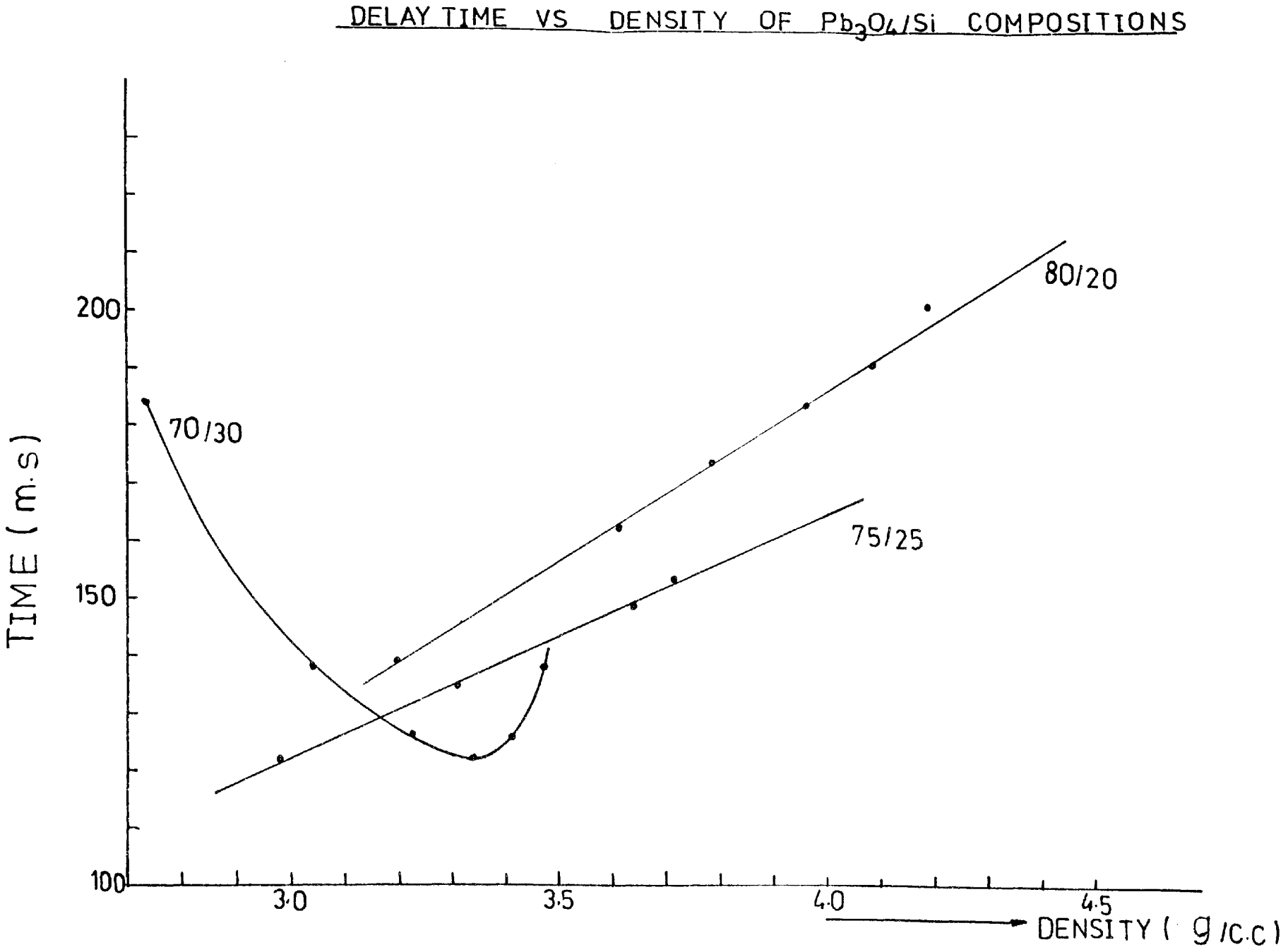
DELAY TIME VS DENSITY OF Pb_3O_4/Si COMPOSITIONS
TIME (m.s)
200
150
100
70/30
80/20
75/25
3·0
3·5
4·0
4·5
DENSITY (g/c.c)

FIG. 5.1.8

This can be explained by the fact that at these weight ratios, the amount of heat generated by the reaction in each layer becomes very large, as can be seen later in 5.1.9 and so some of the products are raised to a temperature at which vaporization takes place and the heat needed to raise temperature of unreacted layers is being carried by the gaseous diffusion of these products through the voids to raise the temperature of the reactants to that of the ignition temperature. So the effect of heat conducted by the particle is of less importance than the heat carried by gases through the pores, and so increasing the pressure of compacting will reduce the voidage and hence hindering the rate at which these gases are transported.

It can also be concluded that the heat transfer in the 30 - 50%, Si region is mainly conducted by the solid particles, though a certain amount of gaseous diffusion will also occur but to a lesser extent. It can be seen later (5.1.10), that temperatures reached for 10 - 30%, Si, exceed the melting point of silicon, and the lead formed will be vapourised so would any unreacted lead oxide. In the 30 - 50%, Si the temperatures are too low, especially at higher Si%, to create enough gases or to raise the pressure high enough to drive these gases through the compacted material to be of significance to rate of burning.

5.1.5 PRESSURE MEASUREMENT INSIDE DETONATOR TUBE

The pressure created in the space above the delay element during burning was measured by using a pressure transducer. The pressure, as the fusehead was fired and the burning has commenced, was sensed by a piezo electric crystal and the signal produced was fed to an oscilloscope and a transient recorder as illustrated in Figures 5.1.9 & 10.

In this apparatus, the delay element acts as a piston and therefore it was adequately lubricated with vacuum grease to enable free sliding inside the aluminium tube.

The pressure variation with time was recorded for red lead/silicon samples of ratios 55/45, 60/40 up to 90/10. It can be seen from Figure 5.1.11 that in all cases the fusehead gases gave a sudden pressure increase to reach a maximum after approximately 10×10^{-3} second. As the heat was lost to the surrounding, the pressure dropped to a level which was governed by the heat of reaction.

For a 55/45 sample, there was a steady pressure at approximately 3500 kN/m^2, but for a 90/10 ratio, the pressure rose sharply until the tube has burst at pressure 8200 kN/m^2. Between these two extremes, there was an increase in the pressure created, which was quite large for 80 or 90% red lead samples.

In the samples containing less than 30% silicon, it was clear that the occurrence of leaks due to inefficient sealing and crimping, will, therefore, affect the delay time considerably. The absence of substantial slags due to vapourisation of products means

FIG. 5.1.9

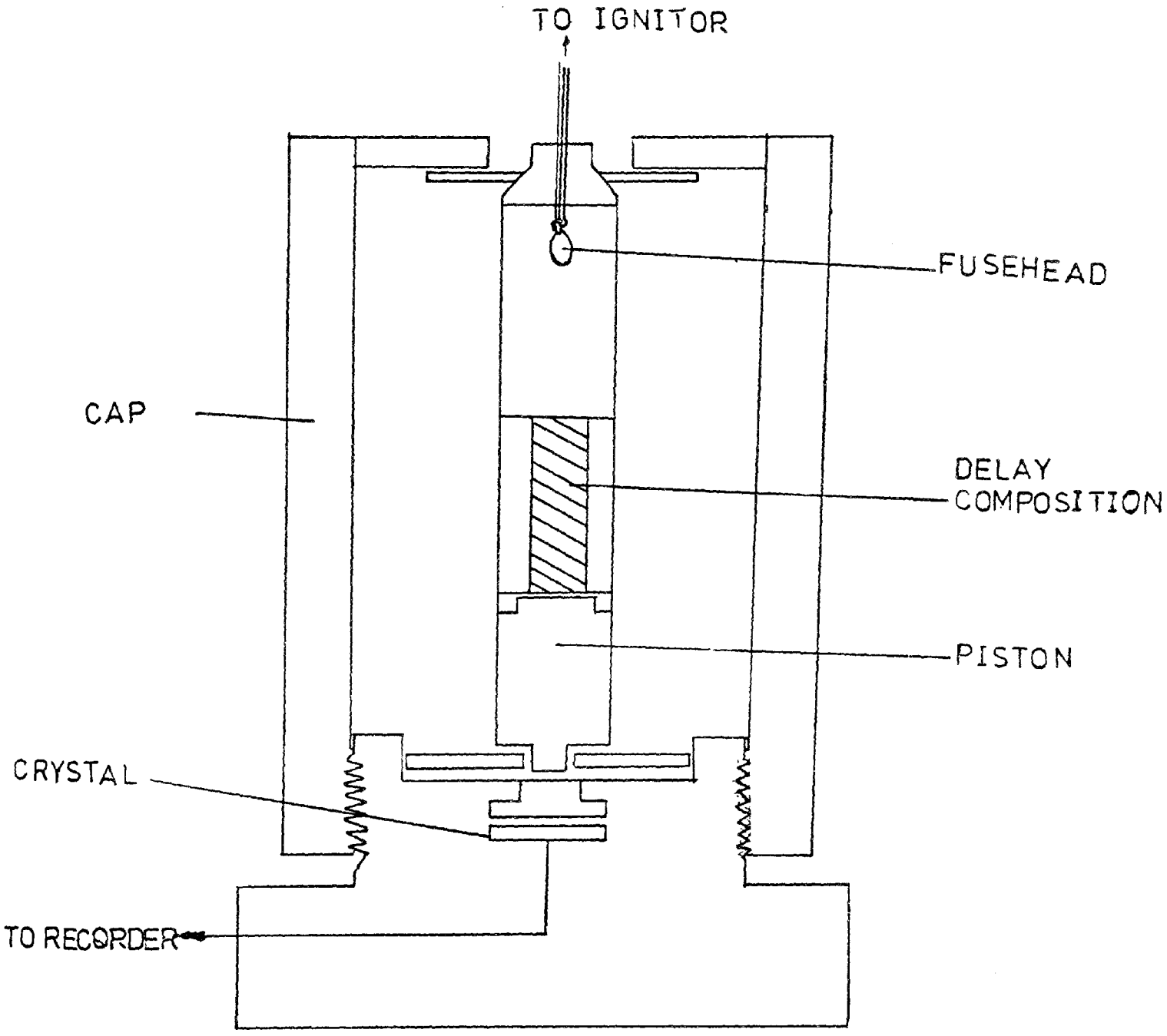

DETONATOR PRESSURE MEASURING APPARATUS

FIG. 5.1.10

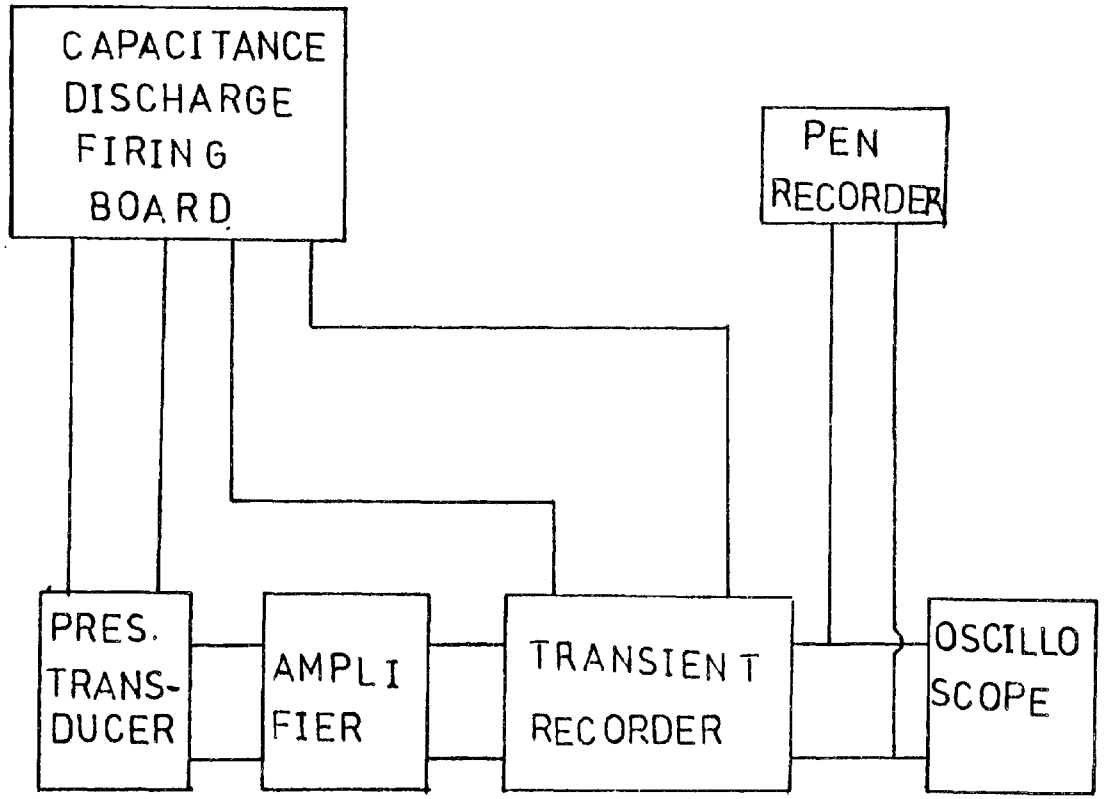

DETONATOR PRESSURE MEASURING ASSEMBLY

FIG. 5.1.11

P VS T FOR FUSEHEAD + Pb_3O_4 / Si

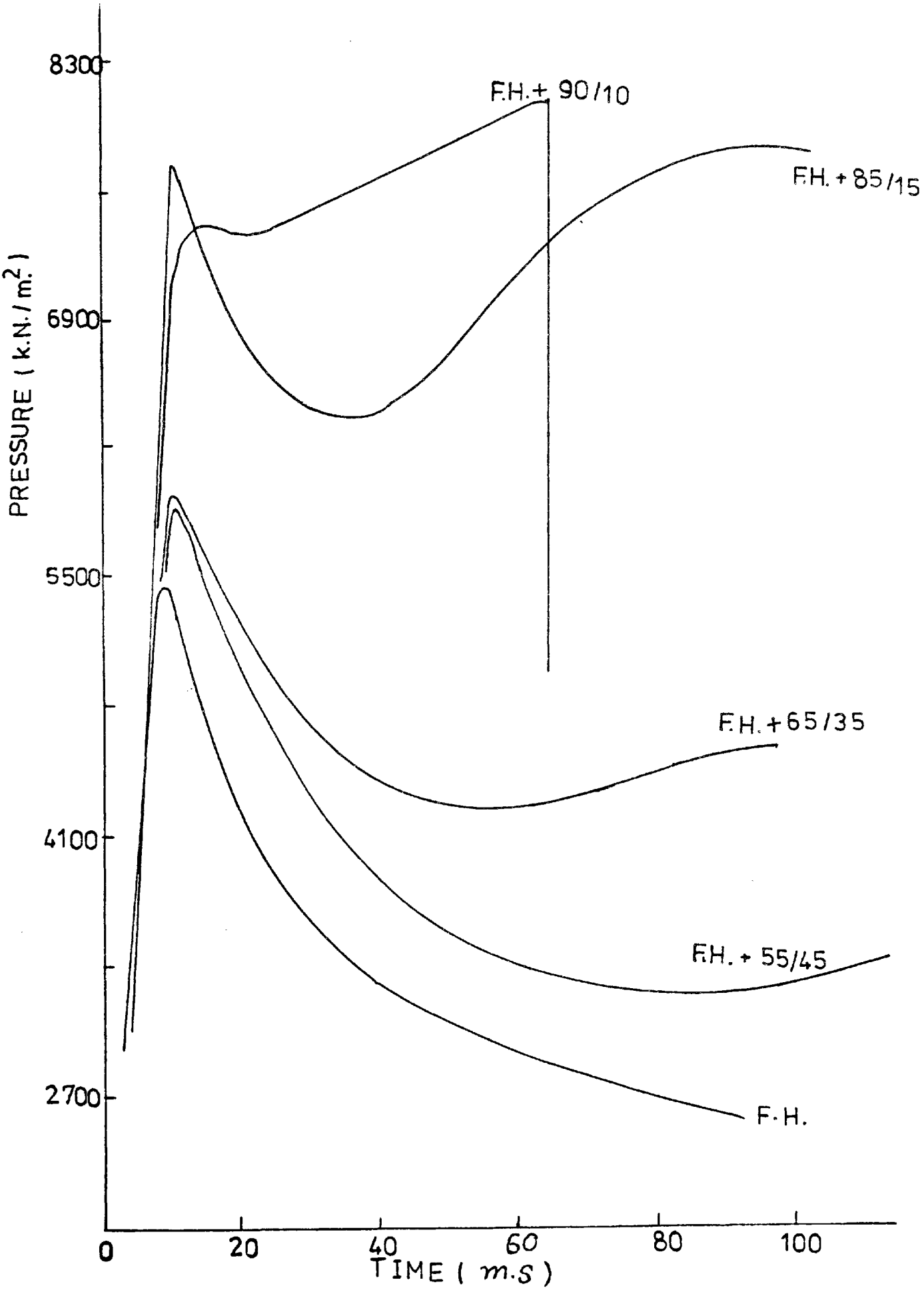

that the heat of reaction will be communicated by radiation, conduction and convection to the free space in the tube, so that the pressure therein, primarily determined by the fusehead, will be affected to a greater extent than by a 50/50 sample where the slag will seal the pores, making the burning independent of pressure.

It is possible to improve the slag forming compositions by the use of finer powders, compacted at higher pressures. The slags formed will also seal off convected and radiated heat from the element, so that the pressure in the free space will be influenced mainly by conducted heat, and will, therefore, not be affected to nearly the same extent as other types of compositions.

5.1.6 STUDY OF EFFECT OF AMBIENT PRESSURE ON RATE OF BURNING

The effect of pressure of anitrogen atmosphere ranging from atmospheric pressure (100 kN/m^2) to 8300 kN/m^2 on (R.B.) of red lead/silicon and lead dioxide/silicon was studied. The detonator tubes containing the delay mixture were vented, then inserted inside a vessel which was constructed to provide for electrical connections and nitrogen supply under pressure, and had a transparent base to make it possible for the light signal emitted from the end of the delay pellet to be picked up by the photoelectric cell located externally in line with the delay assembly as illustrated in diagram

It can be seen from Fig. 5.1.12 that the (R.B.) is influenced slightly by pressure for mixtures containing 30 to 50% silicon but to a greater extent for those containing less than 30% silicon.

For compositions with 30 to 50% silicon, a substantial

FIG. 5.1.12

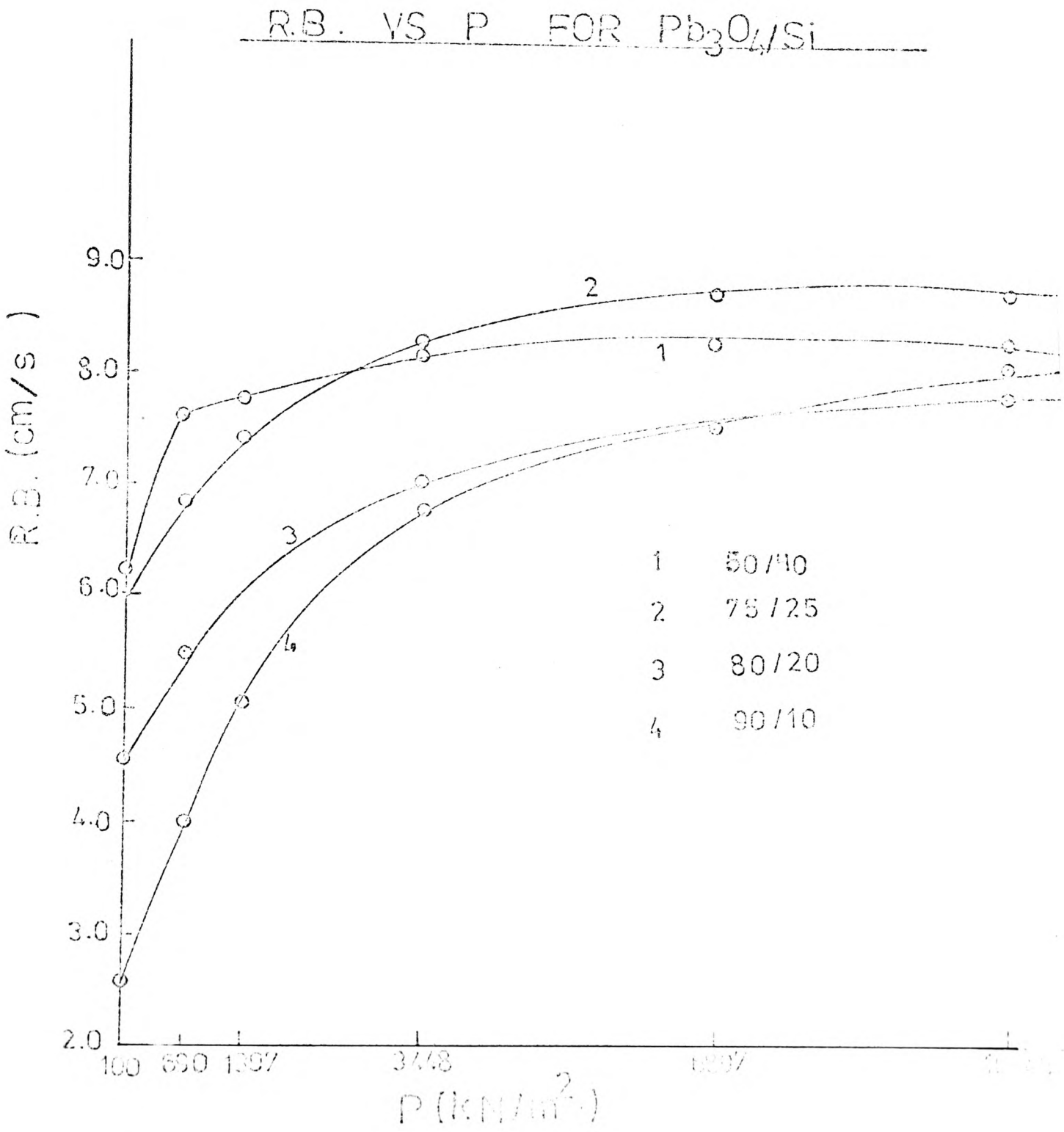
R.B. VS P FOR Pb_3O_4/Si
R.B. (cm/s)
9.0
8.0
7.0
6.0
5.0
4.0
3.0
2.0
1
2
3
4
50/50
75/25
80/20
90/10
100
690
1380
3448
P (kN/m²)

FIG. 5.1.12a

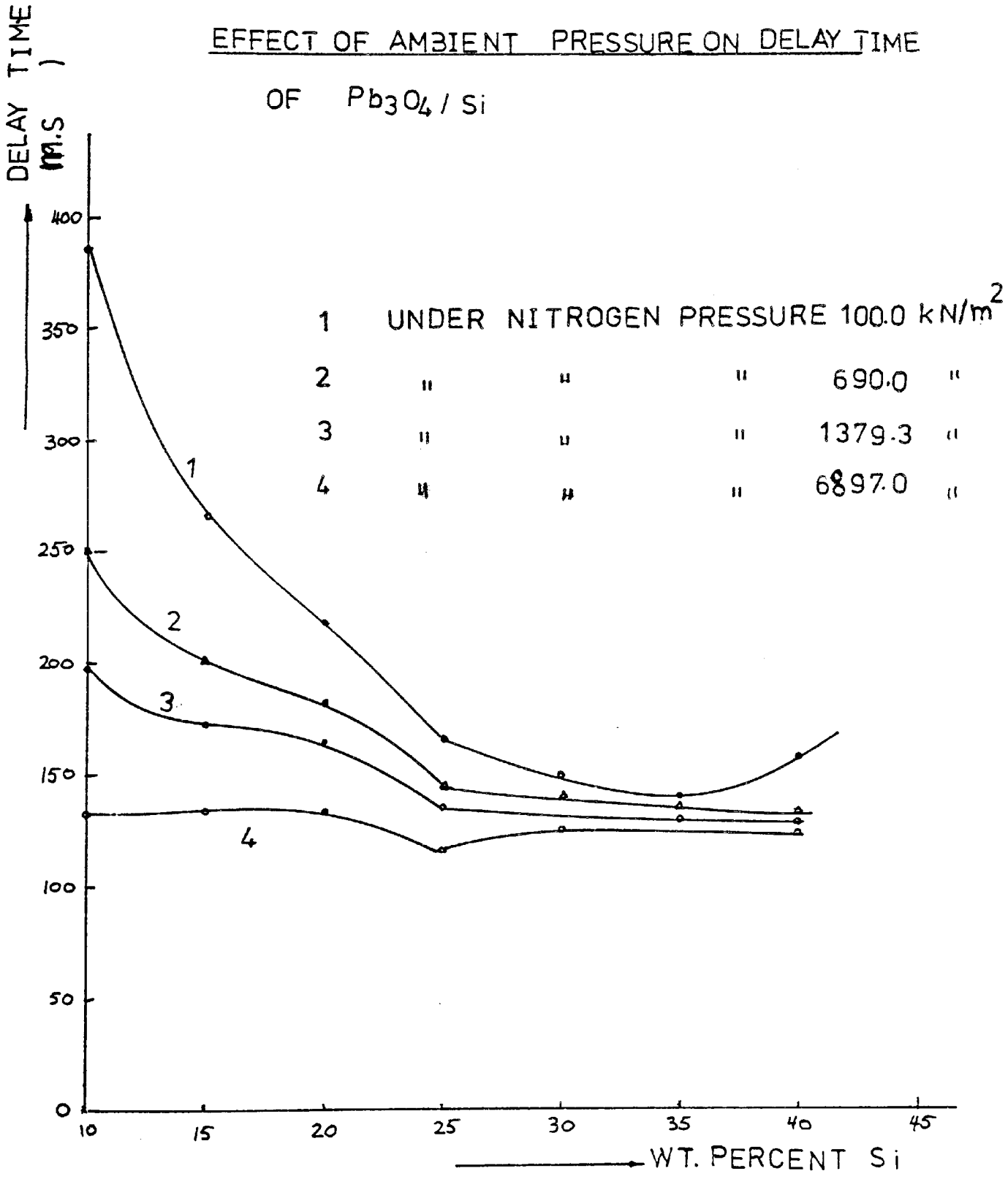
EFFECT OF AMBIENT PRESSURE ON DELAY TIME
OF Pb_3O_4 / Si
DELAY TIME (m.s)
1 UNDER NITROGEN PRESSURE 100.0 kN/m²
2 " " " 690.0 "
3 " " " 1379.3 "
4 " " " 6897.0 "
400
350
300
250
200
150
100
50
0
10
15
20
25
30
35
40
45
WT. PERCENT Si

residue is formed on burning and this residue tends to seal off the burning interface from the external pressure more and more as the burning proceeds, until burning is independent of pressure.

Compositions with less than 30% silicon, when burnt, raise the temperature of products to that at which some of them, such as lead, or lead monoxide, vapourise, and the slag left does not seal the burning front from the external pressure, and therefore, the heat of reaction will be communicated by radiation, conduction and convection to the surrounding nitrogen. At the same time, the passage of these gases through the voids will influence the rate of burning differently at different pressures, making them dependent on external pressure. Hence, in a 10% silicon composition of red lead/silicon, the rate of burning at atmospheric pressure, where the gaseous products escape carrying with them a large amount of heat needed for the reaction, is much slower than that at 8300 kN/m^2.

R.B. at 100 kN/m^2 = 2.6 cm/S

R.B. at 8300 kN/m^2 = 8.04 cm/S

For a 45% silicon of the same mixture, where combustion proceeds mainly in a solid/solid reaction, the external pressure effect is much lower

R.B. at 100 kN/m^2 = 5.17 cm/s

R.B. at 8300 kN/m^2 = 6.09 cm/s.

The ambient pressure is related to the rate of burning (8) by the following equation:

$$V = V_o P^n$$

where V = rate of burning at any pressure

V_o = rate of burning at atmospheric pressure

P = ambient pressure

n = constant

The value of n obtained from a plot of $\ln \left(\frac{V}{V_o}\right)$ against lnP indicates the extent of dependency of (R.B.) on prevailing pressure. From these plots in Fig. 5.1.13 it can be seen that for 55/45 and 60/40 Pb_3O_4/Si, the values of n are 0.042 and 0.026 respectively, confirming a slight dependency. For 80/20, 85/15 and 90/10 red lead/silicon, the (R.B.) is markedly increased by increasing the pressure up to 4900 kN/m^2, but less so as it is increased further to 8300 kN/m^2. The n values for these two pressure ranges are as follows:

80/20	n_1	=	0.162	n_2	= 0.058
85/15	n_1	=	0.208	n_2	= 0.143
90/10	n_1	=	0.357	n_2	= 0.111

In these three compositions, the pressure of the gaseous products will be high due to the high temperature of the reaction and the rate of its increase, so they escape the reaction system to the lower pressure of the ambient atmsophere. As the pressure outside was increased the tendency to vapourise, and the amount of escaped gases will be reduced, so they are driven into the reactants through the voids giving a faster rate of burning. Also at high ambient pressures there is less vapourisation taking place at a certain temperature than at low pressure and so vapourisation may be suppressed altogether as a certain pressure is exceeded.

FIG. 5.1.13

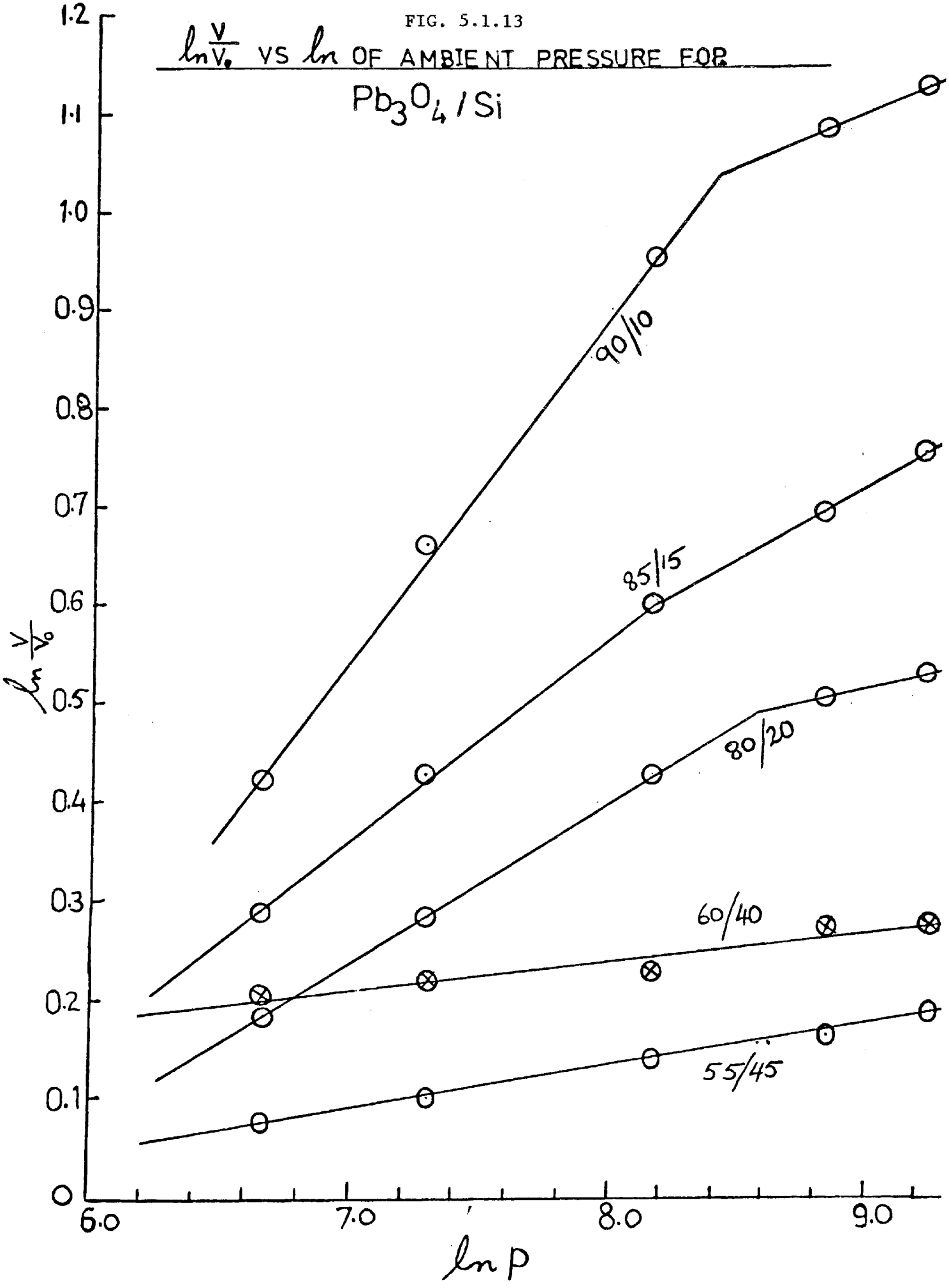
ln V/V0 VS ln OF AMBIENT PRESSURE FOR
Pb3O4 / Si
1.2
1.1
1.0
0.9
0.8
0.7
0.6
0.5
0.4
0.3
0.2
0.1
0
ln V/V0
90/10
85/15
80/20
60/40
55/45
6.0
7.0
8.0
9.0
ln P

FIG. 5.1.14

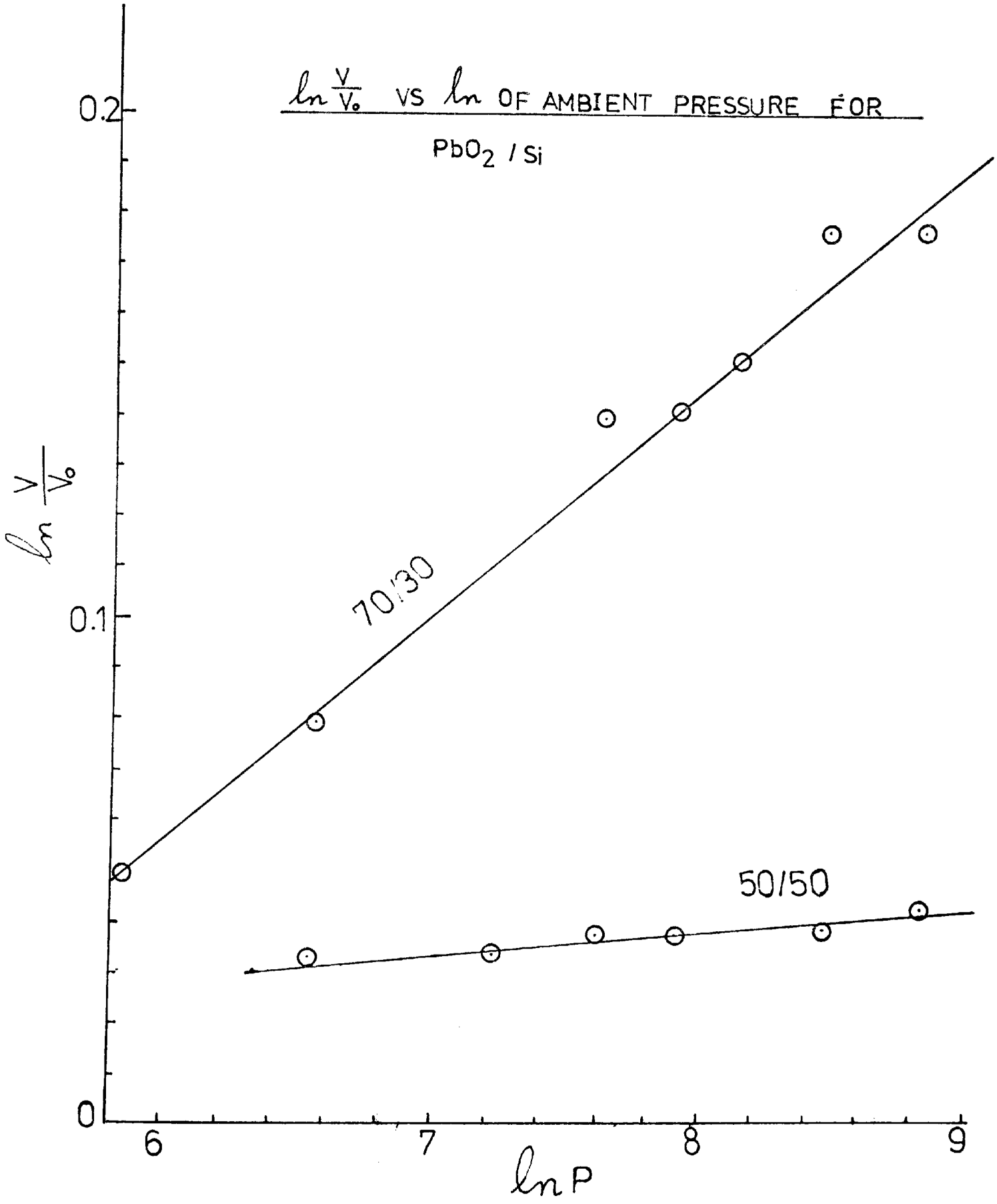
ln V/V₀ VS ln OF AMBIENT PRESSURE FOR
PbO2 / Si
0.2
0.1
0
ln V/V₀
70/30
50/50
6
7
8
9
ln P

From Fig 5.1.14 which shows the variation of ln $\frac{V}{V_o}$ against ln of ambient pressure for 50/50 and 70/30 lead dioxide/silicon samples, the gradients of the resulting straight lines give

$m = 0.005$ for 50/50 sample

and $m = 0.040$ for 70/30 sample

which indicates a very slight dependency of rate of burning of these mixtures on the ambient pressure.

5.1.7 EFFECT OF AMBIENT TEMPERATURE ON RATE OF BURNING

Delay compositions in their assemblies were heated in an oven; with provisions to ensure that all heat sensitive parts of the assemblies (such as wires, neuprene plugs, etc.) were protected. Each assembly was left at a steady temperature for an hour, then fired while it was still in the oven, and the delay time was taken as previously described. An average of ten readings was taken for each sample.

It was not possible to exceed 170°C, as fuseheads ignited, and damage to the photoelectric cell would have been inevitable. For low temperature experiments, ice for 0°C, solid CO_2 in ether for -80°C, solid CO_2 in carbon tetrachloride for -27°C and liquid nitrogen for -185°C were used.

From plots of (R.B.) against absolute temperature, straight lines were obtained for red lead/silicon and lead dioxide/silicon delay compositions. The ambient temperature can be seen to influence significantly samples with 45 and 50% silicon, whilst in

those with 35 and 30% silicon, the effect on rate of burning is very slight as in Figs. 5.1.15 - 17.

The relationship of (R.B.) and absolute temperature can be represented by the equation

$$V = mT + \text{constant}$$

with m, the gradient in $cm/s^{o}K$.

m

(W/W)	Pb_3O_4/Si	PbO_2/Si	
	unvented	unvented	vented
50/50	0.0195	0.0076	0.0143
55/45	0.0163		
60/40	0.0115	0.0055	0.0067
70/30	≃ 0	0.0052	0.0030

The thermal effect on the chemical reactivity or the ease and rate at which a material undergoes a chemical reaction can be studied by assuming that the reactants are at an initial potential energy value of E_R, and that the chemical reaction proceeds through an activated state to form a stable set of reaction products having a potential energy Ep. In the course of the reaction, the reactants have reacted to form products and have given off an amount of heat $\Delta Eo = E_R - Ep$

If energy E_A is supplied to the system prior to the reaction, then the reaction starts at a value $E_R + E_A$ and ends again at E_p giving up an amount of heat:

FIG. 5.1.15 RATE OF BURNING VS AMBIENT TEMP FOR VENTLESS TUBES WITH Pb_3O_4 / Si

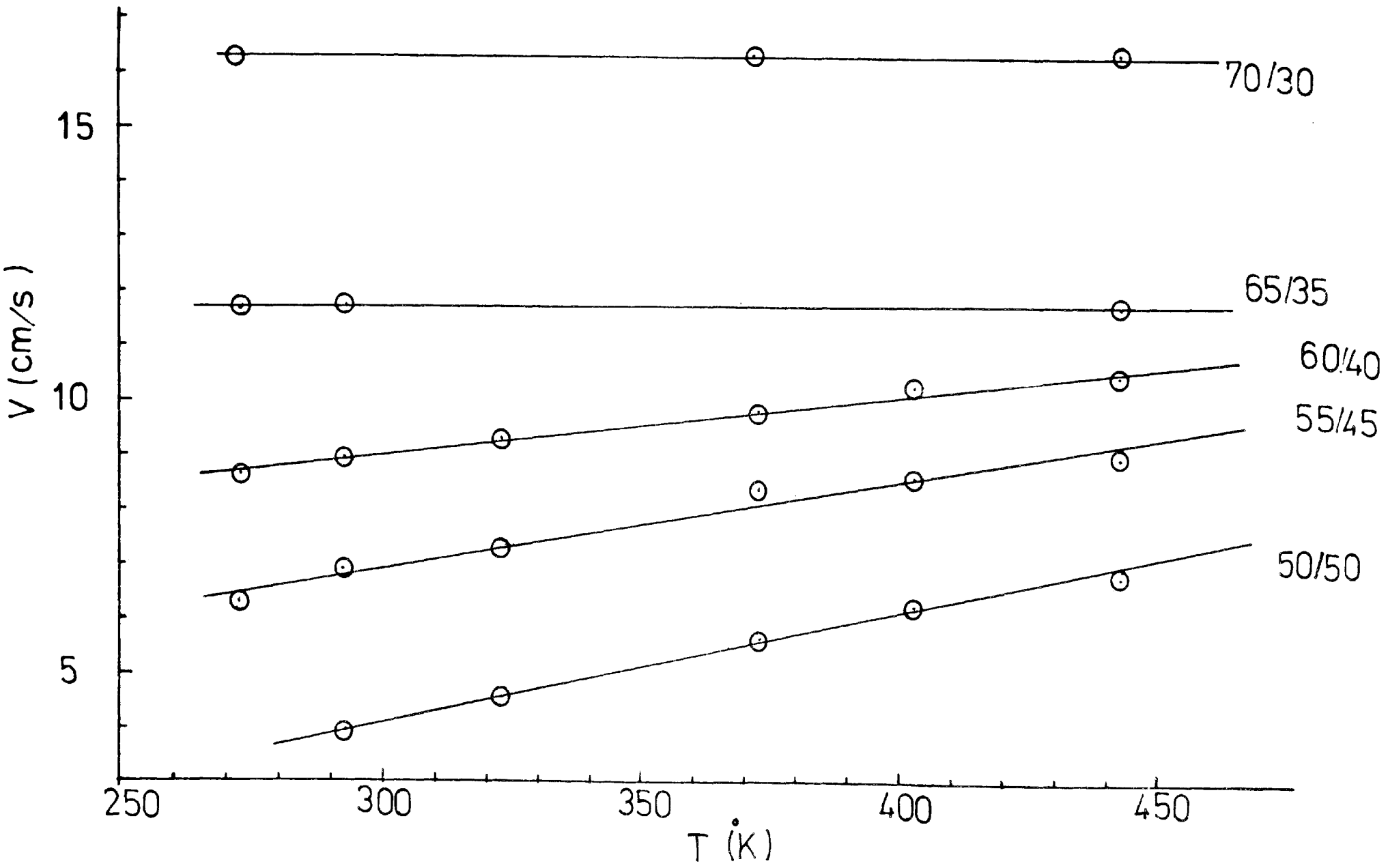

FIG. 5.1.16

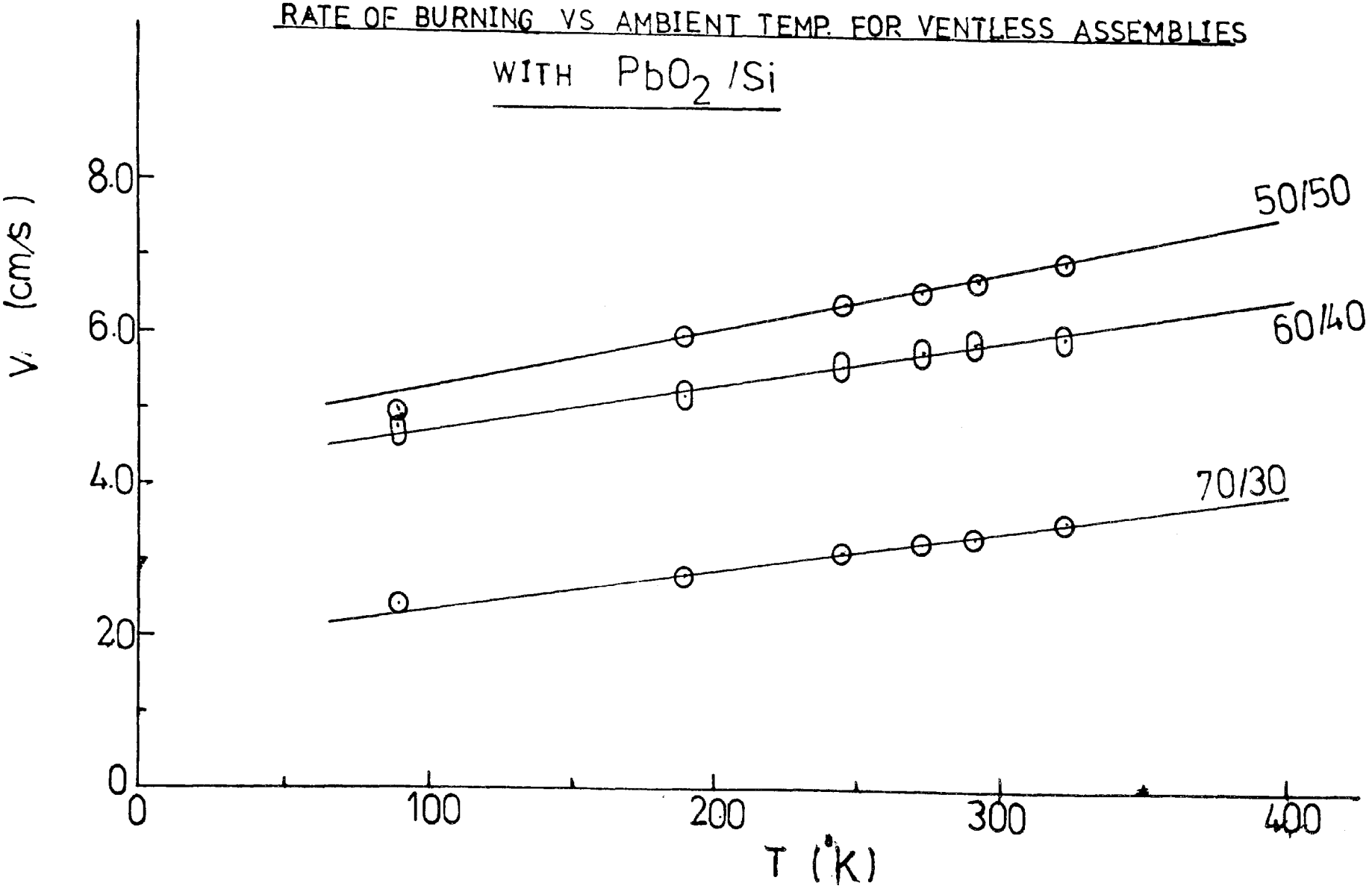
RATE OF BURNING VS AMBIENT TEMP. FOR VENTLESS ASSEMBLIES
WITH PbO_2 /Si
V (cm/s)
8.0
6.0
4.0
2.0
0
0
100
200
300
400
T (°K)
50/50
60/40
70/30

FIG. 5.1.17

RATE OF BURNING VS AMBIENT TEMPERATURE

FOR VENTED ASSEMBLIES WITH PbO_2/Si

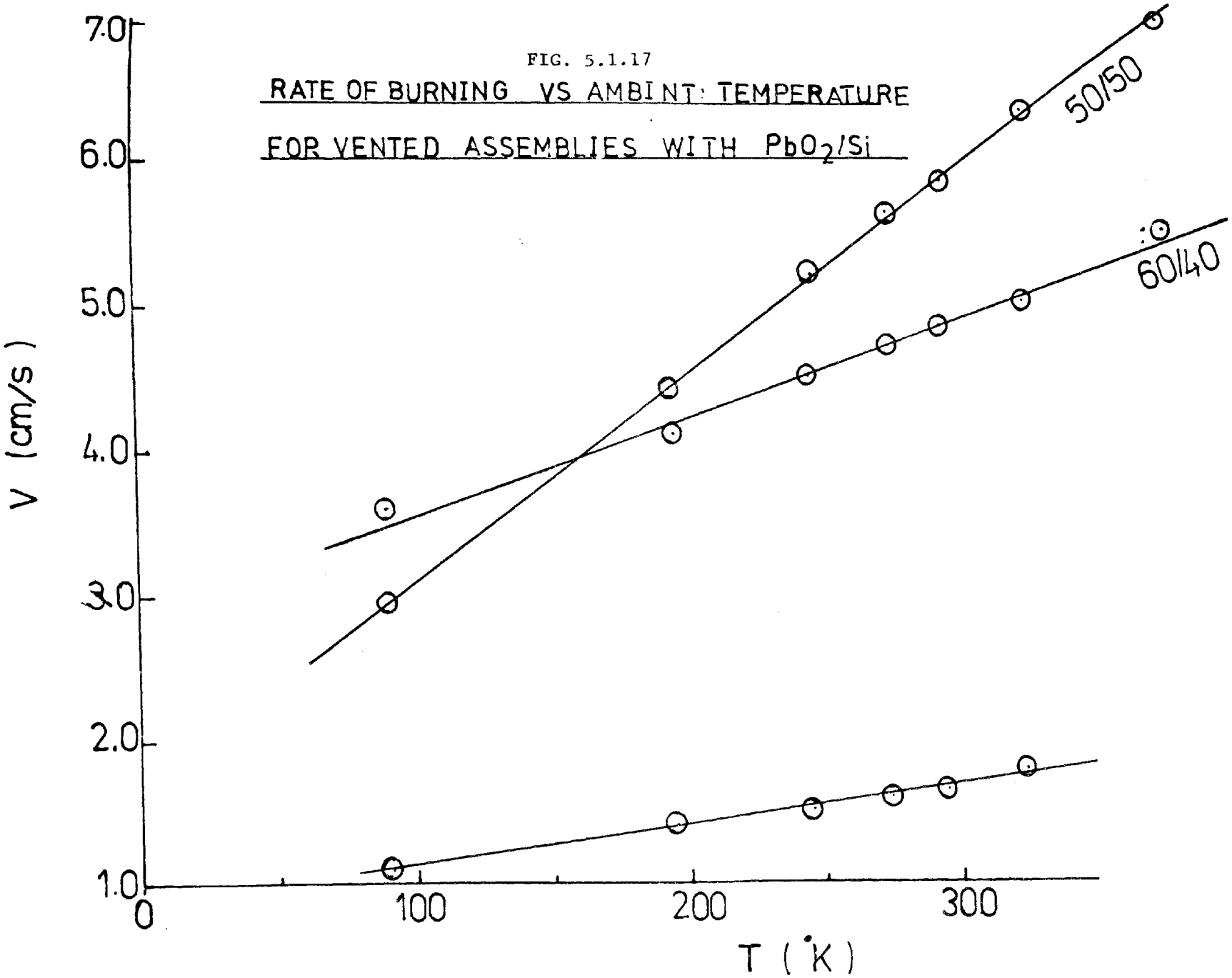

$$\Delta E_1 = E_R + E_A - Ep.$$

So heat produced ΔE_1 is increased by an amount E_A. However, this increase is significant in cases of 50 & 45% silicon compositions, but rather slight for the highly reactive mixtures containing 30 & 35% silicon which produce a large ΔE_1 Therefore the effect on the rate of burning of the latter sample is much smaller than on the former.

The same argument is put for the low temperature experiments. Another factor to be taken into consideration, is that of heat losses through radiation and conduction, which is very important in the case of samples containing 50% silicon, where the ignition temperature may not be sustained along the whole length of the column at temperatures of $0^{o}C$ and below. Firing the compositions at an elevated temperature will reduce this heat loss.

5.1.8 EFFECT OF DILUENTS ON RATE OF BURNING OF RED LEAD/SILICON COMPOSITIONS

As seen previously, it was possible to alter the rate of burning of a composition by altering the ratio of the oxidant to fuel, or the fuel particle size, or by altering the loading pressure, though the effect of this was rather limited. The alternative to this is to add a diluent, which in most cases is used to prolong the delay time, i.e. reducing the (R.B.), possibly by inhibition of reaction brought about by reducing the area of contact between the oxidant and the fuel particles. Also as the diluent absorbs heat to melt or to undergo a physical transformation, the temperature of

reaction products will be lowered leading to a reduction in (R.B.).

If the diluent takes part in the reaction, then it will compete with the fuel for the oxygen available, and depending on heat of reaction, it could reduce the total heat evolved and hence the rate of burning.

The diluents examined with the red lead/silicon system were: powders of iron, calcium fluoride, graphite, lead, lead chromate, potassium chromate, potassium dichromate, and barium sulphate. The effect of varying the amount of binder was also examined.

In all cases, the oxidant and silicon make up the datum weight and any diluent was calculated as a percentage of that weight. In all cases the diluents were passed through a 75 μm sieve, then added to the slurry of the prepared composition. The procedure that followed was identical to previously described.

5.1.8.1. EFFECT OF BINDER

Fig.5.1.18 shows the effect of increasing the percentage binder from 0.5 to 1.0%. It can be seen that the (R.B.) was slowed down for all Pb_3O_4/Si ratios, but the effect was more pronounced in the mixtures 55/45 to 70/30 (W/W). However, with increased binder the standard deviation of delay time readings was increased, making the compositions unreliable.

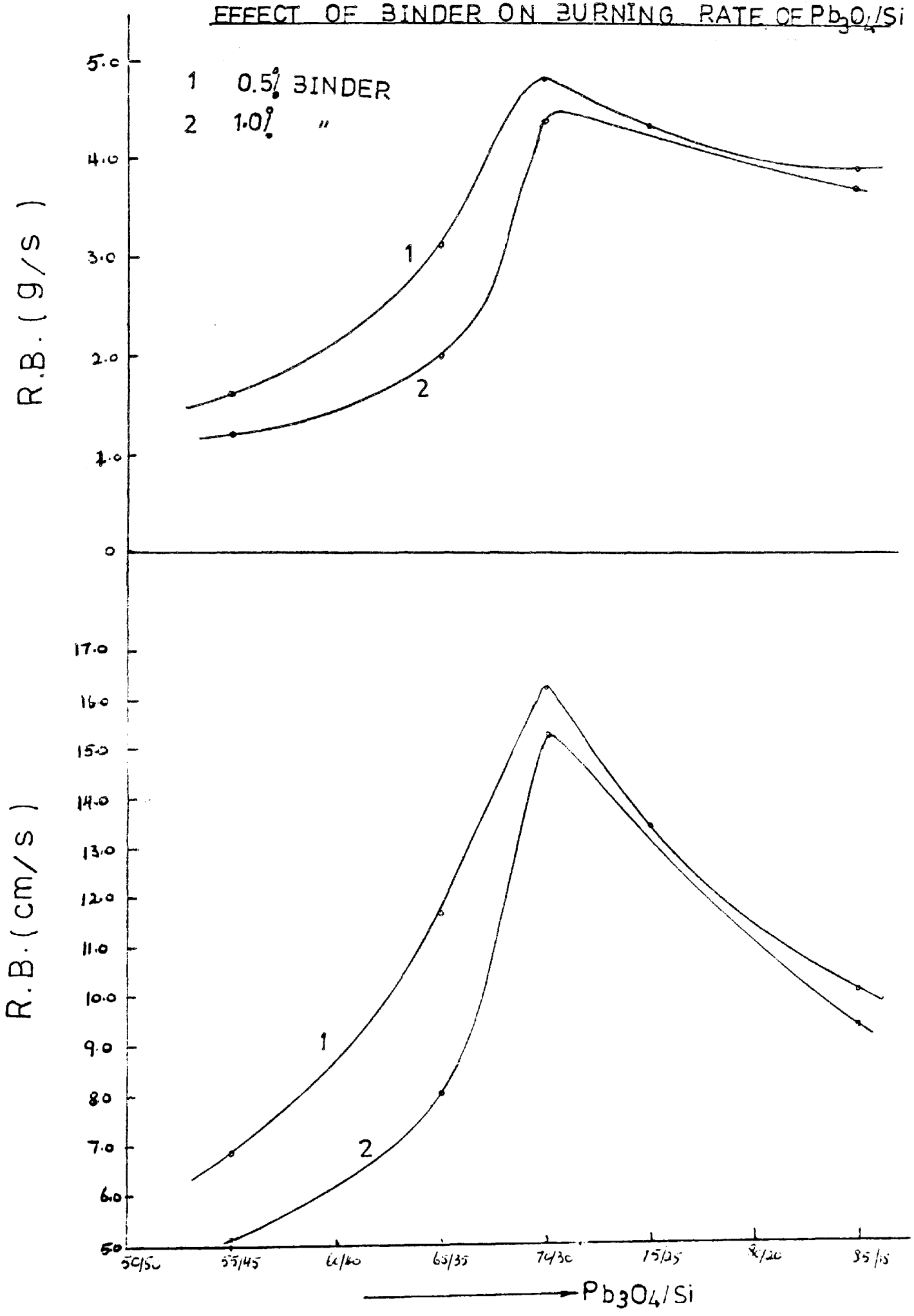
EFFECT OF BINDER ON BURNING RATE OF Pb3O4/Si
1 0.5% BINDER
2 1.0% "
R.B. (g/s)
5.0
4.0
3.0
2.0
1.0
0
1
2
R.B. (cm/s)
17.0
16.0
15.0
14.0
13.0
12.0
11.0
10.0
9.0
8.0
7.0
6.0
5.0
50/50
55/45
60/40
65/35
70/30
75/25
80/20
85/15
Pb3O4/Si

5.1.8.2 EFFECT OF IRON POWDER

A 60/40 (W/W) Pb_3O_4/Si was studied on its own, and then with the addition of different amounts of powdered iron of specific surface area 0.241 m^2/g. Fig.5.1.19 shows that the rate of burning was reduced slightly by adding up to 10.0% Fe, but then dropped sharply as the amount was increased further. The mixture failed to ignite for Fe greater than 40.0%.

The iron itself is a fuel, so its addition to the silicon will cause both to compete for the red lead. Since the heat evolved from the reaction with iron was less than that with silicon, the total heat produced was lowered, hence the rate of burning was reduced in spite of the improved thermal conductivity of the compacted mixture.

5.1.8.3 EFFECT OF CALCIUM FLUORIDE

When CaF_2 of specific surface area 15.28 m^2/g was added to 60/40 Pb_3O_4/Si, the (R.B.) was reduced enormously as in Fig.5.1.20 which shows that 17.0% of calcium fluoride gave the same effect as 40.0% iron.

The CaF_2 was acting purely as a physical barrier reducing the number of contact points between oxidant and fuel. At the same time it absorbed heat from the system to raise its temperature to that of reaction products. The large surface area made the influence of CaF_2 more pronounced.

FIG. 5.1.19

EFFECT OF IRON ON R.B. OF 60/40 Pb_3O_4/Si

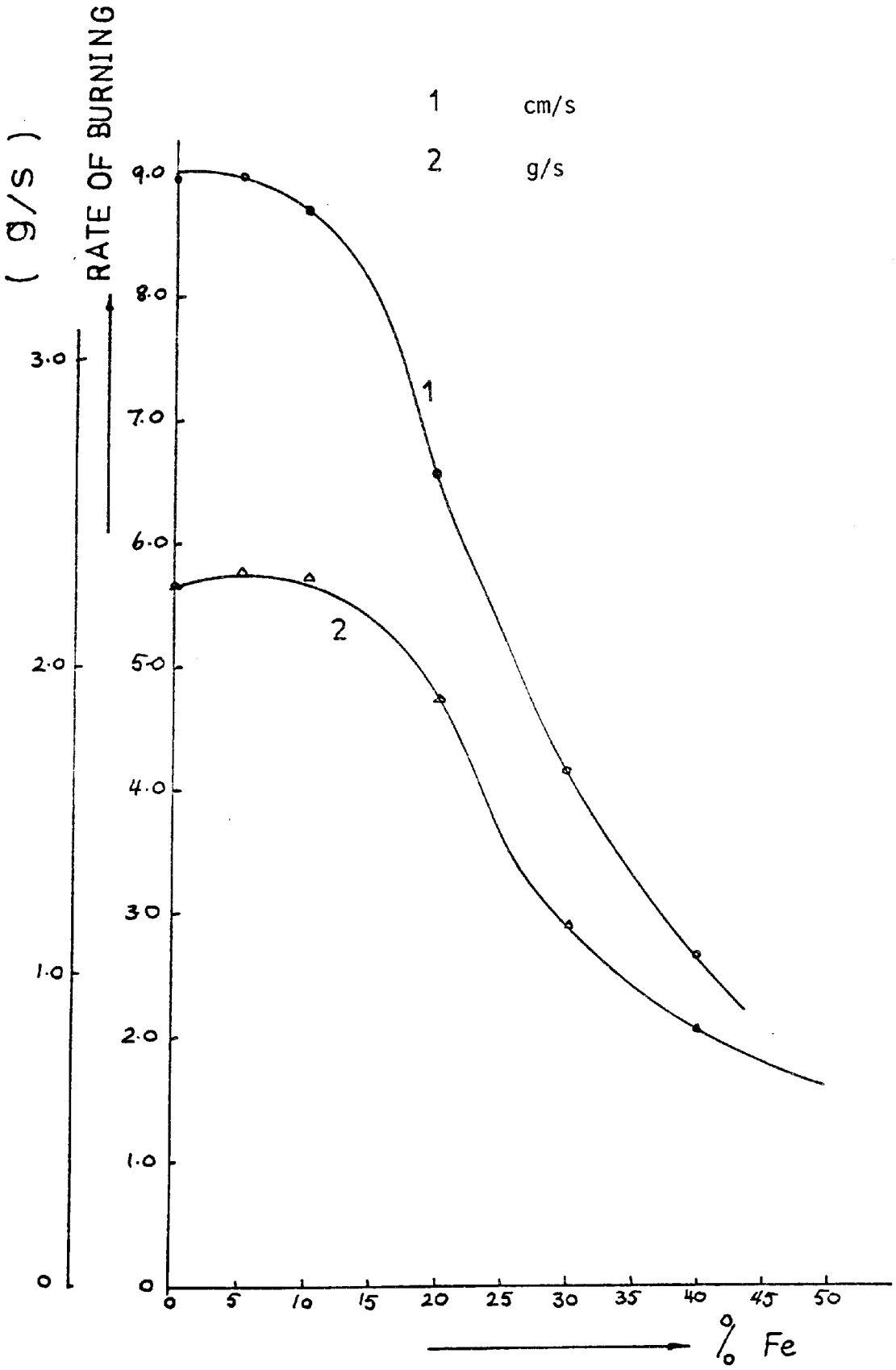

FIG. 5.1.20

EFFECT OF DILUENTS ON RATE OF BURNING OF 60/40 Pb_3O_4/Si

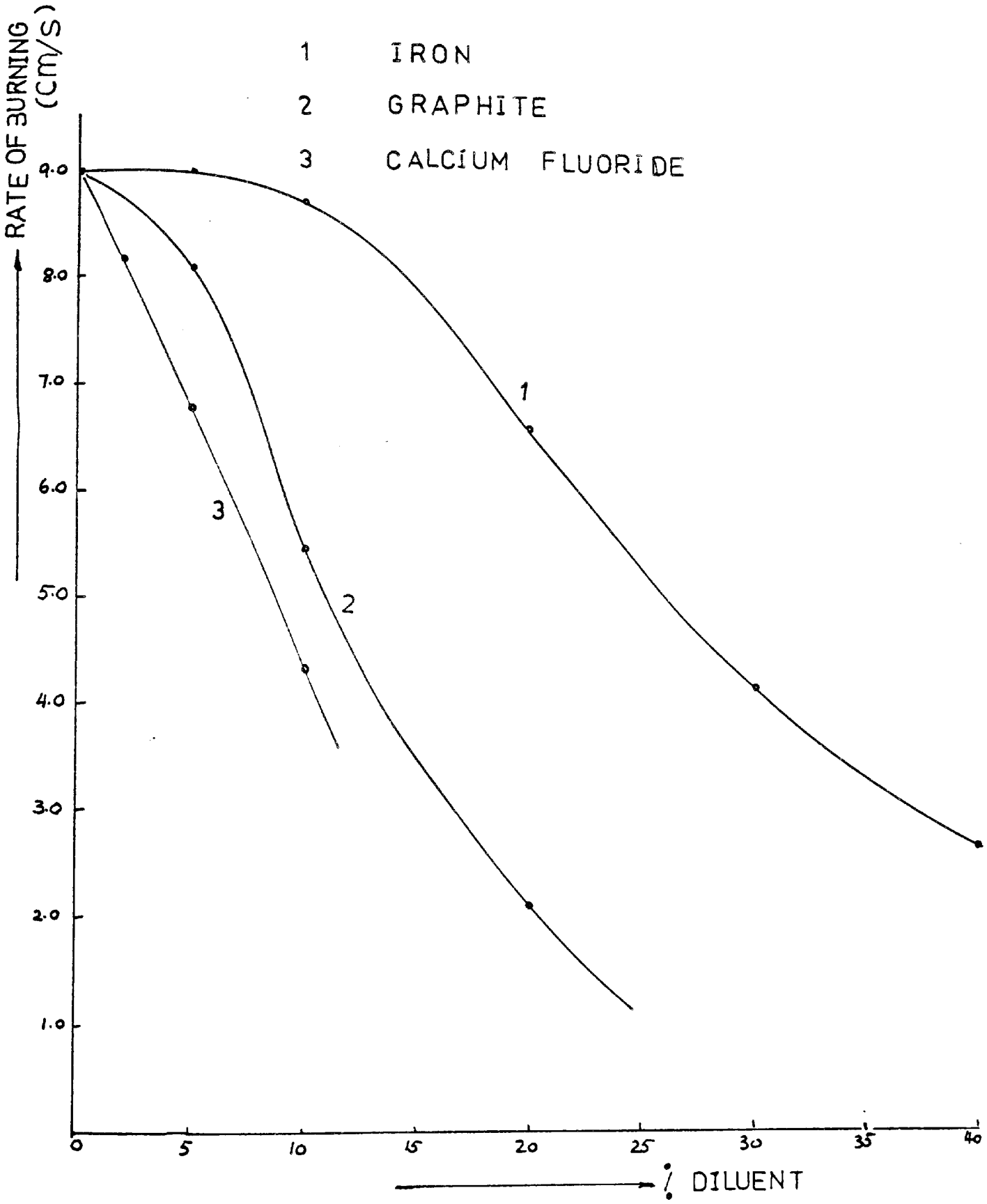

FIG. 5.1.21

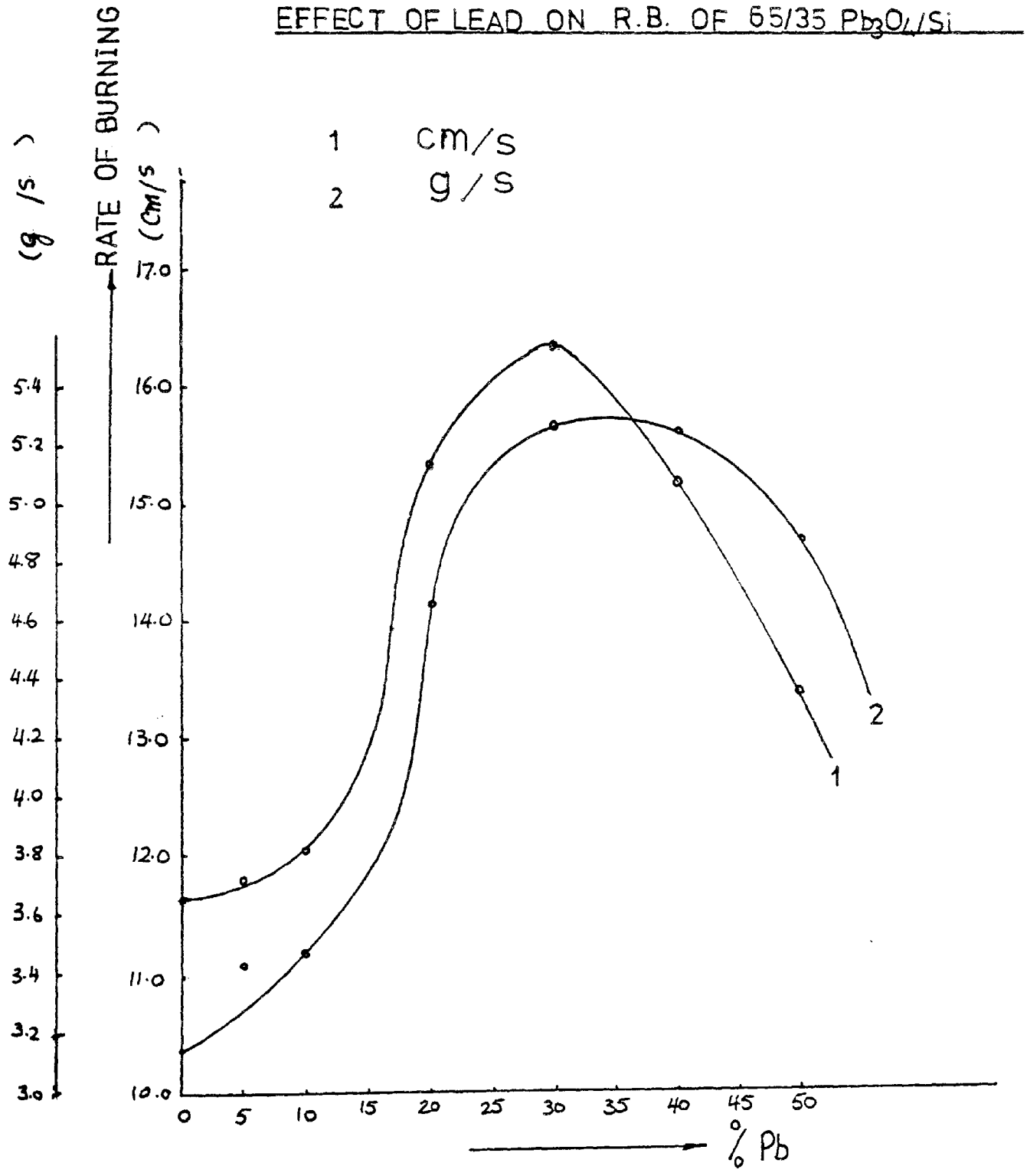
EFFECT OF LEAD ON R.B. OF 65/35 Pb_3O_4/Si
1 cm/s
2 g/s
RATE OF BURNING (cm/s)
(g/s)
17.0
16.0
15.0
14.0
13.0
12.0
11.0
10.0
5.4
5.2
5.0
4.8
4.6
4.4
4.2
4.0
3.8
3.6
3.4
3.2
3.0
0 5 10 15 20 25 30 35 40 45 50
% Pb
1
2

5.1.8.4 EFFECT OF GRAPHITE

Graphite powder of specific surface area 6.29 m^2/g and average particle size 11.2 μm was added in differing amounts to a 60/40 mixture. It is illustrated in Fig. 5.1.20 that the drop in (R.B.) is sharper than with iron or calcium fluoride, even when smaller amounts were used. The (R.B.) decreased in a straight line in relation with an increased percentage of graphite. A mixture containing more than 13% graphite failed to sustain burning.

5.1.8.5 EFFECT OF LEAD POWDER

Lead powder of specific surface area 0.057 m^2/g was added to a 65/35 red lead silicon. Instead of reducing (R.B.), the lead powder increased it when up to 30.0% was added. As this percentage was exceeded, the (R.B.) started to drop rather sharply as illustrated in Fig. 5.1.21. A possible interpretation of this behaviour is that as the lead melts at 327°C it will fill the pores, hence increasing the thermal conductivity of the pellet. It could also react with oxygen from decomposition of red lead, forming PbO which will react with silicon giving rise to higher temperature and subsequently a faster rate of burning.

Above 30.0% the Pb will require a significant amount of heat to melt it and this will counteract the above factors, causing reduction in (R.B.)

5.1.8.6 EFFECT OF OXYGEN CONTAINING SALTS

The effect of adding oxygenated salt was studied and the following were used:

(a) 10% lead chromate

(b) 10% barium sulphate

(c) 5% potassium chromate

(d) 10% potassium chromate

These were added to mixtures of (50/50, 55/45 ... 90/10) red lead/silicon, and as can be seen in Fig. 5.1.22, in all cases there occurred a slowing of (R.B.) over the whole range, except for 10% lead chromate which produced an increase in (R.B.) for mixtures 50/50 to 60/40.

Potassium chromate (10%) gave the slowest (R.B.), but the scatter of readings from which the average values were obtained was too high for practical application.

To produce a very slow burning composition, barium sulphate was added to a 55/45 mixture, and the plot of (R.B.) obtained against percentage barium sulphate resulted in a straight line. The (R.B.) was reduced from 6.3 cm/sec. for no diluent to 2.6 cm/sec. by addition of 20.0% barium sulphate. Further increase of this diluent resulted in the mixture failing to ignite, as shown in Fig. 5.1.23.

FIG. 5.1.22

EFFECT OF DILUENT ON RATE OF BURNING OF Pb_3O_4 /Si

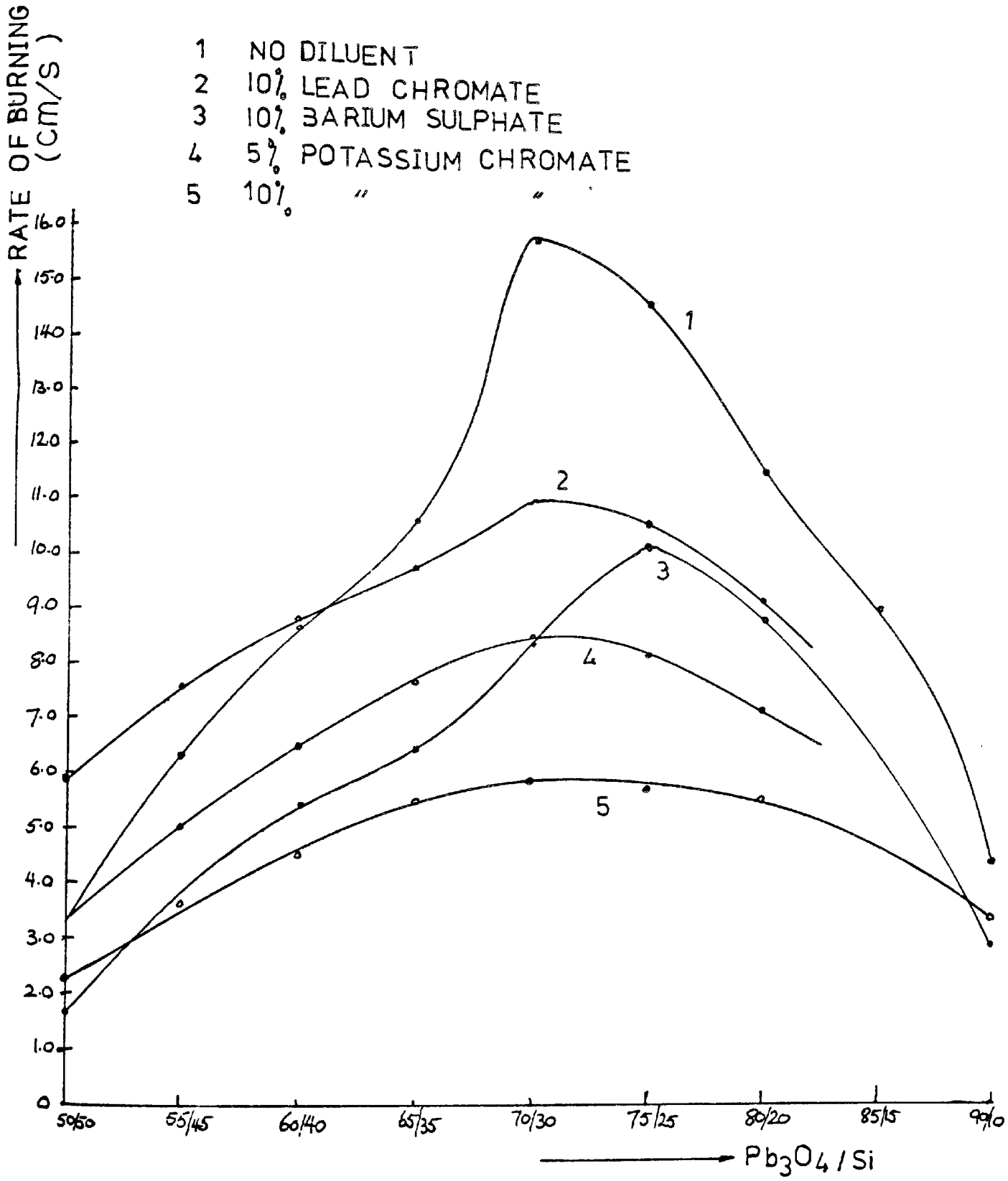

FIG. 5.1.23

EFFECT OF BARIUM SULPHATE ON RATE OF BURNING OF 55/45 Pb_3O_4 / Si

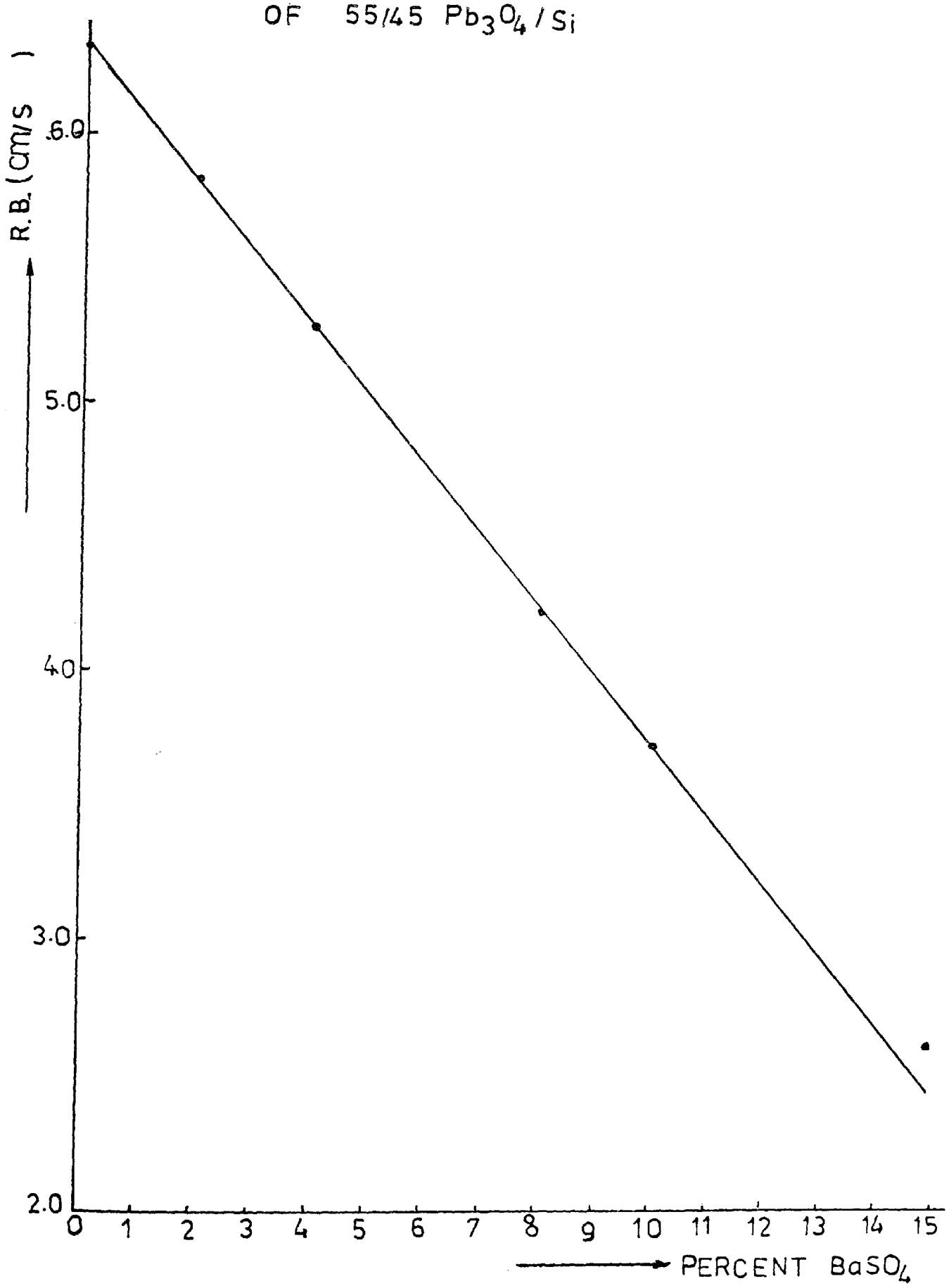

5.1.9 HEATS OF REACTION

The amount of heat evolved per gram of the mixture (Q) was evaluated by firing a known weight of the delay composition which had been prepared and compacted in delay tubes and placed in delay assemblies in the manner used for delay time measurement. The heat evolved was measured by using an adiabatic bomb calorimeter, and the samples were fired by passing a 5 amp current through the firing plug to ignite the fuseheads, which in turn ignited the experimental mixture. The heat generated from the fuseheads alone was measured by a separate experiment under identical conditions.

The heat evolved (Q) was found to increase as the percentage of silicon was reduced; reached a maximum at 10.0 and 13.0% silicon for red lead/silicon and lead dioxide/silicon respectively as illustrated by Figures 5.1.24 and 5.1.25.

Silicon powders A, B and C having respectively the following average particle size and surface area, 1.9 μm and 6.258 m^2/g, 3.9 μm and 2.543 m^2/g, 5 μm and 1.448 m^2/g, were used with the red lead and lead dioxide.

For red lead/silicon compositions containing silicon A, the heats of reaction were found to be in close agreement with calculated values from the equation

$$Pb_3O_4 + 2\ Si \rightarrow 3\ Pb + 2\ Si\ O_2$$

However, the silicon percentage at which maximum heat was evolved was 10.0% compared with 7.6% Si from the equation. With coarser silicon powders, B and C, the values of Q were lower than those of A,

especially for the very silicon rich samples (50/50 and 55/45). It is likely that due to the reduction in contact areas between coarser particles, the reduction of surface area and the low temperature of reaction of the high silicon compositions (i.e. insufficient oxidizer), coupled with absorption of some of the heat evolved by the large excess of silicon, the latter compositons did not undergo complete reaction. However, the three silicon powders gave the same pattern with Q maximum at approximately 10% Si as in Figure 5.1.24.

X-ray diffraction analysis and infra red spectroscopy results confirmed the presence of lead, unreacted silicon, and formation of silicon dioxide.

The theoretical (Q) was calculated by using the above chemical formula, and by using the values of heat of formation given by the National Bureau of Standards (41, 42).

$$\Delta H_f \quad Pb_3O_4 = -718.6 \text{ kJ/mol.}$$

$$H_f \quad SiO_2 = -903.7 \text{ kJ/mol.}$$

If a 90/10 (W/W) Pb_3O_4/Si is considered, then for a one gram sample, the silicon present is more than that required by the formula, hence 0.9 g. of red lead is considered to have completely reached

$$\text{The } SiO_2 = \frac{2 \times 60.1}{685.6} \times 0.9 \text{ g}$$

$$Q = 0.9 \left(-\frac{60.1 \times 2 \times 903.7}{685.6 \times 60.1} + \frac{718.6}{685.6} \right)$$

$$= -1427.7 \text{ J/g}$$

Heat evolved per mole of Pb_3O_4 = H

$$= \frac{1427.7}{1000} \times \frac{685.6}{0.9} = 1088.9 \text{ kJ}$$

For lead dioxide/silicon system; the three silicon sizes were used, and variation of (Q) with percentage silicon in the samples were plotted in Fig. 5.1.25. Q was found to increase with finer silicon particles. The maximum Q occurred at approximately 13.0% silicon, this can be compared with the stoichiometric silicon (10.5%) for the chemical equation

$$PbO_2 + Si \rightarrow Pb + SiO_2$$

From the figure 5.1.25, it can be seen that the amount of heat per gram observed and the amount of heat calculated from the above equation are compatible.

In accordance with the treatment by Spice and Stavely (10) the heat of reaction can be used to determine the chemical nature of the reaction. The method used calculates the amount of heat given off by the weight of mixture which contains one mole of oxidant (H). A plot of H against percentage silicon is made, as seen in Fig. 5.1.26. If (H) continues to increase as the silicon content is increased up to that composition where the silicon uses up all the oxidizer, this point theoretically corresponds to the stoichiometric composition.

For a PbO_2/Si, the possible reactions are

$$3\ PbO_2 + Si \rightarrow SiO_2 + 3PbO + \tfrac{1}{2}\ O_2$$

$$2PbO_2 + 3Si \rightarrow SiO_2 + 2SiO + 2Pb$$

$$PbO_2 + 2Si \rightarrow Pb + 2SiO$$

$$PbO_2 + 3Si \rightarrow Pb + Si + 2SiO$$

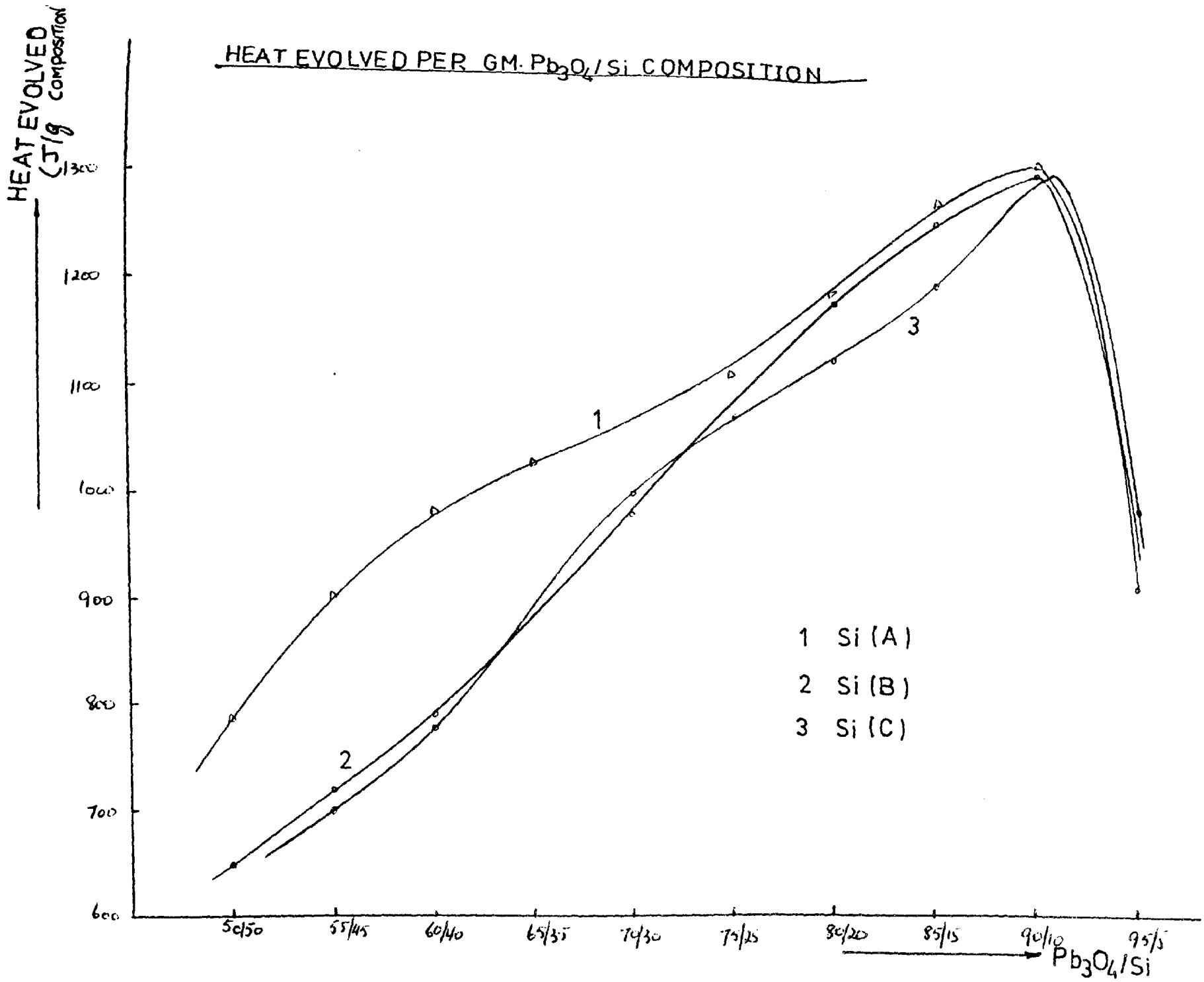
HEAT EVOLVED PER GM. Pb_3O_4/Si COMPOSITION
HEAT EVOLVED (J/g composition)
1300
1200
1100
1000
900
800
700
600
50/50
55/45
60/40
65/35
70/30
75/25
80/20
85/15
90/10
95/5
Pb_3O_4/Si
1
2
3
1 Si (A)
2 Si (B)
3 Si (C)

FIG. 5.1.24

FIG.5.1.25 HEAT EVOLVED PER GM MIXTURE OF PbO_2/Si

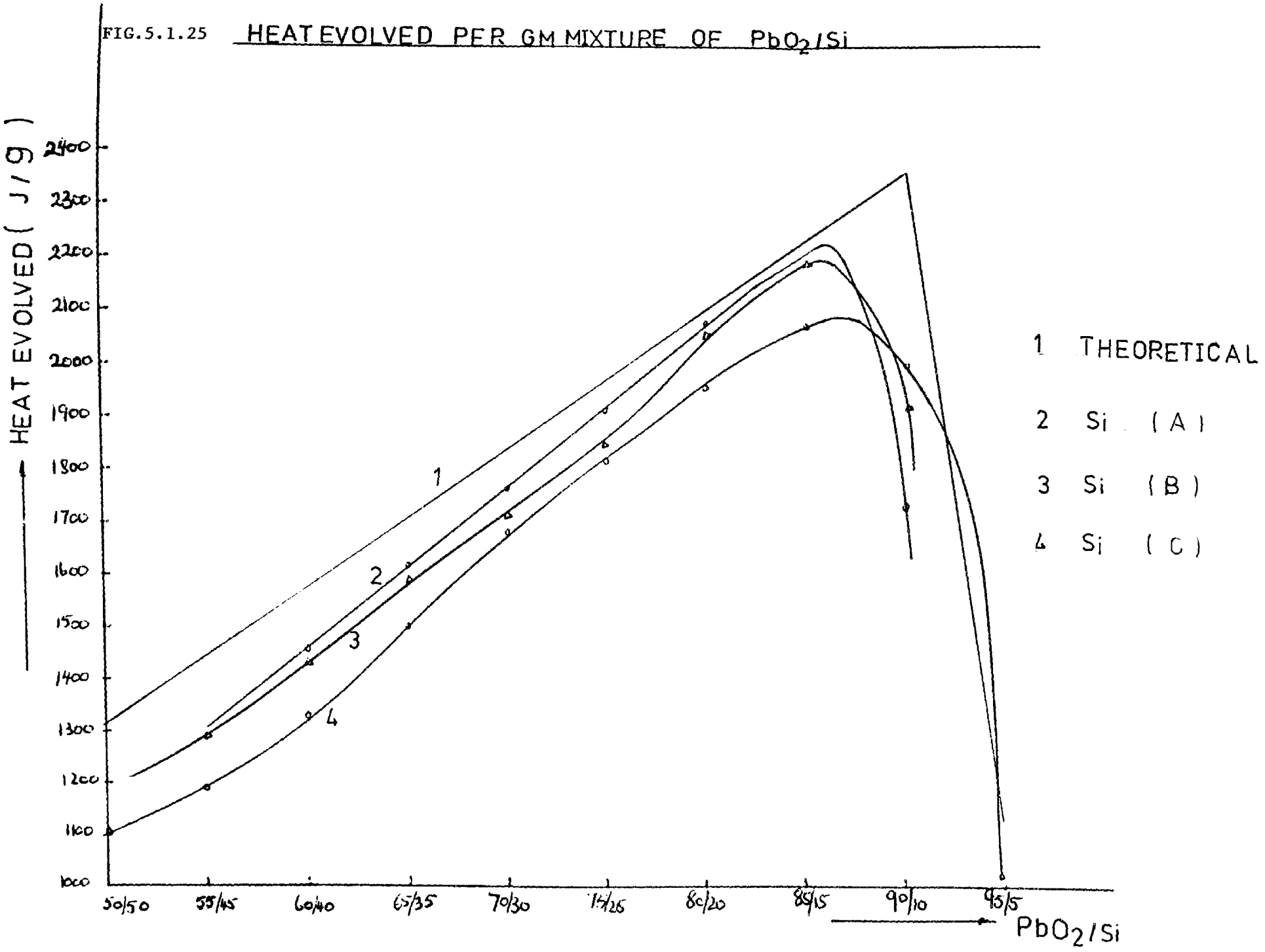

$$2PbO_2 + Si \rightarrow Pb_2 SiO_4$$

$$3PbO_2 + 2Si \rightarrow 2PbSiO_3 + Pb$$

$$PbO_2 + Si \rightarrow Pb + SiO_2$$

(H), from experiments increased up to 15.0% silicon, then stayed approximately constant. Although this is higher than the stoichiometric compositon of the last equation, it seems to be the most likely reaction, as X-ray diffraction analysis and infra red spectroscopy confirmed the presence of lead, silicon and silica in the slag.

From Fig.5.1.27 red lead/silicon compositions gave (H) values which increased up to 15% silicon, then stayed constant up to 30% silicon, but deviated above this point. This suggests that up to 30% silicon there existed only one reaction, the deviation that followed was quite likely due to incompletion of the reactions.

Correlation between heats of reactions and rates of burning

Theoretically, the maximum rate of burning should coincide with the maximum heat of reaction. The observed discrepancies from (Q) and (H) may be interpreted by the fact that as the reactions take place at the surface of the silicon particles, these become coated with a layer of products which prevent complete reaction of the silicon core even when in the molten state. Thus, in approaching the peak of the heat of reaction, the amount of silicon is reduced and the layer of product being thicker causes the rate of reaction, and hence the rate of burning, to drop. This occurs at a point richer in silicon than that for the maximum heat.

Another parameter is the rate of heat evolved, which is

calculated from Q values, and the weight burned per second. This weight of compressed composition burned was found to be directly proportional to the delay time. For silicon A, it was found that the heat evolved per second for various red lead/silicon ratios reached a maximum at approximately the same percentage of silicon as that at which rate of burning was maximum, indicating that the two parameters are significantly related to each other. This pattern was also true for coarser silicon powders, but it was observed that some deviation occurred at approximately 10% Si. However, at this point, the time of burning was markedly influenced by the high pressure generated inside the tubes, due to the rapid rise of temperature, making the rate of burning somewhat unreliable.

The finer the powder, the closer were the values of percentage silicon at which rate of burning and Q were maximum as in Fig. 5.1.28.

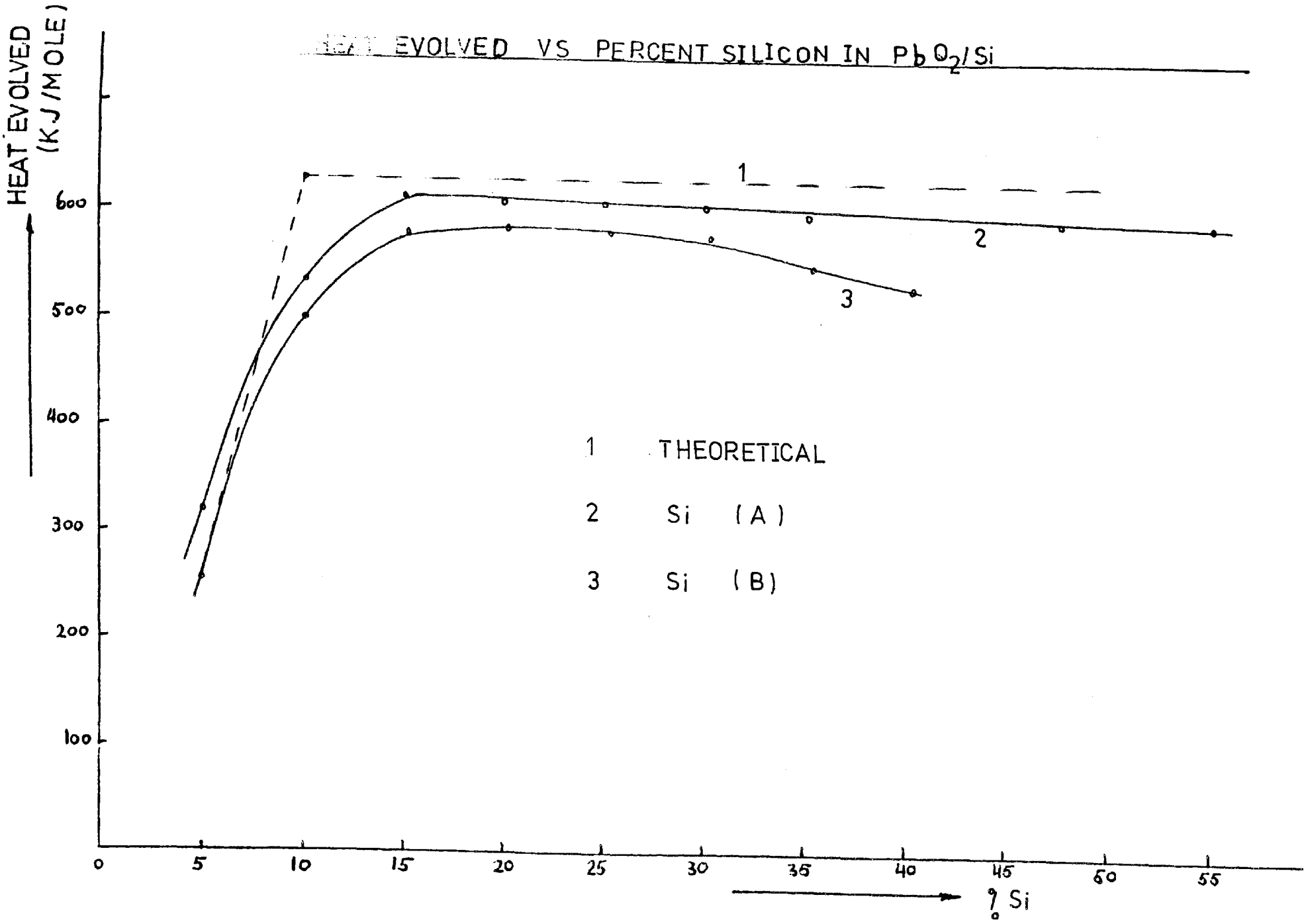
HEAT EVOLVED VS PERCENT SILICON IN PbO_2/Si
HEAT EVOLVED (KJ/MOLE)
600
500
400
300
200
100
0
5
10
15
20
25
30
35
40
45
50
55
% Si
1
2
3
1 THEORETICAL
2 Si (A)
3 Si (B)

FIG. 5.1.26

FIG. 5.1.27 HEAT EVOLVED PER MOLE Pb_3O_4 VS PERCENT SILICON

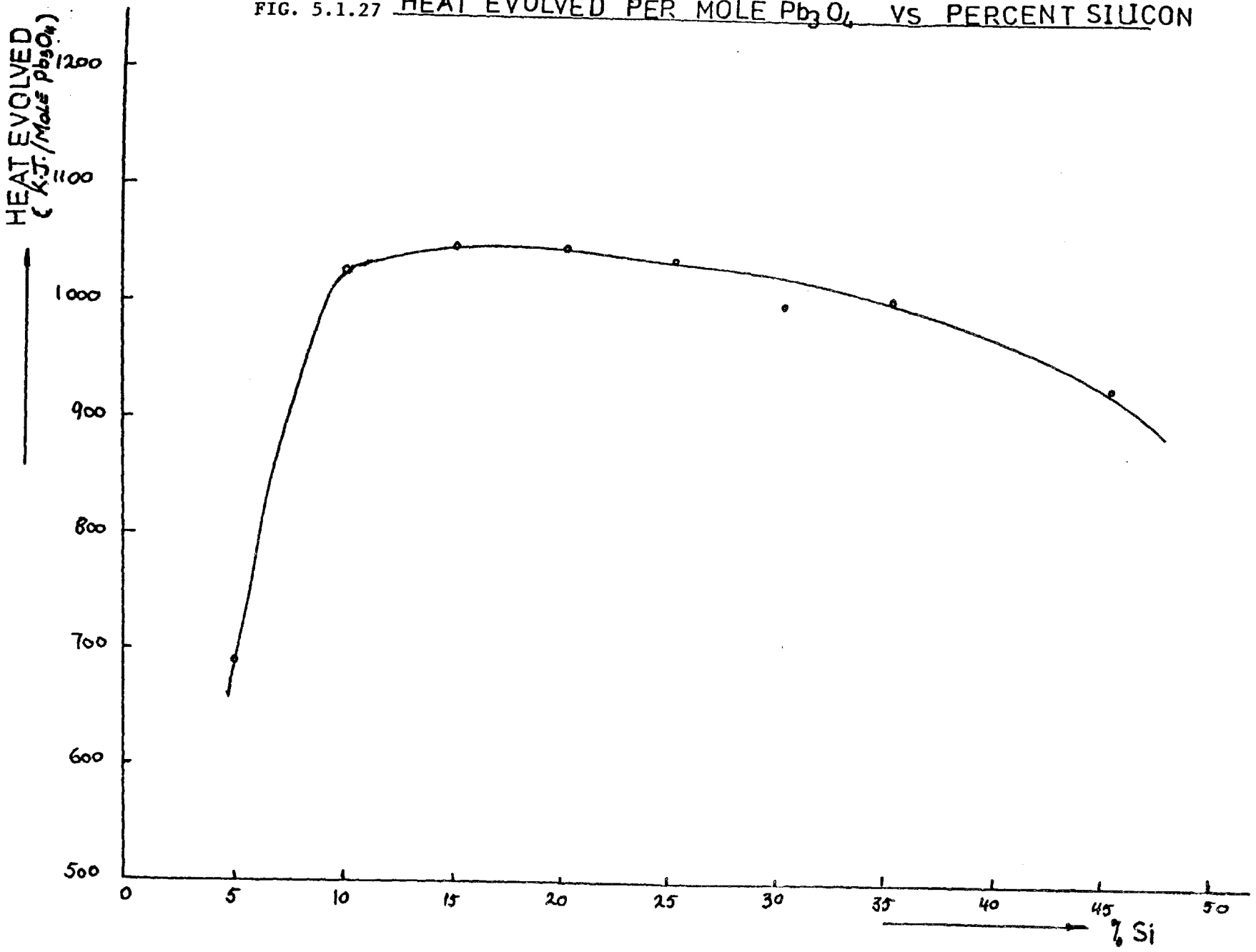

FIG. 5.1.28

1 J/g VS % Si IN Pb_3O_4/Si
2 cm/s " " " "
3 J/s " " " "

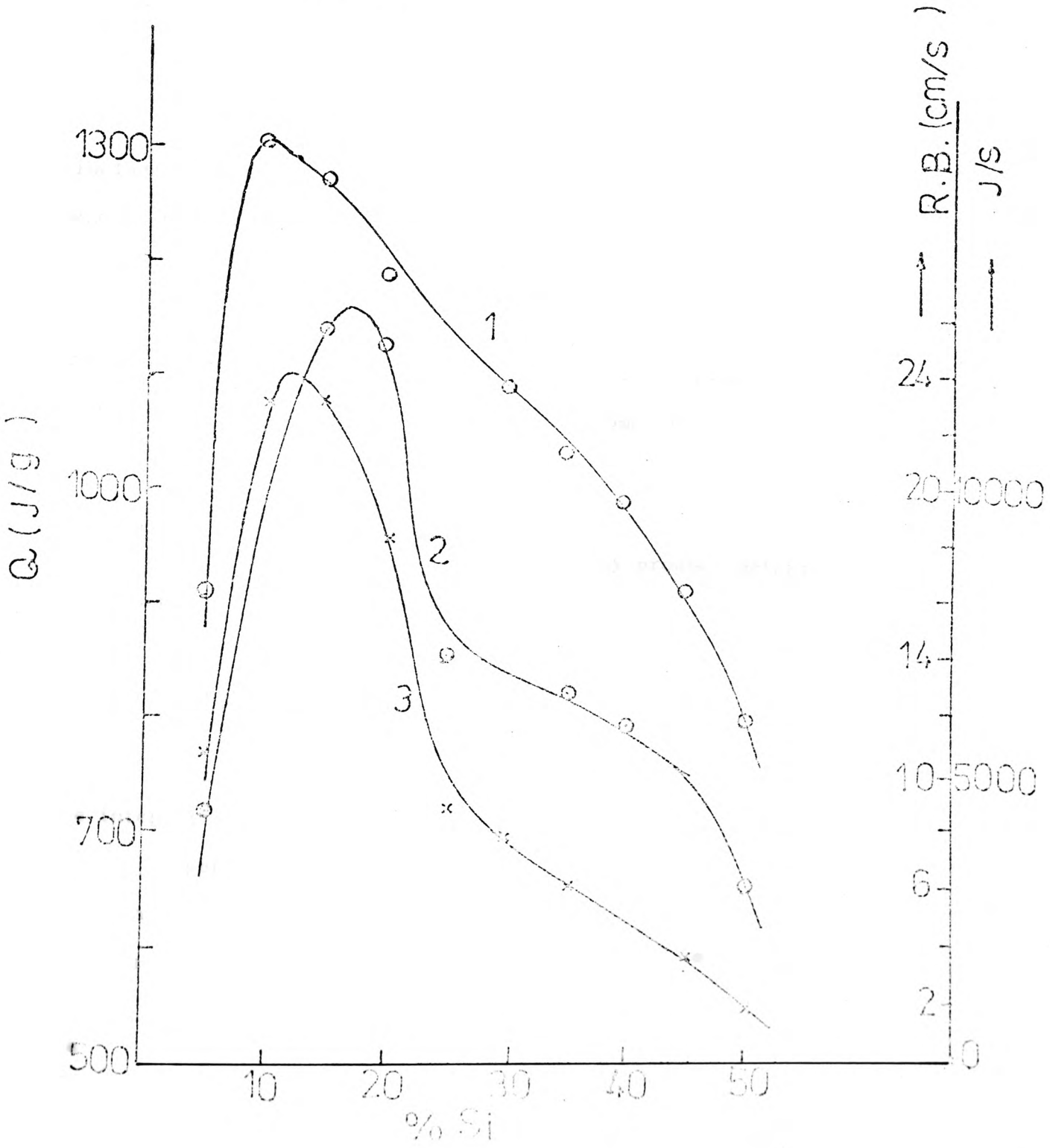

5.1.10 MAXIMUM TEMPERATURE OF REDLEAD/SILICON REACTION:

If it is assumed that in a burning pellet, the reaction proceeds without loss of heat, then the reaction products will assume a definite temperature, sometimes referred to as adiabetic-reaction temperature. In a reaction taking place at a constant pressure where the only energy term involved is internal energy, the enthalpy change is zero. The temperature of the products which corresponds to the total enthalpy may be calculated by expressing the enthalpy of the products as a function of temperature.

The products considered in calculating the maximum temperature include all materials actually present in the final system; inerts and excess reactants as well as the new compounds formed are included.

If the reaction is incomplete, only the standard heat of reaction resulting from the degree of completion actually obtained is considered, and the products will include some of each of the original reactants.

The enthalpy ΣH_p of N_i moles of any product material at a temperature T^oK is expressed by

$$\Sigma H_p = \Sigma n_i \cdot C_i \int_{298}^{T} dT + \Sigma n_i \lambda_i$$

The integration term refers to the change in enthalpy of component i for the temperature change of each phase, and $\Sigma n_i \lambda_i$ refers to all latent heats of all phase changes of component i in being heated from its reference state to the maximum temperature of reaction at constant

pressure. Where heat capacity C_i is expressed as a quadratic function of temperature,

$C_i = a_i + b_i T - c_i T^{-2}$ upon integration:

$$\Sigma H_p = \Sigma n_i \left[a_i (T-298) + \frac{b_i}{2}(T^2-(298)^2) + c_i \left(\frac{1}{T} - \frac{1}{298}\right)\right] + \Sigma n_i \lambda_i$$

The equation is solved by assuming values of T until the equality is satisfied. Temperature values are obtained for both observed and theoretically calculated heats of reactions according to the equation

$$Pb_3O_4 + 2Si \rightarrow 3Pb + 2SiO_2$$

It can be seen from the values of T obtained from observed heats of reaction as in Fig.5.1.29that there are three temperature ranges. The first one for mixtures 50/50 and 55/45, where the temperature rises to below the melting point of silicon 1683K, then for 60/40, 65/35 and 70/30, the temperature stayed constant at 1683°K, the increasing exothermicity of the last three compositions only contributes to melting more of the silicon present in excess. As the percentage silicon is reduced further (25% and below), the heat evolved is found to be more than is required for melting the lead, excess silicon and the silica formed, and the lead will therefore start to vapourise at 2024°K if the reaction proceeds at atmospheric pressure.

The following table shows the adiabatic reaction temperatures for the range 50/50 to 90/10 Pb_3O_4/Si:

Pb_3O_4/Si (w/w)	TEMPERATURE ^oK		
	FROM THEORETICAL H	FROM OBSERVED H	OBSERVED T
50/50	1550	1365	1007
55/45	1683	1620	1243
60/40	1683	1683	1473
65/35	1683	1683	1613
70/30	1683	1683	1743
75/25	2024	2024	1963
80/20	2024	2024	-
85/15	2024	2024	-
90/10	2024	2024	-

A composition fired in a small diameter delay tube (0.33 cm) and contained in an aluminium tube 0.66 cm diameter loses a significant amount of heat to these metal containers and also to the surrounding atmosphere, due to the large temperature difference. The temperatures recorded which are shown in the table above are seen to exhibit a large difference from calculated values for the compositions 50/50 and 55/45 when the temperature is below the melting point of silicon: but for 65/35 and 70/30 the heat losses from the reaction will be mainly that of latent heat of fusion of the silicon and will therefore not give rise to a large discrepancy between them and calculated values.

In sealed assemblies, the pressure inside the detonator tube will rise due to the sharp change in temperature, and vapourisation of lead will take place at higher than 2024^oK. If the pressure is high enough to suppress any vapourisation, and the heat of reaction only contributes to raising the temperature of the products, then the maximum

temperature of reaction will be as follows:

Pb_3O_4/Si	CALCULATED T.^oK
75/25	2030
80/20	2442
85/15	3055
90/10	3862

If the reaction occurs under varying pressure, the temperature can be related to the pressure by the expression

$$\ell n \left(\frac{P_2}{P_1}\right) = - \Delta H_v \left(\frac{1}{T_2} - \frac{1}{T_1}\right)$$

where P_1 is atmospheric pressure

P_2 is any pressure considered.

T_1 and T_2 are temperatures at P_1 and P_2 respectively

ΔH_v is the heat of vapourisation

R universal gas constant.

The assumptions made in the above expressions are:

(i) The vapour behaves as an ideal gas

(ii) ΔH_v is independent of temperature

(iii) The system is at equilibrium

Temperature values at different pressures calculated according to the above relation is shown in the following table:

FIG. 5.1.29

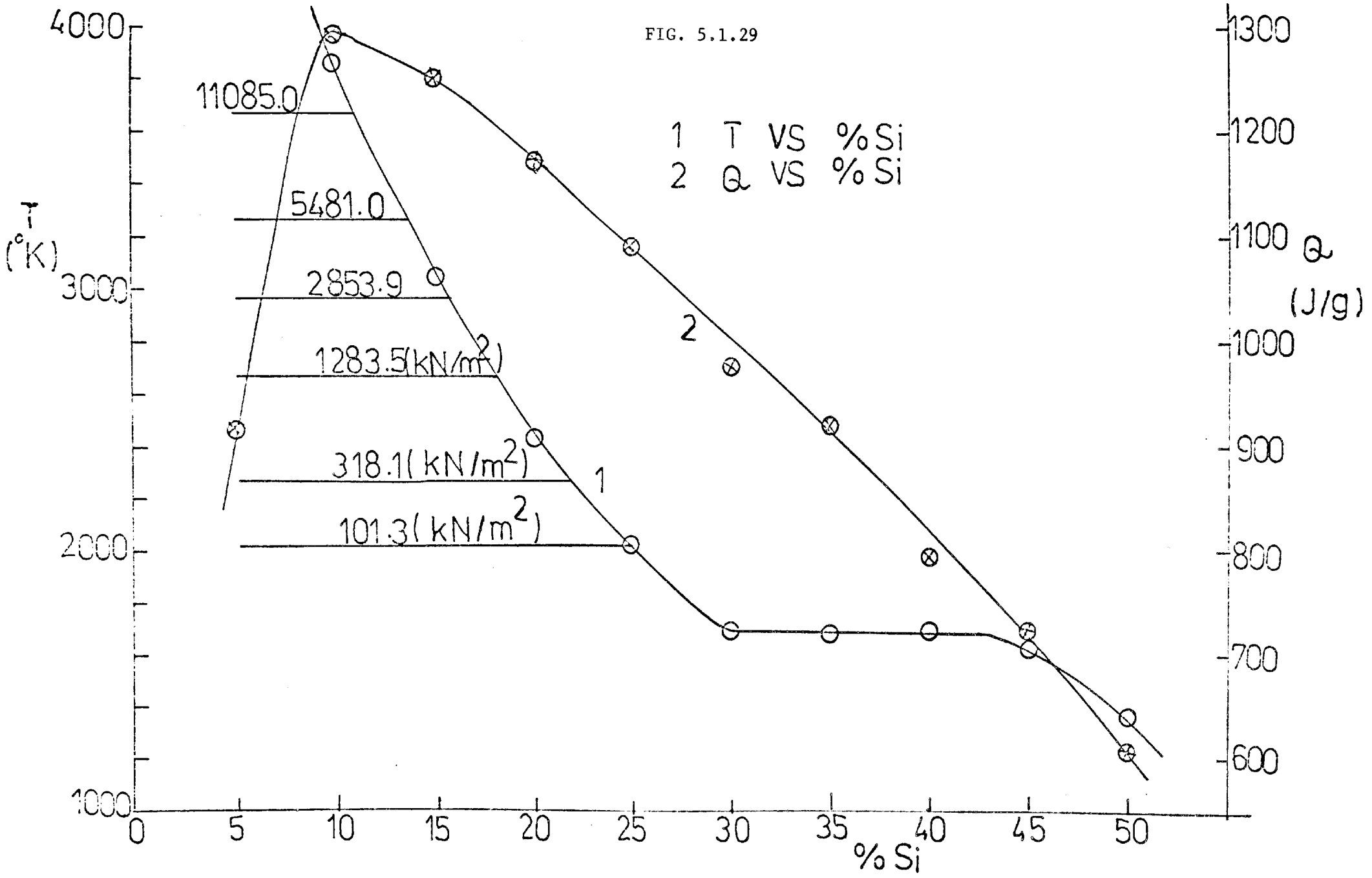
4000
3000
2000
1000
T (°K)
1300
1200
1100
1000
900
800
700
600
Q (J/g)
11085.0
5481.0
2853.9
1283.5(kN/m²)
318.1(kN/m²)
101.3(kN/m²)
1 T VS %Si
2 Q VS %Si
1
2
0
5
10
15
20
25
30
35
40
45
50
% Si

TEMPERATURE ^{o}K	PRESSURE kN/m^2
2024	101.3 (atmospheric p)
2273	318.08
2673	1283.47
2973	2853.88
3273	5481.04
3673	11085.06
4273	24898.53

Delay composition of weight ratio 50/50 Pb_3O_4/Si gives a calculated temperature 1365K. If the silicon content is increased above 50%, the reaction fails to propagate along the whole length of the pellet, therefore the reduction in temperature due to increase of silicon causes the reaction to cease. It can be concluded that for self propagation to be possible, the reaction must be sufficiently exothermic for a reaction zone to reach a calculated temperature of 1365K, or higher.

Measurements are made of how much inert material can be added to a composition before the combustion reaction will no longer propagate. The following results are obtained:

DELAY COMP. Pb_3O_4/Si (w/w)	DILUENT	WT. DILUENT PER g. COMPOSITION	
		CALCULATED (g)	ACTUAL (g)
55/45	$BaSO_4$	0.218	0.200
60/40	CaF_2	0.236	0.250
60/40	Graphite C	0.142	0.130
65/35	Pb	2.412	-

The agreement between calculated and actual amount of diluent required to reduce the adiabatic reaction temperature to 1365^{o}K is seen from the table on the previous page to be fairly good.

5.1.11 THERMAL CONDUCTIVITY OF COMPACTED POWDERS:

Thermal conductivity is the quantity of heat in the steady state condition passing in unit time through an area forming part of a slab of a uniform material of infinite extent with flat and parallel faces.

$$Q = \frac{k\,A(T_{s_1} - T_{s_2})}{L}$$

If, in the equipment previously described, it is assumed that conditions are quasi-steady state, and if edge effects are neglected, it is possible to equate the heat flow through the silica and the specimen so that

$$\frac{k_s}{L_s}(T_H - T_M) = \frac{k_{sp}}{L_{sp}}(T_M - T_C)$$

$$\text{i.e. } \frac{k_{sp}}{L_{sp}} = \frac{k_s}{L_s}\,\frac{(T_H - T_M)}{T_M - T_C}$$

For the equipment $L_s = 1$ cm

$k_s = 0.0142$ J/g.cm^2 deg/cm.

$T_M = 80.2^{\circ}$C

$T_C + 0^{\circ}$C

$$\text{i.e. } k_{sp} = L_{sp} \times 0.0142\,\frac{(T_H - 80.2)}{80.2}$$

where

k_s is the known thermal conductivity of the silica

k_{sp} is the unknown thermal conductivity of the specimen

L_s, L_{sp} are the thickness of the silica and specimen respectively

T_H is the temperature of the lower face of the silica in contact with the copper black

T_M is the temperature of the silica/specimen interface which corresponds to m.pt of naphthalene.

T_c is the temperature of the upper face of the specimen = 0^oC.

TABLE 5.1.28

Thermal Conductivity of Pb_3O_4/Si Compositions

Pb_3O_4/Si	DENSITY g/c.c.	THERMAL CONDUCTIVITY $J.s^{-1}\ cm.^{-2}\ deg\ c.^{-1}\ cm$
50/50	2.31	2.200×10^{-3}
	2.40	2.555×10^{-3}
	2.53	2.31×10^{-3}
60/40	2.47	1.844×10^{-3}
	2.69	2.009×10^{-3}
65/35	2.705	1.903×10^{-3}
	3.05	2.121×10^{-3}
	3.20	2.152×10^{-3}
70/30	2.69	1.527×10^{-3}
	2.82	1.692×10^{-3}
80/20	3.69	1.844×10^{-3}
	3.76	2.092×10^{-3}
	3.82	2.103×10^{-3}

5.1.12 A MATHEMATICAL MODEL FOR THE ANALYSIS OF THE SELF-SUSTAINED COMBUSTION BETWEEN SILICON AND RED LEAD IN A COMPRESSED FORM

In previous studies, with iron/potassium permanganate mixtures, the data were analysed to determine the order of reaction and activation energy with the help of temperature profile analysis developed by Hill (3,4,67) This method was described by Hill et al in 1950-54 and since then few developments, in the method of analysis of combustion results have appeared in the literature.

If finely divided solid powders, composed of mixtures of oxidants and reductants are ignited in pellet form by applying a strong heating source, a reaction zone is formed which spreads through the mixture from the point of ignition. In the reaction zone, the temperature is usually high, and the heat released conducts to the next layer of unburnt mixture due to the temperature gradient that develops, raising it to its ignition temperature. This type of behaviour is only observed when the reaction is strongly exothermic, so that a considerable amount of heat is evolved in the chemical change that occurs in the reaction zone.

With the progress of reaction, the temperature at a point in the pellet will rise and can be measured by a fine thermojunction and recorded to give a temperature-time profile as shown in Fig. 5.1.30-32 This temperature profile can be analysed to obtain reaction rate, burning rate and activation energy.

In a combustion zone, the rate of reaction can be related to the temperature rise through an energy balance over a thin section. This energy balance, assuming negligible heat losses through the

surface of the section, and for one-dimensional heat flow along the direction "x" leads to

$$\rho q \frac{d\varepsilon}{dt} + k \frac{d^2T}{dx^2} - \rho C \frac{dT}{dt} = 0 \qquad \ldots \qquad (1)$$

By substituting dx = Vdt and integrating for temperature between T_o and some value T equation (1) gives

$$\rho q\varepsilon + \frac{\bar{k}}{V^2} \cdot \frac{dT}{dt} - \rho \bar{C} (T - T_o) = 0 \qquad \ldots \qquad (2)$$

where $\bar{c}$ and $\bar{k}$ are average values over the temperature range To to T

Expressing the heat of reaction by

$$q = \bar{C} (T_f - T_o) \qquad \ldots \qquad (3)$$

equation (2) can be expressed by

$$\varepsilon = \frac{1}{T_f - T_o} \left[(T - T_o) - \frac{\bar{k}}{\bar{C}\rho V^2} \cdot \frac{dT}{dt} \right] \qquad \ldots \qquad (4)$$

The equation can be converted into a dimensionless form by defining a dimensionless temperature, θ

$$\theta = \frac{T - T_o}{T_f - T_o} \qquad \ldots \qquad (5)$$

$$\frac{d\theta}{dt} = \frac{dT}{dt} \Big/ (T_f - T_o) \qquad \ldots \qquad (6)$$

and then substituting in equation (4) gives

$$\varepsilon = \theta - \frac{\bar{k}}{\bar{C}\rho V^2} \cdot \frac{d\theta}{dt} \qquad \ldots \qquad (7)$$

An expression for ε can be found if θ is expressed as a function of time.

To describe the temperature profile, θ must range from 0 to 1 over the temperature range

$$T = T_o \text{ to } T = T_f$$

A function of the form

$$\theta = 1 - e^{-\left(\frac{t}{\alpha}\right)^{\beta}} \qquad \ldots \qquad (8)$$

is found to satisfy the above conditions over the period

$$t = 0 \text{ to } \infty$$

From this function, substitution of θ and $d\theta/dt$ in equation (7) gives

$$\varepsilon = 1 - e^{-\left(\frac{t}{\alpha}\right)^{\beta}} \cdot \left[1 + \frac{\bar{k}\beta}{\bar{c}\rho V^2 \alpha} \cdot \left(\frac{t}{\alpha}\right)^{\beta-1} \right] \qquad \ldots \qquad (9)$$

If $\bar{k}$, $\bar{c}$, and ρ remain constant over the reaction time, the rate of reaction can be found from equation (9).

Thus

$$\frac{d\varepsilon}{dt} = K_R \left[(1 - \varepsilon) + \left(\frac{\beta-1}{t}\right) \cdot \frac{\bar{k}}{\rho \bar{c} V^2} \right] \qquad \ldots \qquad (10)$$

where $K_R = \left(\frac{\beta}{\alpha}\right) \left(\frac{t}{\alpha}\right)^{\beta-1}$ $\qquad \ldots \qquad (11)$

For the compositions studied, the thermal diffusivity $(k/C\rho)$ is low as shown in Table 5.1.32 so the second term in the bracket of equation (9) can be neglected and then equation (10) gives

$$\frac{d\varepsilon}{dt} = K_R \ (1 - \varepsilon) \qquad \ldots \qquad (12)$$

Substitution of K_R in equation (12) from equation (11) and integrating from t = o to time t gives

$$\varepsilon = 1 - e^{-(\frac{t}{\alpha})^{\beta}} \quad \ldots \quad (13)$$

which describes the extent of reaction as a function of time

At $t = \alpha$, equation (12) leads to

$$\frac{d\varepsilon}{dt} = (\frac{\beta}{\alpha})\ (1 - \varepsilon) \quad \ldots \quad (14)$$

which is a first order rate equation with a specific rate constant

$$K(T) = (\beta/_{\alpha}) \quad \ldots \quad (15)$$

Replacing $(\frac{t}{\alpha})$ in equation (11) from equation (13), K_R can be written as

$$K_R = (\frac{\beta}{\alpha})\ \left[-\ell n\ (1 - \varepsilon)\right]^{\frac{\beta-1}{\beta}} \quad \ldots \quad (16)$$

which can also be represented by

$$K_R = K_1(\varepsilon).K_2\ (T) \quad \ldots \quad (17)$$

where $K_1(\varepsilon) = \left[-\ell n\ (1 - \varepsilon)\right]^{\frac{\beta-1}{\beta}}$ ... (18)

Expressing (17) in logarithmic form gives

$$\ell n\ K_R = \ell n\ K_1(\varepsilon) + \ell n K_2(T) \quad \ldots \quad (19)$$

Differentiating with respect to T

$$\frac{d\ell nK_R}{dT} = \frac{d\ell nK_1(\varepsilon)}{dT} + \frac{d\ell nK_2(T)}{dT} \quad \ldots \quad (20)$$

and expressing K(T) in Arrhenius form, equation (20) can be

written in the form

$$E\ (T_1\varepsilon) = E_o + RT^2 \frac{d\ell n K_1(\varepsilon)}{dT} \qquad \ldots \qquad (21)$$

Equation (21) indicates that the plot of $\ell n\ K_R$ versus $\frac{1}{T}$ will not yield a straight line, instead a curve is obtained as shown in Fig. 5.1.33 - 35.

To obtain the activation energy E_o, $K_2(T)$ should be used instead of K_R. If the Arrhenius law is applicable, as at $t = \alpha$, $\varepsilon = 0.63$, then a plot of $\ell n(\beta/\alpha)$ against $1/T_{o.63}$ should yield a straight line with a slope equal to E/R, where $T_{o.63}$ is the temperature reached at $\varepsilon = 0.63$.

Fig.5.1.36 shows that the data yielded straight lines to obtain the activation energy for the systems studied.

Propagation Velocity:

An expression for the propagation velocity can be obtained by solving equation (4) which shows

$$V^2 = \frac{\bar{k}}{c\rho} \cdot \frac{d\theta}{dt} \Big/ (\theta - \varepsilon) \qquad \ldots \qquad (22)$$

For small values of $\bar{k}/\bar{c}\rho$, ε approaches θ as can be seen in equation (7), therefore it is necessary to find the velocity at the condition where $\varepsilon = 0$.

Taking $\varepsilon = 0$ at $T \to T_o$, equation (22) becomes

$$V^2 = \frac{\bar{k}}{\bar{c}\rho} \cdot \frac{d\theta}{dt} \Big/ \theta \qquad \ldots \qquad (23)$$

$$\text{or } V^2 = \frac{\bar{k}}{\bar{c}\rho} \left(\frac{dT/dt}{T-T_o}\right) \qquad \ldots \quad (24)$$

equation (24) becomes indeterminate when $T \neq T_o$.

The combustion zone in pellets of compressed fuel and

considered to proceed by burning layer to

Equations (25 - 29) to be deleted

$$V = \frac{\sum_{i=1}^{N} \Delta x}{\sum_{i=1}^{N} \Delta t} \qquad \ldots \quad (25)$$

Since $\sum_{i=1}^{N} \Delta x$ can be taken equal to L, the length of the pellet, and similarly $\sum_{i=1}^{N} \Delta x = t_c$, the time required for the zone to reach the end of the pellet, the burning rate V becomes

$$V = \frac{L}{t_c} \qquad \ldots \quad (26)$$

In equation (26) L is known and t_c can be found from the rate of combustion reaction.

From equation (11) and (16)

$$\frac{d\,\varepsilon}{dt} = \left(\frac{\beta}{\alpha}\right) \left[-\ell n\,(1-\varepsilon)\right]^{\frac{\beta-1}{\beta}} \cdot (1-\varepsilon) \qquad \ldots \quad (27)$$

since $\sum_{i=1}^{N} \Delta t = \int_{o}^{t_c} dt$

equation (27) can be used to find $\int_{o}^{t_c} dt$

Thus $$\int_{o}^{t_c} dt = \int_{o}^{t_f} \frac{d\varepsilon}{\left(\frac{\beta}{\alpha}\right)\left[-\ell n(1-\varepsilon)\right]^{\frac{\beta-1}{\beta}}(1-\varepsilon)}$$

Integrating to a limit $\varepsilon_f = 0.99$

$$t_c = \alpha\,(4.6)^{1/\beta} \qquad \ldots \qquad (28)$$

Substitution of t_c in equation (26) gives

$$V = \frac{L}{\alpha(4.6)^{1/\beta}} \qquad \ldots \qquad (29)$$

Testing the theory against experimental results:

To test the validity of the theory developed, it is essential to check equation (8), and to do so the temperature readings were transformed into the dimensionless number θ by using equation (5). Plotting $\ell n\ \ell n\ (\frac{1}{1-\theta})$ versus $\ell n t$ on a linear graph yielded straight lines as shown in Fig.5.1.37. It can be seen from the plot that equation (8) describes accurately the temperature profiles. From the resulting straight lines α and β are evaluated from the intercept and slope respectively. Table 5.1.37 gives results for three ratios of the red lead/silicon system. By knowing α and β the rate of burning can be calculated by using equation (28). The calculated results are found to agree well with observed values as seen in Table 5.1.38.

Since equation (8) fits the temperature profiles as indicated

by the plots in figure 5.1.37 the rate equation developed from temperature profile can be regarded as true for the reaction between Pb_3O_4/Si in compressed form. This rate equation shows first order kinetics, with a rate parameter dependent upon the temperature and reaction time. Obtaining the reaction rate in this way helps to find the activation energy through the Arrhenius law, and also provides an insight into the mechanism of the reaction.

The reason for the dependence of the rate parameter upon the reaction time can be seen by considering the solid reaction model of Komatsu (40) in which it is shown that reactions between the particles of different species in contact start on the particle surfaces. As the reactions progress, contact areas and contact points change, thus the rate of reaction, in addition to being dependent upon the unreacted materials, also depends on these factors which vary over the reaction time. For the system Pb_3O_4/Si, the reaction rate reaches a maximum value then decreases. The variation of the reaction rate over time, figure 5.1.38 is consistent with the model presented by Komatsu. Since the reaction starts along the contact points of reactant particles and as the area of contact points increases with the reaction time, the rate must increase. This increase continues until enough products are produced to form an intervening layer separating the reactants. For further reaction, reactants must diffuse through this layer. At this stage the reaction is controlled by diffusion, and due to this the rate falls. As the product layer thickens, the rate decreases sharply.

The activation energy has been evaluated from K(T), the temperature dependent part of K_R, by applying the Arrhenius law. A value of 31.4 kJ/mole has been obtained indicating a diffusion controlled reaction (44, 45).

N O T A T I O N

E = activation energy

E_0 = activation energy as defined by the Arrhenius equation

K_1 = specific rate constant dependent on temperature

K_2 = specific rate constant dependent on ε

K_R = rate parameter

κ = thermal conductivity of compacted mixtures

T = temperature

T_0 = initial temperature

T_f = final temperature

t = time

tc = propagation time

V = propagation velocity

L = length of pellet of composition

α, β = constants for a specific composition

ε = fraction reacted

ρ = density of pelleted mixture

TABLE 5.1.37

Values of α and β for various Pb_3O_4/Si Compositions

Pb_3O_4/Si	β	α (sec)	$\ell n\beta/\alpha$	$1/T_{0.63}$ (K^{-1})
50/50	1.94	0.102	2.95	11.71×10^{-4}
55/45	2.00	0.049	3.71	9.83×10^{-4}
60/40	1.83	0.031	4.07	8.69×10^{-4}
70/30	1.69	0.026	4.16	8.56×10^{-4}

TABLE 5.1.38

Observed and Calculated (R.B.)

for Pb_3O_4/Si Compositions

Pb_3O_4/Si (w/w)	Rate of burning, cm/sec	
	observed	calculated
50/50	3.88	3.71
55/45	6.92	6.86
60/40	11.47	11.63
70/30	13.91	12.95

FIG. 5.1.30 T VS t FOR 50/50 Pb_3O_4/Si

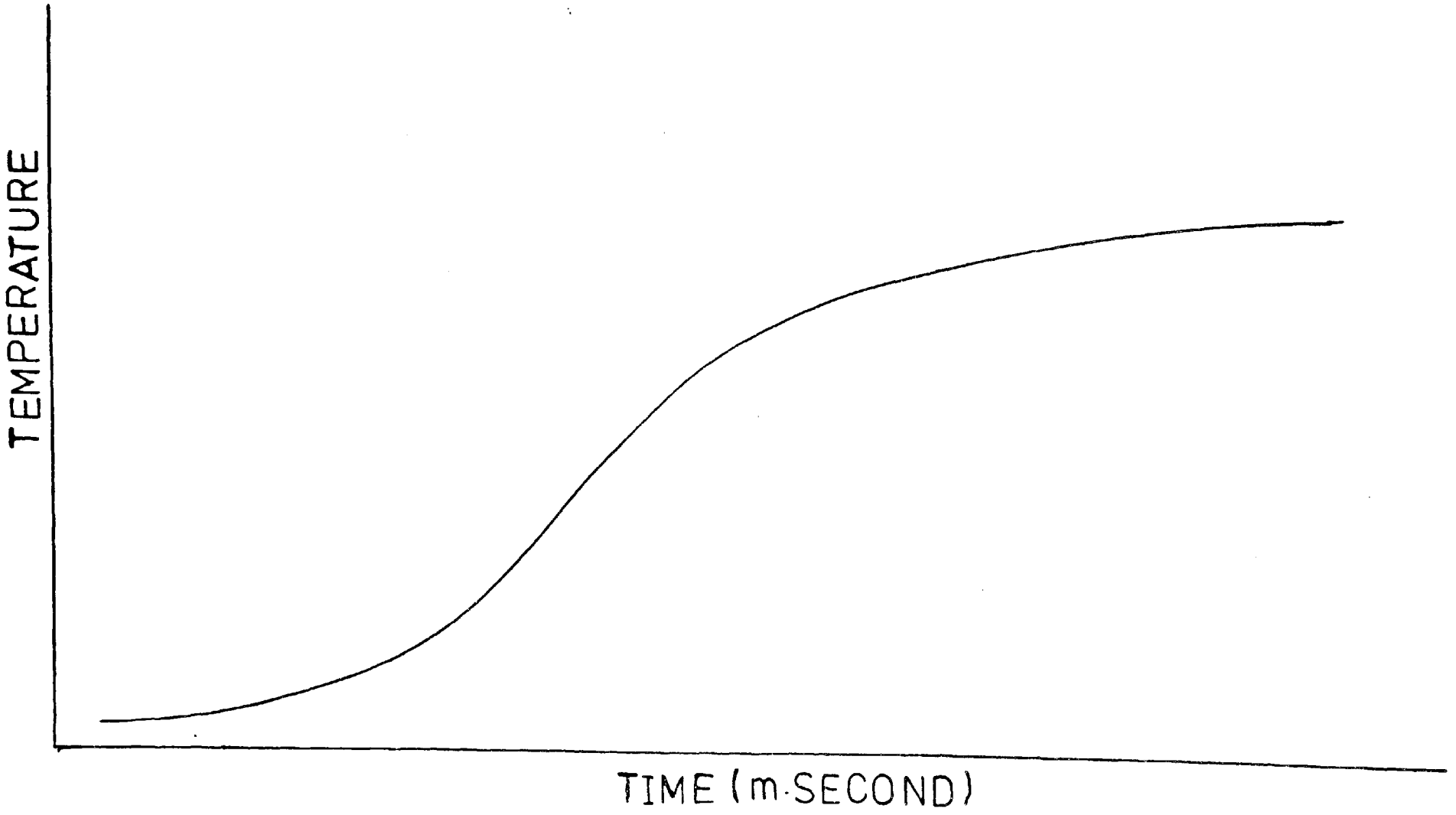

FIG. 5.1.31

TEMPERATURE VS TIME FOR 60/40 W/W) Pb_3O_4/Si

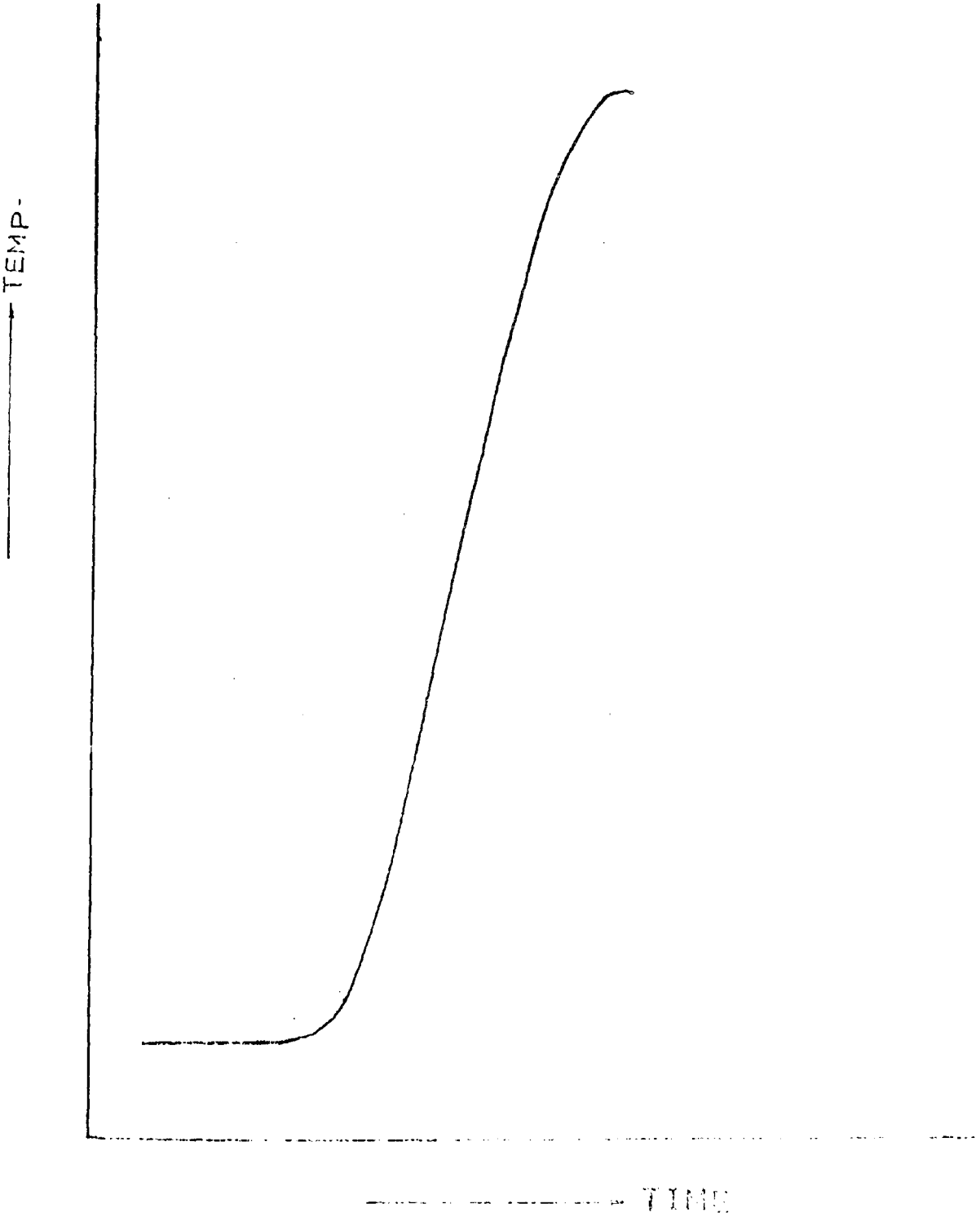

FIG. 5.1.32

TEMPERATURE VS TIME FOR 70/30 W/W Pb_3O_4/Si

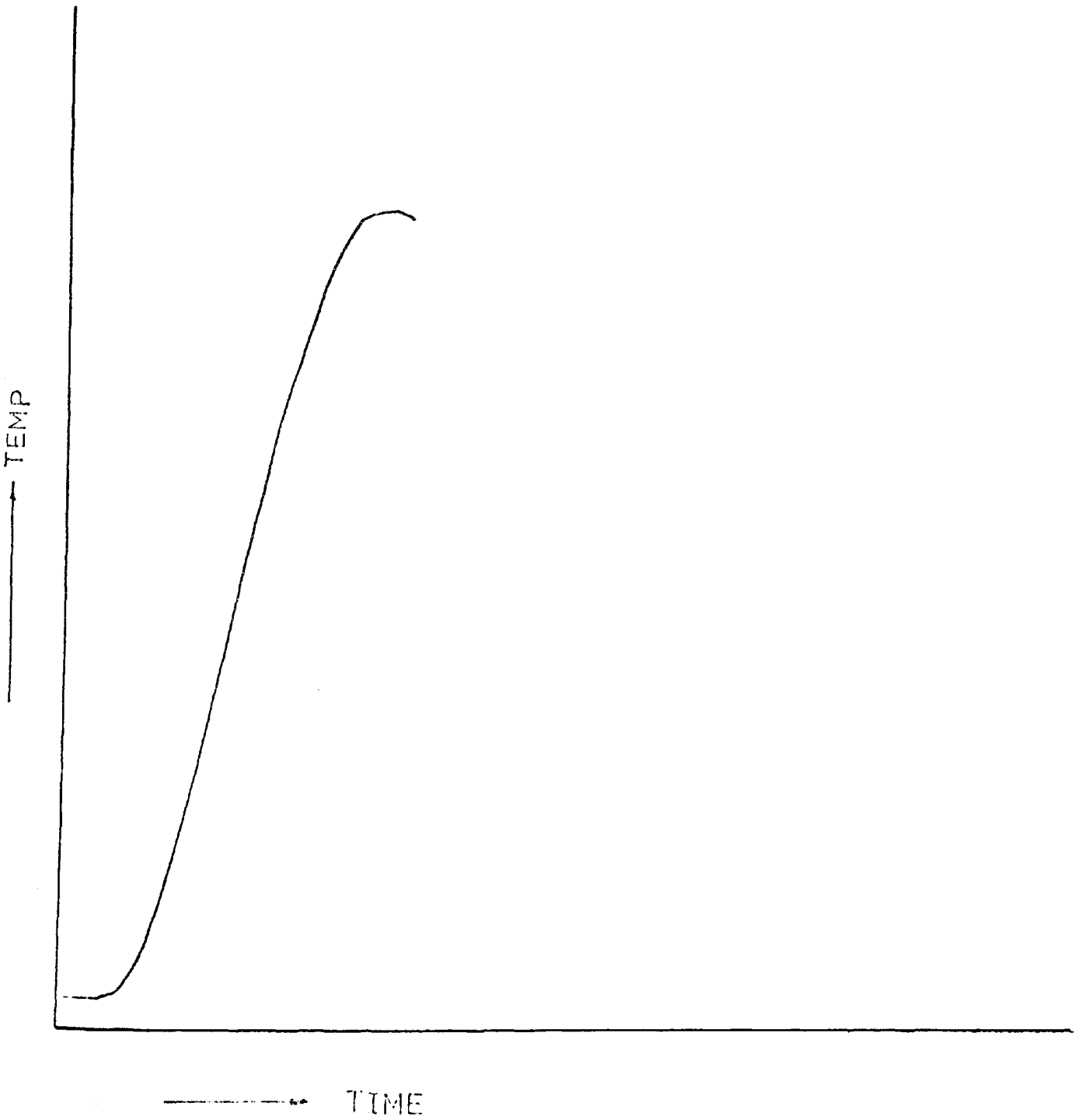

FIG. 5.1.33

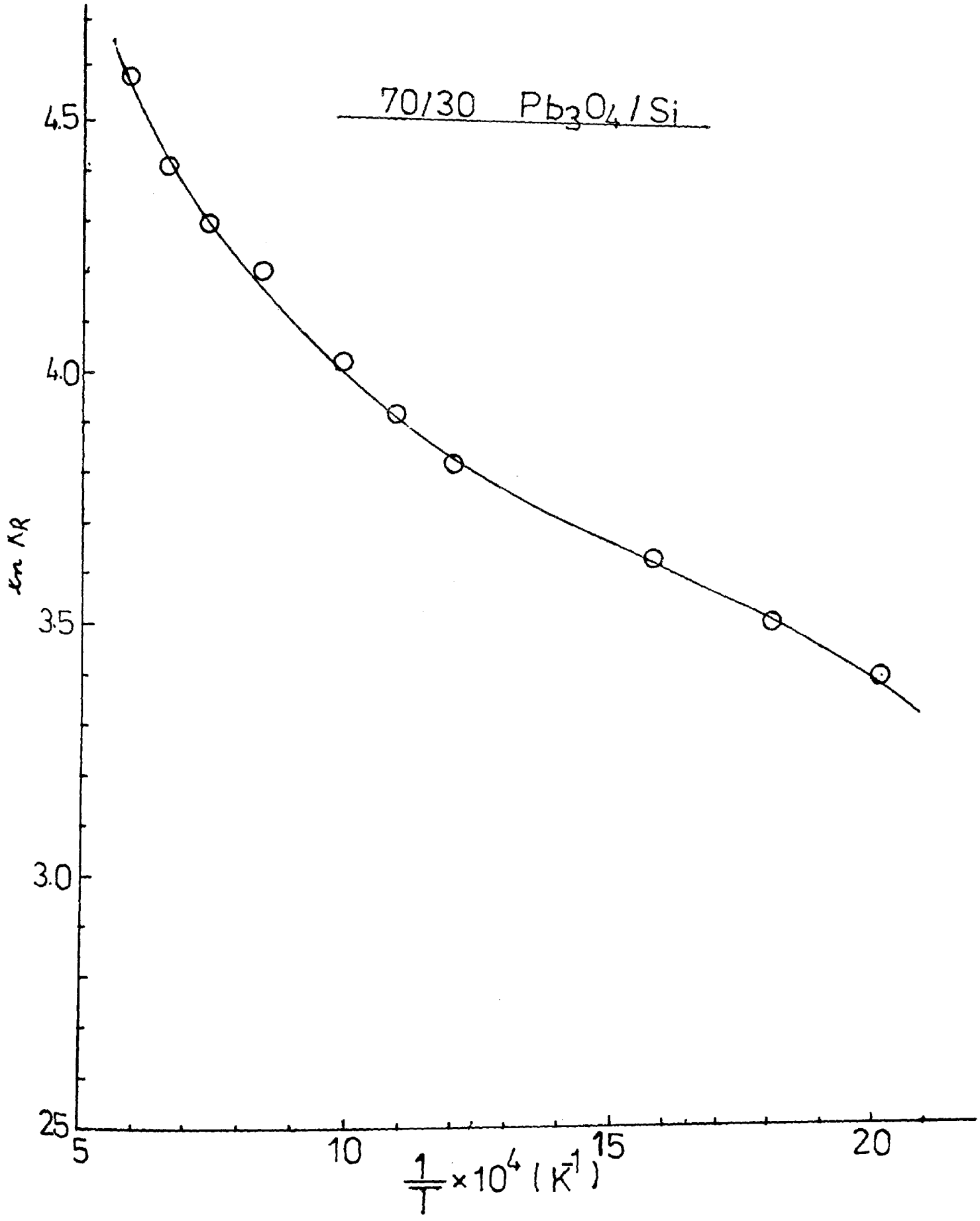

FIG. 5.1.34

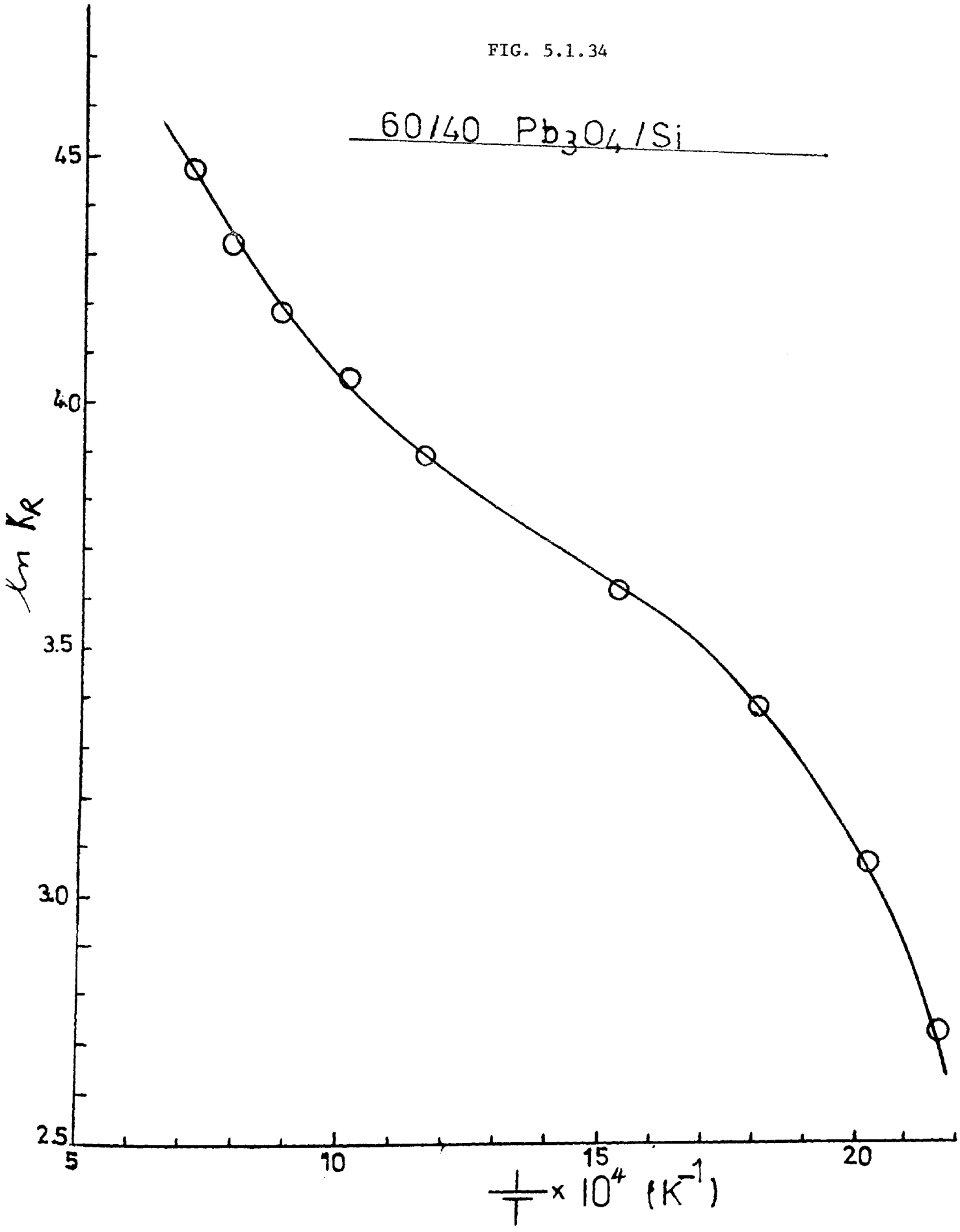

FIG. 5.1.35

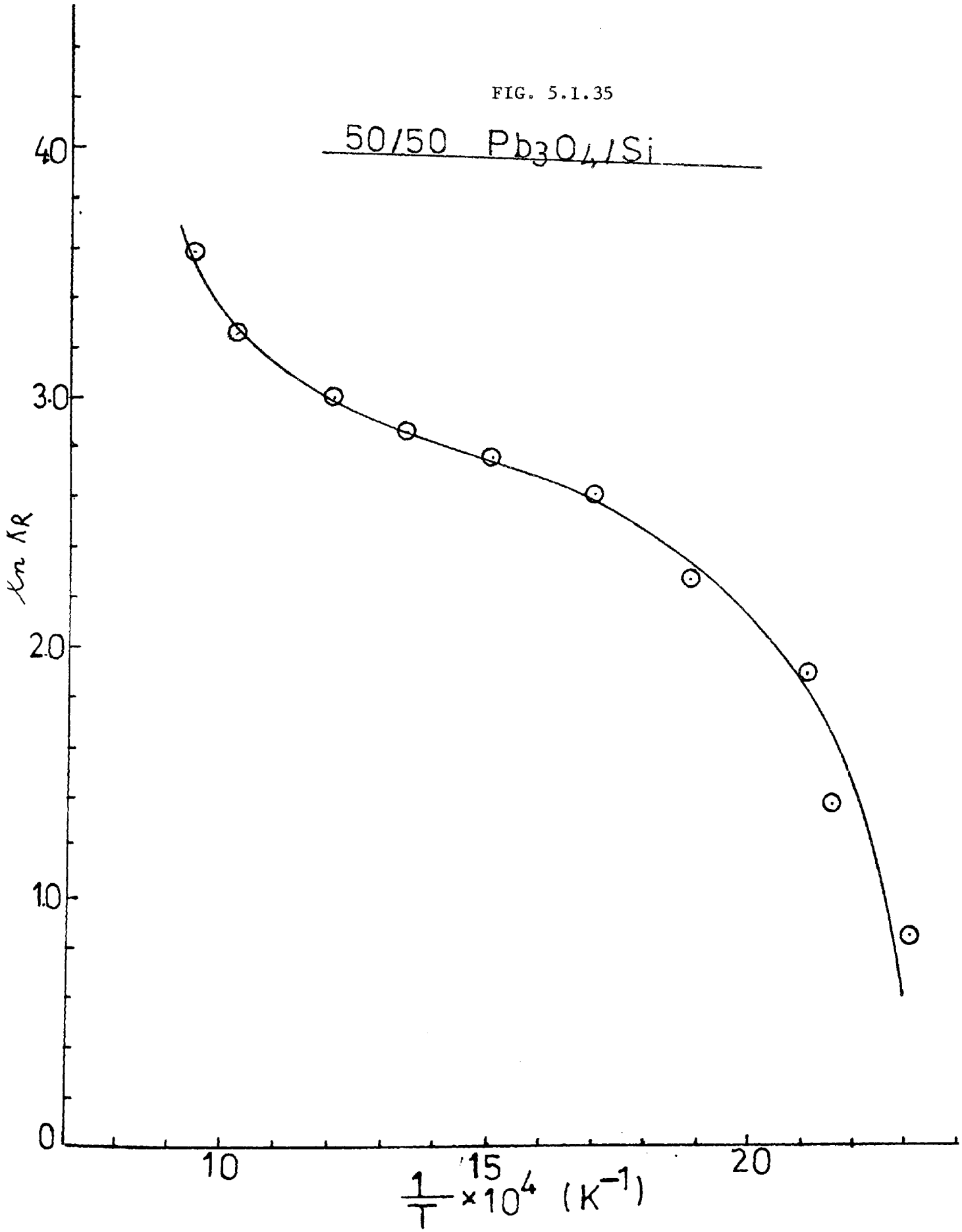

FIG. 5.1.36

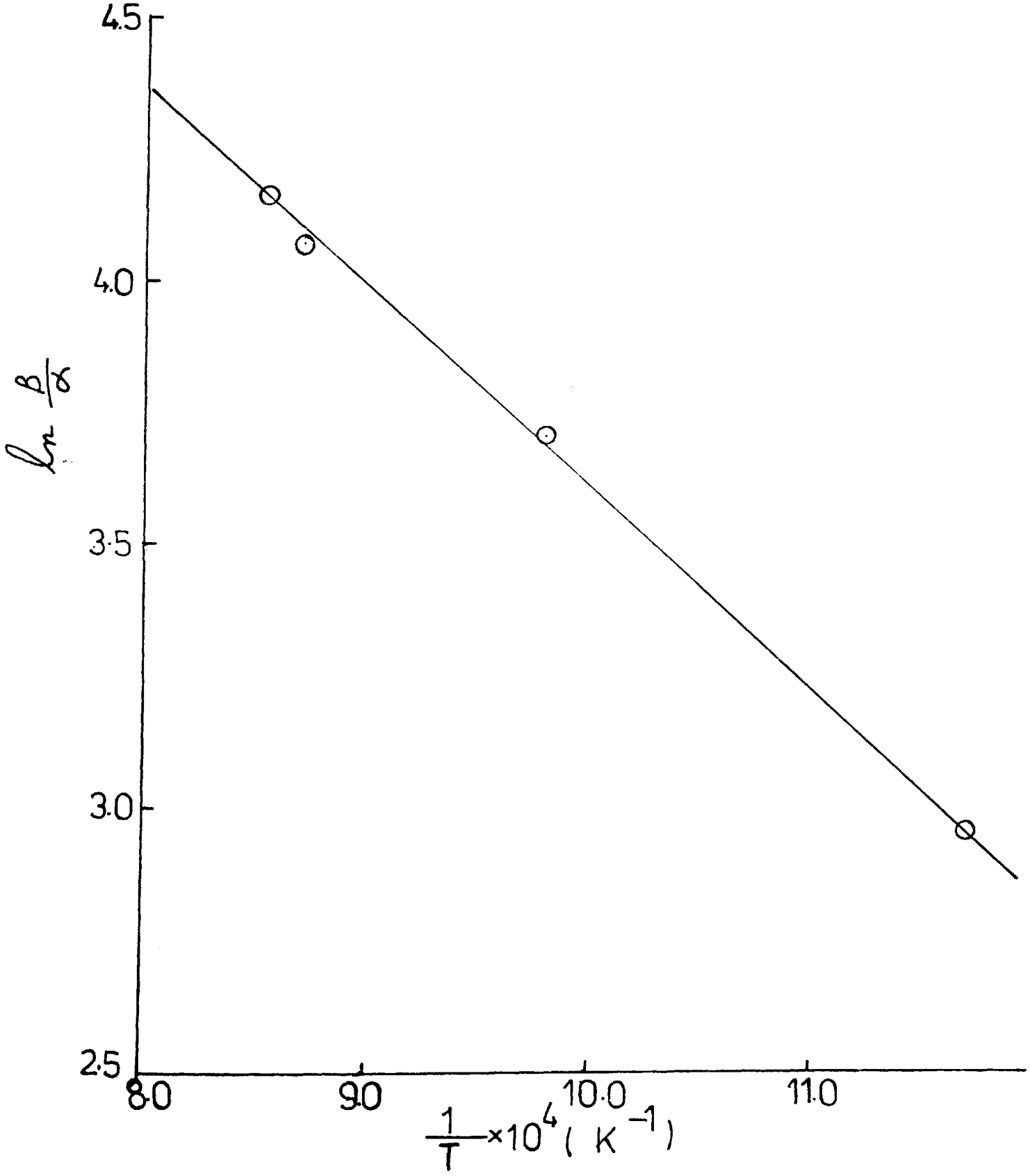

FIG. 5.1.37

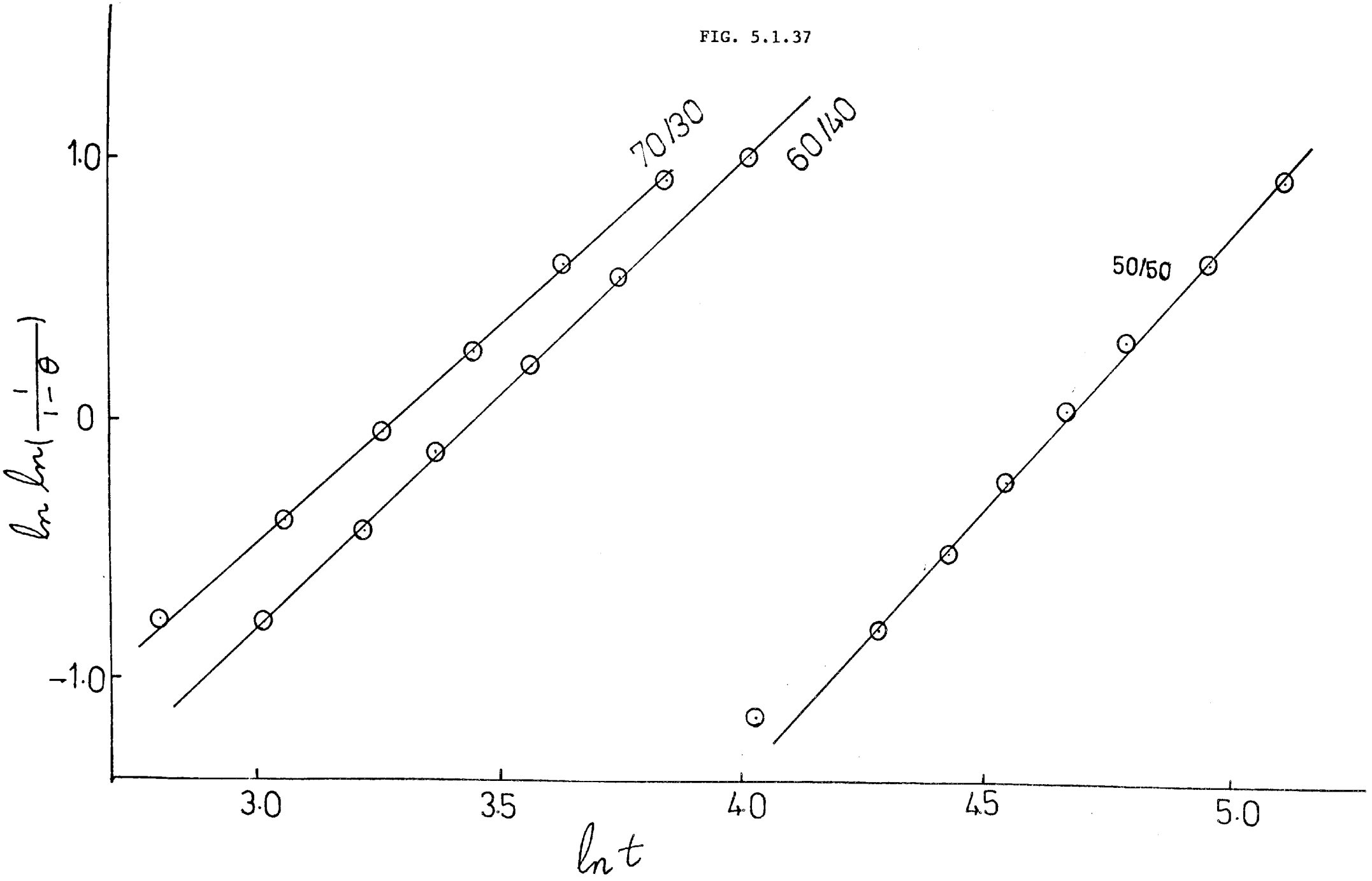

FIG. 5.1.38

Pb_3O_4 /Si

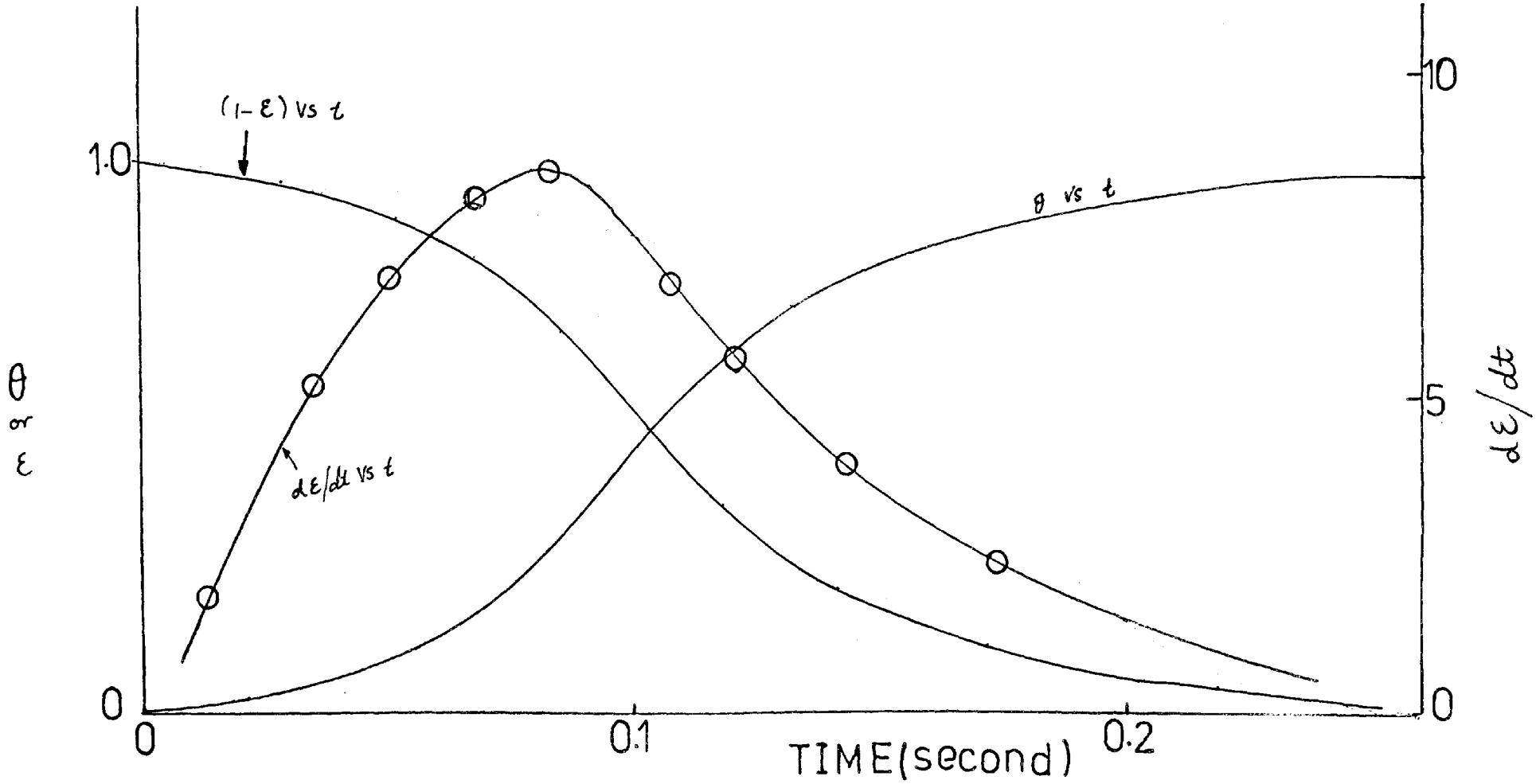

5.2 THERMAL ANALYSIS STUDIES (46-51)

Three methods have been adopted for the studies

1. Differential Thermal Analysis (DTA)
2. Differential Scanning Calorimetry (DSC)
3. Thermogravimetry (TG)

1. DTA: This is a technique in which a record is made of the temperature difference between the sample and reference material against time or temperature, as the specimens are subjected to identical temperature regimes, in an environment heated or cooled at a controlled rate.

The DTA Curve, shows increases or decreases in temperature differences, depending on whether a change in the sample causes absorption or liberation of heat. The method records all changes in enthalpy, whether accompanied by a change in weight or not, e.g. phase transition (change of crystalline structure, boiling, sublimination, evaporation, melting) or chemical reactions such as redox reactions, decomposition, dehydration and dissociation.

DTA is a dynamic method in which equilibrium conditions are not attained; thus the temperatures of changes and reactions determined in this way do not correspond to the thermodynamic equilibrium temperatures.

The experimental procedure consists of heating or cooling both sample and reference material under identical conditions, and simultaneously recording the temperature difference between them. In an ideal case the heating or cooling takes place at a constant

rate, the heat flow is identical in both materials and in the vessels used, the observed temperature difference is constant and the plot is horizontal. This line is called the base line.

The temperatures of the test and reference materials are monitored by two thermojunctions, one of which is placed in the sample and the other in the reference material and connected in opposition. DTA can be carried out in either a static atmosphere or in a gas flowing at a controlled rate. The size of the sample used has a bearing both on the shape of the curve obtained and the significance that can be attached to the results. Very small samples tend to give sharper, narrower peaks, which are easier to interpret. Because of the small mass, changes in heat capacity consequent upon physical or chemical processes have less tendency to cause baseline drift, and give a smaller temperature differential so the errors introduced by ignoring it are consequently reduced.

In all the tests a diluent, which was the same as the inert sample, was used in alternate layers, i.e. inert - sample - inert. This is done to minimise the difference in heat capacities between the test and reference sample, thereby reducing baseline drift. The reference material is chemically and thermally inert, having a negligible tendency to sinter under the experimental conditions used. Alumina was used in all cases, being preheated at the highest temperature required for DTA so as to remove any volatile impurities and stabilise the crystalline structure.

2. DSC: This technique is used for the measurement of heat evolved or absorbed, by a physical change or a chemical reaction, by maintaining the sample and reference material at a

temperature predetermined by the programmed oven during a thermal event in the sample. The amount of energy which has to be supplied to, or withdrawn from, the sample to maintain zero temperature differential between the sample and the reference is the experimental parameter displayed as the ordinate of the thermal analysis curve.

The sample and reference pans on individual bases which each contain a platinum resistance thermometres and thermocouples The temperatures of the two thermocouples are compared, and the elecrical power supplied to each heater adjusted so that the temperatures of both the sample and the reference remain equal to the Programmed temperature, i.e. any temperature difference which results from a thermal event in the sample is "nulled." Unlike DTA, DSC does not require the thermal masses of the sample and reference to be closely matched, since a power difference, not a temperature difference, is measured.

The ordinate signal, the rate of energy absorbed by the sample (millicalories per second), is proportional to the specific heat of the sample, since the specific heat at any temperature determines the amount of thermal energy necessary to change the sample temperature by a given amount.

3. TG: This is a method in which the weight of the sample is continuously recorded during heating or cooling. The TG curve thus obtained, expressing the dependence of the weight change on temperature, gives information on the sample composition, thermal stability, its thermal decomposition and on the products formed on heating.

The equipment provides for experiments involving both rising temperature and isothermal experiments. One factor which can give rise to error is the incorrect reading of temperature, i.e. that of the recording thermocouple. This is important in isothermal operations where the heat capacity of the surrounding equipment is large, and it takes the sample some time to come to the desired isothermal operating conditions.

5.2.1 DTA

This technique was employed to study effect of heating on

1. Pb_3O_4
2. Pb_3O_4/Si in nitrogen atmosphere
3. Pb_3O_4/Si in air
4. Si in air
5. PbO/Si in air and in nitrogen
6. Pb/Si in air
7. PbO_2 in air and in nitrogen

(1) DTA for Pb_3O_4

A sample of 20 mg was sandwiched between two layers of alumina in a platinum crucible, and was then heated at $6^{\circ}C$/min. The DTA curve Fig.5.2.1 shows that an endothermic reaction commenced at $540^{\circ}C$, as shown by a slight devation of the ΔT from the base line at this temperature. This deviation became rather large at $580^{\circ}C$ and reached a maximum at $590^{\circ}C$. A second endothermic peak formed with T max $868^{\circ}C$, this peak being sharper than the first one. As the temperature of the furnace was raised higher, the DTA curve

FIG.5.2.1 DTA & TG FOR Pb_3O_4 IN AIR

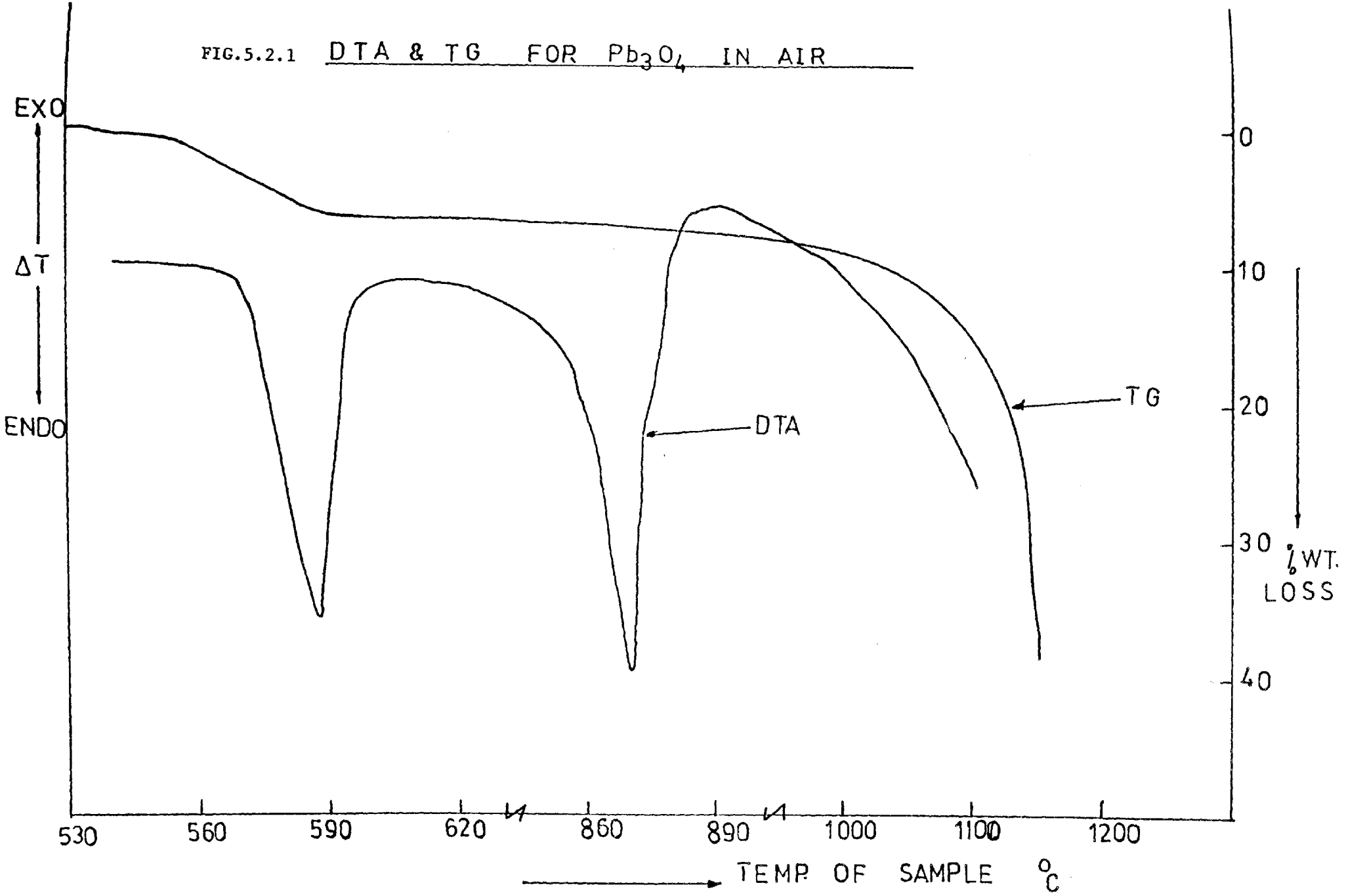

declined continuously without forming a peak, indicating a heat loss from the sample.

(2) DTA for Pb_3O_4/Si in nitrogen

Mixtures of Pb_3O_4/Si of weight ratio 40/60, 50/50, 60/40, 70/30, 80/20 and 90/10 were studied, the DTA curves deviated from the baseline at (530 - 555°C), rose gradually until 560°C, then formed a shoulder followed by a sharper rise to form exothermic peak with its maximum at 585 - 600°C. The temperature at which the peaks maxima occurred could be seen to coincide with the endothermic decomposition reaction of the red lead, namely 590°C. The decomposition of red lead, and the reaction with the silicon, were therefore taking place at the same time.

(3) DTA for Pb_3O_4/Si in air:

The reactions in air, as illustrated by DTA curve fig. 5.2.2 were three exothermic peaks for all the compositions. The first peak was at the sampe temperature as that of the reaction in nitrogen. However the peak size is larger. The second peak started at 626 - 630°C but rose sharply at 660 - 670°. This was a very exothermic reaction, necessitating the use of small samples (10 mg), especially for mixtures with red lead percentage greater than 70%, as the platinum crucible and the thermocouple below it were damaged, due to the high temperature of the reaction products. The third peak was also exothermic, but was rather slow and small compared with the first two peaks, except for samples with very large excesses of silicon (50% & 60%) where this peak was quite significant, fig
The peaks maximum was seen at 730 - 780°C.

FIG.5.2.2 DTA FOR Pb_3O_4 /Si IN AIR

1 60/40

2 80/20

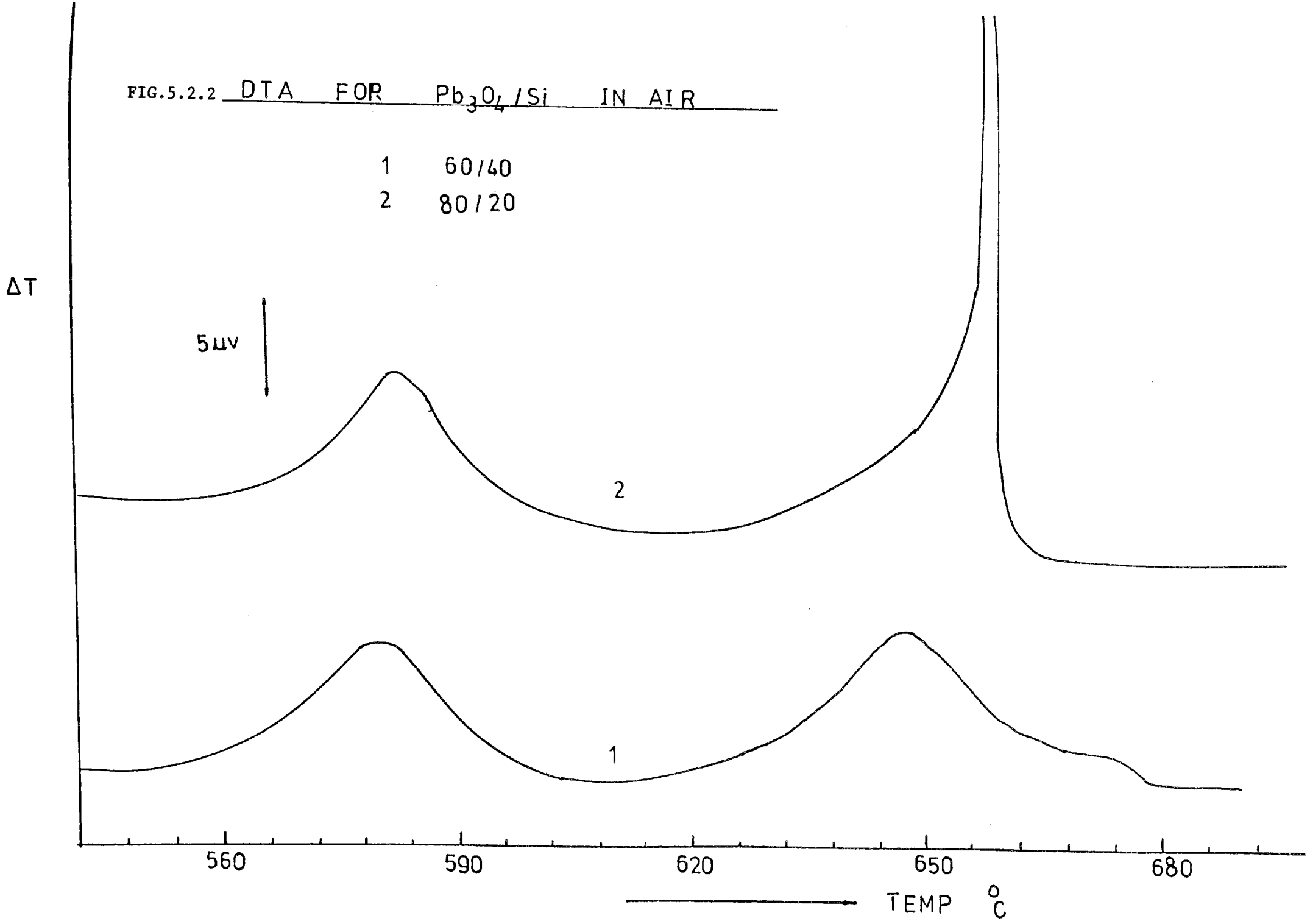

(4) DTA for silicon

No reaction was apparent from DTA curve of silicon in air for temperatures up to 1000°C.

(5) DTA for PbO/Si

A 70/30 (W/W) PbO/Si prepared in the same manner as that of red lead/silicon, was studied in air and in nitrogen. The reactions in air, as can be seen from Fig.5.2.3, are exothermic. The first started at 540°C and peak maximum was at 590°C, a second peak started at 610°C, the ΔT rose gradually as the temperature was increased, the rise becoming very sharp as the temperature approached 665°C, and the reaction terminating soon after. These reactions follow the same pattern, in temperature of occurrence and relative sizes of peaks, as those for red lead/silicon reactions.

It can be interpreted that the lead monoxide was converted to red lead as it reacted with atmospheric oxygen at temperature above 350°C. (52).

$$6\ PbO + O_2 \rightarrow 2Pb_3O_4$$

The red lead was then decomposed at a temperature above 540°C as previously discussed. The same red lead/Si reactions would then follow.

When the same sample was studied in nitrogen, the DTA curve shows that the peaks were formed at the same temperature ranges as the reactions in air, but they were, particularly the second exotherm, less sharp and smaller in size as in Fig. 5.2.4.

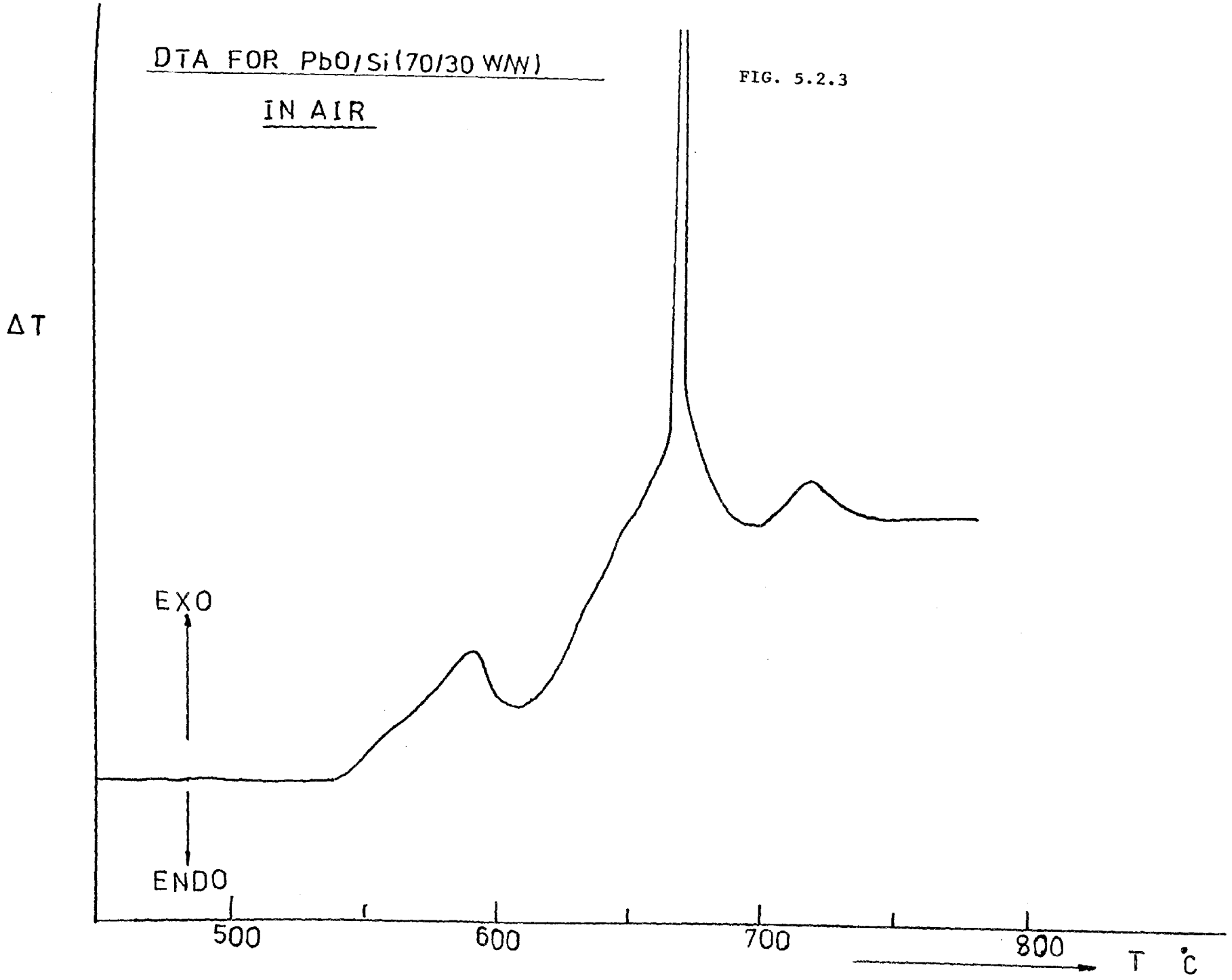
DTA FOR PbO/Si(70/30 W/W)
IN AIR
FIG. 5.2.3
ΔT
EXO
ENDO
500
600
700
800
T °C

FIG. 5.2.4

DTA FOR PbO/Si (70/30W/W) IN NITROGEN

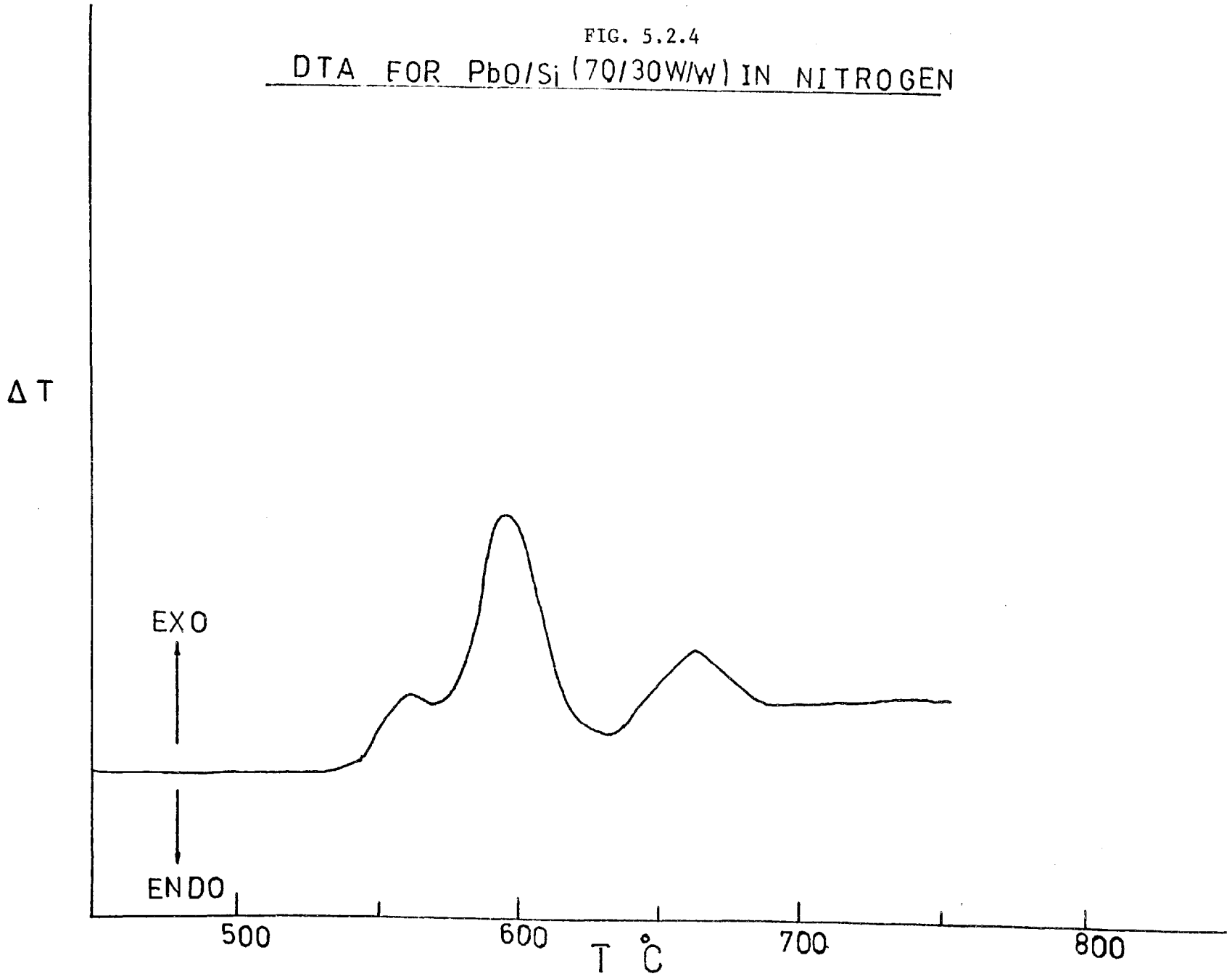

(6) DTA for lead/silicon

Reactions in air of 70/30 (w/w) Pb/Si were studied by DTA. Fig.5.2.5 shows that at 327°C an endotherm representing the melting of lead has formed. The molten lead was then partially oxidised in air, at a temperature above the melting point, and the mixed oxides formed would, on further heating in air at above 350°C, form lead monoxide which was subsequently transformed into red lead. The reactions thereafter were the same as those of red lead/silicon compositions. (52)

There were no reactions between Pb and Si when the study was performed under nitrogen flow, and the melting peak was the only one obtained.

(7) DTA for lead dioxide

DTA curve for PbO_2, under a steady flow of nitrogen, shows that the differential temperature ΔT started to deviate from the baseline at 296°C, forming an endothermic peak with its maximum rate at 386°C. This peak was then followed by two smaller endotherms at 430 and 464°C, then a sharper and much larger endothermic peak formed at 540°C. These four reactions correspond to

$$PbO_2 \rightarrow PbO_{1.56} \rightarrow PbO_{1.43} \rightarrow Pb_3O_4 \rightarrow PbO$$

as confirmed by X-ray diffraction; though there was simultaneous appearance of one oxide with small proportions of the other oxides from the preceeding and following stages.

Another endothermic peak formed at a much higher temperature

FIG.5.2.5 DTA FOR Pb/Si (70/30) IN AIR

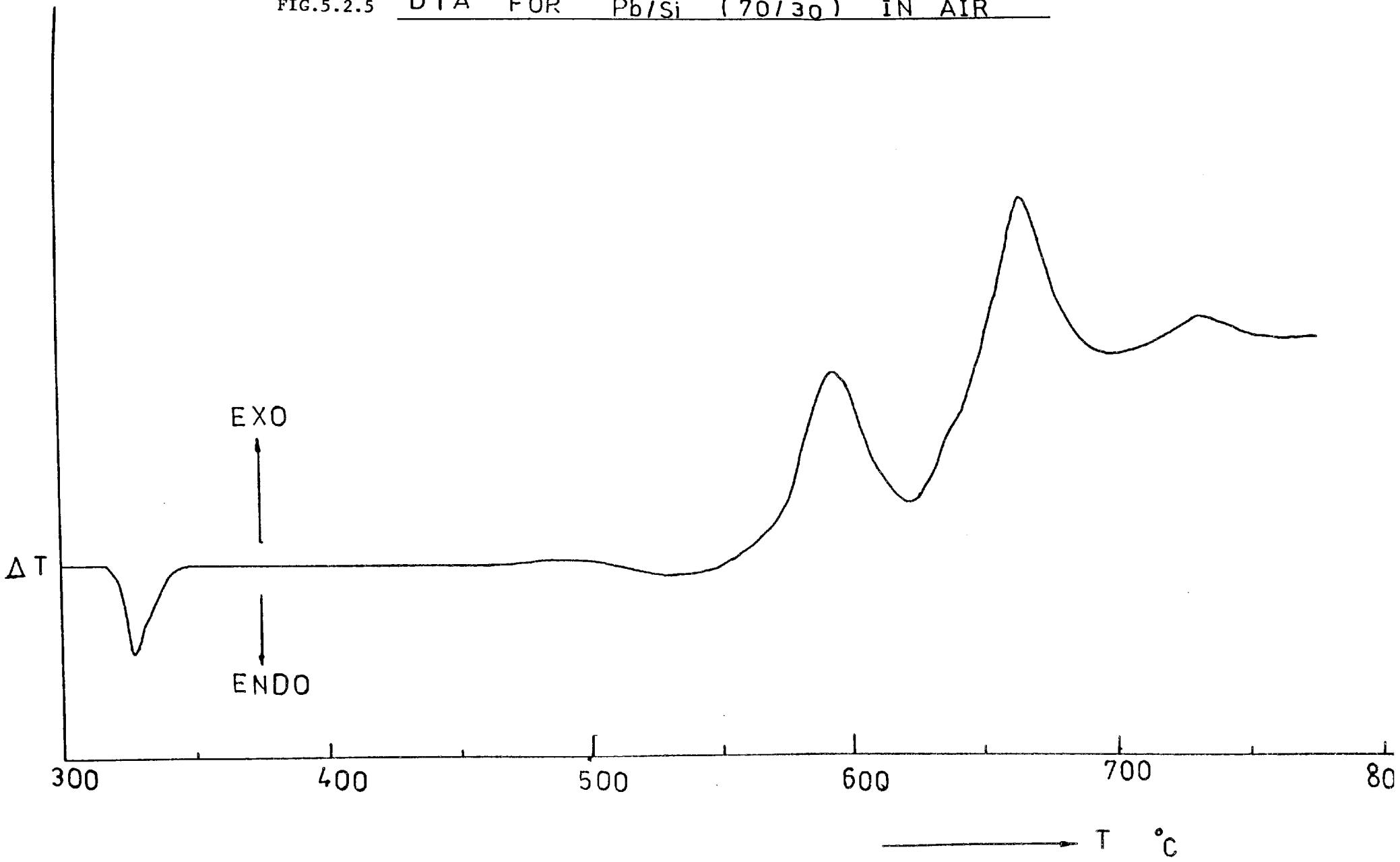

(876°C). This peak, as in the case of red lead, is that of melting of the PbO formed.

When DTA was performed in static air, but at the same heating rate (6°C/min), there were four endotherms at 381, 425, 467 and 589°C. The fifth peak was that of PbO melting, and was noted at 870°C, as in Fig. 5.2.6. The conversion of red lead to lead monoxide is a reversible reaction and can be repeated by

$$2\ Pb_3O_4 \underset{500\ <}{\overset{>\ 500}{\rightleftharpoons}} 6\ PbO + O_2$$

The oxygen from the air would favour the reverse reaction, thereby inhibiting the formation of PbO until a higher temperature was attained. In nitrogen, it is likely that the oxygen formed was immediately driven away by the flowing gas. The difference in the fourth peak's temperature of 540°C and 589°C for reactions in nitrogen and air respectively, was also obtained when red lead samples were studied under these conditions.

5.2.2 DSC

(1) DSC for red lead/silicon:

Samples were prepared by mixing the required amounts of the two powders, passing them through a 75 μm sieve five times to ensure uniform mixing and to break down any powder agglomeration. The samples were then stored for 24 hours in a descicator, prior to test. Each sample was mixed throughly again immediately before the experiment to avoid the segregation of the two species, which have a large

FIG. 5.2.6 DTA FOR PbO_2 IN AIR

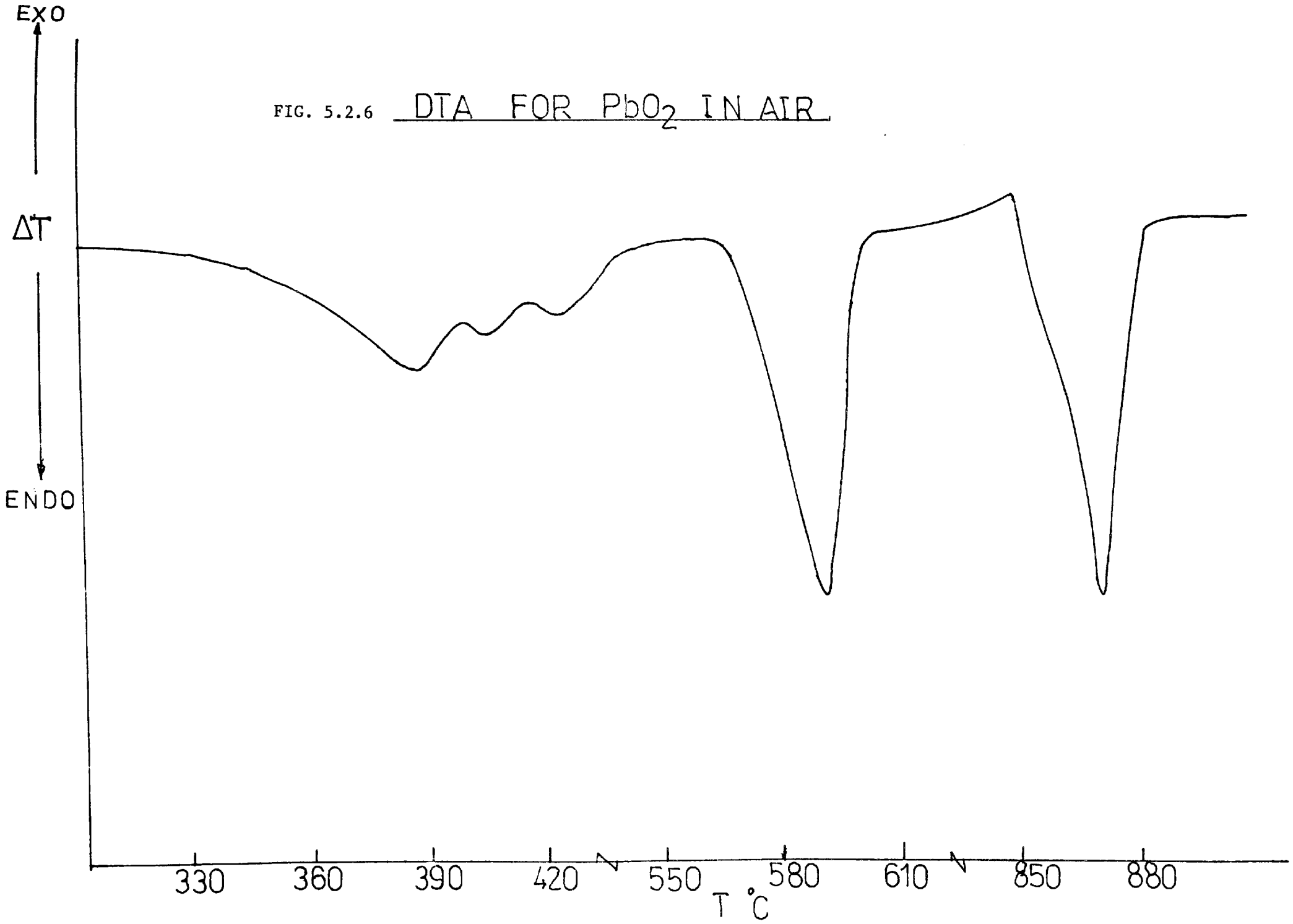

difference in their densities.

The amount needed for testing was approximately 3 mg, and in all cases the tests were carried out under a steady nitrogen flow around the furnace which contains the sample and reference pans.

When the sample was heated at a uniform heating rate of $40^{o}C$/min., it was seen as in Fig.5.2.7 that

a. A very slight exothermic reaction took place at T max = $490^{o}C$

b. A large peak, which was also exothermic, occurred at $T_{max} = 620^{o}C$

c. A third exothermic reaction, which was of a very small peak for a 50/50 and a 70/30 Pb_3O_4 but was rather significant for the 85/15 sample. This peak reached its maximum at $T_{max} = 685^{o}C$

Prior to these exothermic reactions, the base line was seen to drift gradually in an endothermic direction, possibly due to slow decomposition of the red lead at a temperature as low as $370^{o}C$.

The compositions 50/50, 70/30 and 85/15 were seen to reach their peaks maxima at approximately the same temperature. The size of the peaks which can be used to calculate the amount of heat evolved from the reaction was seen to increase with the decrease of percentage silicon in sample. Knowing the quantity of heat per second, dH/dt (m.cal/s) for full scale deflection, rate of heating, and area under each peak, the heat evolved was calculated for the samples. It can be seen from the following table that the total

FIG. 5.2.7 PB30Z/SI [illegible] AT 40 C/MIN

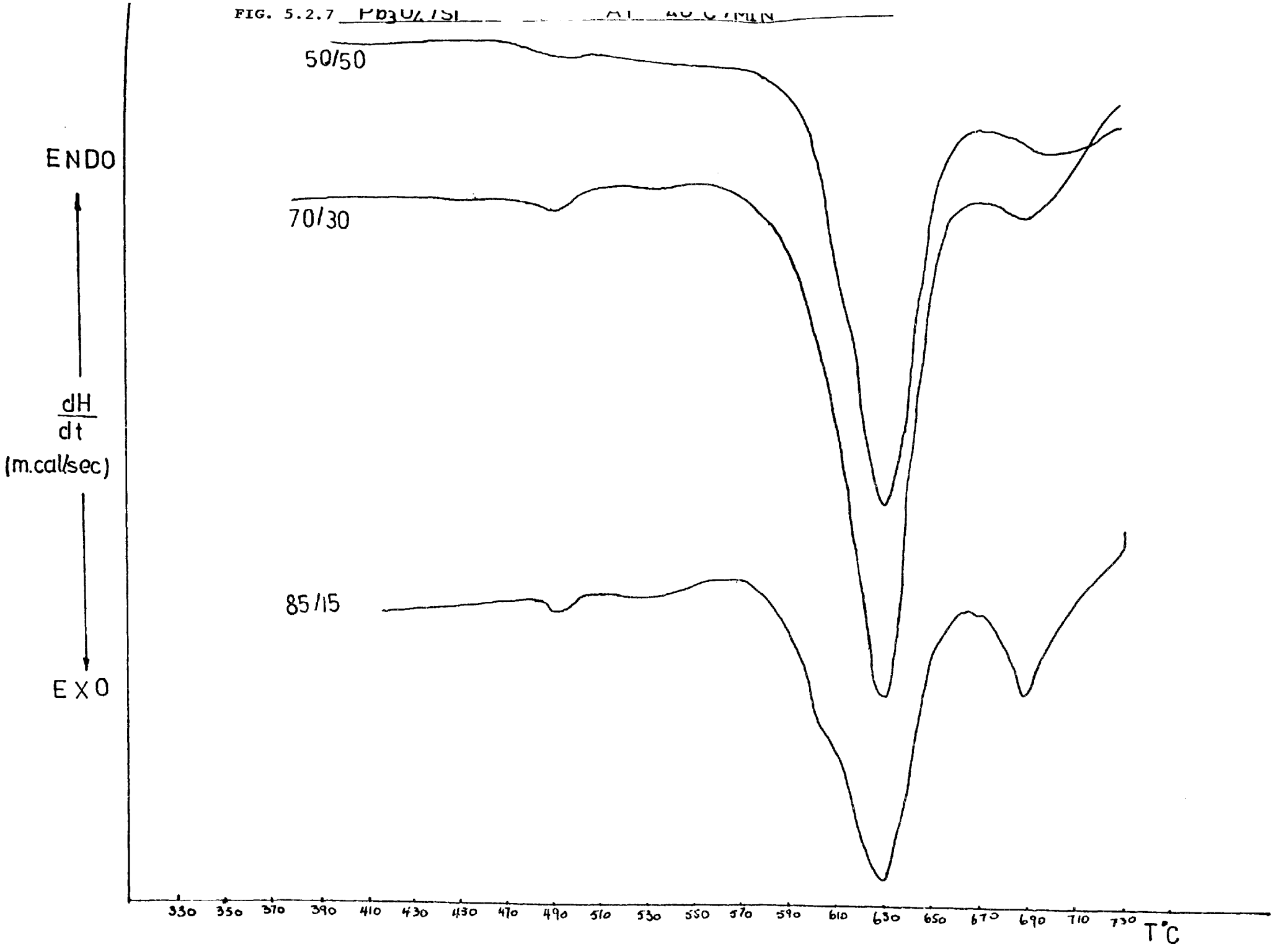

heat evolved per gram of composition increases from 50/50 to 85/15 red lead/silicon.

Pb_3O_4/Si (NO BINDER)	HEATING RATE ^oC/Min.	F.S.D. m.cal/s	AREA cm^2/g	HEAT EVOLVED J/g
50/50	40	20	3605.3	396.0
70/30	40	20	5496.1	603.7
90/10	40	20	6216.3	682.8

(2) DSC for red lead/silicon with binder:

Samples were prepared as previously described, for use in delay tubes. Approximately 3 mg. was used for each test, and conditions were the same as those of the previous study. The curves obtained differed markedly from those of samples which did not include binder, in that the second exothermic reaction was immediately followed by a third exothermic peak; the two reactions appearing as a shoulder followed by a peak. The same sequence was obtained for 50/50, 70/30 and 85/15 red lead/silicon with 0.5% C.M.C as in Fig. 5.2.8.

In the table on the following page, a comparison is being made of the T_{max} for samples with and without binder.

FIG. 5.2.8 85/15 Pb_3O_4/Si + BINDER

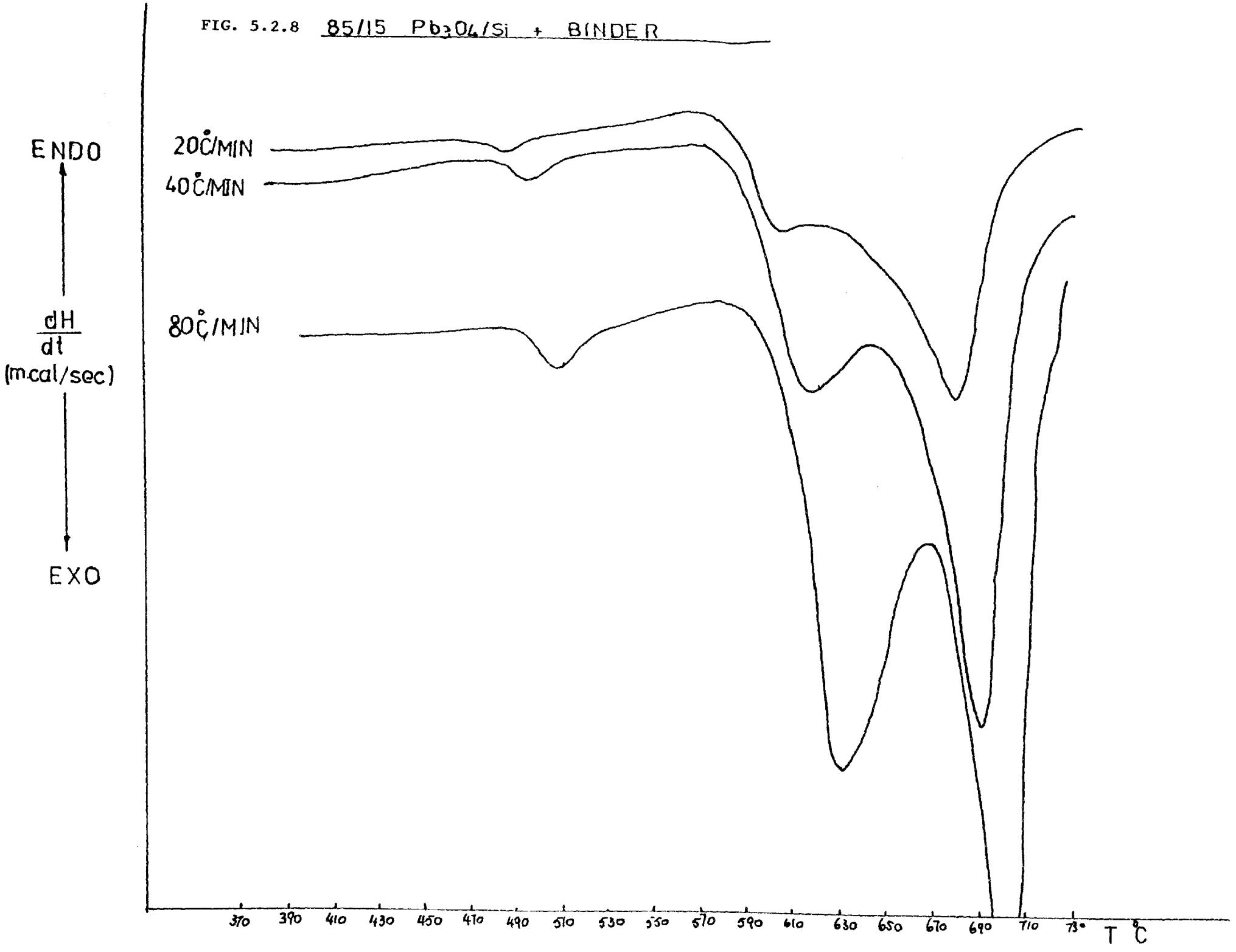

(3) DSC for lead dioxide:

On heating PbO_2 at 40°C/min, the DSC curve was seen to leave the baseline at 180°C and drifted endothermically, gradually at first, then more sharply at 350°C, to reach a peak maximum at 435°C, followed by endothermic peaks at T_{max} 465, 495 and 573°C. as illustrated in Fig. 5.2.9.

The four peaks are the decomposition reactions

$$PbO_2 \xrightarrow{435^\circ C} PbO_{1.56} \xrightarrow{465^\circ C} PbO_{1.43} \xrightarrow{495^\circ C} Pb_3O_4 \xrightarrow{573^\circ C} PbO$$

Though at each T_{max}, there is a simultaneous appearance of one oxide with a small portion of the other oxides from the preceding and following stages.

A study by Aleksandrov et al (53) has shown that at high heating rates, by means of a mass spectrometer at rates of 2.1×10^2 °C/second, there are only two macrokinetic stages at T_{max} 490°C and 580°C, indicating that at a high heating rate, red lead formation extends over an increasingly large temperature range, up to the temperature at which red PbO starts forming.

$$PbO_2 \xrightarrow{490^\circ C} PbO_{1.43} + Pb_3O_4 \xrightarrow{580^\circ C} PbO(red) + Pb_3O_4$$

It can be concluded that with increased heating rate, a fusion of the first stage with the second stage and a fusion of the third stage with the fourth stage of the reactions at slow heating rates occur.

As PbO_2 and Si reactions produce a temperature rise greater than 1000°C per second, it is likely that only two decomposition stages occur.

FIG. 5.2.4 DSC FOR PbO_2

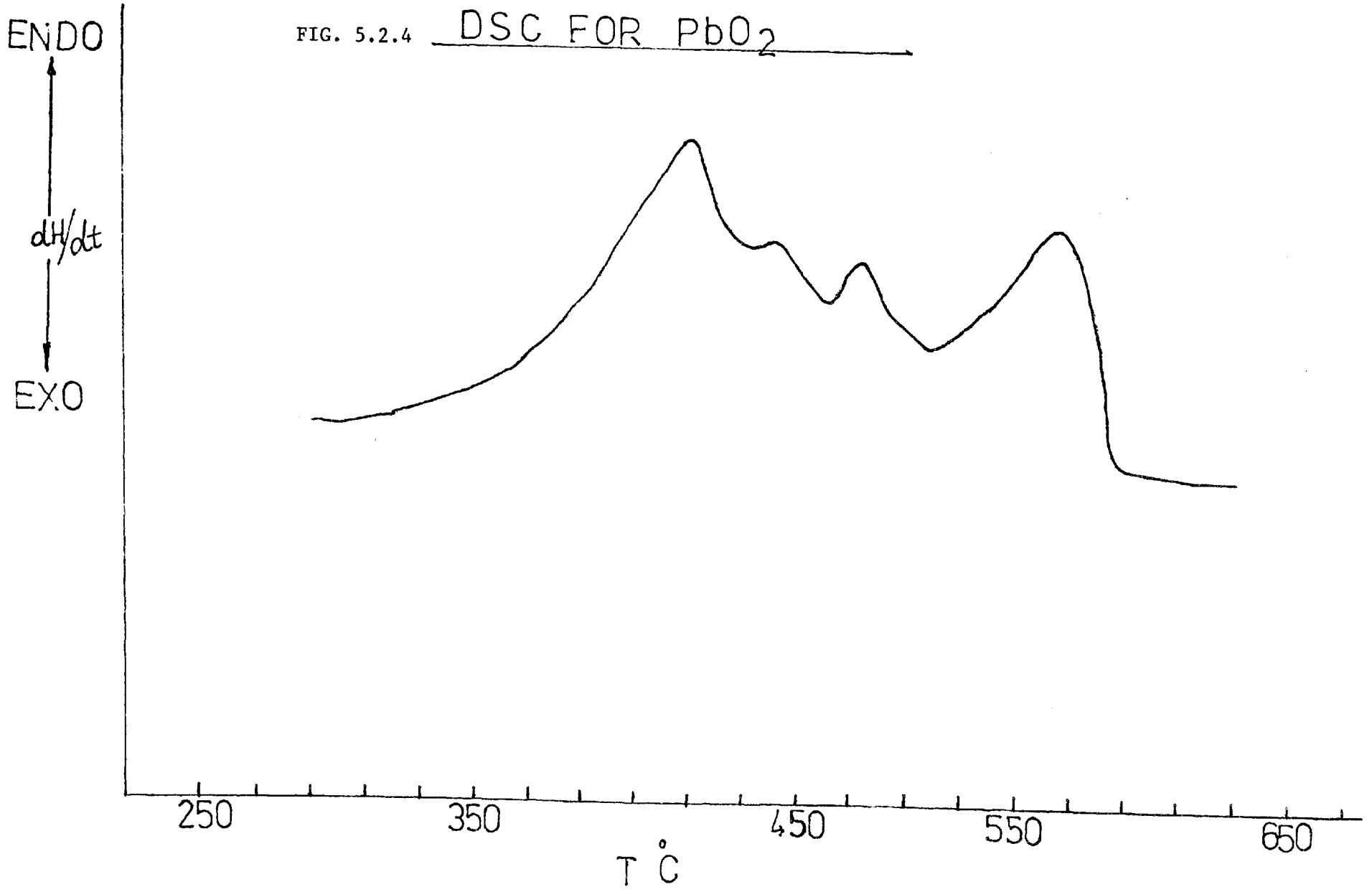

(4) DSC for lead dioxide/silicon:

Mixtures of 50/50, 70/30 and 85/15 (w/w) PbO_2/Si were examined with and without binder. The studies were performed at a heating rate of 40°C min., under a steady flow of nitrogen. The samples were prepared in the same manner as red lead/silicon samples. In each test approximately 3.0 mg. were used.

For samples containing no binder, the DSC curve started to leave the base line gradually, showing an endothermic reaction, with T_{max} at 430°C, followed by a sharp exotherm at T_{max} = (493 - 497)°C. For the 50/50, 70/30 and 85/15 mixtures, though the exothermic reaction was in all cases at approximately the same temperature, it is clear from Fig.5.2.10 that these peaks are much sharper with higher lead dioxide percent samples, indicating more reactive compositions. This reaction was followed by an endothermic peak whose maximum dH/dt took place at T_{max} 542°C as in Figure
This reaction precedes a slow exothermic reaction of a shallow peak at T_{max} 607°C.

When 0.5% of sodium carboxymethyl cellulose was added to the lead dioxide/silicon mixtures as prepared for delay compositions, the endothermic decomposition reaction of PbO_2 was observed at T_{max} 450°C, followed by the major exothermic reaction. The latter peak is of a larger area than the corresponding samples without binder as seen in Fig.5.2.10. The endothermic reaction that followed this exotherm was clearly seen in a 50/50 mixture, but was overlapped by the preceding exotherm in the more reactive mixtures of 70/30 and 85/15 PbO_2/Si.

FIG. 5.2.10 DSC FOR PbO_2/Si (40C/MIN)

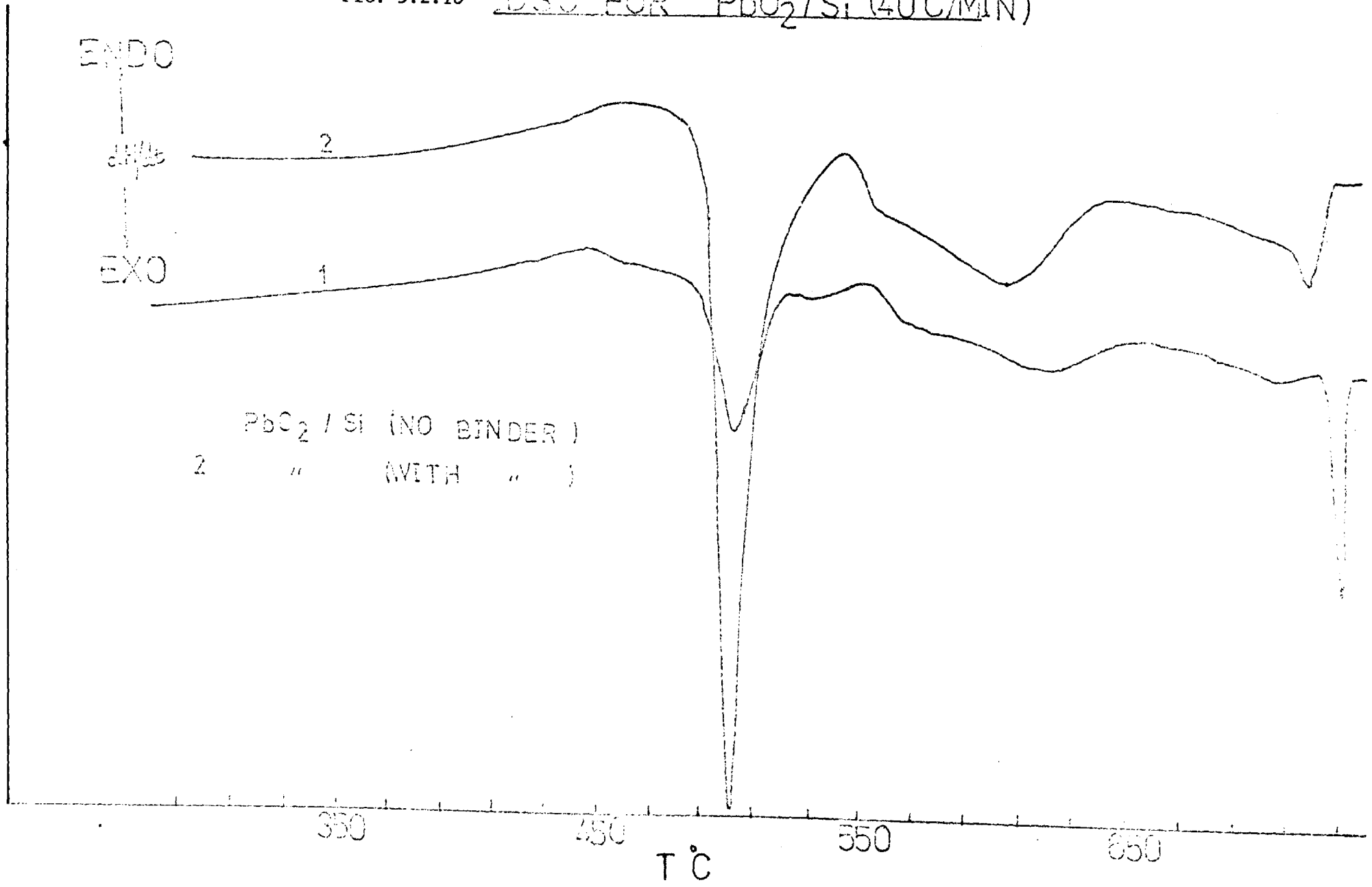

(5) DSC for binder:

Although only 0.5% of sodium carboxymethyl cellulose was used with the oxidizer/fuel compositions, it was seen that it served an important role in the reaction, necessitating an independent study. The binder was heated in controlled conditions, at a heating rate of 40°C/minute, in a nitrogen atmsophere.

An exothermic peak commenced at 280°C, reaching a maximum at 320°C. A second peak which was endothermic, commenced at 345°C, and reached its maximum at 365°C, as seen in Fig. 5.2.11.

When the binder was studied for weight loss by thermogravimetry under the same conditions, it was observed as in Fig. that there was a gradual weight loss at 270°C, which became rather sharp soon after, and gave a maximum rate of loss of weight (DTG) at 310°C. The weight loss from the DTG curve corresponds to the exothermic reaction, but for the endothermic reaction that followed, the TG curve showed no weight variation, and the endothermic peak is likely to be due to a physical change, possibly melting.

The pyrolytic decomposition of the binder involves various processes.[54] The first is a slight weight loss of water, followed by a slight loss of weight that can be attributed to an intermolecular reaction to form a dehydrocellulose. The exothermic process can be ascribed to a reaction of the dehydrocellulose which experiences carbon-carbon and carbon-oxygen bond ruptures, to produce volatile carbon - containing compounds, and intermolecular condensations to produce char. The formation of the carbon-oxygen double bond, or

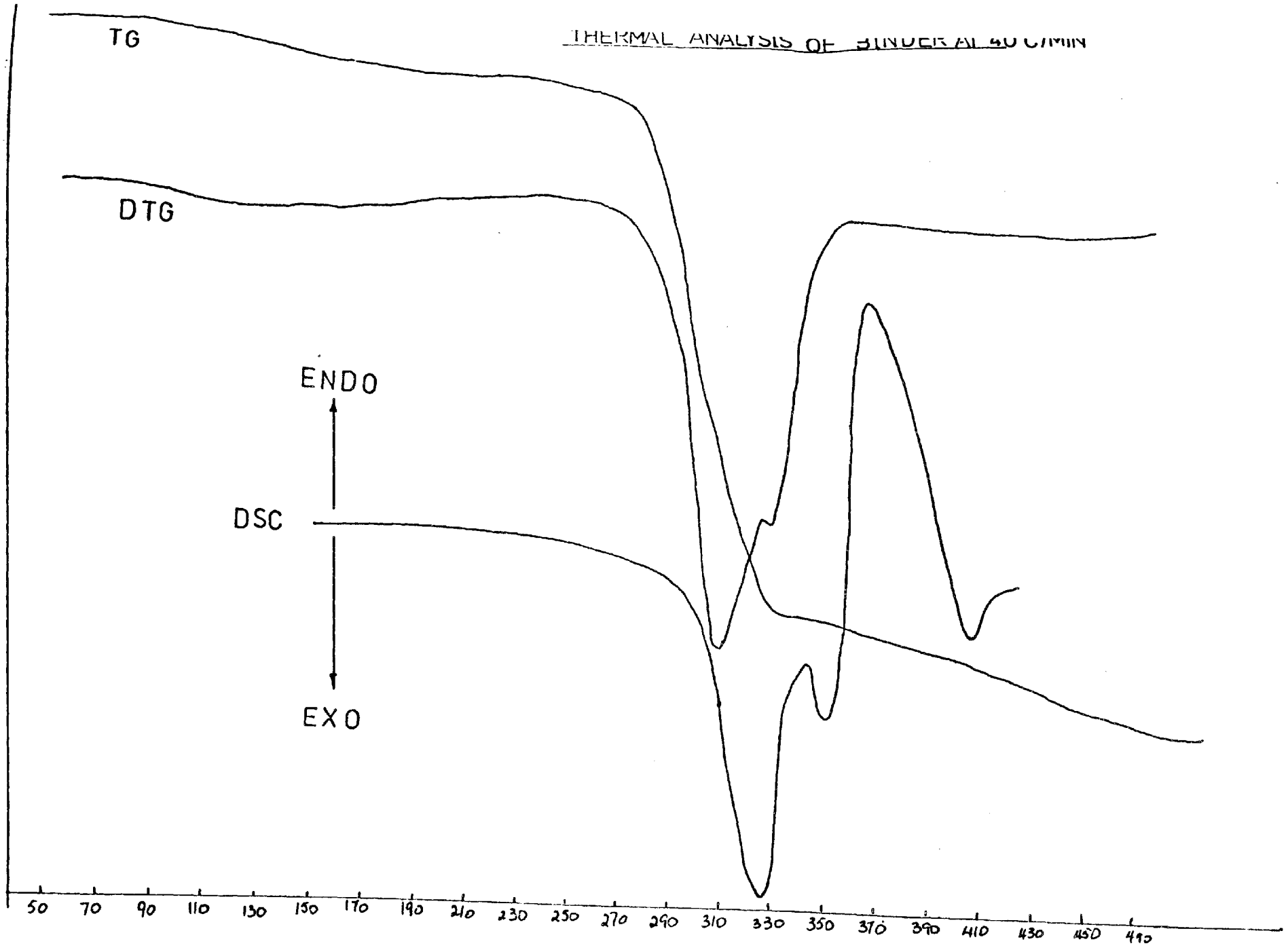
TG
THERMAL ANALYSIS OF BINDER AT 40 C/MIN
DTG
ENDO
DSC
EXO
50 70 90 110 130 150 170 190 210 230 250 270 290 310 330 350 370 390 410 430 450 490
T °C

FIG . 5. 2 .11

carbon monoxide, can provide energy which contributes to the exotherm observed in DSC curve.

(6) Effect of heating rate on temperature of reaction:

When DSC was performed under different heating rates with all other conditions identical, the variation is illustrated by curves for lead dioxide/silicon and red lead/silicon as in figures 5.2.11, 5.2.12 and 5.2.8. It can be seen from the figures and the table below that maximum change in dH/dt, which is the peak maximum, occurs at higher T_{max} as the heating rate increases, but the peaks are larger and much sharper. This may be due to the fact that at lower heating rates, the reactants are given longer times to attain the temperature of the furnace and so reach their maximum reaction rate at a lower temperature than those at a fast heating rate.

HEATING RATE ^{o}C/Min.	85/15 PbO_2/Si T_{max} ^{o}C	85/15 Pb_3O_4/Si T_{max} ^{o}C		
		1st PEAK	2nd PEAK	3rd PEAK
10	475	-	-	-
20	489	483	600	678
40	499	490	610	687
80	511	506	628	703
160	527			

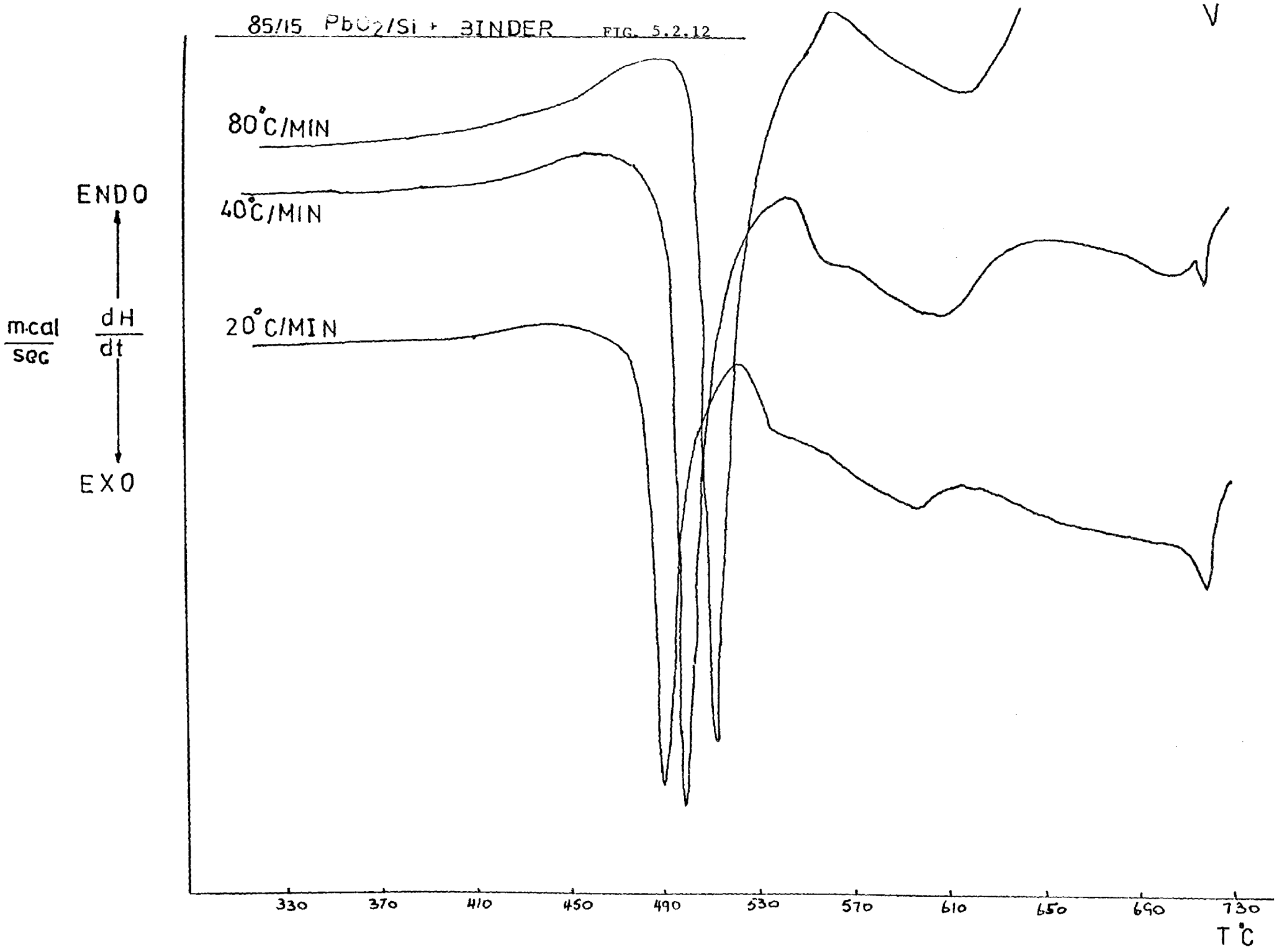
85/15 PbO2/Si + BINDER FIG. 5.2.12
V
80°C/MIN
40°C/MIN
20°C/MIN
ENDO
m·cal/sec
dH/dt
EXO
330
370
410
450
490
530
570
610
650
690
730
T°C

FIG.5.2.13 DSC FOR PbO_2/Si AT 40°C/MIN

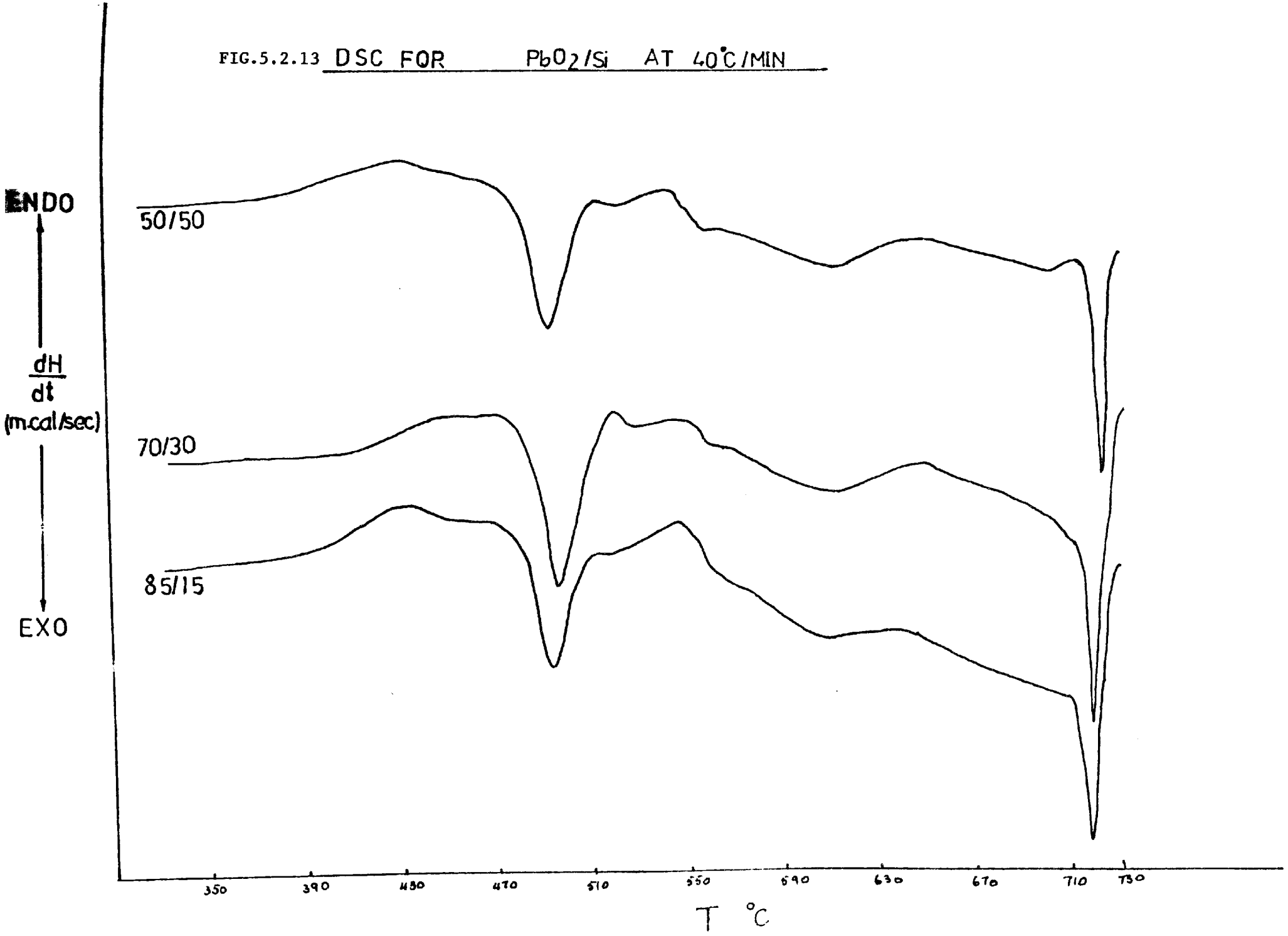

COMPOSITION	T_{max} °C 1st PEAK	T_{max} °C 2nd PEAK	T_{max} °C 3rd PEAK
red lead/silicon + binder	482 - 492	610 - 612	677 - 687
red lead/silicon	487 - 492	625	684 - 690

It appears that though the temperature at which peak maximum occurred was close for mixtures with and without binder, the relative size of the peaks differed. Whereas the third peaks are very small for compositions without binder, they are the largest peaks for samples containing binder. The effect of binder in providing a better contact of the reactants seems to have taken the reaction to a greater extent. Figs.5.2.10 & 13 illustrate this effect on dH/dt against temperature curves.

The heat evolved from samples containing binder is seen from the table below to be greater than that from samples without binder.

Pb_3O_4/Si	HEATING RATE °C/Min.	F.S.D. m.cal./s	AREA cm^2/g	TOTAL HEAT EVOLVED J/g
50/50	40	20	3788.7	416.2
70/30	40	20	6974.2	766.1
85/15	40	20	8034.0	882.5

5.2.3 THERMOGRAVIMETRY TG

(1) TG for Pb_3O_4:

The thermal decomposition of red lead is presented in Fig.5.2.14 which shows that the weight loss, on heating a small sample under nitrogen flow, corresponds to the equation

$$2\ Pb_3O_4 \rightarrow 6\ PbO + O_2$$

The theoretical amount of oxygen evolved for a stoichiometric reaction is 2.33%, the observed values from the TG study were 2.68% - 2.90%, according to rate of heating, as seen in the table following. The loss of a slight amount of water retained by the powder, and loss of some impurities that may decompose or vapourise over the temperature range studied (20 - 730°C) may account partly for the difference between calculated and observed values, but this difference could mainly be due to sublimation of the lead monoxide formed specially at the higher temperatures of the range.

The reaction above is also confirmed by the close agreement of the changes that existed on DSC and TG and DTG results when the experiments were performed in identical conditions, as seen by superimposing the two curves obtained from DSC and TG, as in Figure

Similar to the changes that occurred in the T_{max} for different heating rates on DSC, the DTG peaks were also seen to be influenced by the heating rate, i.e. the maximum rate of weight loss was noted to take place at a higher temperature as the heating rate was increased from 10°C/min. to 160°C/min. as shown on the table.

FIG.5.2.14 Pb3O4 10 C/MIN

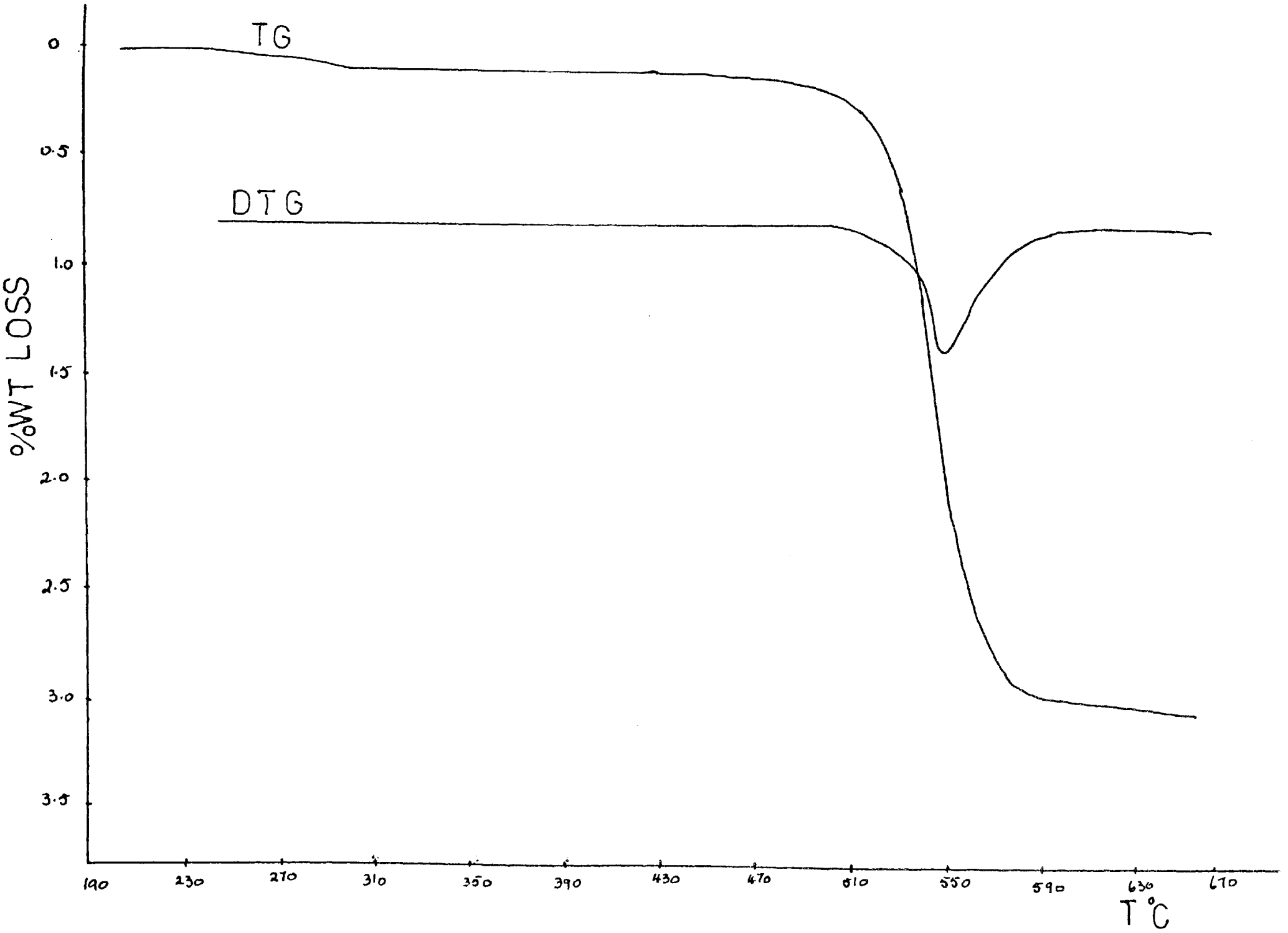

HEATING RATE °C/Min.	PEAK TEMP. °C			% WT.LOSS
	START	MAX.	END.	
10	470	550	600	2.90
40	490	604	660	2.80
80	530	630	700	2.75
160	585	668	735	2.68

(2) TG for Pb_3O_4/Si

When red lead and silicon of weight ratio 85/15 was studied by TG, the weight losses as percentages of the red lead were measured under different heating rates for

1. 85/15 Pb_3O_4/Si
2. 85/15 Pb_3O_4/Si + Binder

The results of these were compared with weight loss from the decomposition of Pb_3O_4 on its own.

HEATING RATE °C/Min.	Pb_3O_4		Pb_3O_4/Si		Pb_3O_4/Si + BINDER	
	T_{max} °C	% Wt. loss	T_{max} °C	% Wt. loss	T_{max} °C	% Wt. loss
10	550	2.90	558	1.24	556	1.25
40	604	2.75			610	1.36

The weight loss from red lead/silicon compositions is much smaller than the weight loss from the red lead under the same

FIG. 5.2.15 THERMAL ANALYSIS OF 85/15 Pb_3O_4/Si + BINDER AT 10°C/MIN

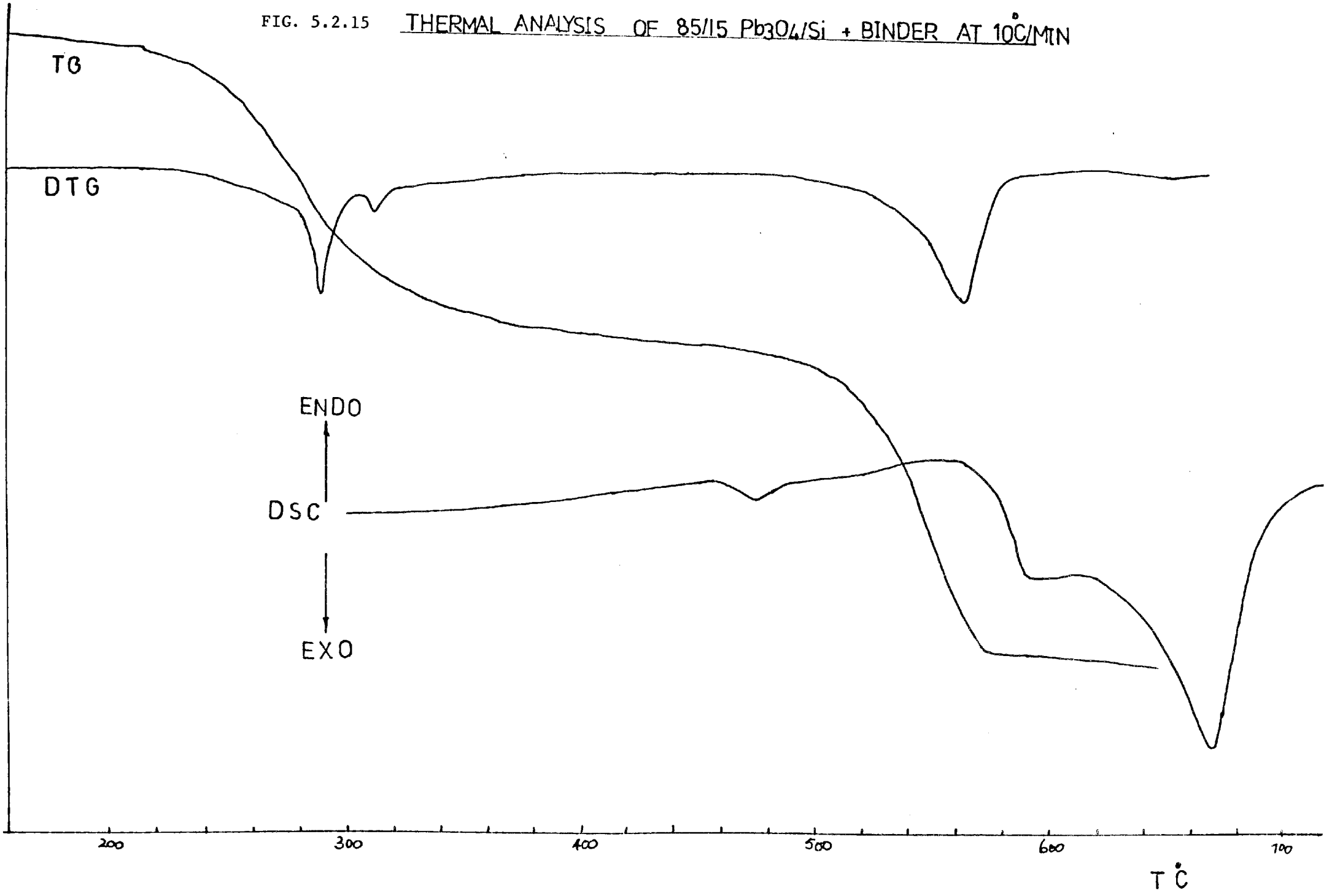

FIG. 5.2.16

THERMAL ANALYSIS OF 85/15 Pb_3O_4/Si + BINDER AT 40°C/MIN

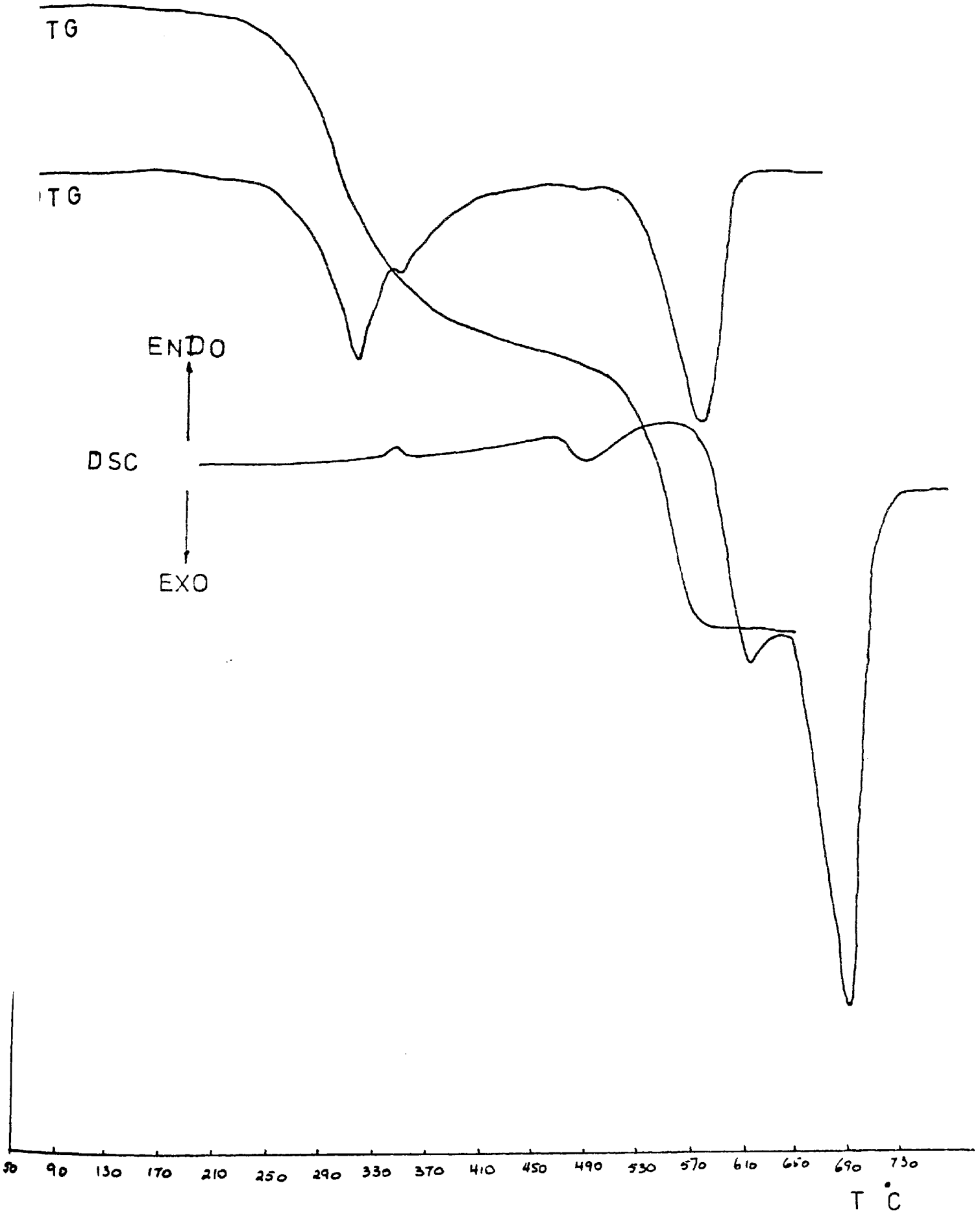

FIG. 5.2.17

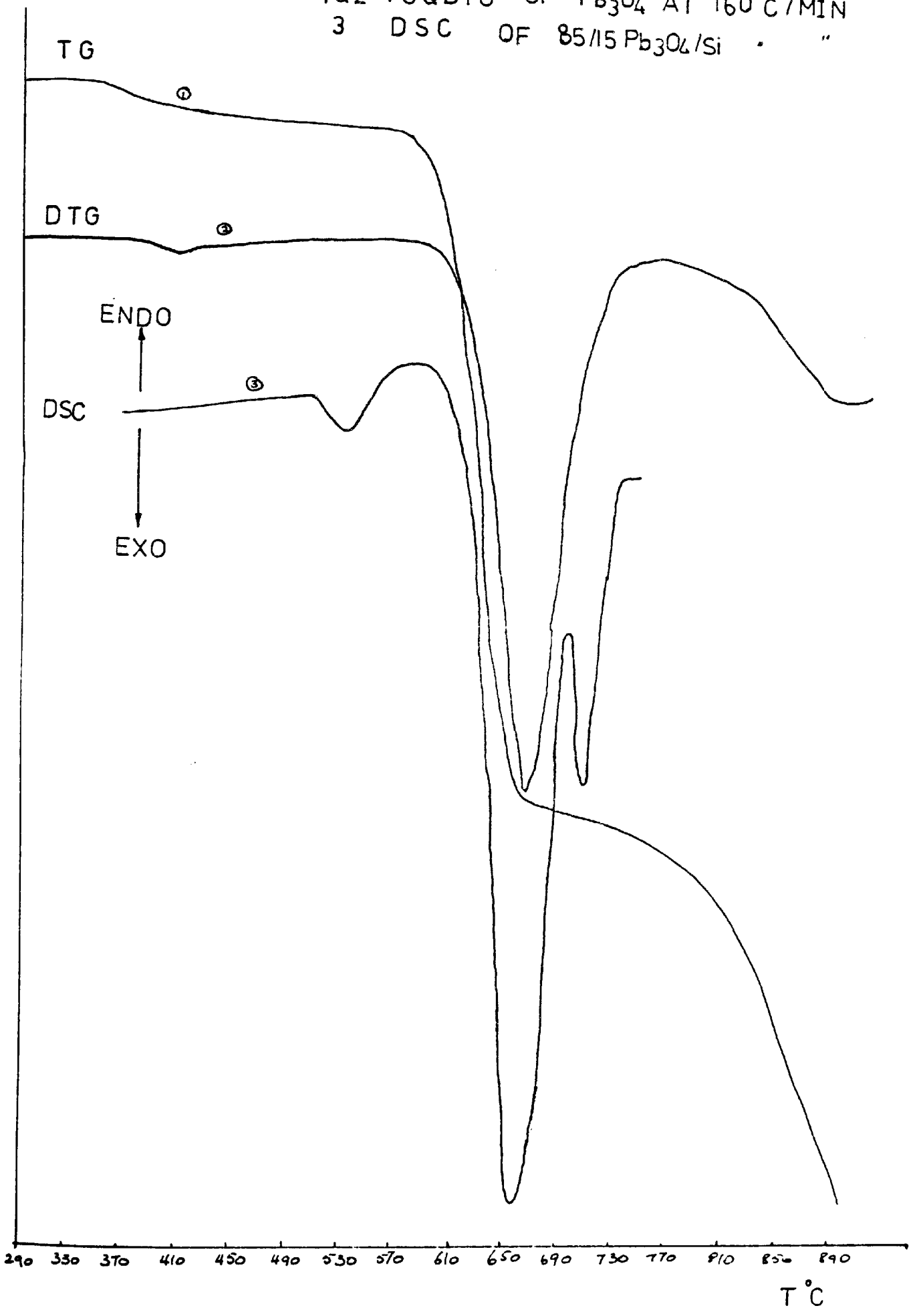
1&2 TG&DTG OF Pb_3O_4 AT 160 C/MIN
3 DSC OF 85/15 Pb_3O_4/Si " "
TG
①
DTG
②
ENDO
DSC
③
EXO
290 330 370 410 450 490 530 570 610 650 690 730 770 810 850 890
T °C

conditions, confirming that part of the oxygen is being lost during the reaction.

There is a distinct DTG peak at approximately 350°C, for samples containing binder only. This is due solely to loss of weight on decomposition of the binder.

TG and DTG for these mixtures are illustrated in Figures 5.2.15, 16 & 17.

(3) TG for PbO_2

On heating a small sample of lead dioxide, approximately 20 mg., under a constant flow of nitrogen, at known heating rates, the weight loss as shown by TG and DTG curves in Figs.5.2.18 - 22 is a result of the decomposition reactions of PbO_2 to give lead monoxide and oxygen, as discussed earlier. The theoretical oxygen that can be lost from the lead dioxide on decomposition is 6.69%, whilst the observed weight loss from this study over the temperature range 350 - 582°C is 6.59%. The temperature of decomposition, and the percentage of weight lost for each of the four reactions involved is shown in the following table.

The weight loss from lead dioxide, on its own or in a mixture with silicon in thefirst decomposition reaction T_{max} (400 - 440°C) constitutes the largest percentage loss among the four reactions.

The proportion of oxygen lost from the PbO_2/Si is much greater than the Pb_3O_4/Si. This is possibly due to the low temper-

FIG.5.2.18

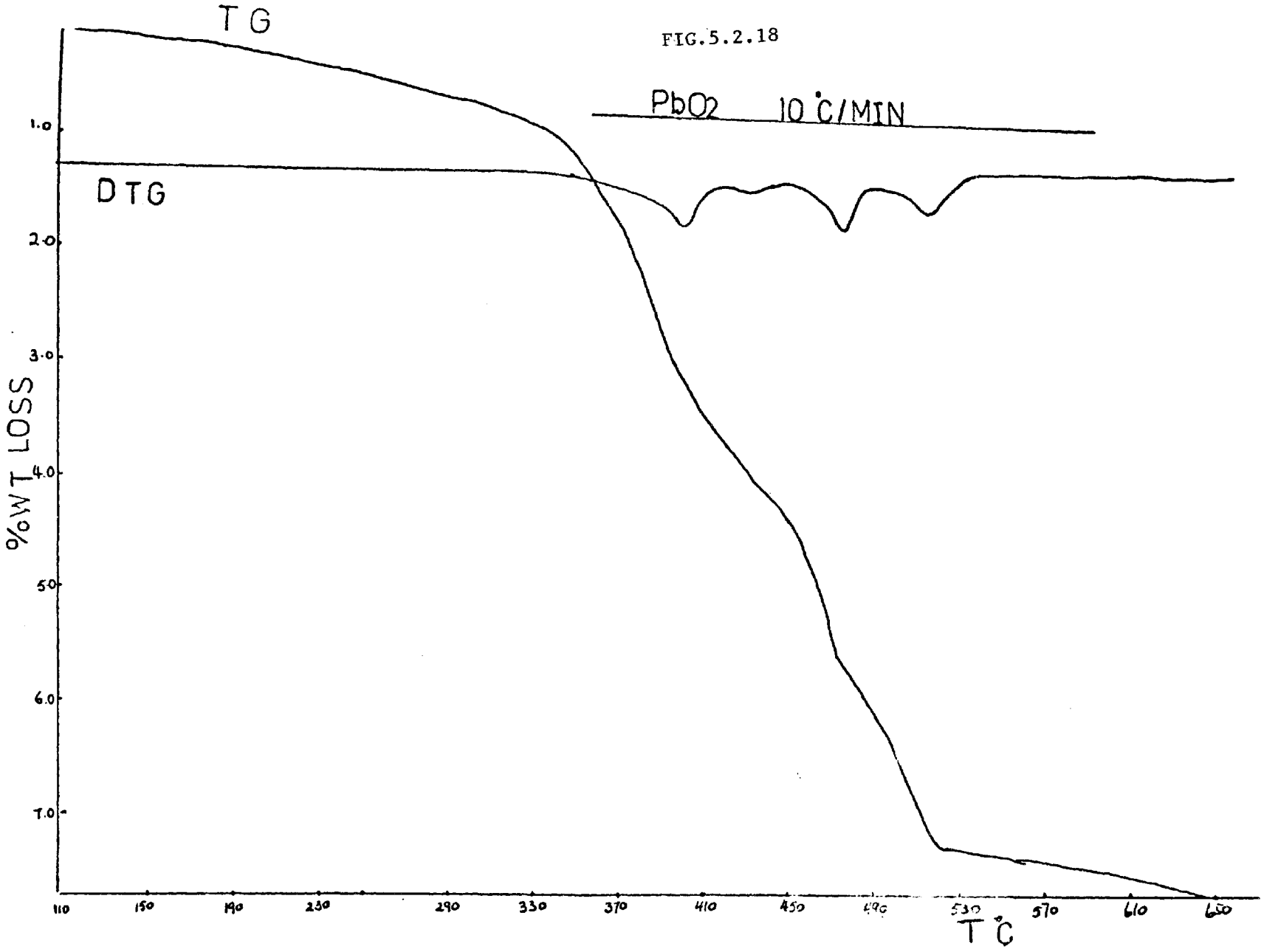
TG
DTG
PbO2 10 °C/MIN
%WT LOSS
1.0
2.0
3.0
4.0
5.0
6.0
7.0
110
150
190
230
290
330
370
410
450
530
570
610
650
T °C

FIG. 5.2.19

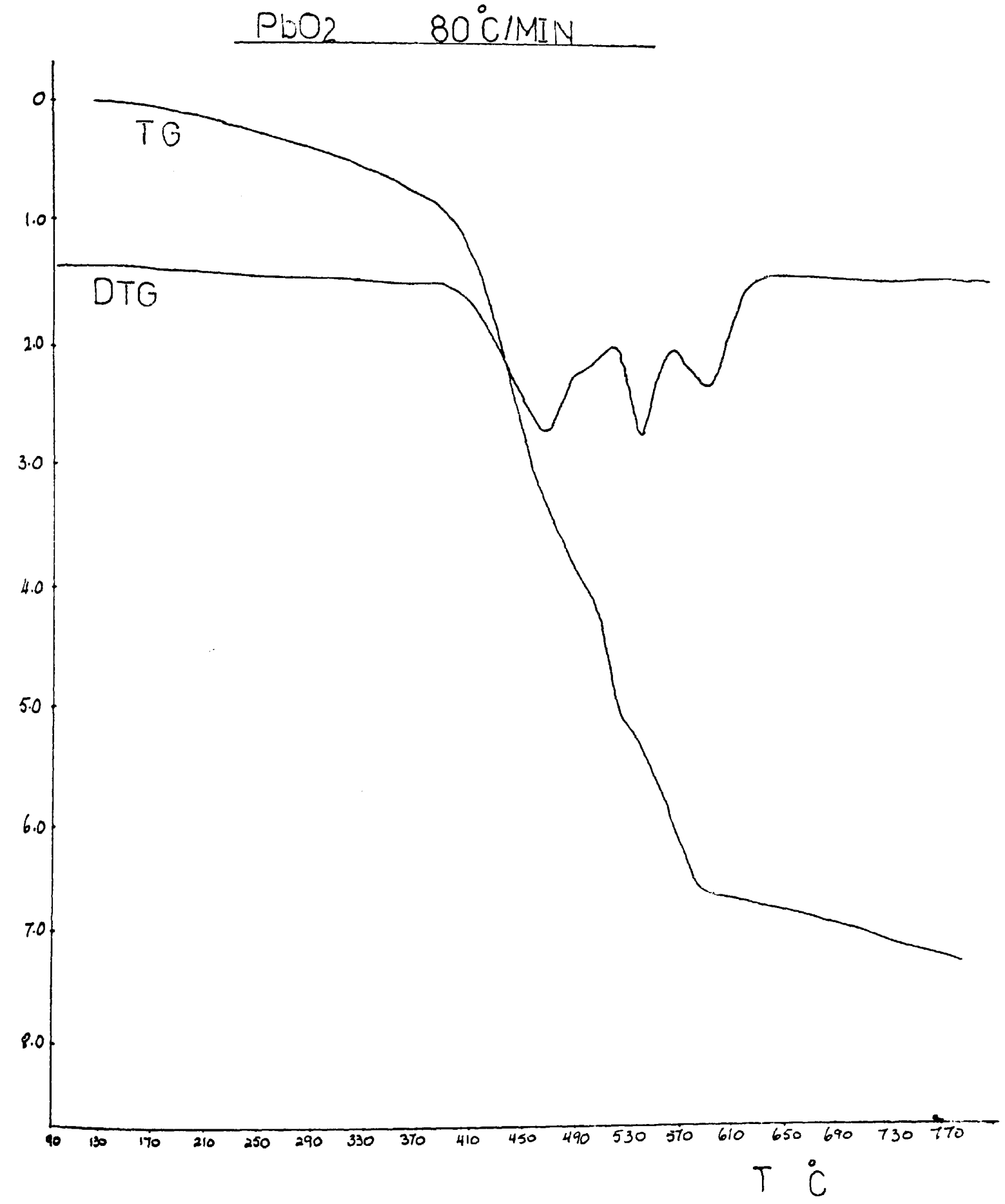
PbO2 80°C/MIN
TG
DTG
0
1.0
2.0
3.0
4.0
5.0
6.0
7.0
8.0
90 130 170 210 250 290 330 370 410 450 490 530 570 610 650 690 730 770
T °C

FIG. 5.2.20

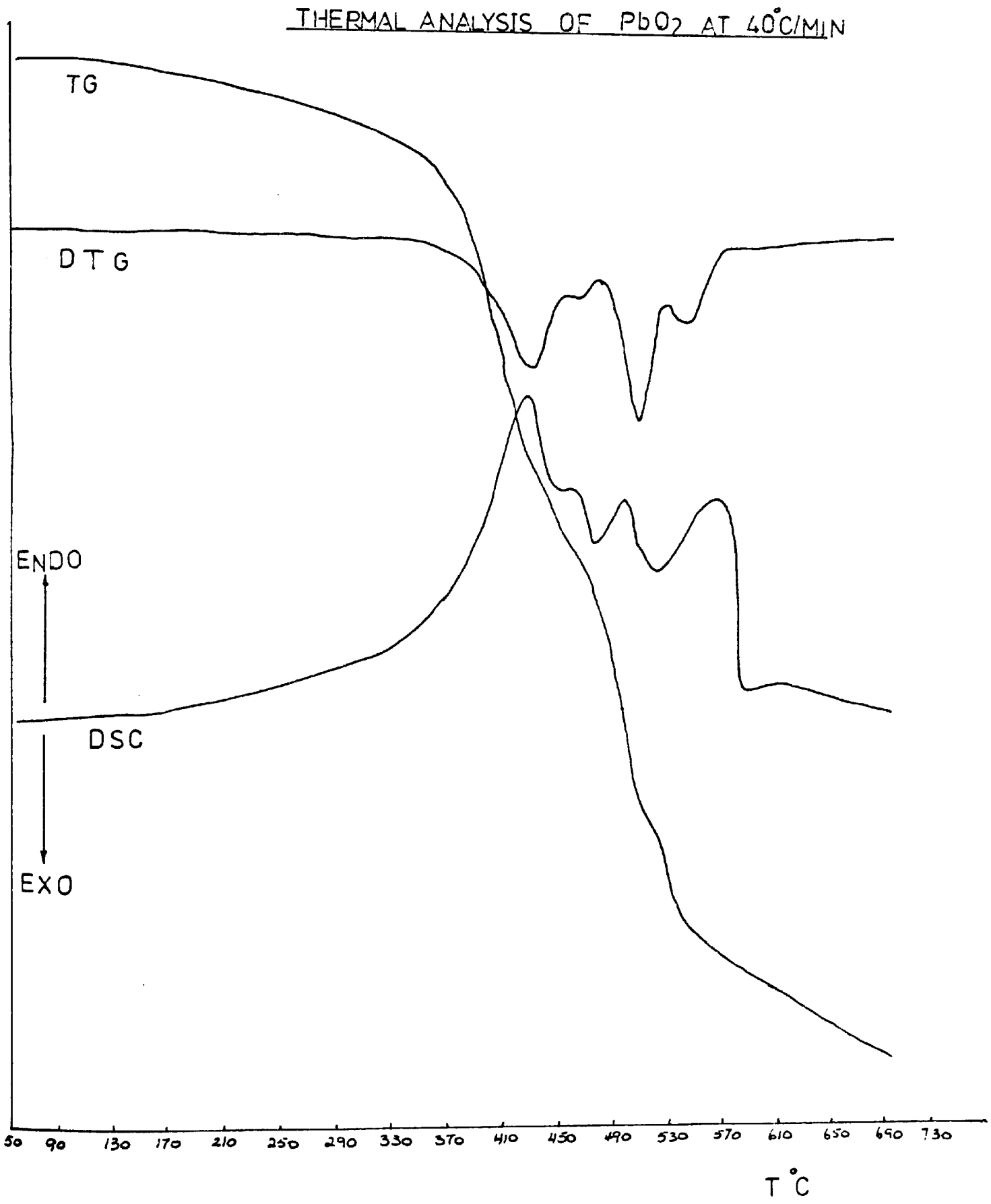
THERMAL ANALYSIS OF PbO2 AT 40°C/MIN
TG
DTG
ENDO
DSC
EXO
50 90 130 170 210 250 290 330 370 410 450 490 530 570 610 650 690 730
T °C

FIG. 5.2.21

THERMAL ANALYSIS OF 85/15 PbO_2/Si AT 40°C/MIN

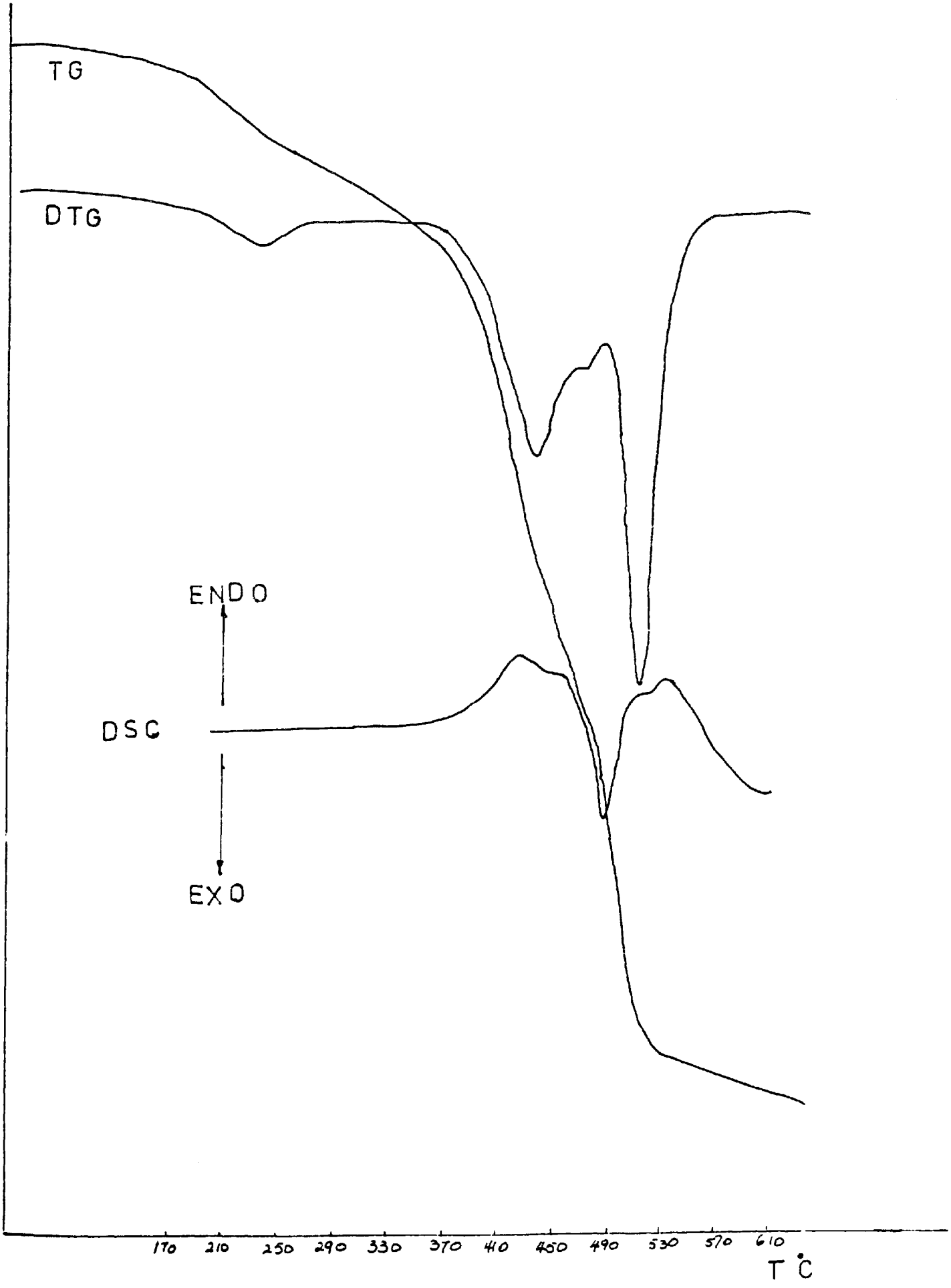

FIG. 5.2.22

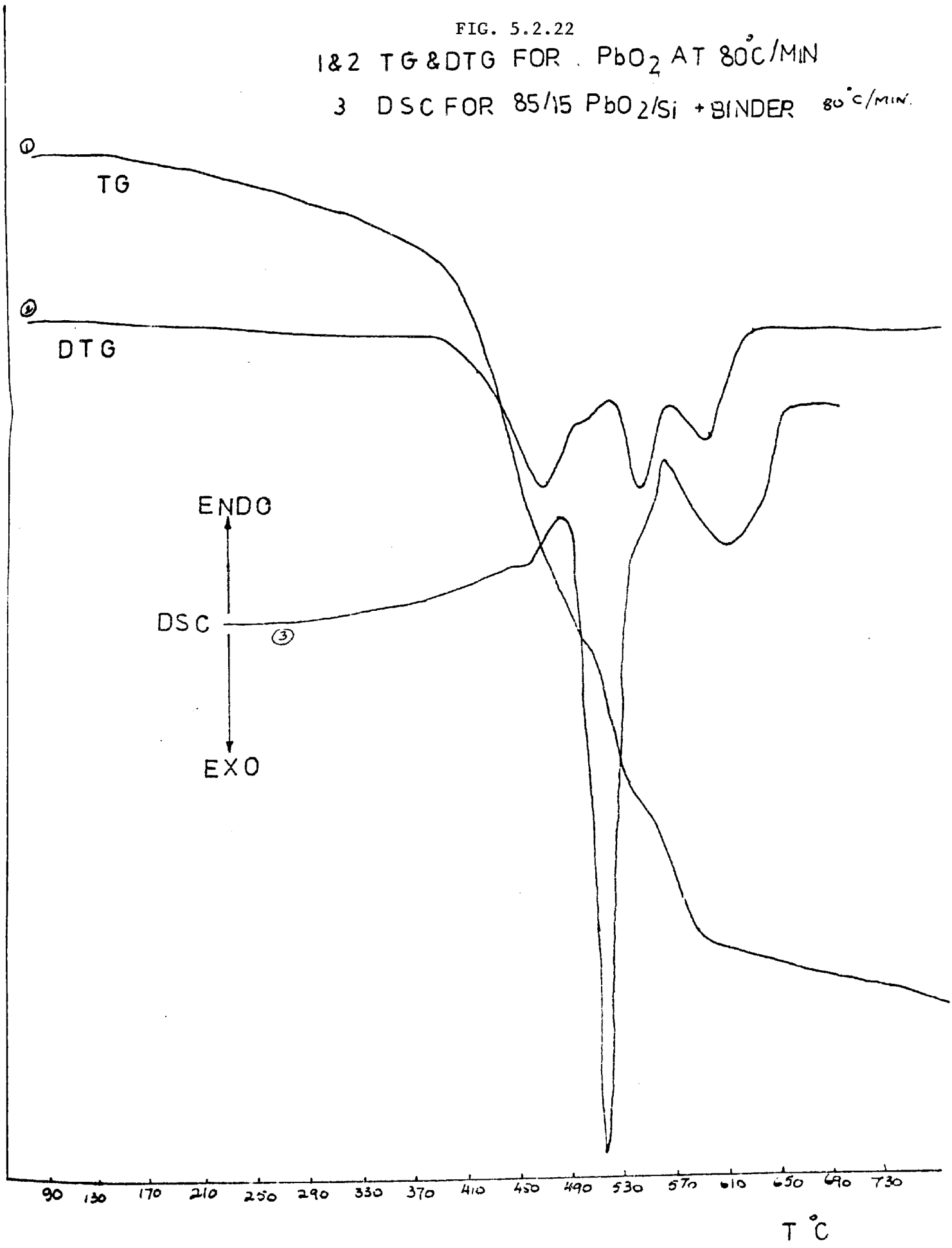
1&2 TG & DTG FOR PbO_2 AT 80°C/MIN
3 DSC FOR 85/15 PbO_2/Si + BINDER 80°C/MIN.
①
TG
②
DTG
ENDO
DSC
③
EXO
90 130 170 210 250 290 330 370 410 450 490 530 570 610 650 690 730
T °C

ature of decomposition, which does not favour the reaction of silicon with oxygen, making the reaction consist almost entirely of Pb_3O_4 and silicon.

HEATING RATE (^oC/min.)	PbO_2		85/15 PbO_2/Si		85/15 PbO_2/Si + BINDER	
	T_{max} ^oC.	WT. LOSS %	T_{max} ^oC.	WT. LOSS %	T_{max} ^oC.	WT. LOSS %
10	-	-	-	-	310	0.46
	404	2.62	400	2.06	420	2.11
	436	0.81	435	0.69	-	-
	478	1.67	482	1.70	478	1.01
	518	1.24	-		-	-
					3.40	0.31
40	438	3.08	440	2.86	435	2.14
	476	0.77	-	-	-	
	518	2.12	518	1.82	-	
	554	0.62	-	-	-	

5.2.4. DISCUSSION OF THERMAL ANALYSIS RESULTS

Thermal analysis of red lead has shown an endothermic peak maximum at 590^o and loss of weight on TG curve. X-ray diffraction analysis revealed the formation of PbO (litharge), hence the following decomposition reaction has occurred

$$2\ Pb_3O_4 \rightarrow 6\ PbO + O_2$$

and weight loss is due to the loss of the oxygen from the system.

The second peak, which was also endothermic on DTA, did

not show a weight loss on TG curve, hence this was merely a physical change. X-ray analysis of the product at this second peak, showed no change from the product of the first reaction, so the temperature 868°C (T_{max} of 2nd peak) was the melting point of the PbO that formed from the decomposition reaction. As the temperature of the sample was raised above the melting point of the PbO, DTA curve declined continuously due to loss of heat on vapourisation of PbO. This was confirmed by weight loss on TG curve, as in Fig. 5.2.1. Studies by Sulacsik (55) on red lead, using 2 g. samples in MOM derivatograph equipment, revealed that litharge was formed on decomposition at 560 - 570°C. A study by Nakahara (56) confirmed the decomposition of red lead at 600°C.

The reaction of Pb_3O_4/Si in nitrogen produced a DTA peak with T_{max} 585 - 600°C. This is approximately the same temperature as T_{max} for red lead decomposition, and so it seems that decomposition of red lead and the reaction with silicon are taking place simultaneously. These reactions can be illustrated by the following

$$2\ Pb_3O_4 \xrightarrow{590^{\circ}C} 6\ PbO + O_2$$

$$Si + O_2 \rightarrow Si\ O_2$$

$$2\ PbO + Si \rightarrow Si\ O_2 + 2Pb$$

Thermal gravimetry study performed on a sample of 85/15 (W/W) Pb_3O_4/Si has shown that the DTG peak and DSC peak occurred at the same temperature, and therefore the maximum rate of weight loss and maximum rate of dH/dt occurred at the same temperature as in Fig. 5.2.16. The weight loss from red lead alone was greater than the weight loss from Pb_3O_4/Si, as shown in the following table.

HEATING RATE °C/MIN	% WT. LOSS Pb_3O_4	% WT. LOSS Pb_3O_4/Si
10	2.9	0.59
40	2.80	0.49
80	2.75	0.48

The theoretical amount of oxygen that can decompose from Pb_3O_4 is 2.33%. As can be seen from the table above, only a fraction of the total oxygen was lost from red lead/silicon system, and the rest must have reacted. It is probable that oxygen freshly formed is more reactive than oxygen from air, or it could be that the oxygen reacted with the silicon after the lead monoxide reacted with silicon.

$$2\ PbO + Si \rightarrow 2\ Pb + SiO_2$$

This is an exothermic reaction which raises the temperature of the silicon to a high temperature, where the reaction of silicon and oxygen would be favoured.

The formation of lead, silica and presence of excess silicon were confirmed by X-ray diffraction analysis and infra-red spectroscopy.

Samples containing up to 70% Pb_3O_4, when heated under nitrogen, produced no further reactions at temperatures above 600°C, as the silicon area available for reaction was sufficient to react with PbO formed from decomposition. Samples with greater Pb_3O_4 than 70%, when studied under the same conditions, displayed two

further exothermic peaks which, though smaller than the first, nevertheless, were quite significant. These last two reactions were noted at T_{max} 670 and 762°C.

It can be interpreted that the reaction was initiated on decomposition of the red lead, and the oxygen formed reacted with the silicon, forming a silica film on the surface of the silicon particles. This proceeds concurrently with the lead monoxide/silicon reaction, resulting in the formation of more silica. This layer of silica makes it difficult for further oxidation reaction to take place, especially for high oxidant mixtures (>70% Pb_3O_4) where the unreacted PbO will form a solid solution with the silica to enable the reaction to progress further.[57,58] These reactions can be represented by

$$Si + O_2 \rightarrow Si\ O_2$$

$$2\ PbO + Si \rightarrow 2\ Pb + Si\ O_2$$

$$YPbO + x\ SiO_2 \rightarrow YPbO\ x\ Si\ O_2$$

The PbO/SiO_2 will exist in a solid solution, and depending on the ratio of the two components, (due to the different compositions ratios used), silicates of varying complexity are formed. Geller et al (59) have shown in the phase diagram of PbO - SiO_2, that when SiO_2 exceeds 29.6% by weight, the SiO_2 will become the main phase on cooling.

The reactions of red lead/silicon in air are illustrated by three exothermic peaks at T_{max} 590, 665 and 730°C as in Fig. 5.2.2. The first peak was formed at the same temperature as that of reaction in nitrogen, but the peak area is larger in air. The second peak

was a very sharp exothermic reaction, and the third peak was relatively small and less sharp than the previous two exotherms. For these reactions, the lead formed during the reaction will react at temperature 600 to 665°C with atmospheric oxygen to form lead monoxide; this in turn will react with the silicon, giving a sharp exothermic reaction, raising the temperature of the excess silicon high enough to react with atmospheric oxygen.

The DTA results in air can be compared with those in nitrogen. In the nitrogen, the lead formed at 600°C could not oxidise and therefore could not react further. The reaction in nitrogen observed at approximately 660°C is that of the unreacted PbO with SiO_2 and Si.

The area under the ΔT versus time curve, which is a function of the amount of heat evolved during the reaction, was measured for each red lead/silicon mixture. Since the temperature range at which the reactions take place was approximately the same for different mixtures, these areas could be compared, by plotting against the percentage silicon of the different compositions. It can be seen from Fig. 5.2.23 that the maximum heat evolved was at 90/10 mixture, which is near the stoichiometric proportion for the reaction

$$Pb_3O_4 + 2\ Si \rightarrow 2\ SiO_2 + 3Pb$$

For samples containing more than 10% silicon, there is less oxidant than is necessary. At the same time, more heat is absorbed in melting products and for raising the temperature of the unreacted materials.

FIG. 5.2.23

AREA UNDER DTA PEAK FOR Pb_3O_4/Si IN NITROGEN

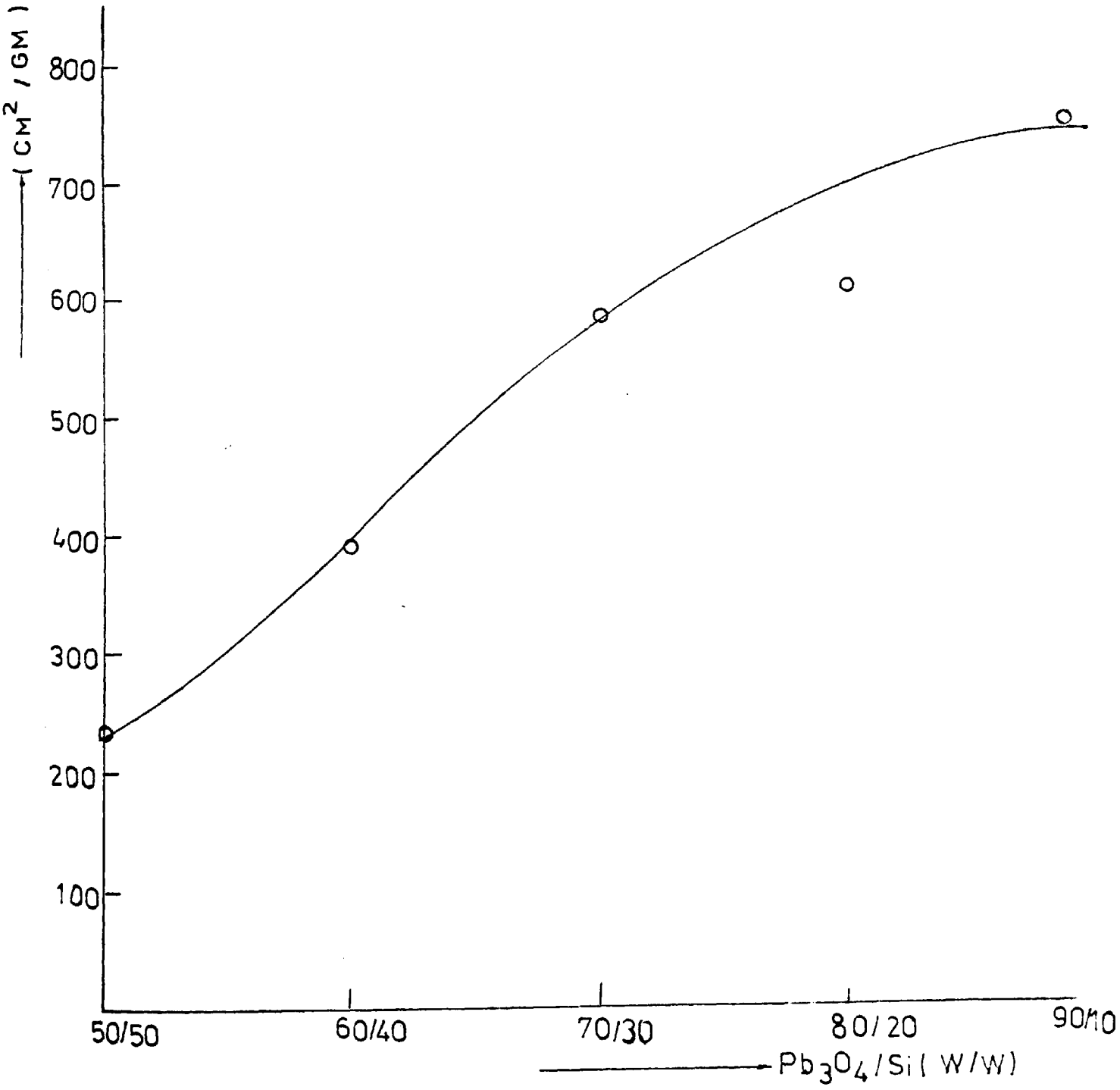

5.2.5 THEORETICAL ASPECTS OF THERMAL ANALYSIS

The measurement and interpretation of the solid state reaction kinetics of metal-oxidant powder mixtures was studied by Spice and Stavely (10) who showed that the preignition reaction between iron and barium peroxide is a true solid state process and deduced from a consideration of the kinetics that the process is not diffusion controlled. In contrast, Schwab and Gerlach (60) investigated the reaction between germanium and molybdenum trioxide and showed that the reaction is diffusion controlled. Beardell et al (30) studied the kinetics of the solid state reaction of zirconium and molydenum trioxide powders by both isothermal and DTA methods. They found that the reaction is a two stage process in which the MoO_3 is first reduced to MoO_2 and then to Mo. The first stage reaction they concluded is a diffusion controlled at the lower temperature but changes to a kinetically controlled mechanism at the higher temperature.

The equations that have been used in kinetic analysis of solid phase reactions can be grouped into

1. Acceleratory period of reaction only

   (a) power law $(\alpha)^{1/n} = Kt$ ... (1)

   (b) exponential law $\ell n\ \alpha = Kt$ ... (2)

2. Sigmoid shaped α - t curves: These are forms of Avrami-Erofeev (61) equation.

   (a) $\left[-\ell n\ (1-\alpha)\right]^{\frac{1}{2}} = Kt$ ... (3)

   (b) $\left[-\ell n\ (1-\alpha)\right]^{1/3} = Kt$ ... (4)

(c) $\left[-\ell n\ (1-\alpha)\right]^{\frac{1}{4}} = Kt$ ... (5)

and a Prout-Tompkins (62) equation

(d) $\ell n\ (\frac{\alpha}{1-\alpha}) = Kt$ ... (6)

3. Diffusion type reactions

(a) diffusion in one dimension $\alpha^2 = Kt$ ... (7)

(b) diffusion in two dimensions

$(1-\alpha)\ \ell n\ (1-\alpha) + \alpha = Kt$ ... (8)

(c) diffusion in three dimensions

$\left[1-(1-\alpha)^{1/3}\right]^2 = Kt$ ... (9)

(d) and the Gistling-Brownshtein equation (63)

$(1-\frac{2\alpha}{3}) - (1-\alpha)^{2/3} = Kt$ ... (10)

Determination of kinetic parameters from DTA, DSC and TG

There are many methods that may be used to determine the kinetics of heterogeneous reaction. One method is that proposed by Kissinger (64), this was derived from the work of Murray and White (65). The method is based on the equation

$$\frac{d(\ell n\ \frac{\theta}{T_m^{\ 2}})}{d\ (\frac{1}{T_m})} = -\frac{E}{R} \qquad \ldots \quad (11)$$

where θ is the rate of heating

and T_m is the activation energy.

Thus by measuring the peak maxima temperatures at a number of different furnace heating rates and by plotting

$$\ell n \frac{\theta}{T_m^2} \quad \text{versus} \quad \frac{1}{T_m} \quad \text{a straight line is obtained}$$

of slope $-\frac{E}{R}$

Borchardt and Daniels (66-70) derived equations based on homogeneous kinetics but was applied to heterogeneous kinetics as well (71-73). The method is based upon the equation derived for the first order reaction

$$K = \frac{Cp\ (d\ \Delta\ T/dt) + k\ \Delta\ T}{k\ (A - a) + Cp\ \Delta\ T} \qquad \ldots \qquad (12)$$

where ΔT is the height of DTA curve

a is the area of DTA curve at T

and k is heat transfer coefficient

Approximation of the above equation gives

$$K = \frac{\Delta T}{(A - a)} \qquad \ldots \qquad (13)$$

The authors have also shown that for stirred liquid phase system, the equation

$$K = \left(\frac{A\ V}{m_o}\right)^{n-1} \cdot \frac{dH}{dt}\ (A-a)^n \qquad \ldots \qquad (14)$$

ie for $n = 1$ (first order reaction)

$$K = \frac{dH/dt}{(A-a)} \qquad \ldots \qquad (15)$$

Piloyan (74) developed a kinetic method which did not require the knowledge of the rate of reaction

$$\ell n \ \Delta T = C_1 - \frac{E}{RT} \qquad \ldots \qquad (16)$$

where C_1 is a constant

ie E can be calculated by plotting $\ell n \ \Delta T$ against $\frac{1}{T}$ and equating the slope of the straight line to $-E/R$

Other methods are the Freeman and Carrol (75) equation and Subramanian (76) equation.

If, during the course of a chemical reaction, it is assumed that the enthalpy change in a small interval of time, dt, is directly proportional to the number dm of moles that react in that interval, then

$$dH = - A \frac{dm}{m_o} \qquad \ldots \qquad (17)$$

where m_o is the number of moles of reactant present initially.

$$\text{Hence} - \frac{dm}{dt} = \frac{m_o}{A} \cdot \frac{dH}{dt} \qquad \ldots \qquad (18)$$

$$\text{and since} - \frac{dm}{dt} = m_o \frac{d\alpha}{dt} \qquad \ldots \qquad (19)$$

where α is the fraction reacted $= \frac{m}{m_o} = \frac{a}{A}$

at time t

$$\text{then} \ \frac{d\alpha}{dt} = \frac{1}{A} \frac{dH}{dt} \qquad \ldots \qquad (20)$$

$$\text{also} \ \frac{d\alpha}{dt} = K(1 - \alpha)^n \qquad \ldots \qquad (21)$$

$$\text{then } K = \frac{A^{n-1}}{(A-a)^n} \cdot \frac{dH}{dt} \quad \ldots \quad (22)$$

$\frac{dH}{dt}$ is the ordinate on the DSC plot

and a is the area at time t

A is the total area under peak

For a first order reaction n = 1

$$K = \frac{1}{(A-a)} \cdot \frac{dH}{dt} \quad \ldots \quad (23)$$

For n = o

$$K = \frac{1}{A} \frac{dH}{dt} \quad \ldots \quad (24)$$

This is also the same equation for negligible values of a, ie. at the start of the reaction, representing the interfacial reaction at the induction period.

The kinetics of solid state reactions are based on the equations relating the fraction α of total product formed to the time of reaction t. These equations are of the form

$$\frac{d\alpha}{dt} = Kf(\alpha) \quad \ldots \quad (25)$$

originally the equation above was considered valid only for isothermal conditions. MacCallum and Tanner (77) suggested that α is a function of time and temperature only in $\alpha = f(t, T)$.

$$\partial\alpha = \left(\frac{\partial\alpha}{\partial t}\right)_T . \partial t + \left(\frac{\partial\alpha}{\partial T}\right)_t . \partial T \quad \ldots \quad (26)$$

$$\frac{\partial\alpha}{\partial t} = \left(\frac{\partial\alpha}{\partial t}\right)_T + \left(\frac{\partial\alpha}{\partial T}\right)_t . \theta \quad \ldots \quad (27)$$

and $\left(\frac{\partial\alpha}{\partial t}\right)_T$ is the rate of reaction with respect to time at temperature T (isothermal) i.e. for $\theta = 0$

However, it is argued by Felder and Stahl (78) that

$\left(\frac{\partial\alpha}{\partial t}\right)_t$, the rate of reaction with respect to temperature at time t, is zero, and therefore, they argued that α is a function of time, temperature and also the reaction path taken. Hence the generalized rate equation

$$\frac{d\alpha}{dt} = Kf(\alpha)$$

is valid for dynamic temperature system.

By plotting α versus t, $d\alpha/dt$ can be found by drawing tangents at different points of the curve. However, the inaccuracy of determining the $d\alpha/dt$ values and the substitution of the correct rate equations for $f(\alpha)$ according to the region of α, make the determination of the reaction kinetics rather unreliable.

Davies, Dollimore and Heal (79) developed a computer programme to determine the tangents from the plot of α versus t then a trial and error procedure was undertaken to determine the rate equation for $f(\alpha)$. The rate equation which produced the best straight line to fit to the equation:

$$\frac{d\alpha/dt}{f(\alpha)} = K = Ae^{-E/RT} \qquad \ldots \qquad (28)$$

$$\text{i.e. } \ell n \frac{d\alpha/dt}{f(\alpha)} = \ell nA - \frac{E}{RT} \qquad \ldots \qquad (29)$$

when $\ell n \frac{d\alpha/dt}{f(\alpha)}$ was plotted against $\frac{1}{T}$

and the slope is equated to $-\frac{E}{R}$

Dankiewicz et al (78) studied the kinetics of the thermal dehydration of syngenite using the isothermal gravimetric method and similar to the treatment used by Davies et al, several equations for $f(\alpha)$ were investigated. They found that their experimental results can be best represented by the Avrami equation

$$\left[- \ell n (\ell - \alpha) \right]^{\frac{1}{2}} = Kt$$

The procedure of trial and error is under criticism on many accounts which have been highlighted by Garn (79 - 80).

In the present work it is found that the existing trial and error method can be avoided if a generalised function is used to describe the reaction kinetics. The function is expressed by

$$\alpha = 1 - e^{-(\frac{t}{\gamma})^{\beta}} \qquad \ldots \qquad (30)$$

where β and γ are parametric constants which can be determined experimentally.

Equation (30) can be expressed in the logarithmic form

$$\ell n\ \ell n\ \left(\frac{1}{1-\alpha}\right) = \beta\ \ell n\ t - \beta\ \ell n\ \gamma \qquad \ldots \qquad (31)$$

By the use of this equation, β can be obtained from the slope of a straight line that should result when the data are plotted as $\ell n\ \ell n\ \left(\frac{1}{1-\alpha}\right)$ vs $\ell n\ t$ and γ can be found from the intercept of the straight line.

Differentiating equation (30) with respect to time gives

$$\frac{d\alpha}{dt} = \left(\frac{\beta}{\gamma}\right)\left(\frac{t}{\gamma}\right)^{\beta-1} . e^{-\left(\frac{t}{\gamma}\right)^{\beta}} \qquad \ldots \qquad (32)$$

substituting $e^{-\left(\frac{t}{\gamma}\right)^{\beta}}$ by the use of equation (30) gives

$$\frac{d\alpha}{dt} = \left(\frac{\beta}{\gamma}\right)\left(\frac{t}{\gamma}\right)^{\beta-1} . (1-\alpha) \qquad \ldots \qquad (33)$$

At $t = \gamma$ equation (33) reduces to

$$\frac{d\alpha}{dt} = \left(\frac{\beta}{\gamma}\right)(1-\alpha) \qquad \ldots \qquad (34)$$

This equation is the rate equation for the first order decay law with a rate constant represented by $\left(\frac{\beta}{\gamma}\right)$

$$\text{i.e. } \ell n\ \left(\frac{\beta}{\gamma}\right) = \ell n\ A - \frac{E}{RT_{0.63}} \qquad \ldots \qquad (35)$$

where $T_{0.63}$ is the temperature corresponding to $\alpha = 0.63$ which, as can be shown by equation (30), is the fraction reacted at $t = \gamma$

For isothermal decomposition of red lead $T_{0\cdot63}$ is the same as decomposition temperature. In the case of decomposition under dynamic conditions, $T_{0\cdot63}$ can be determined from α-T measurements. The temperature in these measurements is increased following a temperature - time relation.

$$T = T_o + \beta t \qquad \ldots \qquad (36)$$

$$\text{and } t = (T - T_o)/\beta \qquad \ldots \qquad (37)$$

where T_o is the temperature at zero time which is fixed at $\alpha = o$

and β is the constant rate of temperature rise

when $\alpha = 0.63$, $t = \gamma$ and hence

$$\gamma = (T_{0\cdot63} - T_o)/\beta$$

β can be obtained from the slope of the plot of

$$\ell n\ \ell n\ \left(\frac{1}{1-\alpha}\right) \text{ Vs } \ell n\ (T - To)/\beta \qquad \ldots \qquad (38)$$

By performing few determinations at different heating rates or at different temperatures, the activation energy can be obtained from equation (35) by plotting $\ell n\ (\frac{\beta}{\gamma})$ versus $\frac{1}{T_{0\cdot63}}$

Experimental

The values of α for thermogravimetric analysis of the oxide are obtained from the weight loss recorded, and the α values for the oxidant/fuel reactions are determined from measurement of area at different temperatures on the DSC peak then using the relation

$$\alpha = \frac{a}{A}$$

(a) Thermogravimetry

The study of the decomposition reaction

$$2Pb_3O_4 \rightarrow 6PbO + O_2$$

was performed isothermally at temperatures 520, 550,565 and 580°C. The results obtained are presented in figure 5.2.24 , and the results of the reaction under dynamic conditions (at heating rates 5, 10, 40 and 80°C/min) are presented in figure 5.2.25 . The Parkin Elmer TGS-2 system was used for measuring the weight loss of the sample as it was subjected to the controlled conditions above. Approximately 20 mg samples were used and thermogravimetry was performed under a constant flow of dry nitrogen (25 cc/min) during both isothermal and dynamic studies.

(b) DSC

The oxidant/silicon reactions were studied by a Perkin Elmer DSC2. Approximately 4.0 mg samples were placed in a graphite crucible, placed in the DSC sample holder and an empty graphite pan was placed in the reference holder to facilitate thermal matching. Both the sample and reference pans were covered with platinum covers to enhance base-line linearity and run to run reproducibility. The temperature was increased at a programmed scan rate until 1000 K was reached. A dry nitrogen atmosphere flowing at a rate 25 cc/min was used and temperature scan, 10, 20, 40 and 80 °C/min. were programmed. The sample and reference are maintained at the same temperature level during a programmed temperature scan rate. The excess energy required to maintain temperature equality during the reaction in a controlled atmosphere is measured and recorded, yielding a curve of dH/dt versus time.

RESULTS AND DISCUSSION

The results of isothermal and dynamic decomposition of red lead are given in figures 5.2.24 and 5.2.25. The results are used to plot $\ell n\ \ell n\ (\frac{1}{1-\alpha})$ VS ℓn t. Figures 5.2.26 and 5.2.27 show that the data fit equation (31) well for values of α = 0.05 to 0.95.

The values of β and γ for the different temperatures were used to plot $\ell n\ (\frac{\beta}{\gamma})$ against $\frac{1}{T}$ for isothermal reactions and the values of β and γ obtained from figure 5.2.27 were used to plot $\ell n\ (\frac{\beta}{\gamma})$ against $\frac{1}{T_{0.63}}$ for the dynamic decomposition of the red lead samples. The two plots are illustrated in figure 5.2.28 yielding activation energy of 240.72 kJ/mol. for the isothermal decomposition and 282.74 kJ/mol for the decomposition reaction under dynamic conditions. The difference between the two values suggests that different mechanisms prevailed under the different conditions.

The reaction of Pb_3O_4/Si was seen to produce two exothermic peaks appearing as a shoulder and a peak in a very narrow temperature range. This makes it difficult to evaluate α for the determination of the activation energy.

The PbO_2/Si mixture, when studied by DSC, it produced a single exothermic peak as the major reaction. The values of α were plotted against t in figure 5.2.29 and the $\ell n\ \ell n\ (\frac{1}{1-\alpha})$ VS ℓn t is illustrated in figure 5.2.30. The latter plot shows that good agreement with equation (31) exists for α values 0.1 - 0.9 and the activation energy was obtained from the plots of $\ell n\ \frac{\beta}{\gamma}$ VS $T_{0.63}$ as previously explained. The straight line obtained from the plot as in figure 5.2.31 gives an activation energy 2 8 1.41 kJ/mol.

Results obtained by application of Kissinger equation as in figure 5.2.32 agree well with the values obtained from the method above, but differ widely from results of the Pilony equation as in figure 5.2.33 and Borchardt equation as in figure 5.2.34. However, the linear relationship of $\ell n\ (\frac{\Delta H}{A-a})$ VS $\frac{1}{T}$ for the Borchardt treatment was true only for values of α 0.05 to 0.4 and the limitations for its use are too great to be of any value.

Activation Energy for PbO_2/ Si Reactions (E)

(1) from proposed model 281.41 kJ/mol
(2) from Kissinger equation 287.26 kJ/mol
(3) from Borchardt equation 1411.11 kJ/mol

FIG. 5.2.24 α VS t FOR Pb_3O_4(ISOTHERMAL)

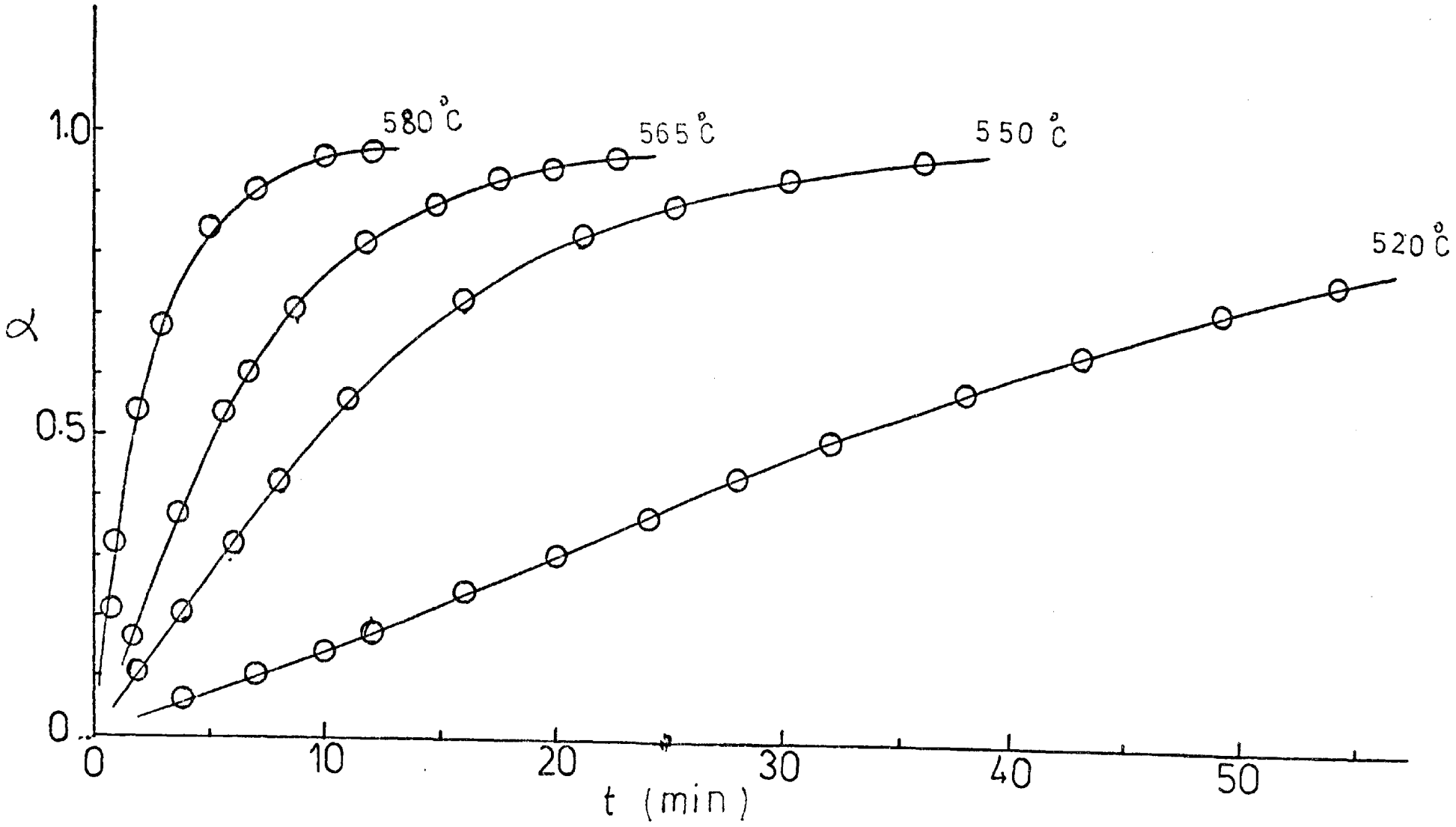

FIG. 5.2.25 α vs t FOR Pb_3O_4 (DYNAMIC)

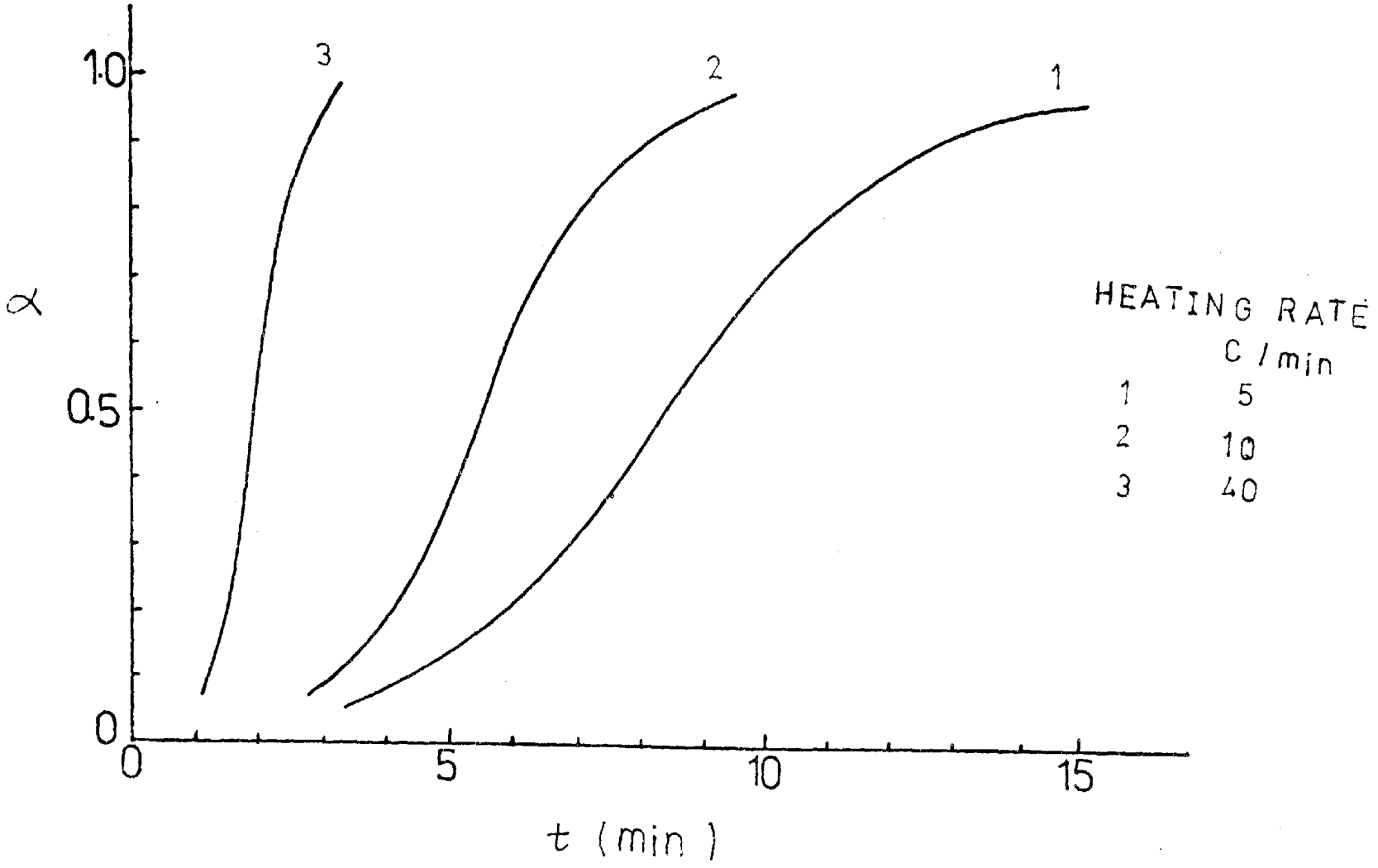

FIG. 5.2.26

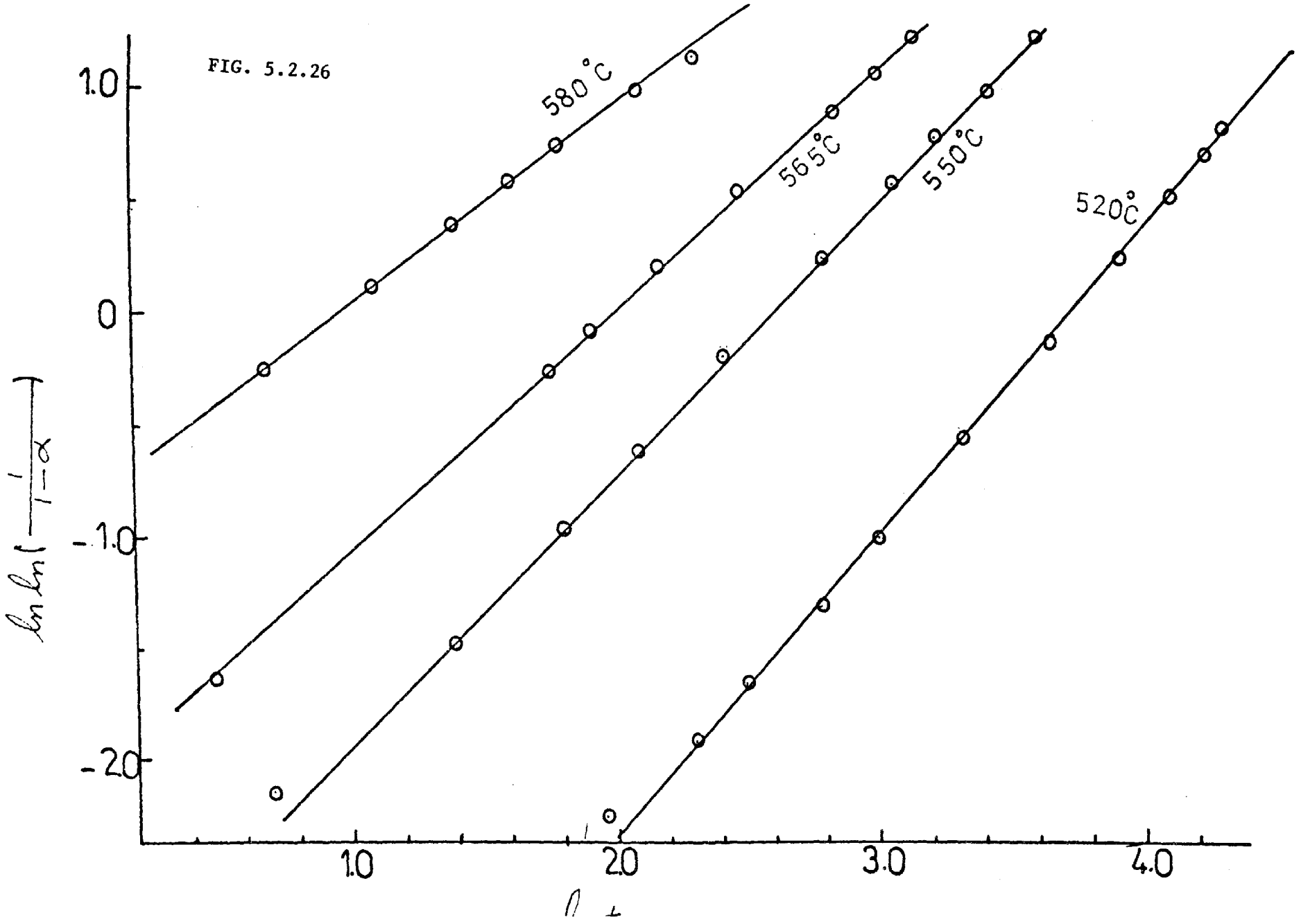

FIG. 5.2.27

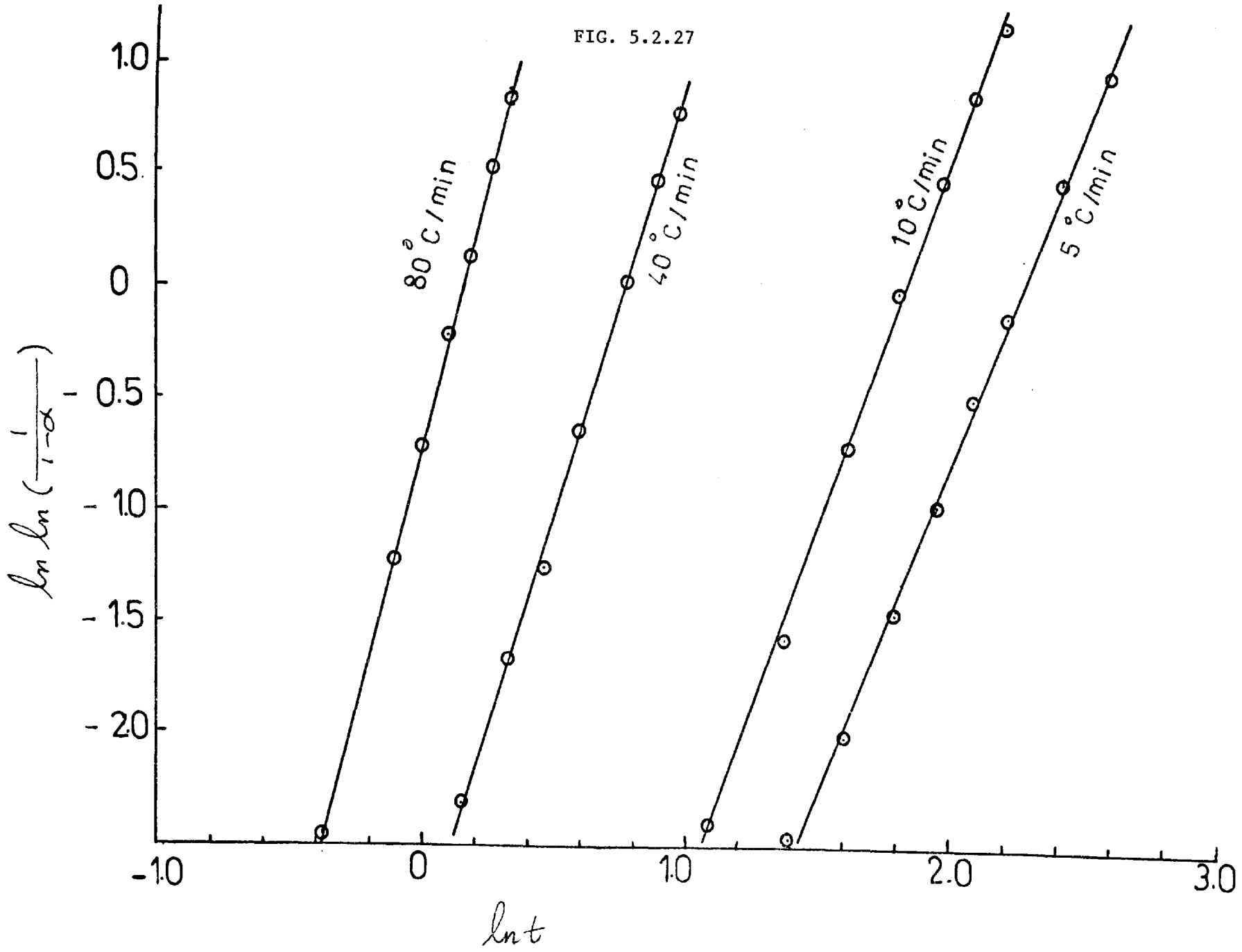
1.0
0.5
0
- 0.5
- 1.0
- 1.5
- 2.0
ln ln (1/1-α)
-1.0
0
1.0
2.0
3.0
ln t
80°C/min
40°C/min
10°C/min
5°C/min

FIG. 5.2.28

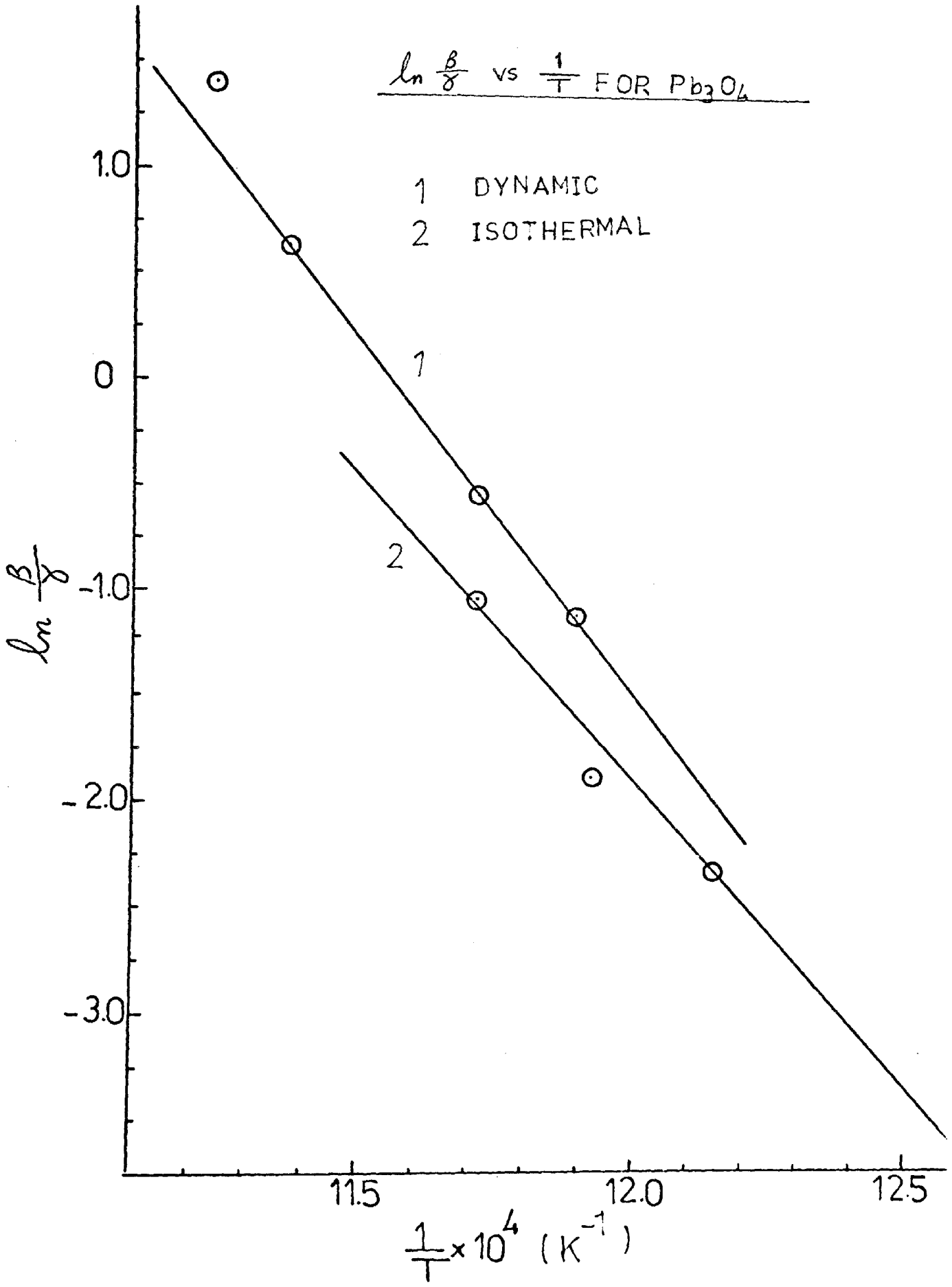
ln β/δ vs 1/T FOR Pb3O4
1 DYNAMIC
2 ISOTHERMAL
1
2
1.0
0
-1.0
-2.0
-3.0
ln β/δ
11.5
12.0
12.5
1/T × 10^4 (K^-1)

FIG. 5.2.29 α VS t FOR PbO_2 / Si

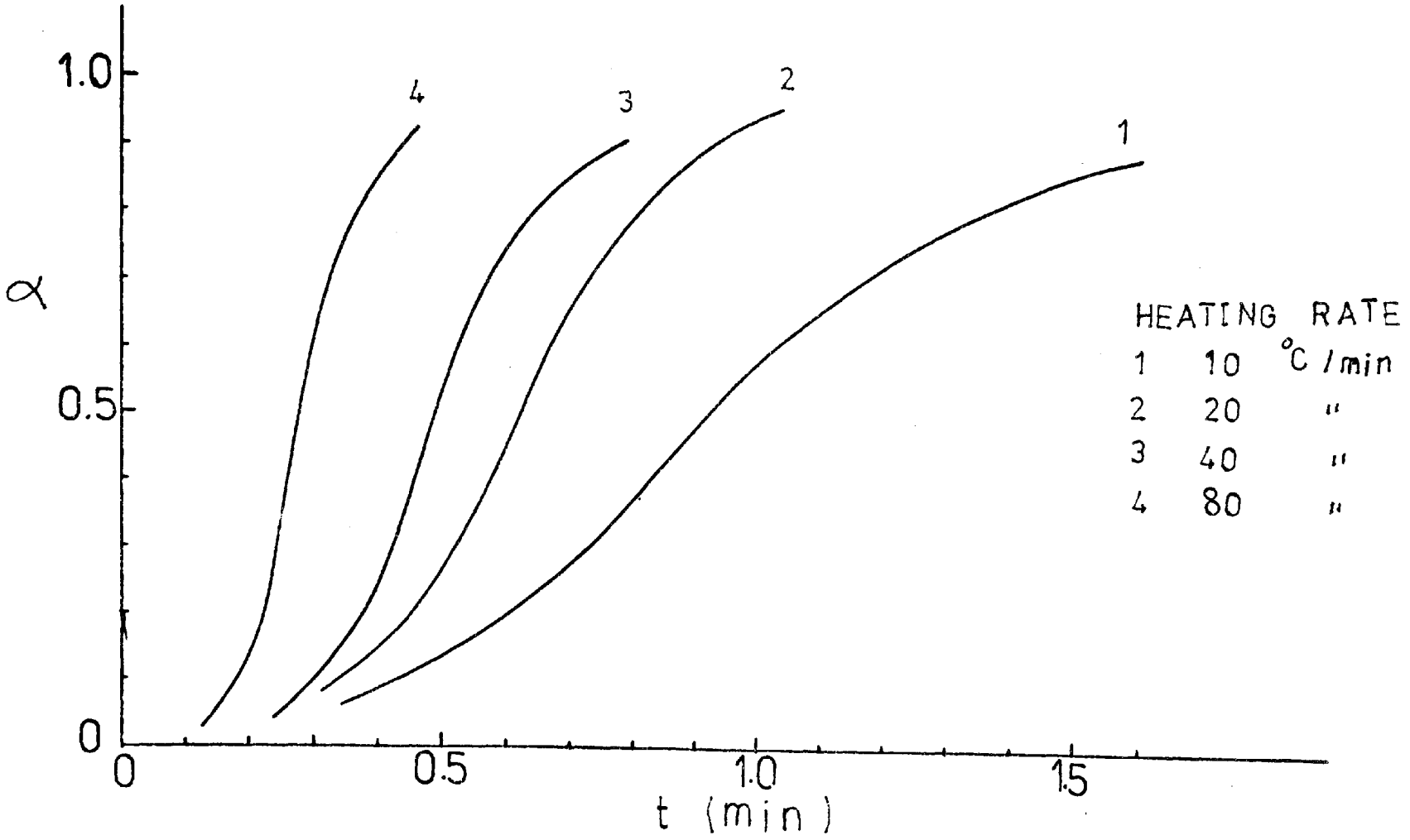

FIG. 5.2.30

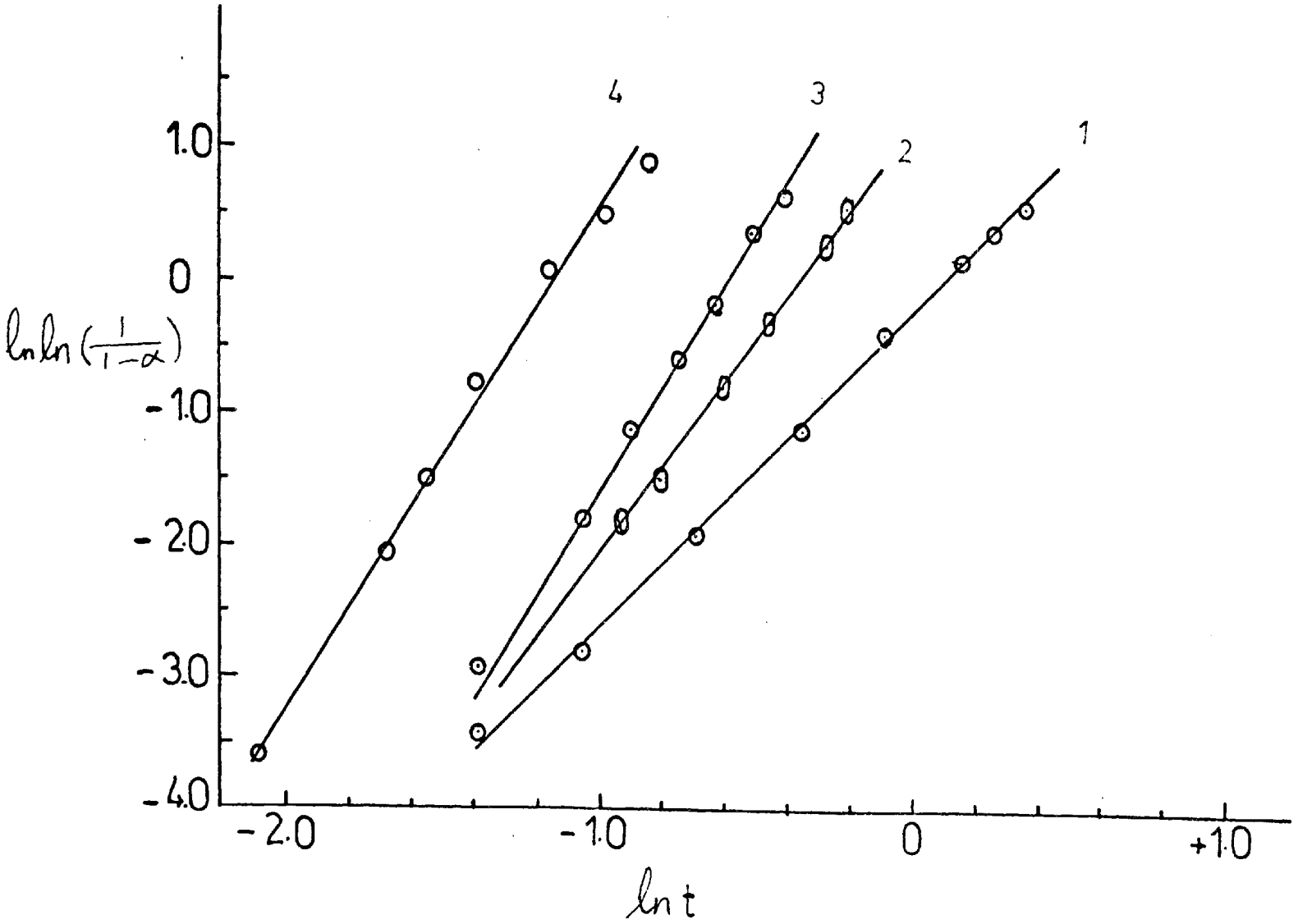

FIG. 5.2.31

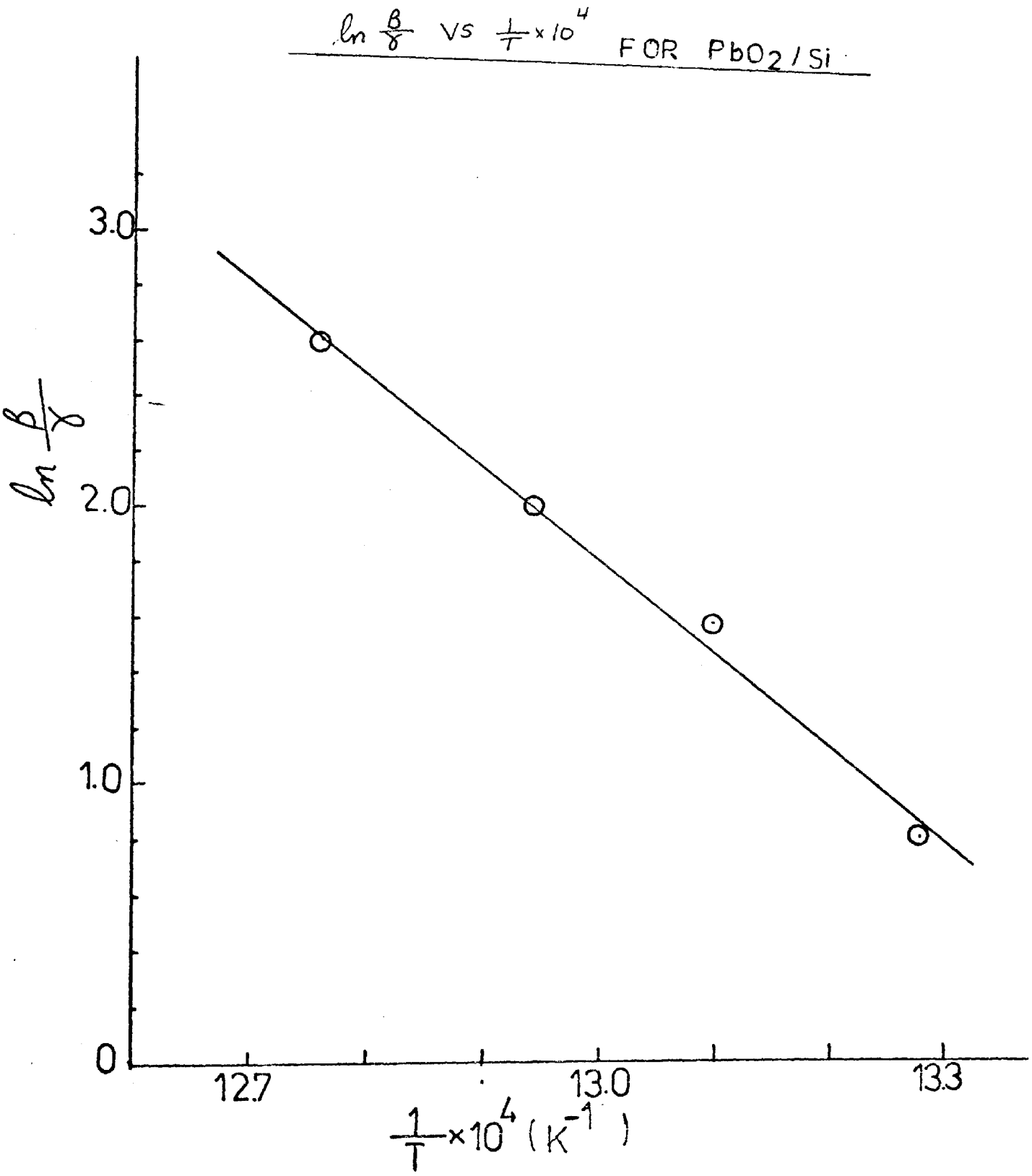

FIG. 5.2.32

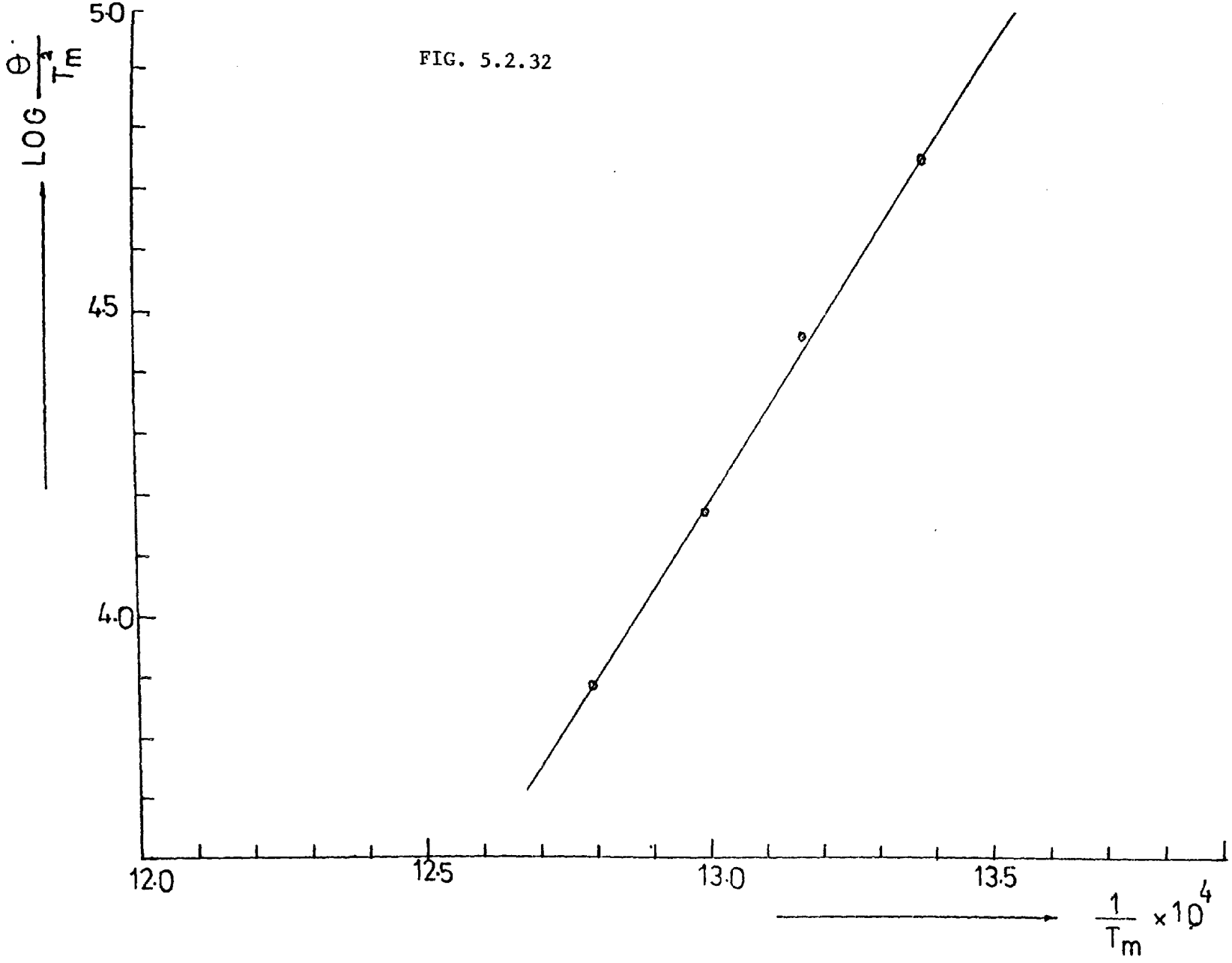
5·0
4·5
4·0
LOG $\frac{\dot{\Theta}}{T_m^4}$
12·0
12·5
13·0
13·5
$\frac{1}{T_m} \times 10^4$

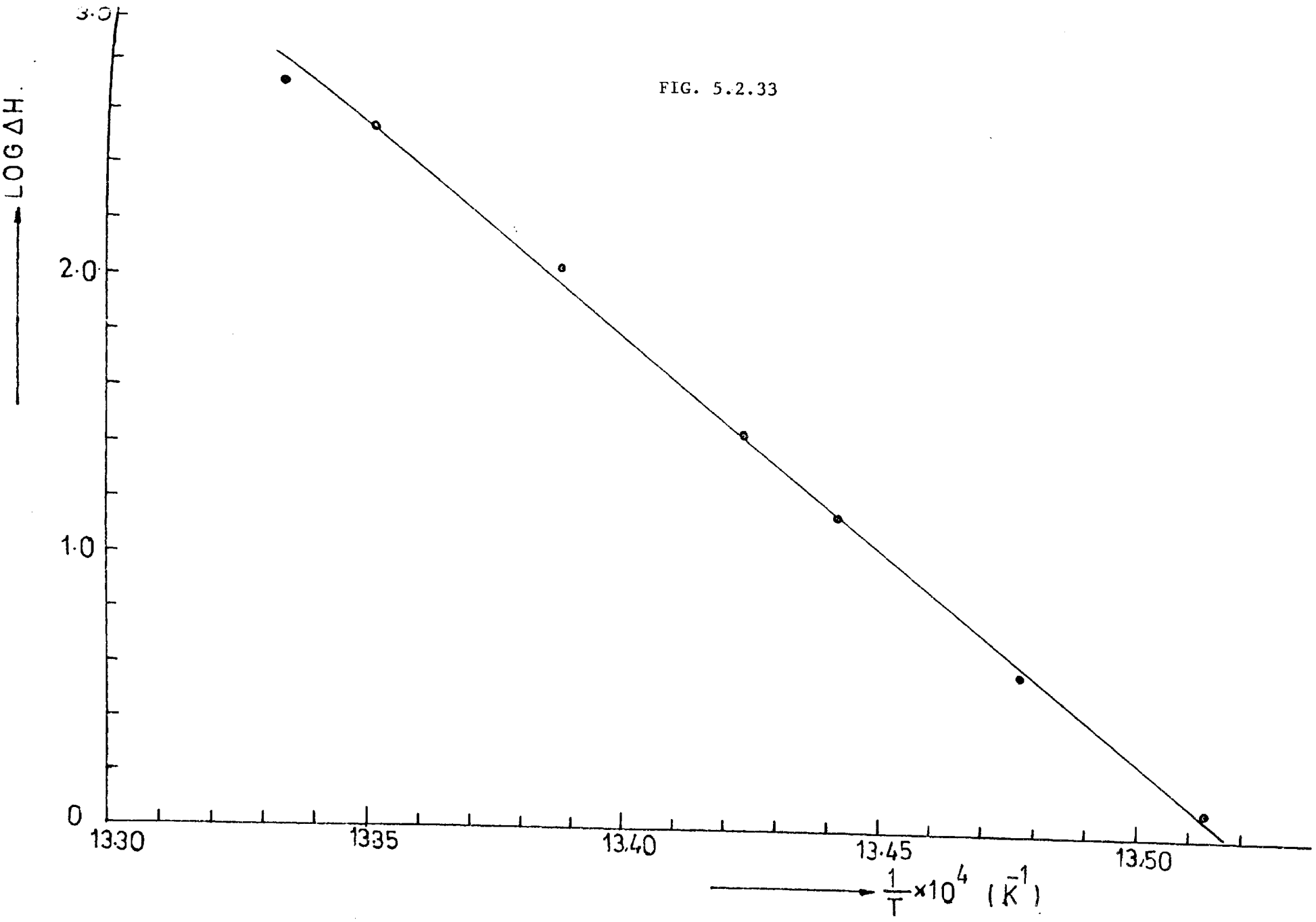

FIG. 5.2.33

FIG. 5.2.34

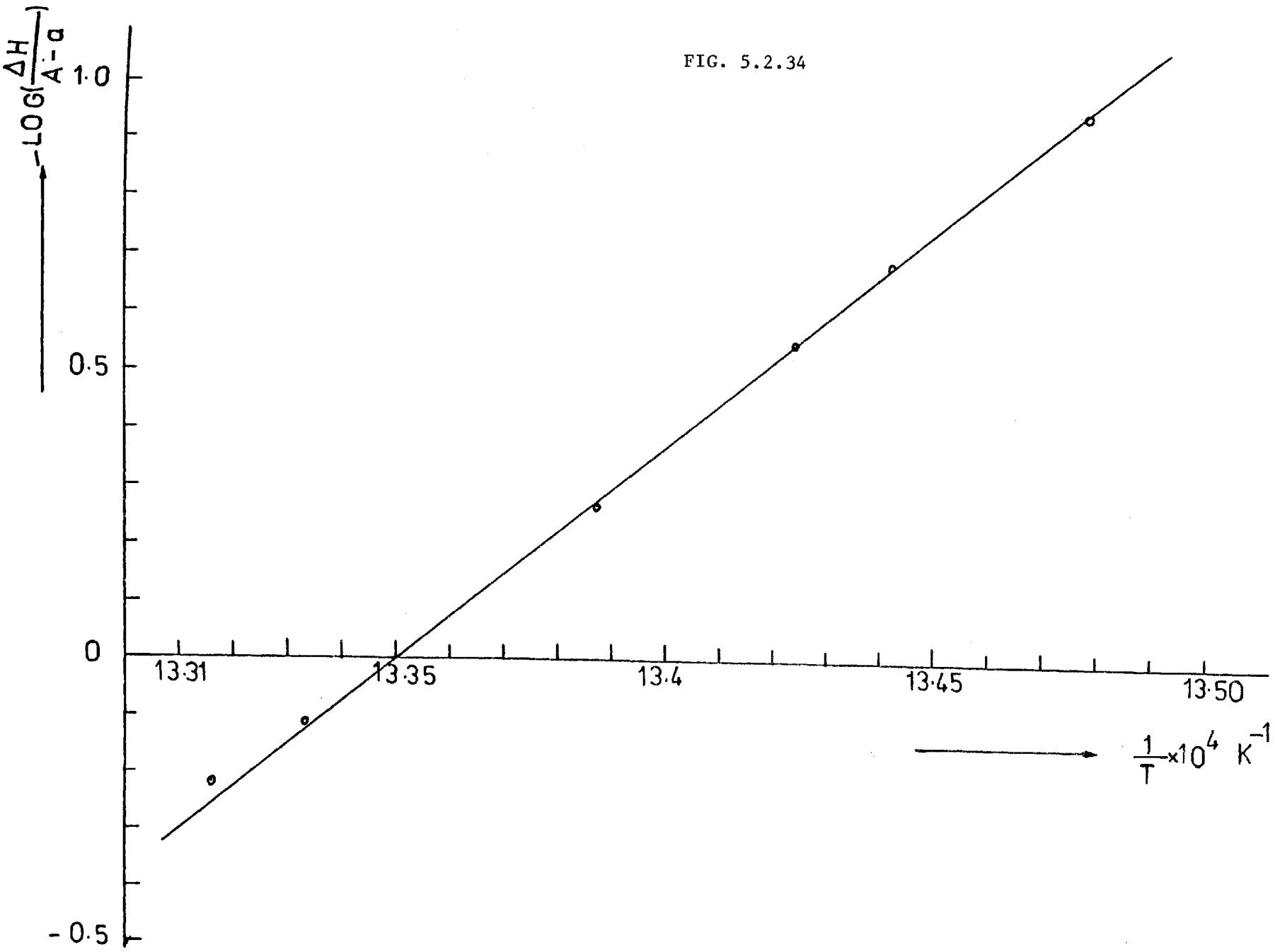
$-\log\left(\frac{\Delta H}{A-a}\right)$
1·0
0·5
0
- 0·5
13·31
13·35
13·4
13·45
13·50
$\frac{1}{T}\times 10^4\ K^{-1}$

FIG. 5.2.35

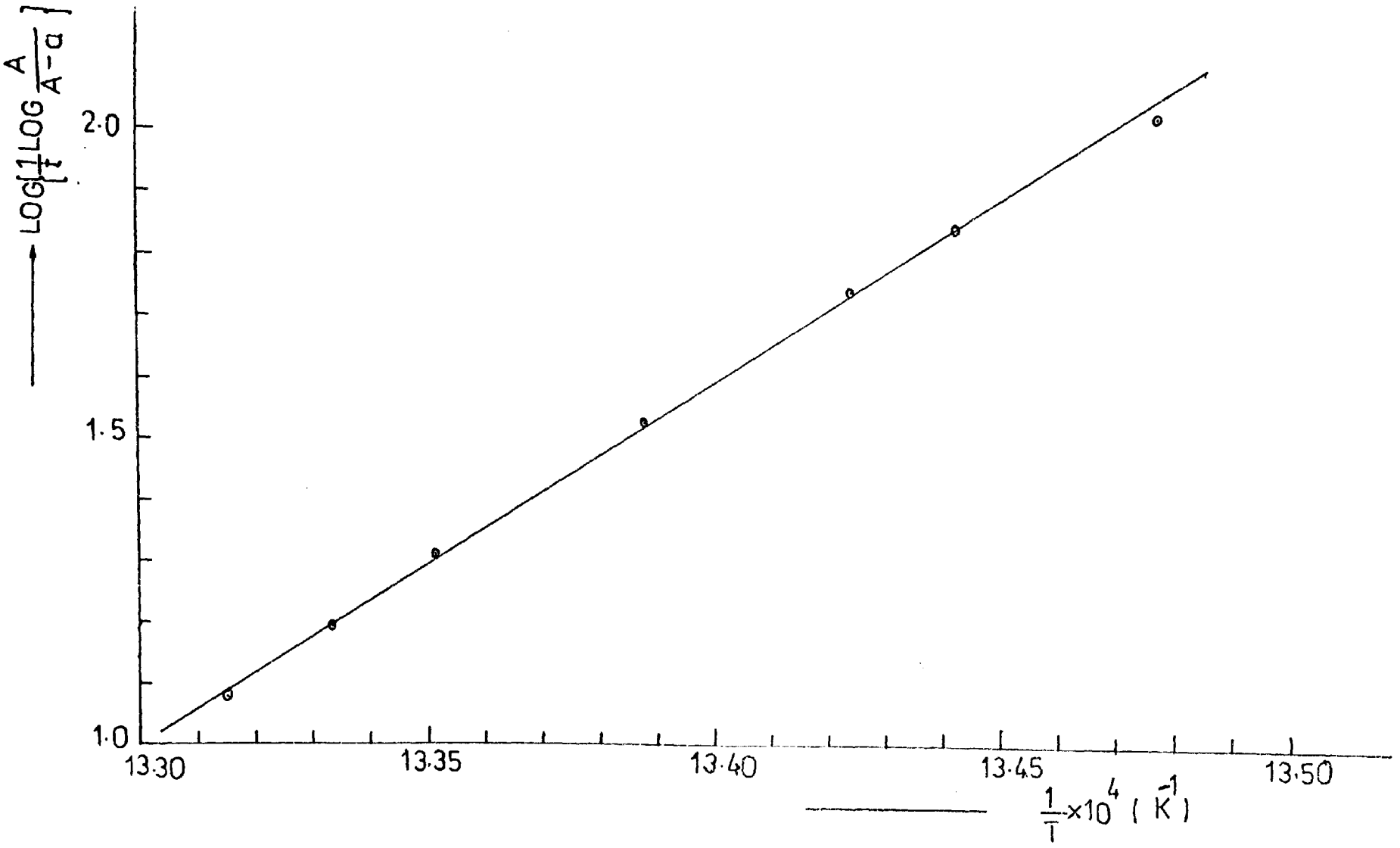

REFERENCES

1. H. Ellern, Military and Civilian Pyrotechnics, Chemical Publishing Company Inc. New York, 1968.

2. R.A.W. Hill, L.E. Sutton, R.B. Temple and A. White, Research, 3, 569-576, (1950).

3. R.A.W. Hill, and T.L. Cottrell, 4th Symposium on Combustion, 349-352. (1958).

4. R.A.W. Hill, Proc. Roy. Soc., 226A, 455-471, (1954).

5. E. Mallard, and Le Chatelier. Ann. Mines, 4, 274, (1895).

6. R.A.W. Hill, and J.N. Welsh. Trans. Faraday Soc. 55, 299-305, (1959).

7. R.A.W. Hill, Trans. Faraday Soc. 53, 1136-1144, (1957).

8. J.C. Cackett, R.G. Hall and T.F. Watkins. Chemical Warfare, Pyrotechnics and the Firework Industry. Pergamon Press, (1968).

9. J.E. Spine, L.A.K. Staveley. J. Soc. Chem. Ind. 68, 313-319, (1949).

10. J.E. Spice, L.A.K. Staveley J. Soc. Chem. Ind., 68, 348-355, (1949).

11. G.J. Rees, Ph.D. Thesis, (London University), (1958).

12. L.B. Johnson, Jr. Ind. and Eng. Chem. 52, 3, 241-244 (1960).

13. B.J. Thomson and A.M. Wild. Pyrochem. Int., 11.1 - 12.1, (1975)

14. J.McLain, Pyroteknikdagen, Stockholm, 1 - 16, (1973.

15. W. Ripley, Proceedings of 1st Pyrotechnic Seminar, 225-262, (1968).

16. A.P. Hardt and P.V. Phung, Combustion and Flame, 21, 77-89, (1973).

17. A.P. Hardt and R.W. Holsinger, Combustion and Flame, 21, 91-97, 1973.

18. G. Hale, U.S. Patent 1805214, (1931).

19. G.U. Graff,
U.S. Patent 2416639, (1947).

20. H. Goldschmidt,
U.S. Patent 906009, (1908)

21. H.E. Nash,
U.S. Patent 1999820, (1935).

22. E.M. Patterson,
U.S. Patent 2478501

23. D.E. Pearsall,
U.S. Patent 2416639, (1947).

24. J.H. McLain, T.A. Ruble,
U.S. Patent 2643946.

25. J. Piccard,
U.S. Patent 1971502, (1934).

26. S.L.H. Howlett & F.G.M. May.
Thermochimica Acta, 9, 213-216, (1974).

27. L. Sulacsik,
J. Thermal Analysis, 5, 1, 33-42, (1973).

28. E.L. Charsley, M.R. Ottaway.
Proceedings of Pyrochemi. Int. 17.1 - 17.16, (1975).

29. C.H. Miller,
Symp. Chem. Prob. Connected with stab. of explosives Proc.
269, (1973).

30. A.J. Beardell, A.D. Kirshenbaum, Thermochimica Acta,
8, 35-44, (1974).

31. T. Boddington, P.G. Laye,
Proceedings of Pyrochem. Int. 12.1 - 12.6, (1975).

32. T. Boddington and P.G. Laye,
Proceedings of Pyrochem. Int., 24.1 - 24.4, (1975).

33. T. Boddington and P.G. Laye,
Combustion and Flame, 24, 137-138, (1975).

34. F.S. Scanes and R.A.M. Martin,
Combustion and Flame, 23, 357-362, (1974).

35. F.S. Scanes,
Combustion and Flame, 23, 363-371, (1974).

36. S. Yoshinaga, M. Matumoto and T. Nagaishi,
Kogyo Kayaku Kyokaishi, 33, 41-48, (1972).

37. D.A. Dadley,
Proceedings Second Int. Pyrotechnics Seminar,
319-345, (1970).

38. A.D. Kirshenbaum and C. Campbell,
The Franklin Institute Research Laboratories.
1.61 - 1.65, (1970).

39. P.H. Bishop and K.F. Rogers, R.A.E. Technical Report
No. 66328, (1966).

40. W. Komatsu,
Proc. 5th Symposium on Reactivity of Solids,
182-191, (1964).

41. National Bureau of Standards, Technical Notes.
(270-273), (1968).

42. F.D. Rossini, D.D. Wagman, W.H. Evans, L. Levine & I. Jaff.
"Selected values of Chemical Thermodynamic Properties"
N.B.S. Circular 500, (1951).

43. G.V. Samsonov, Handbook of the Physiochemical Properties of
Elements, (1968).

44. R.M. Barrer, Diffusion in and through solids,
Cambridge University Press, (1951).

45. W.E. Garner.
The Chemistry of the Solid State, Butterworth Scientific
Publications, London (1955).

46. A. Blazek, Thermal Analysis, Van Nostrand
Reinhold Company, London, (1973).

47. R.C. Mackenzie.
Thermal Analysis, Academic Press, vol. 1 (1970).

48. R.C. Mackenzie and B.D. Mitchell,
Thermal Analysis, Academic Press, (1970).

49. A.D. Cunningham and F.W. Wilburn.
Thermal Analysis, Academic Press, (1970).

50. P.D. Garn.
Thermoanalytical Methods of Investigation,
Academic Press, New York, (1965).

51. G.J. Keattch and D. Dollimore.
An Introduction to Thermogravimetry, 2nd Edition,
Hyden & Son Ltd., (1975).

52. D. Greninger, C. Cline and V. Kollonitsch.
Lead Chemicals, International Lead-Zinc Research Organization, Inc.
New York, (1973).

53. V.V. Aleksandrov, V.V. Boldyrev and V.V. Marusin.
J. Thermal Analysis, 13, 205-212, (1978).

54. F.J. Kilzer and A. Broido,
Pyrodynamics, 2, 151-163, (1965).

55. L. Sulacsik,
J. Thermal Analysis, 6, 2, 215-220, (1974).

56. S. Nakahara,
Kogyo Kayku Kyokaishi, 21, 2, (1960).

57. S. Yoshinaga, M. Matumoto and T. Nagaishi.
Kogyo Kayaku Kyokaishi, 33, 4, 199-206, (1972).

58. J.W. Mellor,
Comprehensive Treatise on Inorganic and Theoretical Chemistry,
vol. VI, 885, (1961).

59. R.F. Geller, A.S. Creamer and E.N. Bunting.
J. Res. National Bureau of Standards, 13, 1, 61, (1958).

60. G.M. Schwab and J. Gerlach.
Z. Phys. Chem., 56, 121, (1967).

61. M. Avrami and B.V. Erofeev.
Smirnova Zhurfig Khim, 26, 1233-43, (1952).

62. E.G. Prout and F.C. Tompkins.
Trans. Far. Soc., 40, 488, (1944).

63. A.M. Ginstling and B.I. Brounshtein.
Zh. Prikl. Khim, 23, 1249, (1950).

64. H.E. Kissinger,
J. Res. Nat. Bur. Standards, 57, 217, (1956).

65. P. Murray and J. White.
Trans. Brit. Ceram. Soc., 79, 41, (1957).

66. H.J. Borchardt,
J. Chem. Educ. 33, 103, (1956).

67. H.J. Borchardt and F. Daniels
J. Am. Chem. Soc. 79, 41-46,(1957)

68. H.J. Borchardt, J. Am. Chem. Soc. 81, 1529-1531, (1959).

69. H.J. Borchardt.
J. Inorganic and Nuclear Chem., 12, 252-254, (1960).

70. H.J. Borchardt,
J. Inorganic and Nuclear Chemistry, 12, 113-121, (1960).

71. W.W. Wendlandt,
J. Chem. Education, 38, 11, 571-573.

72. S.K. Das, S.K. Mookerjee, S.K. Nyogi and R.L. Thakur,
J. Thermal Analysis, 9, 43-51, (1976).

73. E. Segal, D. Fatu.
J. Thermal Analysis, 9, 65-69, 1976.

74. G.O. Piloyan, I.D. Ryabchikov and O.S. Novikova.
Nature, 212, 217, (1966).

75. S. Freeman and B. Carroll.
J. Phys. Chem., 62, 394-397, (1958).

76. K.S. Subramanian, T.P. Radhakrishnan and A.K. Sundaram.
J. Thermal Analysis, 4, 89-93, (1972).

77. J.R. MacCallum and J. Tanner.
Nature, 225, 1127-1128, (1970).

78. R.M. Felder and E.P. Stahl,
Nature, 228, 1085, (1970).

79. P. Davies, D. Dollimore and G.R. Heal.
J. Thermal Analysis, 13, 473-487, (1978).

80. J. Dankiewicz and K. Wieczorek-Crurowa.
J. Thermal Analysis, 13, 543-552, (1978).

81. P.D. Garn.
J. Thermal Analysis, 6, 237-239, (1974).

82. P.D. Garn.
J. Thermal Analysis, 13, (1978).

APPENDIX

1

TABLE 5.1.1

Delay Time of Various Pb_3O_4/Si Compositions

Pb_3O_4/Si(W/W)	TIME ($s \times 10^{-3}$)	STANDARD DEVIATION	DENSITY (g/cm^3)	LENGTH (cm)
50/50	515.61	5.85	2.49	2.0
55/45	289.22	4.95	2.65	2.0
60/40	223.73	4.68	2.85	2.0
65/35	171.54	4.03	3.06	2.0
70/30	122.71	2.58	3.34	2.0
75/25	148.97	5.41	3.64	2.0
80/20	183.95	4.26	3.96	2.0
85/15	198.79	5.56	4.40	2.0
90/10	211.99	6.86	4.87	2.0
95/5	434.10	20.72	5.47	2.0

TABLE 5.1.2

Delay Time for PbO_2/Si Compositions

PbO_2/Si(W/W)	TIME ($s \times 10^{-3}$)	STANDARD DEVIATION	DENSITY (g/cm^3)	LENGTH (cm)
40/60	253.22	7.53	2.28	2.0
50/50	173.10	4.91	2.49	2.0
55/45	159.90	4.14	2.67	2.0
60/40	145.80	3.41	2.84	2.0
65/35	142.10	2.00	3.04	2.0
70/30	148.23	1.73	3.26	2.0
75/25	165.13	3.64	3.54	2.0
80/20	186.29	6.21	3.80	2.0
85/15	259.24	7.65	4.13	2.0
90/10	326.96	25.30	4.50	2.0

TABLE 5.1.3

Delay Time for Various Pb_3O_4/Si Composition Lengths

Pb_3O_4/Si (W/W)	TIME (m.SECOND) s x 10^{-3}			
	0.83(cm)	1.50(cm)	2.00(cm)	3.00(cm)
50/50	214.62	390.42	515.63	
55/45	118.70	212.73	289.21	437.19
60/40	89.51	166.69	223.70	336.90
65/35	76.25	125.38	171.53	
70/30	59.10	92.41	122.76	174.37
72/25	63.57	114.03	149.00	
80/20	76.74	137.20	183.91	280.00
85/15	85.82	153.12	198.85	
90/10	89.32	157.62	212.20	311.21

TABLE 5.1.4

Delay Time of Various PbO_2 /Si Composition Lengths

PbO_2/Si	LENGTH (cm)	TIME ($s \times 10^{-3}$)	S.D.
65/35	0.4	22.20	3.25
"	0.8	71.32	2.96
"	1.0	95.76	3.12
"	1.5	155.30	2.81
"	2.0	210.12	2.54
"	2.5	268.55	2.76
"	3.0	320.70	3.21

TABLE 5.1.5

Delay Time and Rate of Burning for Various Si Particle Sizes in (Pb_3O_4/Si) System

Pb_3O_4/Si (w/w)	SILICON A				SILICON B				SILICON C			
	TIME ($sx10^{-3}$)	S.D.	RATE OF BURNING		TIME ($sx10^{-3}$)	S.D.	RATE OF BURNING		TIME ($sx10^{-3}$)	S.D.	RATE OF BURNING	
			cm/s	g/s			cm/s	g/s			cm/s	g/s
50/50	337.53	12.49	5.93	1.12	515.61	5.85	3.88	0.85	Missfire	-	-	-
55/34	211.95	3.23	9.44	1.92	289.22	4.95	6.91	1.62	376.00	9.58	5.32	1.24
60/40	174.35	6.89	11.47	2.48	223.73	6.17	8.94	2.25	276.54	4.32	7.23	1.82
65/35	157.35	3.37	12.711	2.99	171.54	4.03	11.66	3.15	231.04	4.95	8.66	2.36
70/30	143.83	7.19	13.91	3.56	122.71	2.58	16.30	4.81	174.15	5.35	11.48	3.40
75/25	144.13	6.87	13.88	3.86	148.97	5.41	13.43	4.31	202.72	2.68	9.87	3.23
80/20	80.01	4.64	25.00	7.82	183.95	1.83	10.87	3.80	250.23	4.89	7.99	2.86
85/15	77.71	4.09	25.74	9.10	198.79	5.56	10.06	3.91	279.87	5.93	7.15	2.74
90/10	90.03	2.19	22.22	8.85	211.99	6.86	9.44	4.04	309.85	14.65	6.46	2.84
95/5	183.62	4.59	10.89	4.76	434.10	20.72	4.61		471.43	14.51	4.24	2.09

TABLE 5.1.6

VARIATION OF (R.B.) OF VARIOUS Pb_3O_4/Si COMPOSITIONS WITH SILICON PARTICLE SIZE

SILICON PARTICLE SIZE		50/50 Pb_3O_4/Si				60/40 Pb_3O_4/Si				70/30 Pb_3O_4/Si				80/20 Pb_3O_4/Si				90/10 Pb_3O_4/Si			
RANGE µm	AVERAGE µm	TIME FOR 2 cm ($s \times 10^{-3}$)	S.D.	R.B. (cm/s)	$\frac{1}{(R.B.)}$	TIME PER 2 cm ($s \times 10^{-3}$)	S.D.	R.B. (cm/s)	$\frac{1}{(R.B.)}$	TIME FOR 2 cm ($s \times 10^{-3}$)	S.D.	R.B. (cm/s)	$\frac{1}{(R.B.)}$	TIME FOR 2 cm ($s \times 10^{-3}$)	S.D.	R.B. (cm/s)	$\frac{1}{(R.B.)}$	TIME FOR 2 cm	S.D.	R.B. (cm/s)	$\frac{1}{(R.B.)}$
0.5- 5.0	1.9	337.53	12.49	5.93	0.17	174.35	6.89	11.47	0.09	143.83	7.19	13.91	0.07	80.00	4.64	25.00	0.04	90.03	2.19	22.22	0.05
2.0-15.0	3.9	515.61	5.85	3.88	0.26	223.73	6.17	8.94	0.11	122.71	2.58	16.30	0.06	183.95	1.83	10.87	0.09	211.99	6.86	9.44	0.11
4.0-20.0	7.0	414.87	5.23	4.81	0.21	235.68	5.18	8.42	0.12	190.68	5.26	10.4	0.096	278.71	2.10	7.18	0.14	280.00	4.31	7.11	0.14
4.0-12.0	8.3	546.98	6.10	3.65	0.27	279.12	6.14	7.21	0.14	202.00	5.31	9.87	0.10	290.38	2.36	6.83	0.15	292.80	5.20	6.83	0.15
8.0-30.0	16.0	730.31	17.64	2.74	0.36	395.26	14.27	5.06	0.20	356.21	10.75	5.60	0.18	505.91	8.54	3.94	0.25	435.20	9.72	4.59	0.22
21.0-26.0	24.0	1104.68	28.41	1.81	0.55	580.00	13.00	3.45	0.29	554.15	13.62	3.60	0.28	815.61	19.32	2.46	0.41	738.10	38.10	2.72	0.37
25.0-32.0	30.0	Missfire	-	-	-	697.32	14.85	2.86	0.35	681.54	12.10	2.94	0.34	1011.33	26.41	1.98	0.51	1065.00	50.20	1.88	0.53
32.0-42.0	36.0	"				840.74	17.69	2.37	0.42	828.98	13.24	2.41	0.41	1192.13	27.12	1.67	0.60				
46.0-5=.0	48.0	"				975.61	18.41	2.05	0.49	954.11	17.64	2.10	0.48	1387.84	32.16	1.44	0.69	1510.70	68.91	1.32	0.76

TABLE 5.1.7

Variation of Delay Time and Rate of Burning of PbO_2/Si Composition with Silicon Particle Size

	SILICON A				SILICON B				SILICON C				SILICON D	
PbO_2/Si (W/W)	TIME ($sx10^{-3}$)	S.D.	RATE OF BURNING (cm/s)	RATE OF BURNING (g/s)	TIME ($sx10^{-3}$)	S.D.	RATE OF BURNING (cm/s)	RATE OF BURNING (g/s)	TIME ($sx10^{-3}$)	S.D.	RATE OF BURNING (cm/s)	RATE OF BURNING (g/s)	TIME ($sx10^{-3}$)	RATE OF BURNING (cm/s)
40/60	253.22	6.93	7.90	1.56	253.22	7.53	7.90	1.56					401.28	4.99
50/50	127.33	4.32	15.71	3.04	173.10	4.91	11.56	2.54	213.96	6.23	9.35	1.62	288.60	7.00
55/45					159.92	4.14	12.51	2.95					296.24	6.75
60/40	111.61	2.61	17.92	3.85	145.83	3.41	13.72	3.44	184.59	1.85	10.84	2.18	351.23	5.69
65/35					142.13	2.00	14.07	3.78	208.04	5.23	9.61	2.08		
70/30	85.23	2.02	23.46	5.91	148.27	1.73	13.50	3.88	212.12	4.63	9.43	2.20	599.25	3.34
75/25					165.06	3.64	12.12	3.79					692.25	2.88
80/20	82.04	9.31	24.38	7.29	186.22	6.21	10.74	3.60	262.73	6.21	7.61			
85/15	131.73	12.42	15.18	5.10	259.24	7.65	7.72	2.82						
90/10	BURST				326.97	25.3	6.12	2.43	419.54	20.41	4.77			

TABLE 5.1.8

Variation of Rate of Burning with Density of Pb_3O_4/Si Compositions

LOADING	17.6 N/mm^2		66.5 N/mm^2		110.9 N/mm^2		143.0 N/mm^2		181.0 N/mm^2	
Pb_3O_4/Si	DENSITY (g/cm^3)	R.B. (cm/s)	DENSITY (g/cm^3)	R.B. (cm/s)	DENSITY (g/cm^3)	R.B. (cm/s)	DENSITY (g/cm^3)	R.B. (cm/s)	DENSITY (g/cm^3)	R.B. (cm/s)
50/50	2.15	3.05	2.53	3.30	2.46	3.30	2.50	3.88	2.60	4.07
55/45	2.27	5.18	2.49	6.01	2.58	6.32	2.65	6.92	2.75	7.37
60/40	2.41	6.93	2.66	7.83	2.80	6.86	2.85	8.94	2.95	9.44
65/35	2.57	8.65	2.83	9.82	2.89	10.62	3.06	11.66	3.21	12.55
70/30	2.73	10.89	3.04	14.46	3.23	15.81	3.34	16.30	3.42	15.90
75/25	2.98	16.37	3.31	14.78	3.47	14.47	3.64	13.43	3.91	12.95
80/20	3.20	14.35	3.61	12.35	3.78	11.51	3.96	10.87	4.09	10.47
85/15	3.44	11.77	3.98	10.86	4.18	9.92	4.40	10.06	4.50	9.01
90/10	3.81	-	4.37	10.32	4.69	9.69	4.87	9.43	4.97	9.21
95/5	4.45	BURST	4.87	5.26	5.04	4.28	5.37	4.61	5.69	4.28

TABLE 5.1.9

Effect of Ambient Pressure on Rate of Burning of PbO_2/Si

NITROGEN PRESSURE (kN/m^2)	RATE OF BURNING (cm/s)		
	50/50	60/40	70/30
100	6.61	4.76	6.12
689.6	6.83	4.93	6.63
1379.3	6.83	5.01	6.99
2069.0	6.86	5.16	7.00
2758.6	6.86	5.27	7.05
3448.3	6.89	5.21	7.12
4138.0	6.86	5.35	
4827.7	6.86	5.28	7.27
5517.2	6.84	5.32	
6206.8	6.89	5.29	
6896.6	6.89	5.25	7.27

TABLE 5.1.10

Rate of Burning of Pb_3O_4/Si in Vented and Unvented Assemblies

Pb_3O_4/Si	RATE OF BURNING (cm/s)	
	UNVENTED	VENTED
50/50	3.88	3.42
55/45	6.91	5.69
60/40	8.94	6.73
65/35	11.66	7.79
70/30	16.30	6.44
75/25	13.43	6.36
80/20	10.87	4.70
85/15	10.06	3.92
90/10	9.44	2.54
95/5	4.61	-

TABLE 5.1.11

Effect of Ambient Pressure on Rate of Burning of Pb_3O_4/Si

NITROGEN PRESSURE kN/m^2	RATE OF BURNING (cm/sec.)								
	55/45	60/40	65/35	70/30	75/25	80/20	85/15	90/10	93/7
100.0	5.04	6.22	7.14	6.27	6.02	4.56	3.75	2.60	1.80
689.6	5.42	7.62	7.48	7.14	6.86	5.49	5.00	3.98	3.15
1379.3	5.57	7.74	7.77	8.15	7.37	6.06	5.78	5.06	4.35
3448.3	5.80	8.16	8.92	8.28	8.24	7.02	6.88	6.77	6.31
6896.6	5.94	7.80	9.24	8.34	8.73	7.58	7.56	7.50	7.32
10344.8	6.09	8.20	8.57	8.11	8.68	7.77	8.04	8.04	7.74

TABLE 5.1.12

Variation of (R.B.) of PbO_2/Si with Ambient Temperature in Vented Assemblies

TEMP. ^oK	50/50 (w/w)	60/40 (w/w)	70/30 (w/w)
90	2.94	3.51	1.12
193	4.40	4.10	1.42
245	5.20	4.52	1.50
273	5.61	4.70	1.61
295	5.82	4.83	1.65
323	6.30	5.00	1.80
373	6.95	5.47	1.91

TABLE 5.1.13

Variation of (R.B.) of PbO_2/Si with Ambient Temperature in Unvented Assemblies

AMBIENT TEMP. ^oK	RATE OF BURNING (cm/s)		
	50/50 (w/w)	60/40 (w/w)	70/30 (w/w)
90	5.00	4.80	2.41
193	6.02	3.22	2.80
245	6.41	5.58	3.15
273	6.62	5.79	3.28
295	6.70	5.90	3.32
323	7.00	6.00	3.52

TABLE 5.1.14

Effect of Ambient Temperature on Rate of Burning

of Pb_3O_4/Si System

TEMP. ^oK	50/50 (cm/s)	55/45 (cm/s)	60/40 (cm/s)	65/35 (cm/s)	70/30 (cm/s)
273	Missfire	6.25	8.55	11.66	16.29
293	3.88	6.92	8.94	11.72	16.30
323	4.55	7.30	9.29	11.73	16.33
373	5.60	8.41	9.82	11.73	16.34
403	6.20	8.62	10.30	11.72	16.33
443	6.80	9.03	10.50	11.74	16.34

TABLE 5.1.15

Effect of Adding Barium Sulphate on Burning Rate of Pb_3O_4/Si Delay Compositions

Pb_3O_4/Si	$BaSO_4$%	TIME s x 10^{-3}	S.D.	(R.B.) cm/s	LENGTH (cm)
55/45	0	316.24	7.26	6.32	2.0
55/45	2.0	343.00	5.30	5.83	"
55/45	4.0	378.38	7.34	5.29	"
55/45	8.0	474.22	9.71	4.22	"
55/45	10.0	539.06	6.98	3.71	"
55/45	15.0	767.98	22.67	2.60	"
55/45	20.0	miss-fire			

TABLE 5.1.16

Effect of Binder on Rate of Burning of Pb_3O_4/Si Compositions

Pb_3O_4/Si	COMPO-SITION LENGTH cm.	0.5% BINDER			1.0% BINDER		
		TIME (sx10^{-3})	RATE/BURNING (cm/s)	(g/s)	TIME (sx10^{-3})	RATE/BURNING (cm/s)	(g/s)
55/45	2.0	289.22	6.91	1.62	387.51	5.16	1.20
65/35	2.0	171.54	11.66	3.15	250.34	7.99	1.98
70/30	2.0	122.71	16.30	4.81	130.87	15.28	4.41
75/25	2.0	148.97	13.43	4.31	145.64	13.73	4.33
85/15	2.0	198.79	10.06	3.91	212.88	9.39	3.65

TABLE 5.1.17

Effect of Adding Iron Powder on Rate of Burning of Pb_3O_4/Si Delay Compositions

COMPOSITION Pb_3O_4/Si	Fe%	TIME ($sx10^{-3}$)	S.D.	RATE OF BURNING		LENGTH OF COMPOSITION (cm)
				(cm/s)	(g/s)	
60/40	0	223.73	6.17	8.94	2.25	2.0
60/40	5.0	222.14	6.19	9.00	2.31	"
60/40	10.0	229.38	4.83	8.72	2.30	"
"	20.0	302.94	12.21	6.60	1.89	"
"	30.0	481.20	12.53	4.16	1.15	"
"	40.0	744.07	16.59	2.69	0.83	"
"	50.0	missfire	-	-	-	"

TABLE 5.1.18

Effect of Adding Graphite Powder on Rate of Burning of Pb_3O_4/Si Delay Compositions

Pb_3O_4/Si	% Graphite	TIME ($sx10^{-3}$)	S.D.	RATE OF BURNING		LENGTH cm
				(cm/s)	(g/s)	
60/40	0	223.73	6.17	8.94	2.25	2.0
60/40	2.0	244.65	8.26	8.18	2.02	2.0
60/40	5.0	295.10	7.23	6.78	1.67	2.0
60/40	10.0	461.57	7.19	4.33	1.05	2.0
60/40	15.0	missfire	-	-	-	

TABLE 5.1.19

Effect of Adding Calcium Fluoride on Rate of Burning of Pb_3O_4/Si Delay Compositions

Pb_3O_4/Si	% CaF_2	TIME ($sx10^{-3}$)	S.D.	RATE OF BURNING		LENGTH cm.
				(cm/s)	(g./s)	
60/40	0	223.73	6.17	8.94	2.81	2.0
60/40	5.0	247.13	8.18	8.09	2.80	2.0
60/40	10.0	367.22	7.95	5.45	2.75	2.0
60/40	20.0	954.97	4.40	2.09	2.70	2.0
60/40	25.0	missfire	-	-	-	2.0

TABLE 5.1.20

Effect of Adding Lead on Rate of Burning of Pb_3O_4/Si Delay Compositions

Pb_3O_4/Si	% Pb	TIME ($sx10^{-3}$)	S.D.	RATE OF BURNING		COMPO-SITION LENGTH (cm)
				(cm/s)	(g/s)	
65/35	0	171.54	4.03	11.66	3.15	2.0
65/35	5.0	169.40	6.21	11.81	3.44	2.0
65/35	10.0	165.82	6.53	12.06	3.47	2.0
65/35	20.0	130.42	5.92	15.34	4.66	2.0
65/35	30.0	122.19	3.37	16.37	5.28	2.0
65/35	40.0	131.52	4.05	15.21	5.25	2.0
65/35	50.0	149.45	5.96	13.38	4.88	2.0

TABLE 5.1.21

Effect of Various Diluents on Rate of Burning of Pb_3O_4/Si Delay Compositions

Pb_3O_4/Si	COMPOSITION LENGTH cm.	% DILUENT	TIME ($sx10^{-3}$)	S.D.	RATE OF BURNING (cm/s)
55/45	2.0	NONE	316.24	7.26	6.32
"	"	10% $BaCrO_4$	419.53	11.08	4.77
"	"	10% $CaCO_3$	952.85	24.86	2.10
"	"	10% $K_2Cr_2O_7$	329.41	10.42	6.07
"	"	5% $K_2Cr\ O_4$	398.25	19.50	5.02
"	"	10% $K_2Cr\ O_4$	537.46	28.40	3.72
"	"	10% $PbCO_3$	383.41	15.38	5.22
"	"	10% Al_2O_3	726.22	13.05	2.75
"	"	0.5% Lactose	372.09	14.97	5.37
"	"	1.0% Lactose	548.03	34.60	3.65
"	"	10% $PbCrO_4$	263.05	6.72	7.59

TABLE 5.1.22

Effect of Various Diluents on (R.B.) of Pb_3O_4/Si Delay Compositions

		NO DILUENT			10% LEAD CHROMATE			10% POTASSIUM CHROMATE			5% POTASSIUM CHROMATE			10% BARIUM SULPHATE		
Pb_3O_4/Si	Length cm	TIME ($sx10^{-3}$)	S.D.	R.B. (cm/s)	TIME ($sx10^{-3}$)	S.D.	R.B. (cm/s)	TIME ($sx10^{-3}$)	S.D.	R.B. (cm/s)	TIME ($sx10^{-3}$)	S.D.	R.B. (cm/s)	TIME ($sx10^{-3}$)	S.D.	R.B. (cm/s)
50/50	2.0	606.35	12.58	3.30	337.64	5.53	5.92	888.33	101.9	2.25	616.76	31.1	3.24	1147.16	37.1	1.74
55/45	2.0	316.24	7.26	6.32	263.37	6.72	7.59	537.15	28.4	3.72	398.34	19.5	5.02	519.32	10.0	3.85
60/40	2.0	230.49	4.78	8.68	228.41	12.25	8.76	455.52	29.0	4.39	309.16	16.6	6.47	367.76	12.3	5.44
65/35	2.0	188.71	5.83	10.60	205.56	20.84	9.73	364.46	24.8	5.49	263.66	9.8	7.59	314.55	10.5	6.36
70/30	2.0	126.54	12.13	15.81	182.29	4.60	10.97	346.27	12.3	5.78	234.53	8.4	8.53	236.61	33.6	8.45
75/25	2.0	138.40	5.26	14.55	188.40	4.35	10.62	358.23	11.5	5.58	246.90	6.5	8.10	197.05	6.9	10.15
80/20	2.0	173.39	4.51	11.53	218.16	4.69	9.17	357.16	79.3	5.60	277.42	4.8	7.21	228.44	11.6	8.76
85/15	2.0	221/90	38.30	9.01	-	-	-	-	-	-	-	-	-	-	-	-
90/10	2.0	452.07	76.39	4.42	-	-	-	585.92	110.6	3.41	-	-	-	694.13	14.86	2.88

TABLE 5.1.23

Heat Evolved From Different Pb_3O_4/Si Compositions and Different Silicon Particle Sizes

Pb_3O_4/Si	HEAT EVOLVED PER g OF MIXTURE (J/g)			CALCULATED
	SILICON A	SILICON B	SILICON C	
50/50	788.4	605.6	665.8	794.1
55/45	904.4	720.2	703.5	
60/40	983.1	793.1	780.1	952.9
65/35	1027.0	921.1	918.2	
70/30	1086.4	978.5	999.0	1111.7
75/25	1108.2	1093.1	1076.8	
80/20	1183.1	1174.3	1121.6	1270.5
85/15	1269.3	1251.3	1189.8	
90/10	1303.4	1296.9	1289.8	1429.3
95/5	910.4	916.9	980.1	970.1

TABLE 5.1.24

Heat Evolved from Various PbO_2/Si Mixtures and Different Silicon Particle Sizes

PbO_2/Si	HEAT EVOLVED PER GRAM OF MIXTURE (J/g)			CALCULATED
	SILICON A	SILICON B	SILICON C	
50/50	1238.6	1240.1	1107.3	1312.9
55/45	1307.0	1290.2	1189.6	1444.2
60/40	1456.3	1435.2	1331.3	1575.5
65/35	1616.3	1592.4	1499.4	1706.7
70/30	1763.7	1708.5	1691.2	1838.0
75/25	1312.9	1841.7	1816.3	1969.3
80/20	2048.6	2058.3	1955.5	2100.6
85/15	2202.6	2193.1	2068.7	2231.9
90/10	1728.8	1918.6	1995.5	2350.1
95/5	-	-	1012.3	1118.1

TABLE 5.1.25

Heat Evolved for PbO_2/Si Mixture for Different PbO_2 Origins

PbO_2/Si	PbO_2 1		PbO_2 2	
	J/g mixture	kJ/mol PbO_2	J/g mixture	kJ/mol PbO_2
30/70	742.42	591.95	708.10	564.59
40/60			1010.68	604.38
50/50	1222.02	584.60	1243.78	595.02
60/40			1476.05	588.45
70/30			1768.16	604.20
75/25	1850.61	590.22		
80/20			2035.16	608.51
85/15	2095.01	589.56		
87/13	2055.67	565.19		
90/10	1843.49	489.96	2016.75	536.00
95/5	1260.10	317.28		

TABLE 5.1.26

Heat Evolved per Mole of Pb_3O_4 for Pb_3O_4/Si Compositions

Pb_3O_4/Si	ACTUAL HEAT EVOLVED (H) kJ/mol. Si(A)	Si(B)	Si(C)	H calculated (kJ/mol.)
50/50	1126.1	685.0	775.8	1088.8
55/45	1174.3	935.2	913.5	1088.8
60/40	1170.2	944.0	928.5	"
65/35	1128.4	1012.0	1000.8	"
70/30	1108.4	998.3	1019.2	"
75/25	1056.0	1040.9	1025.3	"
80/20	1056.2	1048.3	1000.1	"
85.15	1060.5	1051.3	999.7	"
90/10	1034.3	1029.1	1023.4	"
95/5	684.4	689.3	736.8	665.1

TABLE 5.1.27

Heat Evolved per Mole PbO_2 for PbO_2/Si System

PbO_2/Si	ACTUAL HEAT EVOLVED (H) kJ/mol. Si(A)	Si(B)	Si(C)	H calculated (kJ/mol.
50/50	592.6	593.0	529.7	628.1
55/45	568.4	561.1	517.4	"
60/40	580.6	572.4	530.8	"
65/35	594.8	586.0	551.8	"
70/30	604.2	585.3	577.8	"
75/25	610.1	587.4	578.9	"
80/20	612.5	614.8	584.7	"
85/15	619.8	617.4	582.2	"
90/10	459.5	508.9	502.5	"
95/5			254.9	281.5

TABLE 5.1.28: Thermal Conductivity of Pb_3O_4/Si Compositions

see Page 72

TABLE 5.1.29

STANDARD VALUES OF VARIOUS SUBSTANCES

SUBSTANCE	ATOMIC OR MOL.WT.	MELTING POINT (K)	BOILING POINT (K)	HEAT OF FUSION (J/mol)	HEAT OF VAPORIZATION (J/mol)	(a) HEAT OF FORMATION ΔH_f^o (kJ/mol)	(b) HEAT OF FORMATION $\Delta^o H_f$ (kJ/mol)
Si	28.09	1684	2890	46473.50		0	0
Pb	207.21	600.6	2024	4777.14	177021	0	0
Pb_3O_4	685.60	DECOMP.	-	-		-718.564	-734.886
PbO_2	239.21	DECOMP.	-	-		-277.465	-276.712
PbO	223.21	1160	1745	25528.5	207283	-217.369	-217.913
SiO_2	60.09	1873	2023 (Sublimes)	8788.5		-903.709	-859.600

(a) ref. (41)

(b) ref. (42)

TABLE 5.1.30

Specific Heats of Some Chemicals Used

SUBSTANCE	C (J/mol.K)	TEMP.RANGE (K)
LEAD Pb(s)	$23.5617 + 3.7552 \times 10^{-3}T$	298 - 600
LEAD Pb(1)	$32.4477 - 3.092 \times 10^{-3}T$	600 - 2024
LEAD Pb(g)	20.7995	T>2024
SILICON Si(s)	$24.1160 + 2.3446 \times 10^{-3}T - 4.5636 \times 10^{5}T^{-2}$	298 - 1684
SILICON Si(1)	25.6232	1684 - 2024
CaF_2	$61.5195 + 0.0159T$	298 - 1684
GRAPHITE C	$11.1865 + 10.9521 \times 10^{-3}T - 4.8923 \times 10^{5}T^{-2}$	298 - 1684
$BaSO_4(s)$	$89.3498 + 59.009 \times 10^{-3}T$	298 - 1684

TABLE 5.1.31

Calculated Temperature from Observed Heats of Reaction

Pb_3O_4/Si (w/w)	OBSERVED ΔH (J/g)	UNREACTED Si (g)	SiO_2 (g)	Pb (g)	PbO (g)	CALCULATED T (^oK)
50/50	605.44	0.469	0.067	0.346	0.108	1365
55/45	720.24	0.413	0.079	0.411	0.087	1620
60/40	793.06	0.359	0.087	0.453	0.091	1683
65/35	921.12	0.303	0.102	0.526	0.063	1683
70/30	978.45	0.249	0.108	0.559	0.076	1683
75/25	1093.12	0.194	0.121	0.624	0.056	2024
80/20	1174.31	0.139	0.130	0.670	0.055	2024
85/15	1251.32	0.085	0.138	0.714	0.056	2024
90/10	1296.93	0.033	0.143	0.740	0.076	2024

TABLE 5.1.32

Physical Properties of Pb_3O_4/Si Compositions

Pb_3O_4/Si	Thermal conductivity (J/s.cm.K)	Density of pellet (g/cc)	Specific heat (J/g.K)	Thermal diffusivity (cm^2/s)
50/50	2.200×10^{-3}	2.31	0.504	1.753×10^{-3}
60/40	2.009×10^{-3}	2.85	0.481	1.466×10^{-3}
70/30	1.723×10^{-3}	3.34	0.448	1.151×10^{-3}

TABLE 5.1.33

CALCULATED VALUES OF ε AND θ

50/50 Pb_3O_4/Si		60/40 Pb_3O_4/Si	
θ	ε	θ	ε
0.170	0.169	0.144	0.143
0.220	0.219	0.169	0.168
0.292	0.290	0.220	0.219
0.359	0.358	0.301	0.300
0.457	0.455	0.479	0.478
0.552	0.550	0.712	0.711
0.655	0.653	0.936	0.936
0.845	0.844		
0.948	0.947		

TABLE 5.1.34

DATA FOR 50/50 Pb_3O_4/Si COMPOSITION

TIME(t) s x 10^{-3}	θ	$d\theta/dt$	$\ell n\ t$	$\ell n\ \ell n(\frac{1}{1-\theta})$
10.8	0.17	1.92	- 4.53	- 1.68
19.0	0.21	3.13	- 3.96	- 1.45
33.2	0.22	5.20	- 3.40	- 1.39
49.2	0.29	6.84	- 3.01	- 1.07
71.9	0.38	8.27	- 2.63	- 0.80
83.4	0.46	8.02	- 2.48	- 0.49
93.7	0.55	7.92	- 2.37	- 0.22
105.7	0.65	6.82	- 2.25	0.06
118.7	0.75	5.61	- 2.13	0.31
141.2	0.84	4.03	- 1.96	0.62
190.6	0.95	1.86	- 1.66	1.09

TABLE 5.1.35

DATA FOR 60/40 Pb_3O_4/Si COMPOSITION

TIME(t) s x 10^{-3}	θ	$d\theta/dt$	$\ell n\ t$	$\ell n\ \ell n(\frac{1}{1-\theta})$
6.2	0.14	13.06	- 5.09	- 1.89
9.2	0.17	17.75	- 4.69	- 1.68
13.5	0.22	22.86	- 4.30	- 1.39
20.2	0.30	26.05	- 3.90	- 1.03
25.0	0.48	25.45	- 3.69	- 0.43
30.3	0.59	23.33	- 3.51	- 0.11
35.3	0.71	18.74	- 3.34	0.22
42.2	0.83	13.12	- 3.17	0.56
50.0	0.94	5.58	- 3.00	1.01

TABLE 5.1.36

DATA FOR 70/30 Pb_3O_4/Si COMPOSITIONS

TIME(t) s x 10^{-3}	θ	$\frac{d\theta}{dt}$	ℓn t	$\ell n \ \ell n \ (\frac{1}{1-\theta})$
8.2	0.23	22.28	-4.80	-1.34
15.6	0.34	25.35	-4.16	-0.88
16.4	0.37	28.26	-4.11	-0.76
18.2	0.43	28.55	-4.00	-0.58
20.9	0.49	28.22	-3.87	-0.39
25.8	0.62	24.47	-3.66	-0.04
30.9	0.73	19.54	-3.48	0.27
37.3	0.84	13.06	-3.29	0.61
44.7	0.91	2.03	-3.11	0.90

TABLE 5.1.37: Values of α and β for Various Pb_3O_4/Si Compositions

TABLE 5.1.38: Observed and Calculated (R.B.) for Pb_3O_4/Si Compositions

See page 82

TABLE 5.1.39

50/50 Pb_3O_4/Si		60/40 Pb_3O_4/Si		70/30 Pb_3O_4/Si	
$\ell n \frac{d}{dt} - \ell n(1 - \varepsilon)$	$\frac{1}{T} \times 10^3 (K^{-1})$	$\ell n \frac{d\varepsilon}{dt} - \ell n(1 - \varepsilon)$	$\frac{1}{T} \times 10^4 (K^{-1})$	$\ell n \frac{d\varepsilon}{dt} - \ell n(1 - \varepsilon)$	$\frac{1}{T} \times 10^4 (K^{-1})$
0.84	5.90	2.72	21.60	3.39	20.20
1.37	4.83	3.06	20.30	3.50	18.10
1.90	4.54	3.38	18.11	3.63	15.78
2.27	3.43	3.62	15.42	3.80	12.00
2.62	2.76	3.89	11.65	3.91	10.95
2.76	2.19	4.05	10.10	4.02	9.92
2.87	1.81	4.18	8.83	4.16	8.42
2.98	1.53	4.32	7.91	4.29	7.39
3.26	1.18	4.47	7.15	4.41	6.61
3.58	1.05			4.59	5.84

TABLE 5.1.40

DATA FROM TG FOR ISOTHERMAL DECOMPOSITION OF Pb_3O_4

520°C				550°C				565°C				580°C			
t(min)	α	$\ell n \ell n(\frac{1}{1-\alpha})$	ℓn t	t(min)	α	$\ell n \ell n(\frac{1}{1-\alpha})$	ℓn t	t(min)	α	$\ell n \ell n(\frac{1}{1-\alpha})$	ℓn t	t(min)	α	$\ell n \ell n(\frac{1}{1-\alpha})$	ℓn t
4	0.054	-2.89	1.39	4	0.21	-1.47	1.39	1.7	0.17	-1.69	0.53	0.5	0.11	-2.13	-0.69
7	0.092	-2.34	1.95	6	0.32	-0.95	1.79	2.7	0.22	-1.39	0.99	1.5	0.33	-0.68	0.41
12	0.164	-1.72	2.30	8	0.42	-0.60	2.08	3.7	0.37	-0.78	1.31	2.5	0.60	-0.10	0.92
18	0.256	-1.22	2.89	11	0.56	-0.18	2.40	5.7	0.54	-0.26	1.74	3.5	0.73	0.27	1.25
24	0.350	-0.85	3.18	16	0.73	0.26	2.77	7.7	0.66	0.08	2.04	4.5	0.81	0.51	1.50
35	0.510	-0.33	3.56	21	0.84	0.60	3.05	9.7	0.75	0.34	2.27	5.5	0.87	0.70	1.70
43	0.615	-0.05	3.76	25	0.89	0.80	3.22	10.7	0.79	0.44	2.37	6.5	0.90	0.85	1.87
49	0.680	0.13	3.89	30	0.94	1.00	3.4	13.7	0.86	0.69	2.62	7.5	0.93	0.97	2.01
59	0.770	0.38	4.08					14.7	0.88	0.77	2.69	8.5	0.94	1.06	2.14
66	0.820	0.54	4.14					16.7	0.92	0.91	2.82				
77	0.850	0.64	4.26												

TABLE 5.1.41

DATA FROM TG FOR (DYNAMIC) DECOMPOSITION OF Pb_3O_4

HEATING RATE 5°C/min.				10°C/min.				40°C/min.				80°C/min.			
t(min)	α	$\ell n \ell n(\frac{1}{1-\alpha})$	ℓn t	t(min)	α	$\ell n \ell n(\frac{1}{1-\alpha})$	ℓn t	t(min)	α	$\ell n \ell n(\frac{1}{1-\alpha})$	ℓn t	t(min)	α	$\ell n \ell n(\frac{1}{1-\alpha})$	ℓn t
4	0.08	-2.48	1.39	3	0.085	-2.42	1.10	1.2	0.09	-2.30	0.18	0.7	0.083	-2.44	-0.36
5	0.13	-1.98	1.61	4	0.19	-1.57	1.39	1.4	0.18	-1.65	0.34	0.9	0.26	-1.21	-0.105
6	0.21	-1.45	1.79	5	0.40	-0.68	1.61	1.6	0.25	-1.23	0.47	1.0	0.39	-0.70	0
7	0.32	-0.94	1.95	6	0.63	0	1.79	1.7	0.33	-0.90	0.53	1.1	0.56	-0.20	0.10
8	0.46	-0.48	2.08	7	0.81	0.50	1.95	1.8	0.41	-0.63	0.59	1.2	0.69	+0.16	0.18
9	0.59	-0.11	2.20	8	0.91	0.87	2.08	1.9	0.49	-0.39	0.64	1.3	0.83	0.55	0.26
11	0.81	0.50	2.40	9	0.96	1.17	2.20	2.15	0.65	0.05	0.77	1.4	0.91	0.87	0.34
12	0.88	0.74	2.48					2.4	0.81	0.51	0.88				
13	0.92	0.95	2.57					2.6	0.89	0.79	0.96				
14	0.95	1.11	2.64					3.1	0.97	1.24	1.13				

TABLE 5.1.42

DATA FROM DSC FOR PbO_2/Si (85/15) REACTION

10°C/min.				20°C/min.				40°C/min.				80°C/min.			
t(min)	α	$\ell n \ell n(\frac{1}{1-\alpha})$	ℓn t	t(min)	α	$\ell n \ell n(\frac{1}{1-\alpha})$	ℓn t	t(min)	α	$\ell n \ell n(\frac{1}{1-\alpha})$	ℓn t	t(min)	α	$\ell n \ell n(\frac{1}{1-\alpha})$	ℓn t
0.35	0.06	-3.43	-1.05	0.25	0.05	-2.89	-1.39	0.28	0.06	-1.11	-2.83	0.125	0.028	-3.62	-2.08
0.50	0.14	-1.89	-0.69	0.40	0.15	-1.82	-0.92	0.34	0.15	-0.86	-1.90	0.187	0.124	-2.02	-1.67
0.70	0.28	-1.13	-0.36	0.45	0.20	-1.49	-0.80	0.41	0.28	-0.65	-1.26	0.212	0.195	-1.53	-1.55
0.80	0.38	-0.74	-0.22	0.50	0.28	-1.13	-0.69	0.47	0.44	-0.47	-0.82	0.250	0.376	-0.75	-1.39
0.90	0.51	-0.35	-0.11	0.55	0.36	-0.79	-0.60	0.53	0.61	-0.28	-0.49	0.280	0.600	-0.10	-1.27
1.05	0.62	-0.05	-0.05	0.63	0.52	-0.30	-0.47	0.59	0.77	-0.10	-0.26	0.312	0.67	0.11	-1.16
1.17	0.71	0.21	0.16	0.75	0.74	0.30	0.29	0.66	0.84	0.07	0.17	0.375	0.81	0.51	-0.98
1.29	0.78	0.42	0.26	0.82	0.83	0.56	0.20	0.72	0.89	0.24	0.12	0.437	0.91	0.86	-0.83
1.42	0.84	0.59	0.35												

TABLE 5.1.43

RESULTS FROM TG OF (ISOTHERMAL) DECOMPOSITION OF Pb_3O_4

TEMP K	β	γ (min)	$\ell n \frac{\beta}{\gamma}$	$\frac{1}{T} \times 10^4 (K^{-1})$
793	1.25	45.40	-3.59	12.61
823	1.23	12.88	-2.35	12.15
838	1.08	7.25	-1.90	11.93
858	0.97	2.86	-1.05	11.72

TABLE 5.1.44

RESULTS FROM TG OF (DYNAMIC) DECOMPOSITIONS OF Pb_3O_4

HEATING RATE ^oC/Min.	β	γ	$\ell n \frac{\beta}{\gamma}$	$\frac{1}{T_{0.63}} \times 10^4 (K^{-1})$
5	3.08	9.53	-1.13	11.90
10	3.50	6.05	-0.55	11.72
40	4.00	2.14	0.63	11.38
80	4.71	1.16	1.40	11.25

TABLE 5.1.45

RESULTS FROM DSC FOR PbO_2/Si 85/15) REACTIONS

HEATING RATE ^{o}C/min.	β	γ	$\ell n \frac{\beta}{\gamma}$	$\frac{1}{T_{0.63}} \times 10^{4}(K^{-1})$
10	2.40	1.087	0.79	13.28
20	3.42	0.710	1.57	13.10
40	4.00	0.543	2.00	12.92
80	4.10	0.301	2.60	12.76

TABLE 5.1.46

RESULTS FROM DSC FOR PbO_2/Si REACTION

HEATING RATE θ $^{o}C/min.$	$\ell n \frac{\theta}{T_m^2}$	$\frac{1}{T_m} \times 10^4 (K^{-1})$
10	-4.75	13.37
20	-4.46	13.16
40	-4.17	12.99
80	-3.88	12.79
160	-3.61	12.32

TABLE 5.1.47

RESULTS OF DSC FOR PbO_2/Si REACTION

dH/dt (cm)	$\ell n \frac{dH}{dt}$	T(K)	$\frac{1}{T} \times 10^4 (K^{-1})$
1.8	0.59	742	13.477
3.2	1.16	744	13.441
4.3	1.46	745	13.423
7.8	2.05	747	13.387
12.9	2.56	749	13.351
15.2	2.72	750	13.333
16.4	2.80	751	13.316
15.6	2.75	752	13.300

TABLE 5.1.48

RESULTS FROM DSC FOR PbO_2/Si REACTION

T(K)	$\frac{1}{T} \times 10^4$ (K^{-1})	$\ell n \frac{dH/dt}{(A-a)}$	α
742	13.477	-4.14	0.053
744	13.441	-3.54	0.085
745	13.423	-3.21	0.112
747	13.387	-2.52	0.193
749	13.351	-1.83	0.330
750	13.333	-1.50	0.433
751	13.316	-1.17	0.560
752.5	13.299	-0.94	0.668
753.7	13.267	-0.76	0.763
754.9	13.246	-0.60	0.834
756.2	13.224	-0.43	0.888
757.4	13.203	1.40	0.920

APPENDIX
2

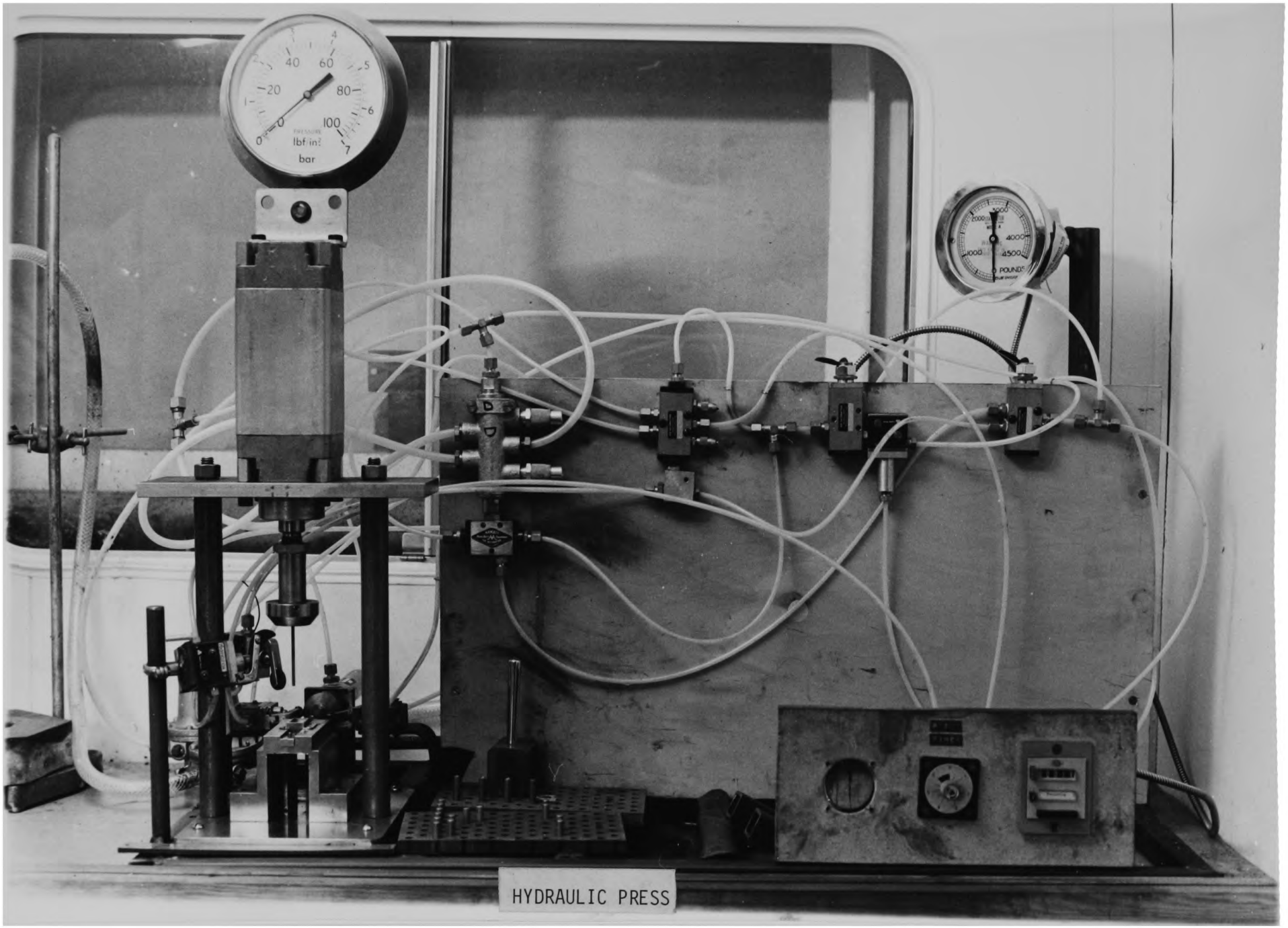

HYDRAULIC PRESS

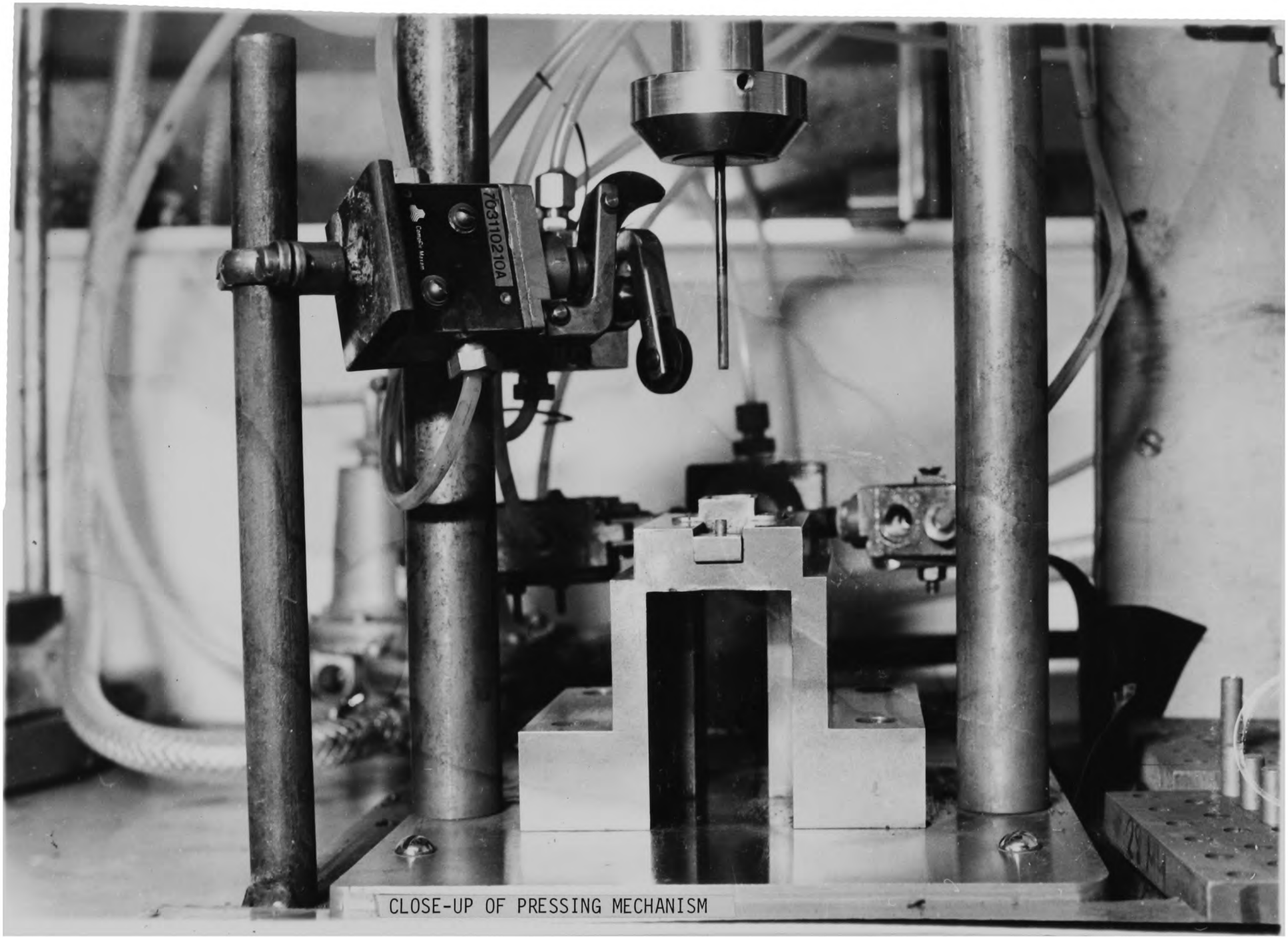

CLOSE-UP OF PRESSING MECHANISM

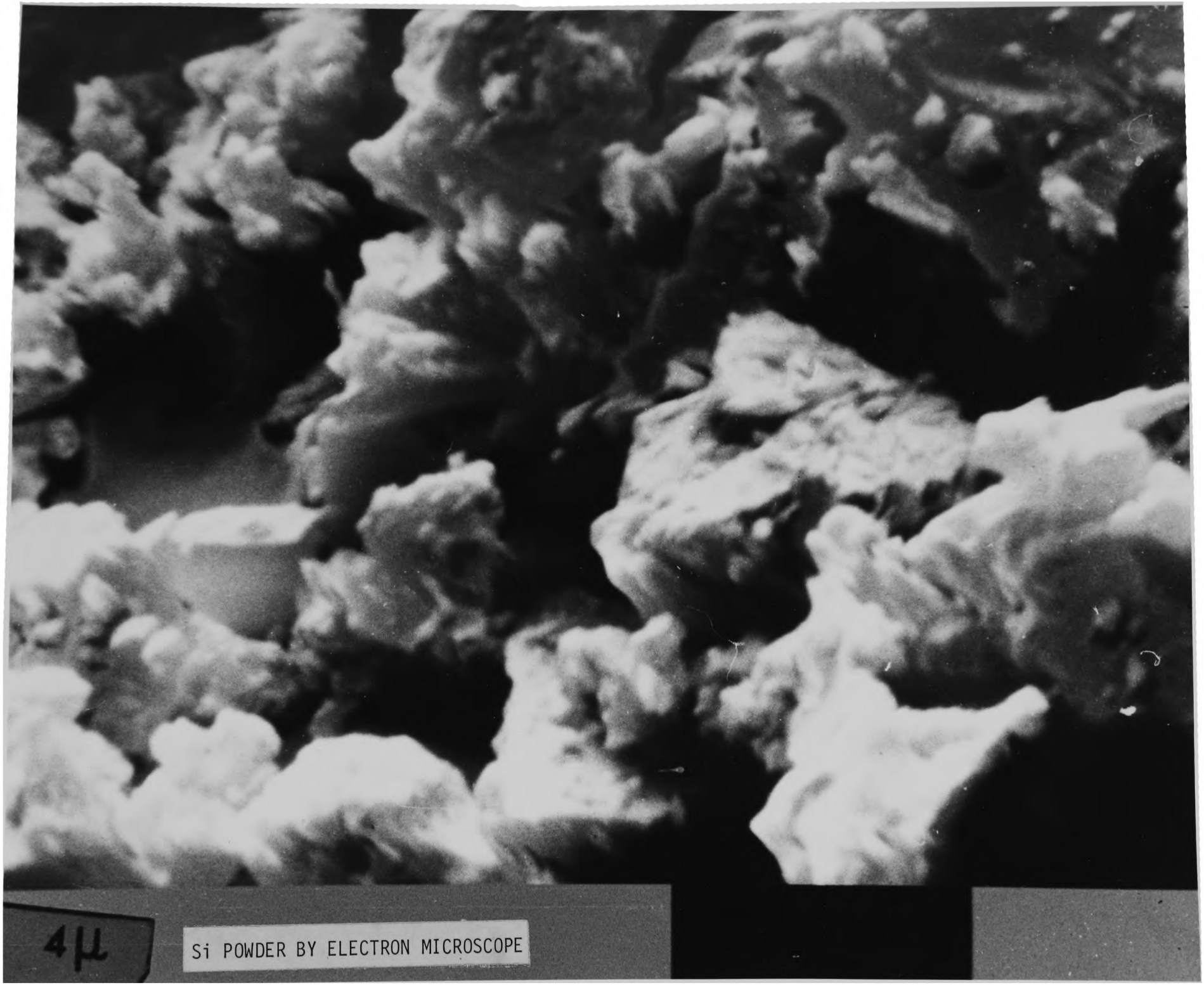
4μ
Si POWDER BY ELECTRON MICROSCOPE

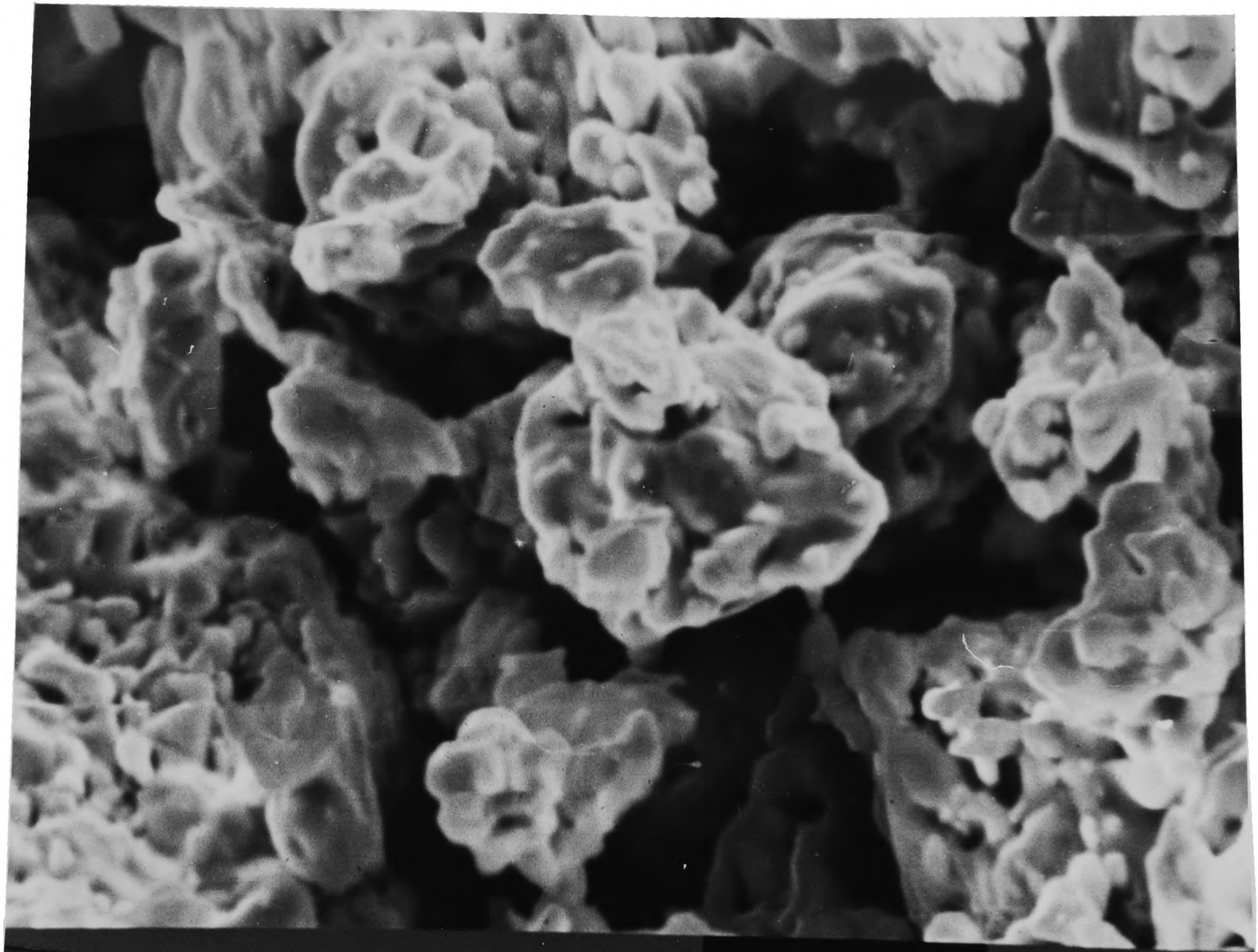

4μ

Pb_3O_4 POWDER BY ELECTRON MICROSCOPE

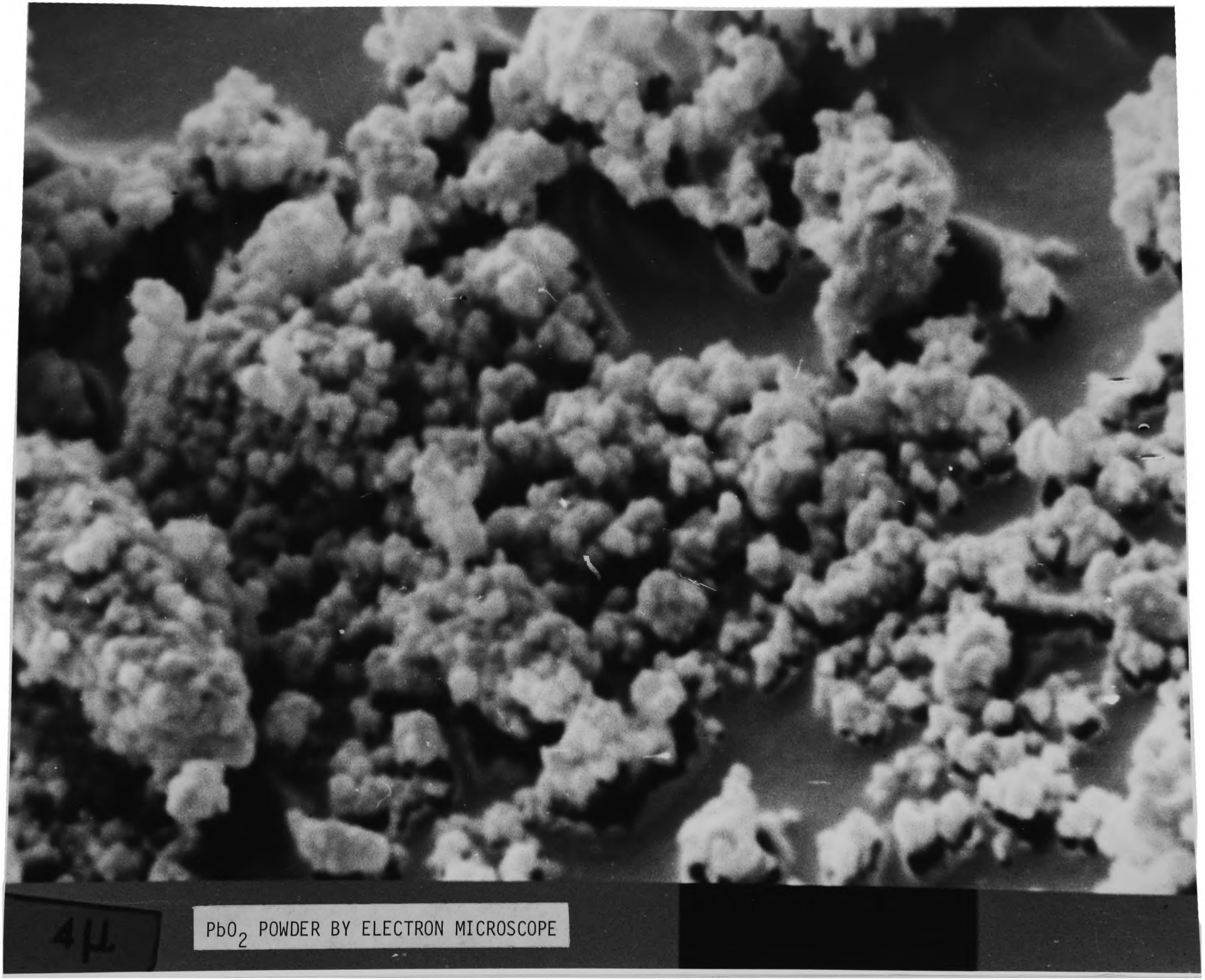
4μ
PbO2 POWDER BY ELECTRON MICROSCOPE

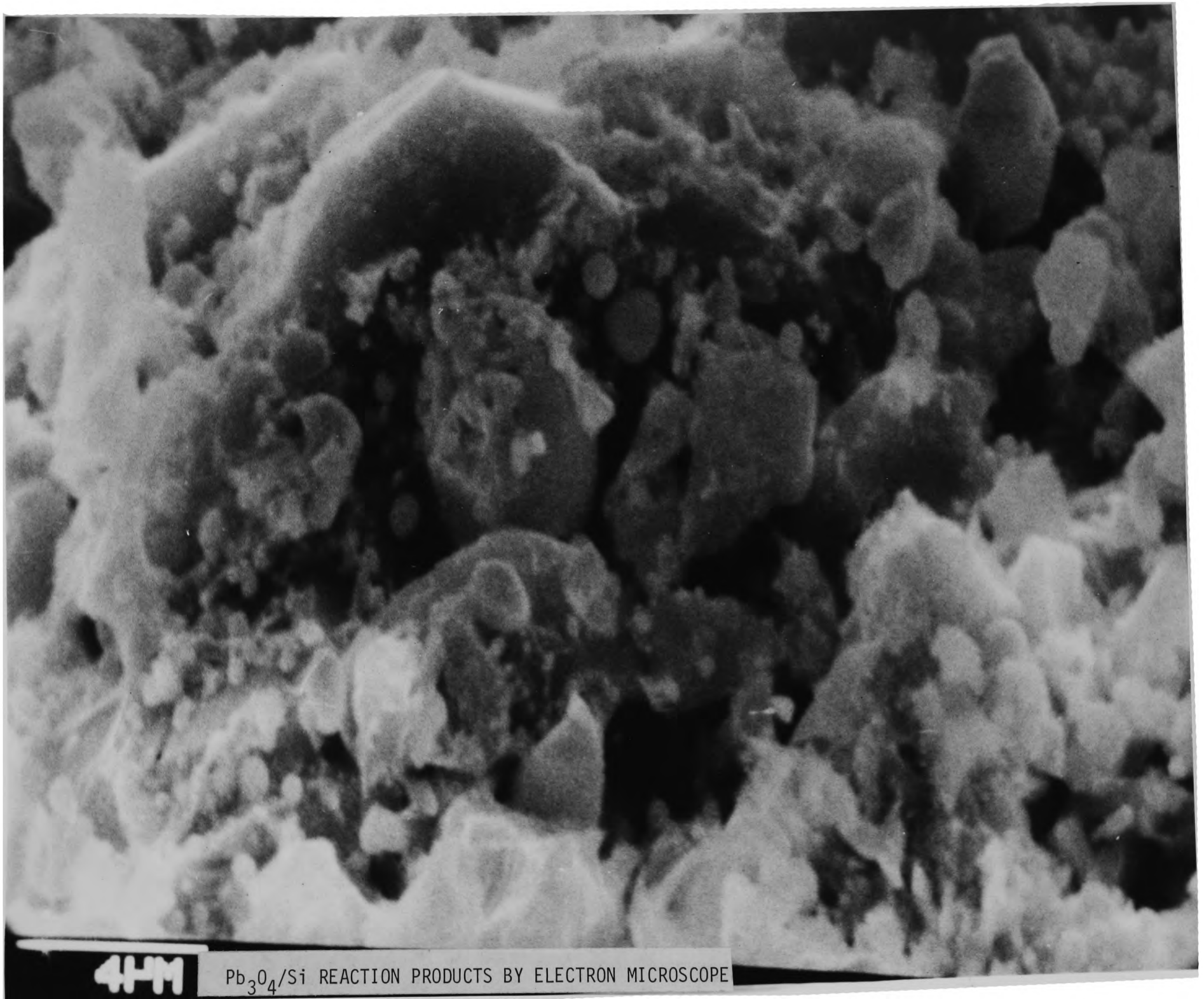

4HM Pb_3O_4/Si REACTION PRODUCTS BY ELECTRON MICROSCOPE